

## 16

# Aircraft Drag Analysis

## O U T L I N E

<b>16.1 Introduction</b>	<b>658</b>	<b>16.4.5 Drag of Landing Gear</b>	<b>717</b>
16.1.1 The Content of This Chapter	658	16.4.6 Drag of Floats	722
16.1.2 Quick-Guide: How Do I Estimate the Drag of My Airplane?	659	16.4.7 Drag of Deployed Flaps	724
<b>16.2 The Basics of Drag Modeling</b>	<b>659</b>	16.4.8 Drag of Deployed Spoilers	725
16.2.1 Fundamental Definitions	659	16.4.9 Drag Correction for Cockpit Windows	725
16.2.2 Quadratic Drag Modeling	662	16.4.10 Drag of Canopies	727
16.2.3 Correcting the Drag Coefficient at High AOA	668	16.4.11 Drag of Blisters	728
16.2.4 Drag Modeling using Higher Order Polynomials	670	16.4.12 Drag of Antennas	729
16.2.5 Drag of a 2D Body in a Wind-Tunnel	670	16.4.13 Drag of Windmilling and Stopped Propellers	729
16.2.6 Additional Topics on Drag	672	16.4.14 Drag of Parachutes	730
16.2.7 Various Means to Reduce Drag	672	16.4.15 Drag of Various Sources	731
<b>16.3 Estimating the Drag of a Complete Aircraft</b>	<b>678</b>	<b>16.5 Special Topics Involving Drag</b>	<b>736</b>
16.3.1 Estimating Skin Friction Drag: $C_{Df}$	680	16.5.1 Step-by-Step: Extracting Drag from $LD_{max}$	736
16.3.2 Estimating Lift-Induced Drag: $C_{Dl}$	691	16.5.2 Step-by-Step: Extracting Drag From a Flight Polar Using the Quadratic Spline Method	737
16.3.3 Estimating Wave Drag: $C_{Dw}$	695	16.5.3 Step-by-Step: Extracting Drag Coefficient for a Piston Powered Propeller Aircraft	740
16.3.4 Calculate $C_{D_{min}}$ Using the Rapid Drag Estimation Method	701	16.5.4 Extracting Drag Coefficient From Published Data for Piston Aircraft	742
16.3.5 Calculate $C_{D_{min}}$ Using the Component Drag Buildup Method	701	16.5.5 Determining Drag Characteristics From Wind Tunnel Data	743
16.3.6 Form Factors	704	<b>16.6 Additional Information—Drag of Selected Aircraft</b>	<b>744</b>
16.3.7 Interference Factors	711	16.6.1 General Range of Subsonic Minimum Drag Coefficients	745
16.3.8 Cumulative Result of Undesirable Drag (CRUD)	712	16.6.2 Drag of Various Aircraft by Class	745
16.3.9 Total Drag Coefficient: $C_D$	712	<b>Exercises</b>	<b>745</b>
<b>16.4 Miscellaneous or Additive Drag</b>	<b>713</b>	<b>References</b>	<b>750</b>
16.4.1 Trim Drag	713		
16.4.2 Cooling Drag	714		
16.4.3 Drag of Simple Wing-like Surfaces	716		
16.4.4 Drag of Streamlined Struts and Landing Gear Pant Fairings	716		

## 16.1 INTRODUCTION

Few tasks in aircraft design are as daunting as the estimation of drag. It puts a lid on creativity and, sometimes, transforms inspiration into disappointment. In aircraft design, the primary objective is usually to minimize drag. However, there is more to drag than meets the eyes. Ideally, we want to control it. During climb and cruise, we want low drag. During approach to landing, we want higher drag. This makes it easier to land. Sailplane pilots can attest to how challenging it would be to land without means to increase drag. Some aircraft, including many sailplanes, allow the drag polar to be shifted around using a cruise flap. This de-cambers the airfoil, moving the maximum glide ratio to a higher airspeed. Or increase camber to reduce drag during climb. This chapter provides the aircraft designer with methods to estimate drag and details of its causes and prevention.

Many areas of the aircraft design process rely on accurate drag estimation. This includes performance analysis, engine selection, and requirements for fuel capacity, to name a few. The subject must be approached with respect and caution. Drag is hard to predict accurately: it is easy to over- and underestimate. In part, this is because it is hard to identify and quantify its sources. An underestimation results in an airplane that performs far worse than predicted, risking a costly “drag-cleanup” effort, if not a program cancellation. In contrast, an overestimation by overly conservative approach may render the design so bad on paper the project it might be canceled before it even begins.

Recall [Figure 1-14](#), which shows how the design project can be broken into manageable tasks. Among tasks are the *lift model* (see [Sections 9.5.2](#) and [24.2.5](#)) and *weight model* (see [Section 6.4, Statistical Weight Estimation Methods](#)). This chapter focuses on the *drag model*. The goal of drag analysis is clear: create a realistic drag model. This is accomplished per the flow chart of [Figure 16-21](#). This chapter presents classical methods for this purpose.

The aspiring designer should not think that drag estimation is simple. “We’ll just model it using CFD,” is an idea often expressed by students of aerospace engineering who have yet to be humbled by Mother Nature by comparing predictions to wind tunnel or flight test data. While *Navier-Stokes Computational Fluid Dynamics* (NS-CFD) is a promising and exciting scientific advancement, it is not yet robust enough to allow novice users to estimate drag reliably.<sup>1</sup> In 2001, researchers from several aviation and science organizations, including the *American Institute of Aeronautics and Astronautics* (AIAA), conducted the

first of several workshops on drag estimation using CFD methods [[1](#), [2](#)]. An Airbus-style passenger transport aircraft, consisting of a fuselage and wing only [[3](#)], was modeled by 18 participants using 14 different NS solvers. The analysis results were compared to wind tunnel data that were made available to the participants after they had submitted their estimates. In short, the lift and drag predictions left a lot to be desired. Some predictions were close to the wind tunnel data, while others (drag) were off by 50%–200% of the wind tunnel value [[1](#), [2](#)]. These predictions were performed by experts. If they have a hard time performing such predictions, the novice analyst should take note. The drag analyst is between a rock and a hard place—a dreaded place shared by the weights engineer.

Today, the state of the art in low drag aircraft is the modern sailplane (see [Figure 16-1](#)). *Natural laminar flow* (NLF) airfoils, segmented tapered wing planform, tadpole fuselage, sealed control surfaces, carefully tailored wing root fairings, T-tail, and disciplined attention to any detail that reduces drag, combine to make some sailplanes achieve glide ratio in excess of 50. No other aircraft are capable of this feat. The aircraft designer interested in developing low drag aircraft should pay special attention to sailplanes. There is a lot that can be learned.

### 16.1.1 The Content of This Chapter

- [Section 16.2](#) discusses the nature of drag, what contributes to it, how it is modeled, and how it can be estimated. The section also discusses limitations of various estimation methods.
- [Section 16.3](#) discusses the drag characteristics of the airplane as a whole and presents methods to estimate the total drag of aircraft. It is a go-to section for the reader interested in starting a drag estimation of a new aircraft.
- [Section 16.4](#) presents methods to estimate the drag caused by the addition of necessary imperfections to aircraft, such as antennas, fairings, landing gear, and so on. Additionally, methods to estimate trim drag and cooling drag are presented.
- [Section 16.5](#) presents methods to estimate the drag of existing aircraft using published performance data. These are intended to obtain drag characteristics for rival aircraft and are used to compare own drag coefficients to reduce chances of poor estimation.
- [Section 16.6](#) tabulates the drag coefficients and maximum lift-to-drag ratios for selected aircraft, accumulated from various sources. These help the designer assessing the drag of comparable aircraft.

<sup>1</sup> Then again, many would argue that novices shouldn’t be estimating drag in the first place.



**FIGURE 16-1** No aircraft generate as little drag as the modern sailplane. A Rolladen-Schneider LS4 sailplane, moments before touchdown with wing spoilers deployed. *Photo by Phil Rademacher.*

### 16.1.2 Quick-Guide: How Do I Estimate the Drag of My Airplane?

Chances are you are reading this chapter to seek help in estimating the drag for your airplane. For immediate help, head to [Section 16.3, Estimating the Drag of a Complete Aircraft](#).

## 16.2 THE BASICS OF DRAG MODELING

This section introduces various means to model the drag of an airplane. A *drag model* is a mathematical expression of the drag coefficient for a body. It primarily describes how the drag of the body changes with orientation in the flow field, but also includes effects of flow properties ( $R_e$ ,  $M_\infty$ ). Unsurprisingly, higher fidelity modeling calls for mathematical complexity. A good drag model accounts for contributions from the deflection of control surfaces, deployment of landing gear, and growth of flow separation at high AOA and AOY. This is challenging to do analytically. Wind tunnel and flight testing remain the most reliable methods for this purpose.

### 16.2.1 Fundamental Definitions

#### (1) Definition of the Drag Model

A drag model is a mathematical representation of the drag coefficient of a body. It is denoted by  $C_d$  for 2D bodies and  $C_D$  for 3D bodies. For aircraft, the drag model is an expression of the form

$$C_D = f(\text{geometry}, R_e, M_\infty, \alpha, \beta, \delta_e, \delta_f, \delta_s, \delta_{LDG}, \dots) \quad (16-1)$$

Where:  $R_e$  = Reynolds number,

$M_\infty$  = Mach number,

$\alpha$  = Angle-of-attack,

$\beta$  = Angle-of-yaw,

$\delta_e$  = Elevator deflection,

$\delta_f$  = Deflection of high-lift devices,

$\delta_s$  = Deflection of spoilers,  $\delta_f$ ,

$\delta_{LDG}$  = Deployment of landing gear.

A good drag model accounts for (A) regions of laminar and turbulent boundary layer, as well as the location of laminar-to-turbulent transition, (B) flow separation regions, (C) compressibility, and (D) deployment of flight control and landing systems. A good drag model shows good agreement with experiment.

#### (2) Classification of Drag Analysis Methods

There are two basic classes of drag analysis methods: *Prediction* and *postdiction*. The former attempts to estimate the drag of a new aircraft before it flies. The latter does so for an existing aircraft. Prediction methods estimate an aircraft's drag based on its geometry. Postdiction methods evaluate drag using wind tunnel, or performance data derived from flight testing. This chapter primarily presents prediction methods, but a few basic postdiction methods are presented in [Section 16.5, Special Topics Involving Drag](#).

### (3) Sources of Drag

The total drag of a body stems from (A) pressure difference (*pressure drag*) and (B) skin friction (*skin friction drag*). Major contributors to each are

- (1) **Pressure drag** is the component of the resultant aerodynamic force that is parallel to the tangent to the flight path. It is generated by the pressure differential formed by the body (see [Equation 8-20](#)).
- (2) **Skin friction drag** is caused by molecules “rubbing” against the body’s surface. The resulting friction primarily acts tangent to the flight path.
- (3) **Lift-induced drag** is a pressure drag caused by the formation of wingtip vortices, which tilts the lift vector backward and creates a force component that adds to the total drag.
- (4) **Wave drag** is caused by the localized rise in pressure around a body due to the formation of normal and oblique shocks on the airplane. This effect begins at high subsonic Mach numbers.
- (5) **Miscellaneous drag** is caused by a number of “small,” often overlooked, contributions such as small inlets and outlets, access panels, fuel caps, and antennas, to name a few.

In addition to the discussion presented in this chapter, the reader should also refer to [Sections 8.1.7, Forces and Moment per Unit Span](#) and [8.1.10, Boundary Layer Basics](#).

### (4) Drag Model Fidelity

Drag models come in many shapes and forms. Their fidelity can be split into three classes:

#### *Class 3—Simplified Drag Model*

This is a *quadratic drag model* (see [Section 16.2.2, Quadratic Drag Modeling](#)) that assumes drag increases with the lift coefficient squared. It is the simplest and least accurate model at our disposal. It is acceptable for missiles and other axisymmetric vehicles, and a handful of fixed-wing aircraft. It is a poor predictor of drag for aircraft whose geometry features mean-line curvature (camber). It is useful for explaining important concepts in performance theory, where its simplicity permits closed-form solutions of complex performance concepts. However, this does not mean those solutions are accurate, just closed-form. The simplified drag model is typically presented in the following form

$$C_D = C_{D_{\min}} + kC_L^2 \quad (16-2)$$

Where  $C_{D_{\min}}$  is the minimum drag coefficient,  $C_L$  is the lift coefficient, and  $k$  is the *lift-induced drag constant*.

#### *Class 2—Adjusted Drag Model*

This is a correction of the simplified model. It requires the position of the minimum drag coefficient ( $C_{L_{\min D}}$ ) to be specified. Its inclusion shifts the quadratic drag polar

to the left or right. This significantly improves the shortcomings of the simplified model. However, it too becomes gradually inaccurate at higher AOA. The adjusted drag model is typically presented in the following form

$$C_D = C_{D_{\min}} + k(C_L - C_{L_{\min D}})^2 \quad (16-3)$$

#### *Class 1—Advanced Drag Model*

Refers to any drag model that (A) corrects for the effect of flow separation at high AOA and AOV and (B) introduces contributions of configuration changes, such as the deflection of control surfaces, flaps, slats, spoilers, and deployed landing gear. A Class 1 drag model is in excellent agreement with experiment over the entire normal operating range of the aircraft and is sometimes defined between  $-180^\circ < \alpha \leq 180^\circ$ . Such drag models are created in serious development programs, where they are used for performance as well as stability and control (e.g., for use in flight simulators). An example of such a model is presented below (also see [Section 24.2.6, The Drag Model](#)).

$$\begin{aligned} C_D = & C_{D_{\min}} + C_{D_\alpha} \alpha + C_{D_\beta} \beta + C_{D_{\delta_e}} \delta_e + C_{D_{\delta_f}} \delta_f + C_{D_{\delta_s}} \delta_s \\ & + C_{D_{\delta_{LDG}}} \delta_{LDG} + C_{D_w} + \dots \end{aligned} \quad (16-4)$$

Where:  $C_{D_\alpha}$  = Drag curve slope,

$C_{D_\beta}$  = Change in drag due to yaw,

$C_{D_w}$  = Wave drag contribution,

$C_{D_{\delta_e}}$  = Change in drag with elevator deflection,  $\delta_e$ ,

$C_{D_{\delta_f}}$  = Change in drag with deployment of high-lift devices,  $\delta_f$ ,

$C_{D_{\delta_s}}$  = Change in drag with deployment of spoilers,  $\delta_s$ ,

$C_{D_{\delta_{LDG}}}$  = Change in drag with deployment of landing gear,  $\delta_{LDG}$ .

#### *Look-up Tables*

Exemplifies another version of an advanced drag model. These are developed using wind tunnel testing or, analytically, using specialized analyses. They incorporate flow separation and other nonlinearities captured by experiment. Their primary use is in flight simulation and advanced performance theory.

#### *(5) Drag Polar*

A *drag polar* is a graph that plots the drag coefficient,  $C_D$ , as a function of the lift coefficient,  $C_L$  (see [Figure 16-2](#)).

#### *(6) Total Drag Force, $C_D$*

Once the drag model is known, the drag force is calculated using the expression below.

$$D = \frac{1}{2} \rho V_\infty^2 S C_D \quad (16-5)$$

Where  $\rho$  is air density,  $V_\infty$  is far-field airspeed, and  $S$  is reference area (typically wing area).

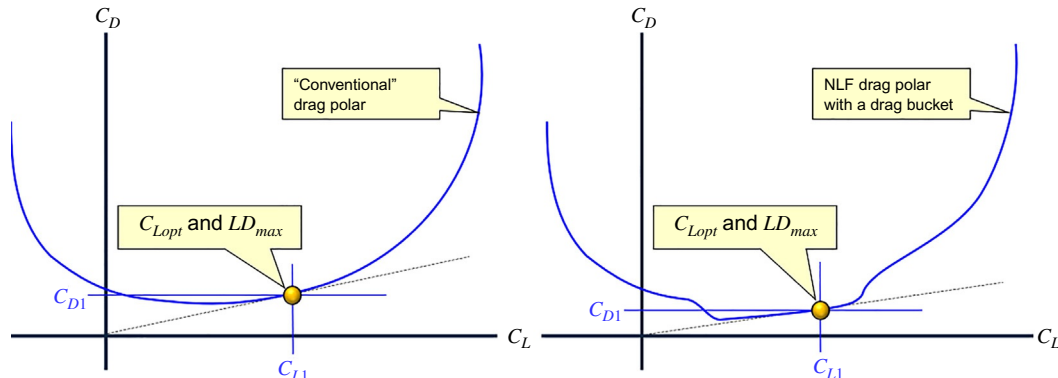


**FIGURE 16-2** Graphical determination of  $LD_{max}$  and  $C_{L_{opt}}$  for conventional (left) and NLF polars (right).

### (7) Dragcounts

A *dragcount* is the drag coefficient multiplied by a factor of 10,000. For instance, 250 dragcounts is equivalent to a  $C_D=0.0250$ ; 363 dragcounts is equivalent to a  $C_D=0.0363$ , and so on.

### (8) Wetted Area, $S_{wet}$

Refers to the surface area of the airplane that is directly exposed to the outside air. As a rule of thumb, if the airplane was dipped in water, everything that gets wet externally belongs to the wetted area.

### (9) Minimum Drag, $C_{D_{min}}$

*Minimum drag* is the lowest value of the drag coefficient. It combines contributions from pressure (pressure drag) and shear stresses (friction). It is easily identifiable in the drag polar. If the body to which it applies features *curvature*, its value occurs at a nonzero lift coefficient. *Parasitic drag* is another name for  $C_{D_{min}}$ . Methods to estimate its value are presented in [Section 16.3, Estimating the Drag of a Complete Aircraft](#). Strictly speaking,  $C_{D_{min}}$  depends on airspeed and altitude and, thus, should be evaluated at each flight condition. However, it is frequently evaluated as an *averaged value* to keep the performance analysis more manageable.

### (10) Lift-Induced Drag, $C_{D_l}$

*Lift-induced drag* is defined in Bullet (3). It is denoted as  $C_{D_l}$ . Methods to estimate its value are presented in [Section 16.3, Estimating the Drag of a Complete Aircraft](#).

### (11) Wave Drag, $C_{D_w}$

As an aircraft approaches the speed of sound, its lift, drag, and moment characteristics change. This is called the *compressibility effect*. It greatly increases the drag of an airplane approaching and exceeding the speed of sound. The drag is called *wave drag* and is denoted by  $C_{D_w}$ . It is discussed for airfoils in [Section 8.3.8, The Effect of Compressibility](#), for wings in [Section 9.3.3, Wing Sweep Angle](#), and for drag in [Section 16.3.3, Estimating Wave Drag](#).

### (12) Effective Aspect Ratio, $AR_e$

The product  $AR \cdot e$ , where  $AR$  is the wing's aspect ratio and  $e$  is the *Oswald's span efficiency* (see [Section 9.5.12, Determination of Span Efficiency](#)), is often referred to as the *effective aspect ratio*, denoted by  $AR_e$ . In this respect, the Oswald efficiency can be considered a factor that renders the  $AR$  less effective than the geometric value indicates. The designer can consider planform and other geometric modifications, such as endplates or winglets, to increase the effective  $AR$ , but should be aware that such modifications increase the skin friction drag (and weight).

### (13) Lift-Induced Drag Constant, $k$

It is the constant whose product with the lift coefficient squared yields the lift-induced drag (see Equations (16-2) and (16-3)). It is given by:

$$k = \frac{1}{\pi \cdot AR \cdot e} = \frac{1}{\pi \cdot AR_e} \quad (16-6)$$

Note that for a clean wing, if  $AR_e \rightarrow \infty$  then  $k \rightarrow 0$  and therefore  $C_D \rightarrow C_d$ , i.e., the drag coefficient becomes that of the airfoil.

### (14) Lift-to-Drag Ratio, $LD_{max}$ , and Optimum Lift Coefficient, $C_{L_{opt}}$

The ratio of lift-to-drag is hugely important in aircraft design. It plays a vital role in performance analysis, where it is a primary indicator of an airplane's efficiency. In this text, the lift-to-drag ratio is denoted by  $LD$  (rather than  $L/D$ ) and is defined as follows:

$$LD \equiv \frac{L}{D} = \frac{C_L}{C_D} \quad (16-7)$$

The  $LD$  is primarily a function angle-of-attack and, thus, airspeed. It has secondary dependency on angle-of-yaw. The maximum value of  $LD$  is of particular interest to the designer (and the pilot). It is denoted by  $LD_{max}$ . The lift coefficient at which  $LD_{max}$  occurs is called the *optimum lift*

coefficient, denoted by  $C_{L_{opt}}$ . If we know  $C_{L_{opt}}$ , we can calculate the airspeed at which it occurs using the expression

$$V_{opt} \cong \sqrt{\frac{2W}{\rho SC_{L_{opt}}}} \quad (16-8)$$

Where  $W$  is weight,  $\rho$  is density, and  $S$  is the reference area. This airspeed is also called the *best glide speed*. The expression shows the optimum speed is a function of wing loading. This turns it into a design variable for aircraft that cruise at (or close to)  $LD_{max}$  (e.g. electric aircraft and commercial jetliners).

### (15) Graphical Determination of $LD_{max}$

In the absence of knowing the exact numbers of a particular drag polar, it is possible to estimate the  $LD_{max}$  and  $C_{L_{opt}}$  graphically. This is shown in Figure 16-2 for a conventional drag polar and one for a NLF aircraft (airfoil) featuring a drag bucket (see Bullet (19)). This is done by fairing a line from the origin such it becomes a tangent to the polar. The reason for why this yields  $LD_{max}$  can be visualized by recognizing that the tangent aligns with the smallest value of  $C_D$  at the greatest value of  $C_L$ .

### (16) Equivalent Flat Plate Area (EFPA)

The *equivalent flat plate area* (denoted by  $f$ ) is a value that is helpful when comparing the relative drag of different aircraft. It is simply the product of the minimum drag coefficient and the reference area, as shown below. Alternatively, it is the minimum drag force at the given airspeed,  $D_{min}$ , divided by the dynamic pressure,  $q_\infty$ :

$$f = SC_{D_{min}} = \frac{D_{min}}{q_\infty} \quad (16-9)$$

The concept assumes the drag of the airplane is equivalent to that of a fictitious plate that has a drag coefficient  $C_D = 1.0$ . Thus, if the flat plate area of an airplane is  $10 \text{ ft}^2$ , it means its drag amounts to that of a flat plate of the same area moving normal to the flight path. The concept is bogus in many respects. It disregards the effect of Reynolds and Mach numbers, the  $C_D$  of a flat plate at  $R_e$  around  $10^5$  is actually closer to 1.17 (e.g., see Figure 16-76), and no notion is given as to the true geometry of this “plate” (i.e., is it rectangular or circular or any other shape?). In spite of these shortcomings, like stated earlier, it is helpful mostly for comparison purposes. Table 16-22 lists the EFPA for a number of different aircraft.

### (17) Profile Drag

For wing-only drag, refers to the difference between the total and lift-induced (and wave) drag, i.e.,  $C_{D_p} = C_D - C_{D_i} - C_{D_w}$ . Sometimes refers to the drag of an

aircraft due to friction only (e.g., see Ref. [4]). For airfoils, see Bullet (10) in Section 8.1.4, *Properties of Typical Airfoils*.

### (18) Zero-Lift Drag

*Zero-lift drag* is the value of the drag coefficient where  $C_L = 0$ . It is equal to  $C_{D_{min}}$  only for the simplified drag model.

### (19) Drag “Bucket”

Refers to a sharp drop in the profile drag of an airfoil. It is a consequence of sustained *natural laminar boundary layer* forming over the airfoil. An example of such a drag bucket is shown in center graph of Figure 8-39.

### (20) Dependency of $CD$ on $\alpha$ and $\beta$

When a body’s orientation (denoted by  $\alpha$  and  $\beta$ ) changes with respect to the oncoming flow, its resultant force,  $R$  (see Figure 8-1), changes as well. Thus, so will lift and drag. See additional discussion in Section 16.2.6.

## 16.2.2 Quadratic Drag Modeling

First, let us establish the difference in how the drag of an airfoil and a wing changes with lift. For an airfoil, this is solely caused by changes in the distribution of pressure and shear stress over the airfoil’s surface (see Figure 16-3). Note that the data to the left terminate just before a large vertical jump occurs. Regardless, it is evident that describing the drag using a quadratic model at large  $C_L$  leaves a lot to be desired.

The same changes happen for a wing, but are compounded by the aft-tilting of the lift-force. This introduces an additional contribution, called *lift-induced* or *vortex drag*. At low angles-of-attack, lift-induced drag is explained by theoretical predictions as a function of  $C_L^2$ . This theory agrees well with experiment at low angles-of-attack. However, as for the airfoil, extreme values of  $C_L$  cause a flow separation too significant for the  $C_L^2$  contribution to capture. This is not a surprise; the contribution of  $C_L^2$  originates in Prandtl’s inviscid *lifting line theory* (see Section 9.7, *Prandtl’s Lifting-Line Theory*)—whereas the flow separation is a viscous phenomenon.

This highlights the limitations of the quadratic modeling. Neglecting to correct for the sharp rise in drag at high  $C_L$  leads to very poor low-speed and high-g performance predictions.

### (1) Simplified Drag Model

As discussed in Section 16.2.1, the simplified drag model is given by Equation (16-2), repeated below for convenience. The variables are defined there.

$$C_D = C_{D_{min}} + kC_L^2 \quad (16-2)$$

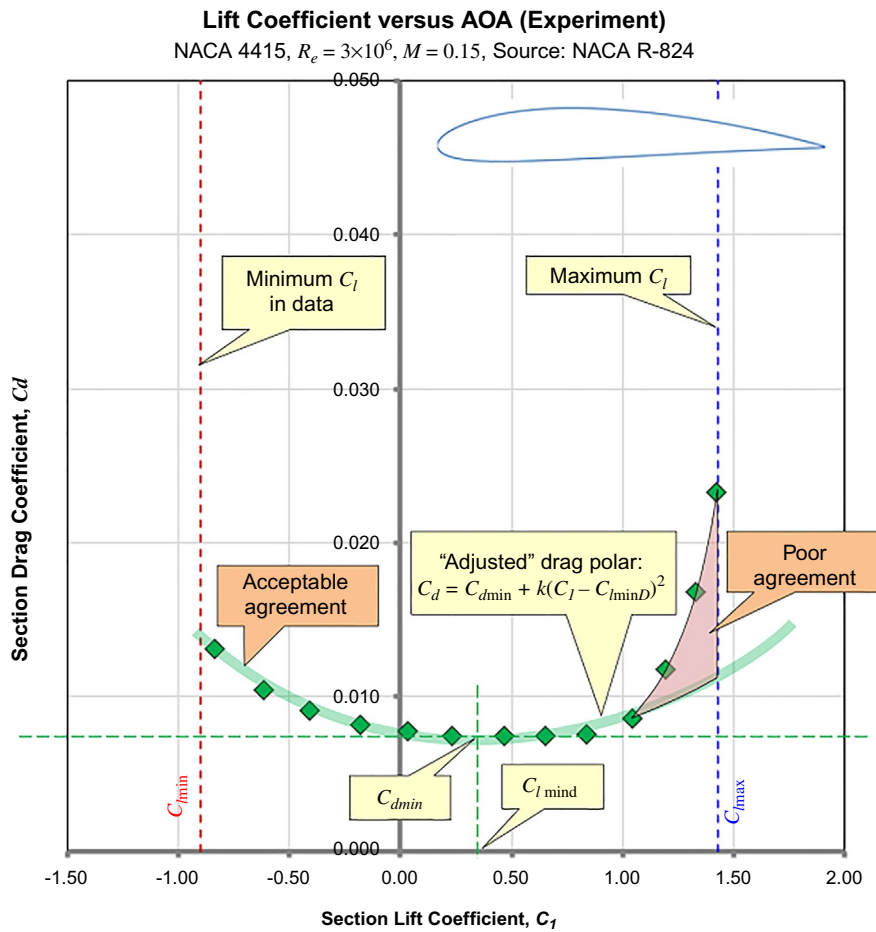


**FIGURE 16-3** Quadratic assumption is in poor agreement with experiment for airfoils.

Where the lift-induced drag constant,  $k$ , is given by Equation (16-6). The optimum lift coefficient and maximum lift-to-drag ratio obtained using this model is

$$C_{L_{opt}} = \sqrt{\frac{C_{D_{min}}}{k}} \text{ and } LD_{max} = \frac{1}{\sqrt{4kC_{D_{min}}}} \quad (16-10)$$

### DERIVATION OF EQUATION (16-10)

First, determine the  $C_L$  of the optimum lift-to-drag ratio,  $C_{L_{opt}}$ :

$$\begin{aligned} \frac{C_L}{C_D} &= \frac{C_L}{C_{D_{min}} + kC_L^2} \xrightarrow{\text{Quotient Rule}} \\ \frac{d}{dC_L} \left( \frac{C_L}{C_D} \right) &= \frac{(C_{D_{min}} + kC_L^2)(1) - (2kC_L)(C_L)}{(C_{D_{min}} + kC_L^2)^2} = 0 \end{aligned}$$

$$\begin{aligned} &\Leftrightarrow (C_{D_{min}} + kC_L^2) - (2kC_L^2) = 0 \\ &\Rightarrow C_{L_{opt}} = \sqrt{\frac{C_{D_{min}}}{k}} \end{aligned}$$

Substituting this into the expression for the lift-to-drag ratio and manipulating algebraically yields:

$$LD_{max} = 1 / \sqrt{4kC_{D_{min}}}$$

### (2) Adjusted Drag Model

As stated in Section 16.2.1, the adjusted drag model corrects the simplified model. The correction is very effective, despite its simplicity. It is far more realistic than the simplified one (see Figure 16-4). However, both models must be corrected for high lift coefficients.

$$C_D = C_{D_{min}} + k(C_L - C_{L_{minD}})^2 \quad (16-11)$$

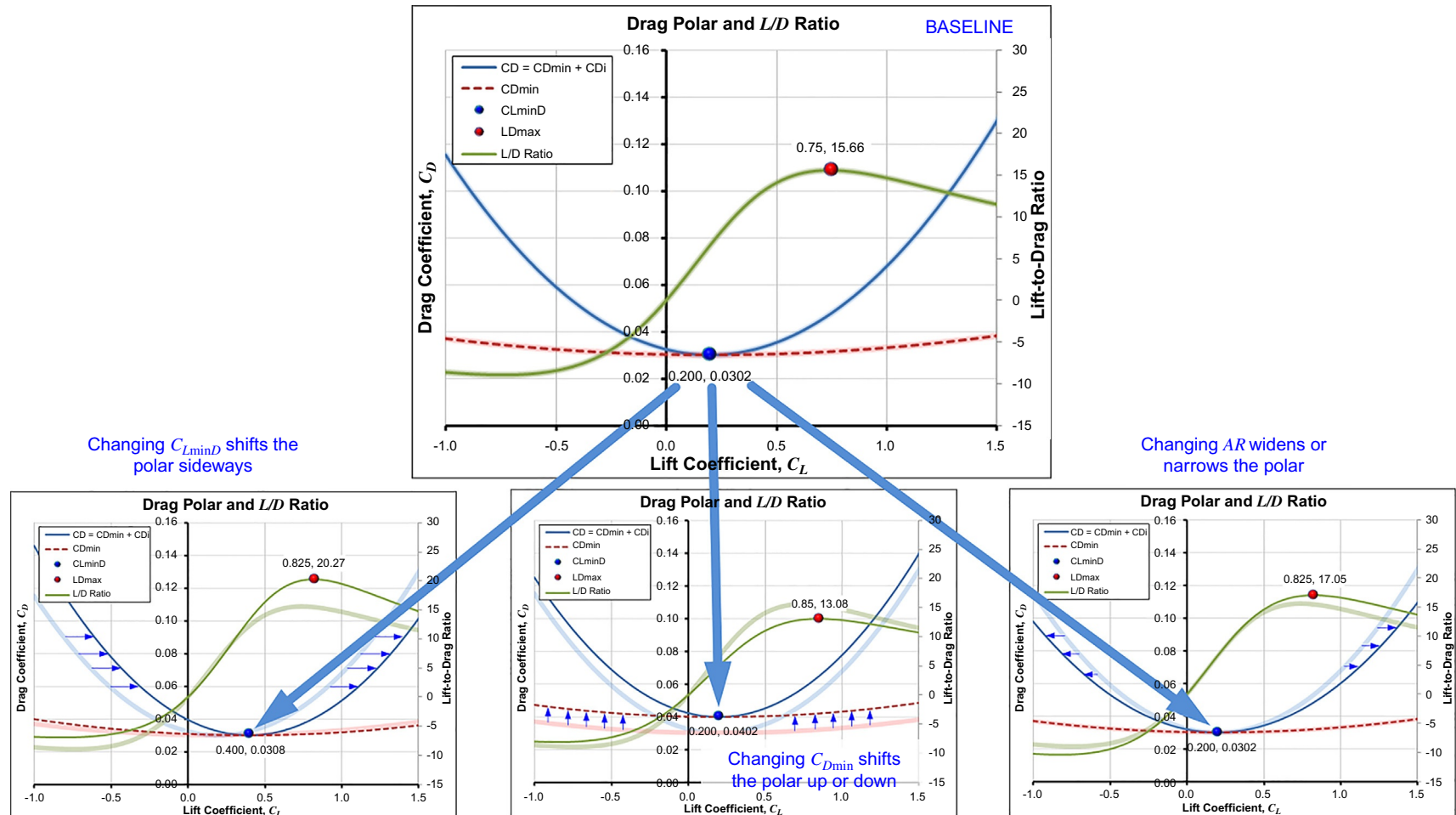


FIGURE 16-4 A schematic showing the effect of changing  $C_{LminD}$ ,  $C_{Dmin}$ , and  $AR$  on the drag polar.

Where  $C_{L_{\min D}}$  is the lift coefficient where drag becomes a minimum. The maximum lift-to-drag ratio obtained using this model is (here using form that resembles that of Equation (16-10))

$$C_{L_{\text{opt}}} = \sqrt{\frac{C_{D_{\min}}}{k} + C_{L_{\min D}}^2} \quad \text{and} \quad LD_{\max} = \frac{1}{\sqrt{4kC_{D_{\min}} + (2kC_{L_{\min D}})^2 - 2kC_{L_{\min D}}}} \quad (16-12)$$

## DERIVATION OF EQUATION (16-12)

First, determine the  $C_L$  of the optimum lift-to-drag ratio,  $C_{L_{\text{opt}}}$ . To do this, we follow a parallel approach as that used for the derivation of Equation (16-10). The quotient rule of differentiation yields the following expression for the numerator:

$$(C_{D_{\min}} + k(C_L - C_{L_{\min D}})^2)(1) - 2k(C_L - C_{L_{\min D}})(C_L) = 0$$

To obtain  $C_{L_{\text{opt}}}$ , we solve this expression for  $C_L$ . This gives  $C_{L_{\text{opt}}} = \sqrt{C_{D_{\min}}/k + C_{L_{\min D}}^2}$ . Substituting this into the expression for the lift-to-drag ratio and manipulating algebraically yields Equation (16-12).

### (3) Impact of Geometry on the Drag Polar

The designer can shape the drag polar using the aircraft's geometry. Three effective means are through  $C_{L_{\min D}}$ ,  $C_{D_{\min}}$ , and AR. This makes these parameters *design variables* as illustrated in Figure 16-4. The curvature of  $C_{D_{\min}}$  (red) represents the contribution of  $m(C_L - C_{L_{\min D}})^2$  in Equation (16-14).

#### AR as a Design Variable

Increasing aspect ratio reduces lift-induced drag, but in a similar fashion as  $C_{L_{\min D}}$ : Increased  $LD_{\max}$  and  $C_{L_{\text{opt}}}$ .

#### $C_{L_{\min D}}$ as a Design Variable

The general effect of  $C_{L_{\min D}}$  is to shift the polar sideways using curvature. For instance, increasing airfoil camber increases  $C_{L_{\min D}}$ . If  $C_{L_{\min D}} < 0$  then the curve is shifted left and right if  $C_{L_{\min D}} > 0$ . As evident in Figure 16-4, shifting  $C_{L_{\min D}}$  right increases  $LD_{\max}$ , but pushes it to a higher  $C_{L_{\text{opt}}}$ . This means the airplane will achieve its maximum range at a *lower* airspeed. Generally, our goal is to increase  $LD_{\max}$  and push it to a *higher* airspeed (low  $C_{L_{\text{opt}}}$ ). Note that high Mach numbers increase  $C_{L_{\min D}}$  slightly, albeit much less than  $C_{D_{\min}}$  (e.g., see Ref. [5]).

#### $C_{D_{\min}}$ as a Design Variable

It is easy to relate to  $C_{D_{\min}}$ . Changing  $C_{D_{\min}}$  shifts the drag polar up or down (see Figure 16-4). Decrease it to increase  $LD_{\max}$  and reduce  $C_{L_{\text{opt}}}$ . Thus, reducing  $C_{D_{\min}}$  is

an effective means to improve  $LD_{\max}$  and  $C_{L_{\text{opt}}}$ . This reduction implies aerodynamic clean-up.

### (4) Transformation of $C_D = A \cdot C_L^2 + B \cdot C_L + C$ to

$$C_D = C_{D_{\min}} + k(C_L - C_{L_{\min D}})^2$$

A drag polar in the form  $C_D = A \cdot C_L^2 + B \cdot C_L + C$  can be transformed to the more familiar form as follows:

$$\left. \begin{aligned} k &= A \\ C_{L_{\min D}} &= -B/(2A) \\ C_{D_{\min}} &= AC_{L_{\min D}}^2 + BC_{L_{\min D}} + D \end{aligned} \right\} \Rightarrow C_D = C_{D_{\min}} + k(C_L - C_{L_{\min D}})^2 \quad (16-13)$$

The derivation of these expressions is provided in Section 16.5.5, *Determining Drag Characteristics From Wind Tunnel Data*.

### (5) Application of the Adjusted Drag Model to Airfoils and Wings

The total drag coefficient of a "clean" wing can be approximated using the drag polars of its constituent airfoils. Figure 16-5 shows a symmetric, single-airfoil wing. Assume we know the distribution of section lift coefficients at some specific flight condition. The airfoil drag polar inserted in the figure shows how this leads to a spanwise distribution of drag along the wing (see the three span stations presented).

To estimate the  $C_D$  for the wing, the variation in spanwise drag must be properly accounted for. Using the adjusted drag model, the airfoil's drag coefficient ( $C_d$ ) can be expressed in terms of the spanwise section lift coefficients ( $C_l$ ) as follows

$$C_d = C_{d_{\min}} + m(C_l - C_{l_{\min D}})^2 \quad (16-14)$$

Where  $m$  is a constant that accounts for the increase in the airfoil's profile drag. Assume the distribution of section lift coefficients is given by the function  $f$  of spanwise position,  $y$ :

$$C_l = f(y) \quad (16-15)$$

Thus, we can determine the wing's *effective profile drag coefficient* at condition as

$$\begin{aligned} C_{D_p} &= \frac{2}{b} \int_0^{b/2} [C_{d_{\min}} + m(f(y) - C_{l_{\min D}})^2] dy \\ &= C_{d_{\min}} + \frac{2m}{b} \int_0^{b/2} (f(y) - C_{l_{\min D}})^2 dy \end{aligned} \quad (16-16)$$

Therefore, we can express the total drag of the wing by including its lift-induced drag as shown below:

$$C_D = \overbrace{C_{d_{\min}} + \frac{2m}{b} \int_0^{b/2} (f(y) - C_{l_{\min D}})^2 dy}^{=C_{D_p}} + \overbrace{k(C_L - C_{L_{\min D}})^2}^{\text{wing lift induced drag}} + \overbrace{k(C_L - C_{L_{\min D}})^2}^{\text{change in airfoil } C_d \text{ due to spanwise } C_l} \quad (16-17)$$

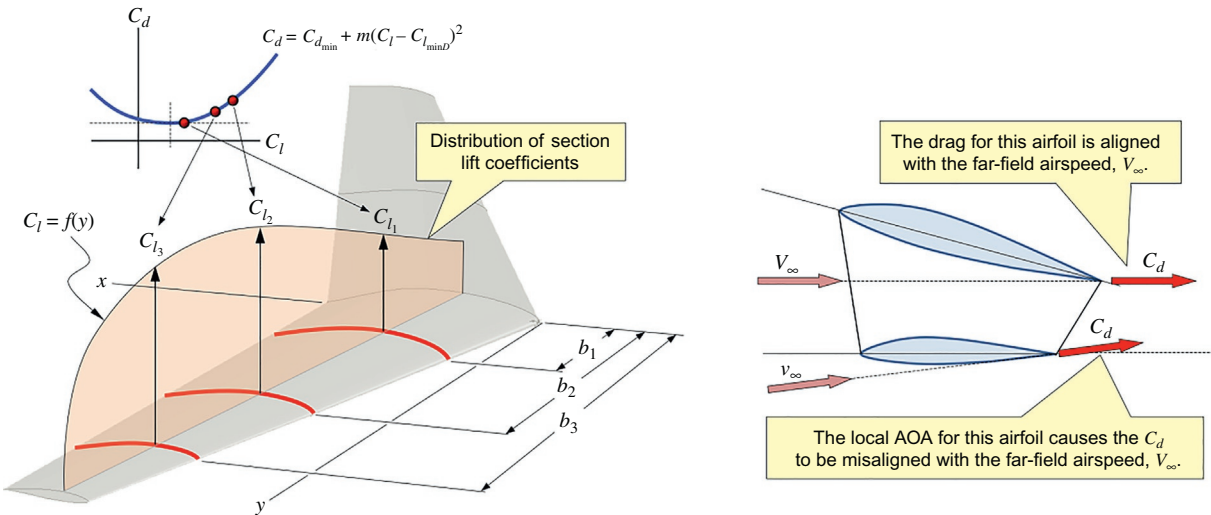


**FIGURE 16-5** The distribution of section lift coefficients dictates the wing's total drag.

The expression reveals that changes in  $C_D$  with  $C_L$  are far more complex than standard models show. Such models “average” the drag. Equation (16-17) shows what it takes to estimate it more accurately. Note that at high  $\alpha$ , the flow-field may introduce local misalignments in the lift and drag vectors that are significant enough to violate the small angle approximation (see Figure 16-5). The aerodynamicist can estimate this by comparing the local AOA to the chord-line orientation of the airfoil on the wing and correct if needed.

## (6) Limitations of the Quadratic Drag Model

(A) Predictions at very low (negative) and high (positive) angles-of-attack are poor (see Figure 16-6). See Section 16.2.3, *Correcting the Drag Coefficient at High AOA* for a remedy. (B) Predictions for aircraft with unmasked drag buckets is poor (see Figure 16-6). It is not guaranteed that the drag bucket in the drag polar of aircraft with NLF-lifting surfaces will be “visible.” For many such aircraft, the drag associated with the

### EXAMPLE 16-1

Estimate the lift coefficient and effective profile drag coefficient for a Hershey bar wing, whose  $S=130\text{ ft}^2$ ,  $b=32.5\text{ ft}$ ,  $c=4\text{ ft}$ , and for which the distribution of section lift coefficients at some angle-of-attack is given by  $C_l=0.5 \cdot \cos(\pi y/b)$ . The airfoil's profile drag is given by  $C_d=0.007166+0.003646(C_l-0.3922)^2$ .

#### SOLUTION:

Determine the lift coefficient per Equation (9-58). Note this lift distribution is only for demonstration.

$$C_L = \frac{2}{S} \int_0^{b/2} C_l(y) c(y) dy = \frac{4}{130} \int_0^{32.5/2} \cos\left(\frac{\pi y}{32.5}\right) dy \\ = \frac{4}{130} \frac{32.5}{\pi} = 0.3183$$

Determine the effective profile drag coefficient per Equation (16-16):

$$C_{D_p} = C_{d_{min}} + \frac{2m}{b} \int_0^{b/2} (f(y) - C_{l_{minD}})^2 dy \\ = C_{d_{min}} + \frac{2m}{b} \int_0^{b/2} \left(0.5 \cos\left(\frac{\pi y}{b}\right) - C_{l_{minD}}\right)^2 dy \\ = C_{d_{min}} + \frac{2m}{b} \int_0^{b/2} \left(0.25 \cos^2\left(\frac{\pi y}{b}\right) - \cos\left(\frac{\pi y}{b}\right) C_{l_{minD}} + C_{l_{minD}}^2\right) dy \\ = C_{d_{min}} + \frac{2m}{b} \left[ \frac{2\pi y + b \sin(2\pi y/b)}{16\pi} - \frac{b C_{l_{minD}}}{\pi} \sin\left(\frac{\pi}{b}y\right) + C_{l_{minD}}^2 y \right]_0^{b/2} \\ = C_{d_{min}} + 2m \left[ \frac{1}{16} - \frac{C_{l_{minD}}}{\pi} + \frac{C_{l_{minD}}^2}{2} \right] \\ = 0.007166 + 2(0.003646) \left[ \frac{1}{16} - \frac{0.3922}{\pi} + \frac{0.3922^2}{2} \right] = 0.007272$$

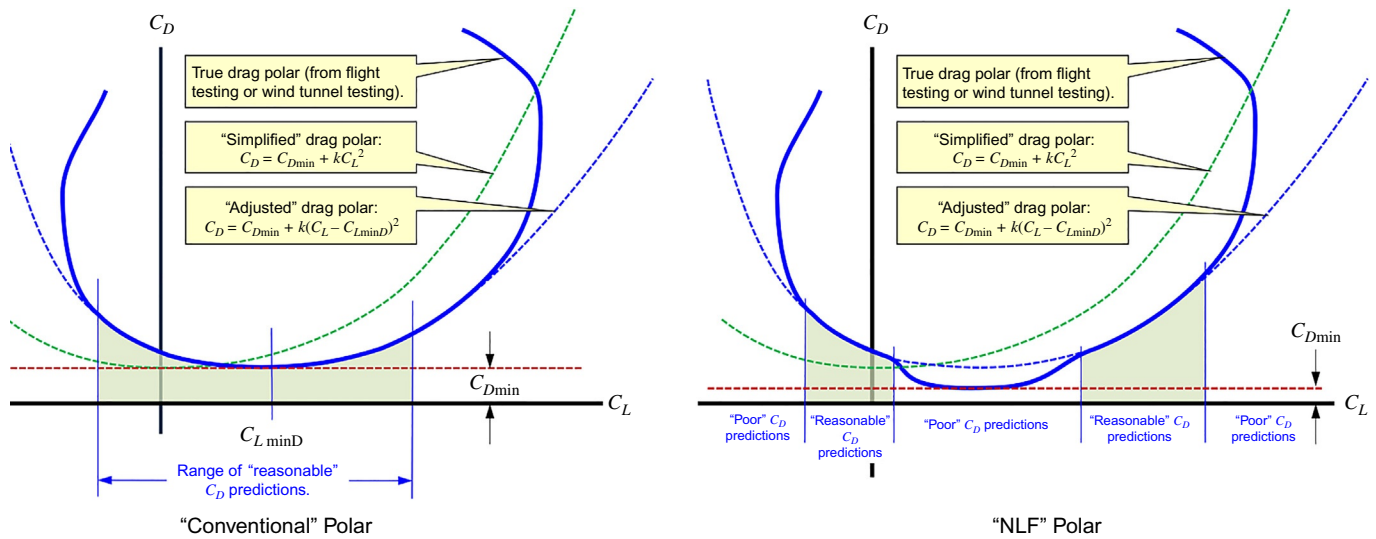


**FIGURE 16-6** Approximating the *true* drag polar illustrates primary sources of error for both the simplified and adjusted drag models. The simplified one is like a stopped clock—it is correct in two places.

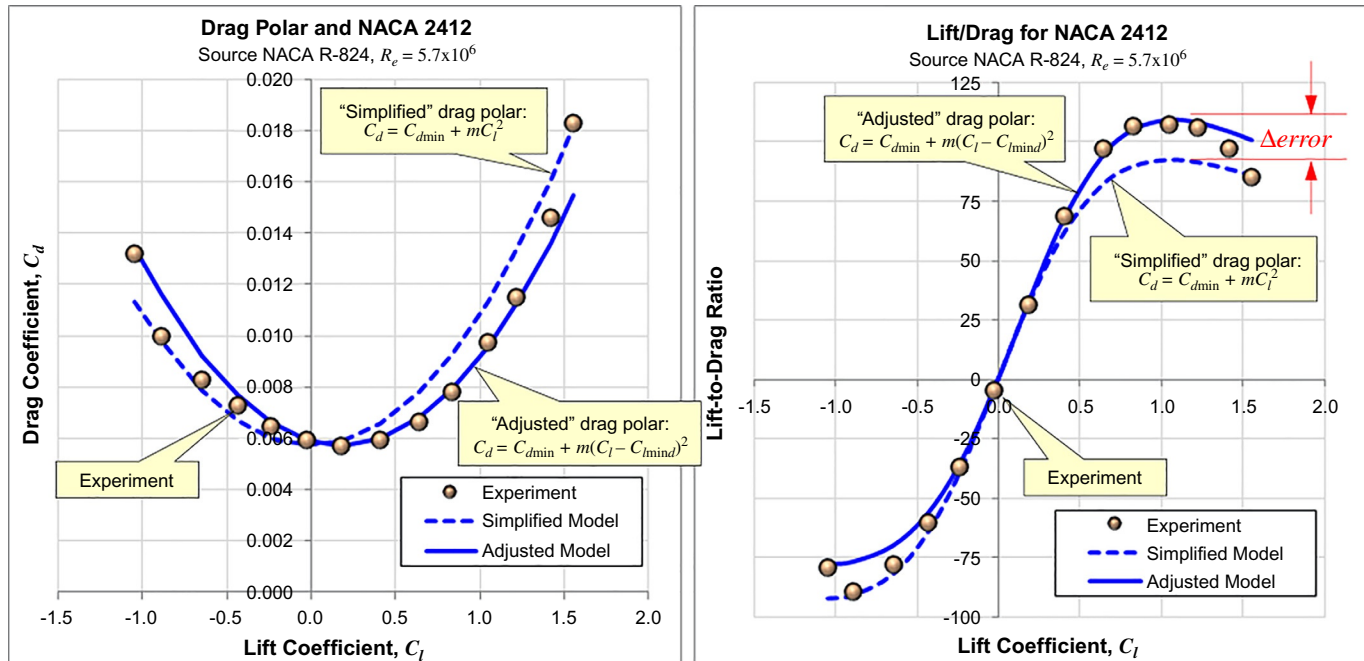


**FIGURE 16-7** A comparison of the simplified and adjusted drag models to experimental data.

fuselage, powerplant, fixed landing gear, and so on, is large enough mask it. Quadratic drag models can treat those aircraft, because the resulting drag polar looks more like a “conventional” one. Otherwise, it is unwise to select this model for aircraft-like sailplanes.

#### (7) Comparing the Accuracy of the Simplified and Adjusted Drag Models

Differences between the simplified and adjusted drag models are best illustrated by a direct comparison to

wind tunnel data (see Figure 16-7). It compares wind tunnel data for the NACA 2412 airfoil from Ref. [6]. This airfoil is used on a number of Cessna aircraft, for instance, the Model 150, 152, 172, and 182, to name a few. To do this, the drag polar was digitized and the smallest experimental value of the  $C_d$  selected as  $C_{d\min}$  for each drag model. The value of  $C_{l\min D}$  for the adjusted model was determined by trial-and-error before being used in the term  $m(C_l - C_{l\min D})^2$ . The term  $m$  was varied to get the best fit of each model (both models use the same  $k$ ). A value of

$k \approx 62$  was found to best fit the experiment. Larger values (e.g., 200 or 400) only flatten the polar. The graphs show the adjusted drag model provides a substantially better fit to experiment. Another lesson to be learned is the dire consequences of estimating range for an aircraft using the simplified model. Since range depends explicitly on  $C_L/C_D$  (see Section 21.3, Range Analysis), any prediction based on the simplified drag model yields a range well below that indicated by the experiment. The opposite conclusion can also happen. The important lesson is that the adjusted model better matches experiment; the simplified does not and should be avoided.

### 16.2.3 Correcting the Drag Coefficient at High AOA

The problem of inaccurate drag modeling at high (and low) lift coefficients has already been discussed. This section develops a method to approximate the drag coefficient at higher lift coefficients.

Consider the hypothetical wind tunnel test data in Figure 16-8. The quadratic polar (blue curve) only approximates the data satisfactorily at lower lift coefficients.

cients for a handful of data points. This model is given by Equation (16-11), reproduced below for convenience:

$$C_D = C_{D_{\min}} + k(C_L - C_{L_{\min D}})^2 \quad (16-11)$$

The test data in Figure 16-8 deviate sharply from the curve starting at  $C_L = 1.15$  (and  $C_L = -0.45$ ). Here, we are primarily interested in the positive lift coefficient, which is needed for low-speed performance predictions. To work around this predicament, the author has used the following methodology in the past with satisfactory results. In this method, once the  $C_L$  exceeds a certain value, from hereon called  $C_{Lm}$ , a quadratic spline is used to replace the values of the adjusted drag model. Other splines are possible; however, the advantage of the quadratic spline is simplicity and acceptable accuracy. The method blends the spline smoothly with the underlying adjusted drag model. First, define a *modified* drag coefficient ( $C_{D\text{mod}}$ ) to be used when  $C_L > C_{Lm}$ . It can be represented with:

$$C_{D\text{mod}} = AC_L^2 + BC_L + C \quad \text{if } C_L > C_{Lm} \quad (16-18)$$

To determine the constants  $A$ ,  $B$ , and  $C$  requires two conditions to be satisfied at  $C_{Lm}$ :

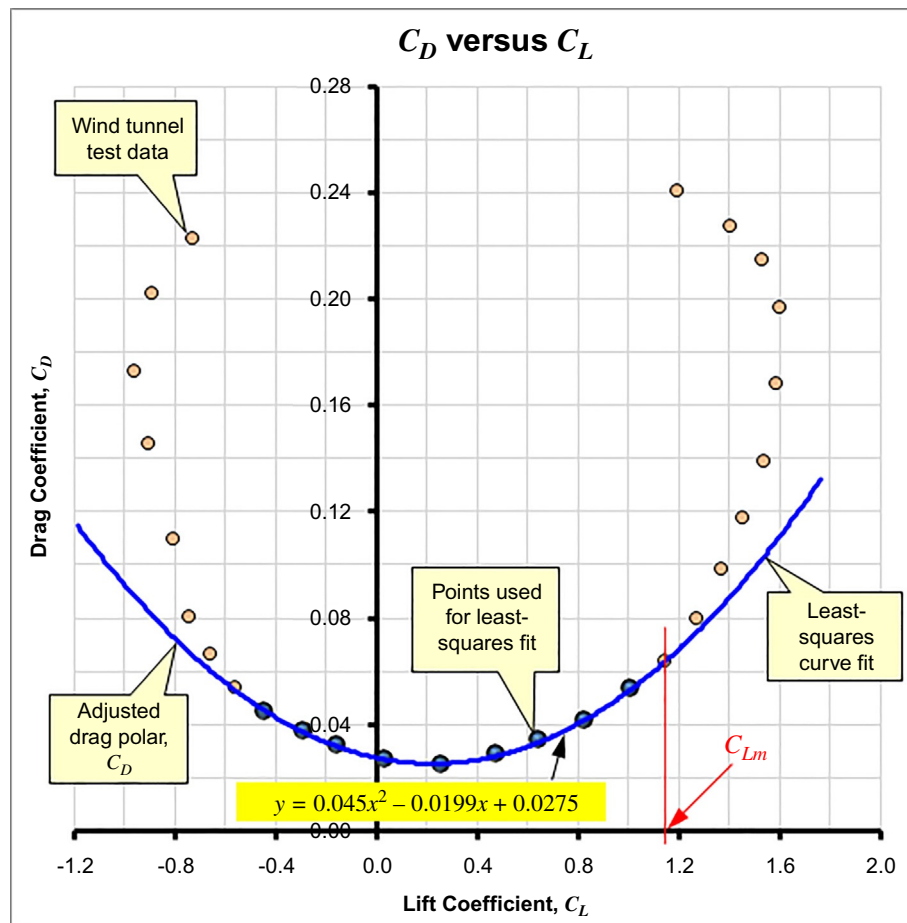


FIGURE 16-8 A hypothetical drag polar for an aircraft, showing the inaccuracy of the quadratic drag model at higher (or lower) lift coefficient.

Condition (1)—Equal drag at  $C_{Lm}$ :

$$C_{D\text{mod}}(C_{Lm}) = C_D(C_{Lm})$$

Condition (2)—Equal slope at  $C_{Lm}$ :

$$\frac{\partial C_{D\text{mod}}}{\partial C_L} \Big|_{at\ C_{Lm}} = \frac{\partial C_D}{\partial C_L} \Big|_{at\ C_{Lm}}$$

A third condition is needed to finalize the determination of  $A$ ,  $B$ , and  $C$ : The value of  $C_{D\text{mod}}$  at  $C_{L\text{max}}$  must match that of the wind tunnel data.

Since the function for  $C_{D\text{mod}}$  has three constants ( $A$ ,  $B$ , and  $C$ ), we need three equations to determine them. One of those requires the derivatives of  $C_D$  and  $C_{D\text{mod}}$  to be determined. These are presented below. Slope of  $C_D$ :

$$\frac{\partial C_D}{\partial C_L} = \frac{\partial}{\partial C_L} [C_{D\text{min}} + k(C_L - C_{L\text{min},D})^2] \\ = 2k(C_L - C_{L\text{min},D})$$

$$\text{Slope of } C_{D\text{mod}}: \frac{\partial C_{D\text{mod}}}{\partial C_L} = \frac{\partial}{\partial C_L} [AC_L^2 + BC_L + C] = 2AC_L + B$$

We now have three equations with three unknowns ( $A$ ,  $B$ , and  $C$ ):

$$\text{Equation (1): } AC_{Lm}^2 + BC_{Lm} + C = C_{D\text{min}} + k(C_{Lm} - C_{L\text{min},D})^2$$

$$\text{Equation (2): } 2AC_{Lm} + B = 2k(C_{Lm} - C_{L\text{min},D})$$

$$\text{Equation (3): } AC_{L\text{max}}^2 + BC_{L\text{max}} + C = C_{D\text{stall}}$$

Rearranging this in a matrix form yields the following expression that allows  $A$ ,  $B$ , and  $C$  to be determined using matrix methods like Cramer's rule or matrix inversion:

$$\begin{bmatrix} C_{Lm}^2 & C_{Lm} & 1 \\ 2C_{Lm} & 1 & 0 \\ C_{L\text{max}}^2 & C_{L\text{max}} & 1 \end{bmatrix} \begin{Bmatrix} A \\ B \\ C \end{Bmatrix} = \begin{Bmatrix} C_{D\text{min}} + k(C_{Lm} - C_{L\text{min},D})^2 \\ 2k(C_{Lm} - C_{L\text{min},D}) \\ C_{D\text{stall}} \end{Bmatrix} \quad (16-19)$$

Then, once  $A$ ,  $B$ , and  $C$  have been determined, the drag model is further refined as follows:

$$C_D = \begin{cases} C_{D\text{min}} + k(C_L - C_{L\text{min},D})^2 & \text{if } C_L \leq C_{Lm} \\ AC_L^2 + BC_L + C & \text{if } C_L > C_{Lm} \end{cases} \quad (16-20)$$

This model is implemented in Figure 16-9. Note that while the wind tunnel data are used here to pick  $C_{Lm}$ , it is reasonable to select  $C_{Lm}$  as the value  $\frac{1}{2}(C_{L\text{min},D} + C_{L\text{max}})$  as a first guess.

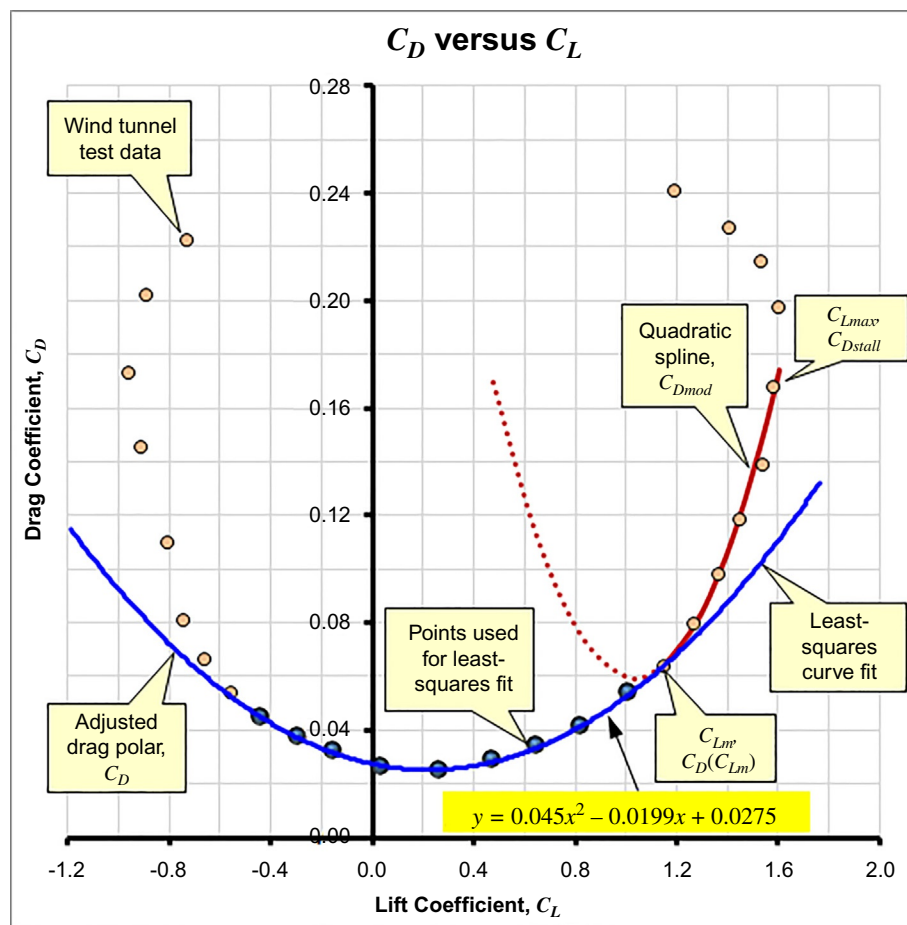


**FIGURE 16-9** Prediction is improved at higher lift coefficients by the quadratic spline,  $C_{D\text{mod}}$ .

## EXAMPLE 16-2

The hypothetical wind tunnel data in Figure 16-10 represent an airplane whose  $AR=9$ . The least-squares quadratic curvefit for the data points is given by  $C_D=0.045C_L^2 - 0.0199C_L + 0.0275$ . Determine the quadratic spline, assuming a  $C_{Lm}=1.15$ , and write the complete drag coefficient.

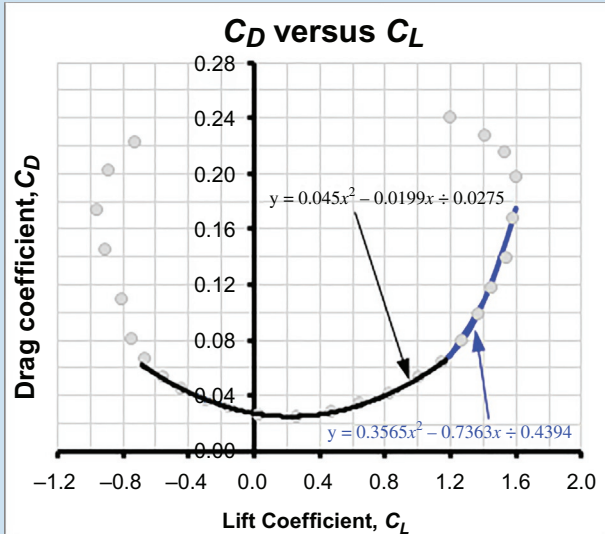


**FIGURE 16-10** The modified drag model better fits experiment than the regular quadratic model.

## SOLUTION:

Using the previously mentioned drag polar, extract  $C_{Dmin}$ ,  $C_{LminD}$ , and the Oswald span efficiency ( $e$ ) using the conversion method of Section 16.5.5. In particular, see Equations (16-194)–(16-196). The section presents an example as well, so only the results based on the previously mentioned polynomial will be presented.

$$C_{Dmin} = 0.02530, C_{LminD} = 0.2211, e = 0.78595$$

Using  $e$ , we find the  $k=1/(\pi \cdot AR \cdot e)=0.045$ . Using this data, the matrix of Equation (16-19) becomes:

$$\begin{bmatrix} 1.3225 & 1.15 & 1 \\ 2.3 & 1 & 0 \\ 2.5113 & 1.5847 & 1 \end{bmatrix} \begin{Bmatrix} A \\ B \\ C \end{Bmatrix} = \begin{Bmatrix} 0.06413 \\ 0.08360 \\ 0.16783 \end{Bmatrix}$$

From which we find that  $A=0.3565$ ,  $B=-0.7363$ , and  $C=0.4394$ . The resulting  $C_D$  can thus be represented by:

$$C_D = \begin{cases} 0.0253 + 0.045 \cdot (C_L - 0.2211)^2 & \text{if } C_L \leq 1.15 \\ 0.3565 \cdot C_L^2 - 0.7363 \cdot C_L + 0.4394 & \text{if } C_L > 1.15 \end{cases}$$

Note the resulting graph is shown in Figure 16-10.

#### 16.2.4 Drag Modeling using Higher Order Polynomials

It is also possible to better approximate the drag polar using higher order polynomials or parametric splines. However, there are limits. Figure 16-11 shows a fourth-order polynomial in good agreement at higher lift coefficients, although it does not approach the minimum drag value as closely as the quadratic one. It is somewhat unwieldy compared to the quadratic form, although this is not an issue in spreadsheets or coding.

Generally, the presence of the drag bucket prevents the use of polynomials, as these do not follow the sharp change in curvature of the drag polar. Even polynomials of order as high as 16+ will not suffice, as they tend to oscillate inside the prediction region. Methods that can be used to represent such drag polars include a spline (e.g., B-spline) or a lookup table. These are outside the scope of this edition of the book.

#### 16.2.5 Drag of a 2D Body in a Wind-Tunnel

Drag force of a 2D body (e.g., an airfoil) is estimated in wind tunnel testing by two means: (1) Using a force

balance and (2) based on velocity profile in front and aft of model using the momentum theorem (see Section 14.2.1, *Conservation Laws*). The former is outside the scope of this book. The latter warrants a short introduction.

The momentum equation of Equation (14-26) can be simplified to allow the extraction of drag of a body in a wind tunnel, by assuming steady flow, absence of body forces, and uniformity of pressure in front and aft. Thus, only the momentum flux term remains. For instance, as shown in references such as Refs. [7–9], this leads to the following expression for drag force *per unit length*:

$$D' = \int_{-h/2}^{h/2} \rho u_e (u_i - u_e) dy \quad (16-21)$$

Where  $h$  is the height of the test section,  $u_i$  and  $u_e$  are the velocity profiles at the inlet and exit of the test section, respectively. It is assumed the body is placed near the vertical center of the test section (where  $y=0$ ). See Example 16-3 for details of its use.

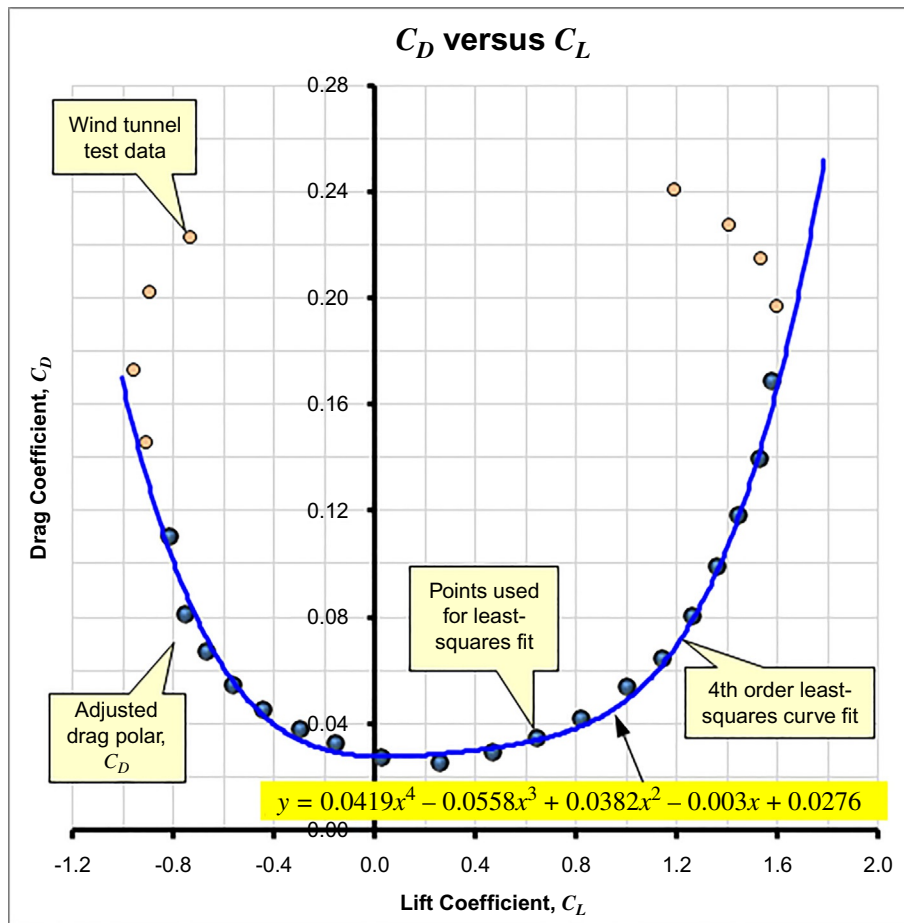


FIGURE 16-11 A quartic polynomial drag polar.

### EXAMPLE 16-3

The wind tunnel setup shown in Figure 16-12 is used to measure drag of an airfoil. The distribution of velocity is measured at the inlet and exit of the test section. The air-speed profile at the inlet is uniform, but at the exit is

$u_e(y) = \frac{1}{2}u_i(1 + 4y \operatorname{sgn}(y)/h)$  between  $-h/4 \leq y \leq h/4$  and  $\operatorname{sgn}(y)$  is the sign function. Elsewhere,  $u_e = u_i$ . Assume equal and uniform static pressures at entry and exit. Determine the *drag force per unit length* ( $D'$ ) acting on the airfoil.

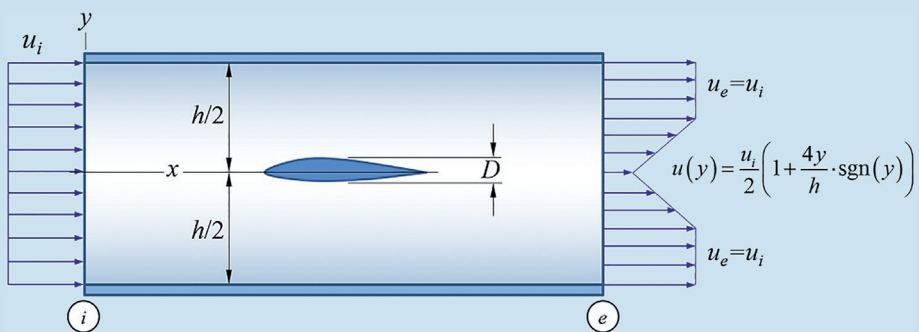


FIGURE 16-12 A 2D body in a wind tunnel.

## EXAMPLE 16-3 (cont'd)

**SOLUTION:**

Let us break the integral of Equation (16-21) into four smaller integrals

$$\begin{aligned} D' &= \int_{-h/2}^{h/2} \rho u_e (u_i - u_e) dy \\ &= \underbrace{\int_{-h/2}^{-h/4} \rho u_i (u_i - u_i) dy}_{=0} + \int_{-h/4}^0 \rho u_e (u_i - u_e) dy \\ &\quad + \int_0^{h/4} \rho u_e (u_i - u_e) dy + \underbrace{\int_{h/4}^{h/2} \rho u_i (u_i - u_i) dy}_{=0} \end{aligned}$$

As shown, the upper and lower fourths of the region return zero (because  $u_e = u_i$ ). Due to the symmetry of this problem, the center two integrals are equal. Therefore, we

can drop the sign function and integrate from 0 to  $h/4$  and multiply the result by two, which reduces this to

$$D' = 2\rho \int_0^{h/4} \left( \frac{u_i}{2} \left( 1 + \frac{4y}{h} \right) \right) \left( u_i - \frac{u_i}{2} \left( 1 + \frac{4y}{h} \right) \right) dy$$

Substitute the given velocity profiles into Equation (16-21) and evaluate the integrals to give

$$\begin{aligned} D' &= \rho u_i^2 \int_0^{h/4} \left( 1 + \frac{4y}{h} \right) \left( 2 - \left( 1 + \frac{4y}{h} \right) \right) dy \\ &= \rho u_i^2 \left[ y - \frac{16y^3}{3h^2} \right]_0^{h/4} = \frac{\rho u_i^2 h}{6} \end{aligned}$$

Note that this velocity profile does not satisfy mass conservation. This is done to simplify this example. Assuming the given profile, mass conservation would require  $u_e > u_i$ .

## 16.2.6 Additional Topics on Drag

This section discusses additional topics of interest.

### (1) Effect of Aspect Ratio on Drag

In 1923, Prandtl [10] presented the results of an experiment that revealed the effect aspect ratio has on lift and drag of a wing. A copy of his results is shown in Figure 16-13. The left graph shows the impact of AR on drag, while the right graph shows its effect on lift.

### (2) Effect of Yaw Angle $\beta$ on Drag

As discussed in Section 16.3.2, *Estimating Lift-Induced Drag*, drag varies greatly with AOA. It also varies with yaw as shown in Figure 16-14. The yaw always increases drag. This fact is frequently used by pilots when landing. Pilots “coming in too high” yaw the airplane to decrease its  $L/D$  ratio, increasing its rate of descent. How much, depends on geometry. For analysis, the flow may be assumed unseparated for  $\beta$  up to  $\pm 10$  degrees. Beyond that, flow separation is certain, as is the associated drag increase.

### (3) Effect of Control Surface Deflection on Drag

Deflecting control surfaces beyond neutral deflection increases the drag of the aircraft. Deflecting the elevator shifts the drag polar vertically, increasing the  $C_{D_{min}}$ . This increases *trim drag* and calls for tail sizing that results in neutral elevator deflection in cruise (called an elevator “in trail”).

Trim drag is most accurately estimated using wind tunnel tests. A graph similar to the one in Figure 16-15 is usually obtained, with several curves showing the drag polar for various elevator deflection angles. This allows the performance engineer to better estimate the capability of the airplane at different loading and flight conditions. In the absence of wind tunnel testing, this drag can be estimated by various means that include various airfoil codes.

A method to estimate trim drag based on CG location and thrust setting is presented in Section 16.4.1, *Trim Drag*.

### (4) Effect of Flap Deflection on Drag

Deflecting flaps significantly shifts the drag polar to the right and up as shown in Figure 16-16. It increases the  $C_{D_{min}}$  and  $C_{L_{minD'}}$  in addition to  $C_{L_{max}}$ . It affects the drag at stall,  $C_{D_{stall}}$ , less significantly.

### (5) Effect of Waviness on Drag of NLF Surfaces

The British aerodynamicist Melville Jones (1887–1975) rose to fame in 1929 for introducing aircraft manufacturers to the importance of streamlining [11]. In 1938, he pointed out the importance of smooth, waveless surfaces for sustaining extensive laminar boundary layer [12].

Surface waviness expedites (trips) laminar-to-turbulent transition. By quantifying the waviness of a surface, it is possible to implement quality control of NLF surfaces. In this capacity, Carmichael [13] summarizes research on NLF surfaces, listing experimental evidence and lessons learned. He presents methods, based on the work presented in Refs. [14–16], that can help the

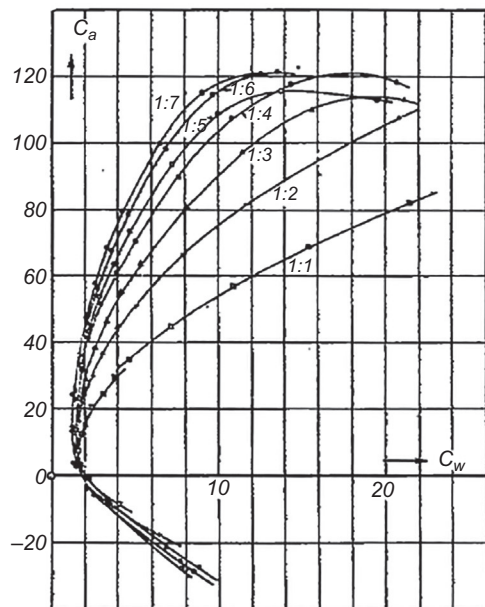


FIG. 16.—Polar diagrams for seven wings, aspect ratios 1:7, 1:6, etc., 1:1.

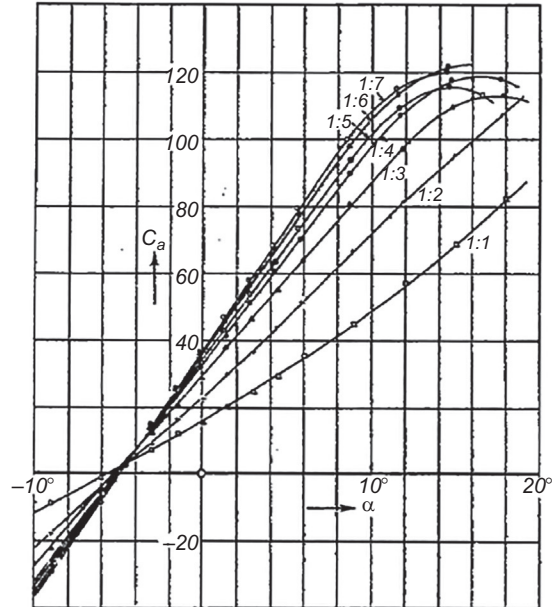


FIG. 47.—Lift coefficients plotted as function of angle of attack for aspect ratios 1:7 to 1:1.

**FIGURE 16-13** Ludwig Prandtl's original research reveals how lift and drag of a wing changes with AR. From L. Prandtl, *Applications of Modern Hydrodynamics to Aeronautics*, NACA R-116, 1923.

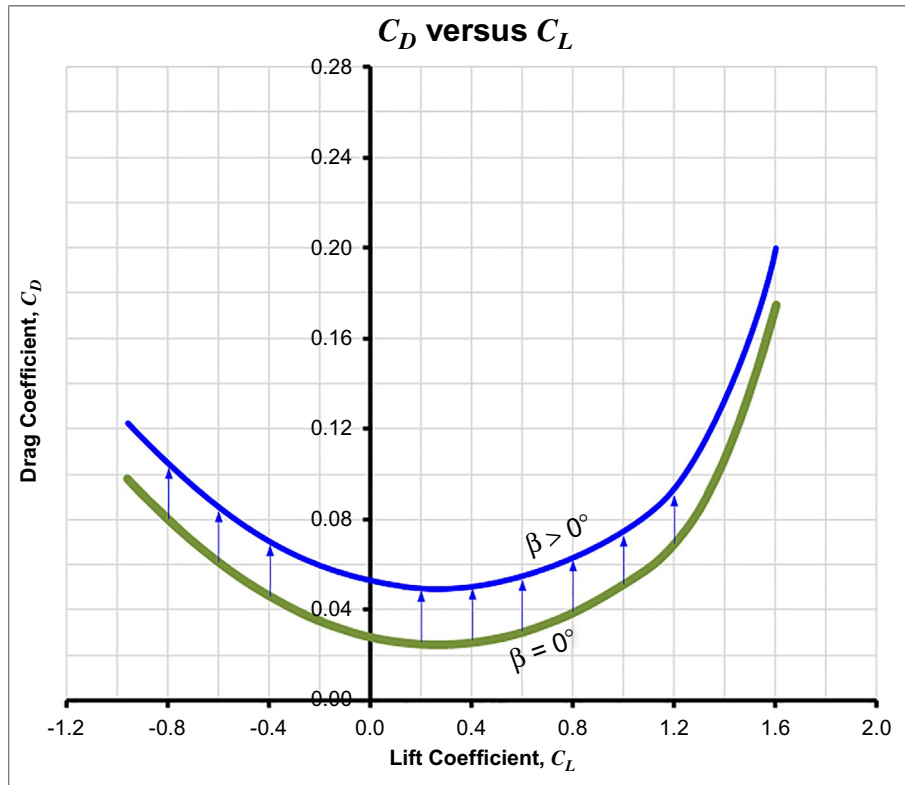
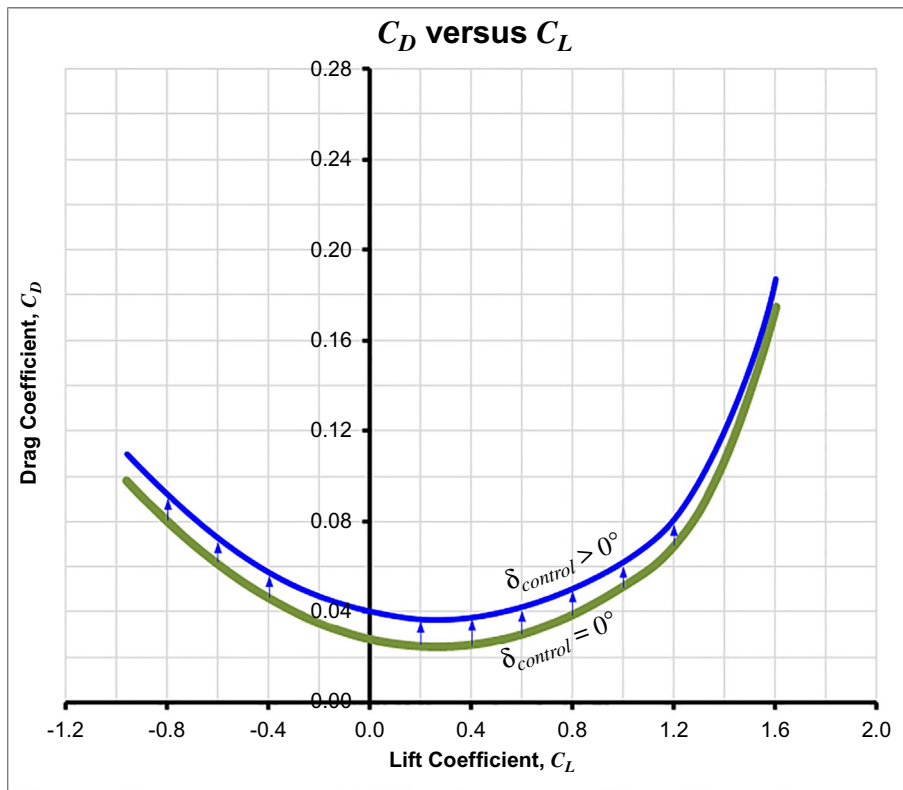
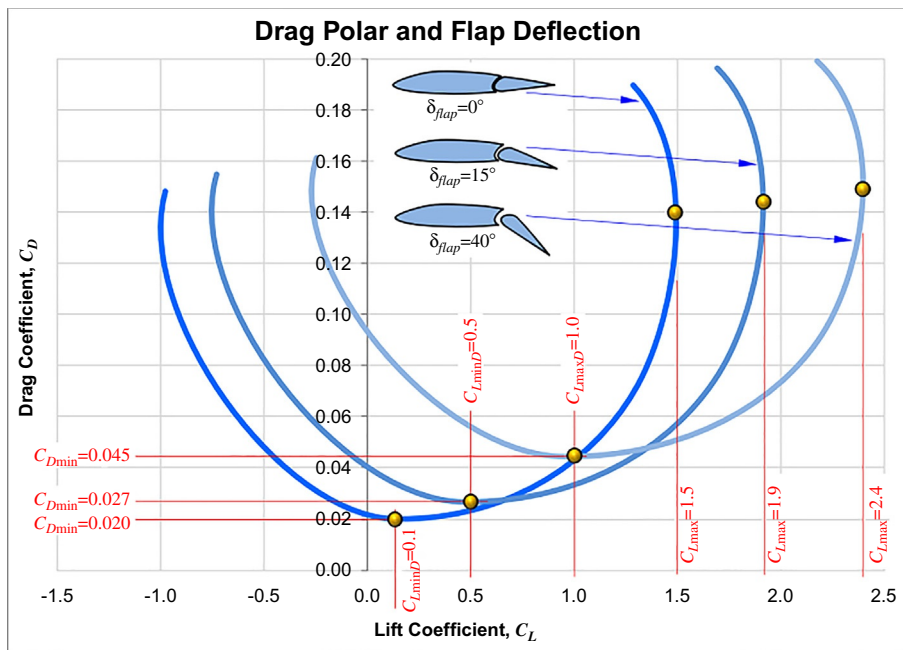


FIGURE 16-14 The effect of yawing the airplane to some yaw angle  $\beta$ .



**FIGURE 16-15** The effect of deflecting a control surface.



**FIGURE 16-16** Deflecting flaps has significant impact on the drag polar. Typical numbers are shown.

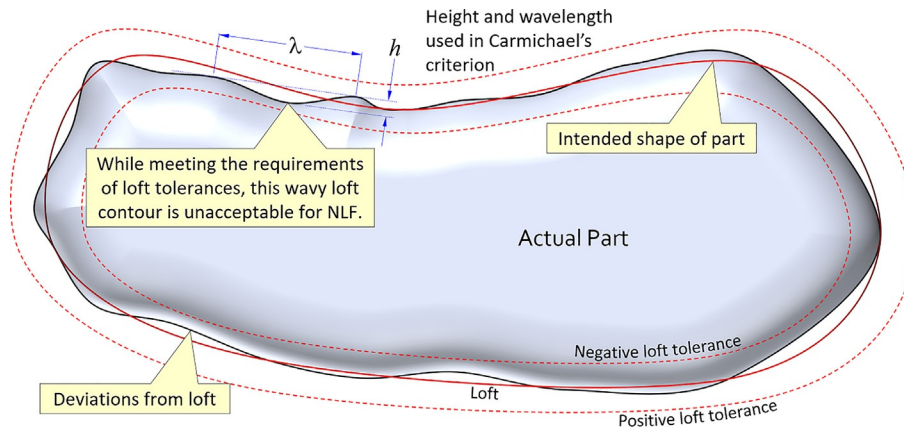


**FIGURE 16-17** Definition of local contour deviations.

manufacturer evaluate the quality of the NLF surface. The expression is widely used and is often referred to as *Carmichael's criterion*. Presented below, it shows the maximum wave height-to-length (see Figure 16-17) below which early transition is avoided.

$$\frac{h}{\lambda} \leq \sqrt{\frac{59,000c \cos^2 \Lambda_{LE}}{\lambda R_e^{1.5}}} \quad (16-22)$$

Where  $h$  is the double-amplitude wave height in inches,  $\lambda$  is wavelength in inches,  $c$  is streamwise chord in inches,  $\Lambda_{LE}$  is the wing leading edge sweep, and  $R_e$  is the Reynolds number based on chord.

## (6) Musings on Prediction Accuracy

In 1940, NACA released the wartime report WR-L-489 [17] in which 11 military aircraft were investigated to determine why they failed to meet their predicted performance. The aircraft were wind tunnel tested in the NACA *Full-Scale Wind Tunnel* (FSWT) in Langley, Virginia.<sup>2</sup> The aircraft were stripped to a clean configuration by gradually removing components. The drag coefficient was measured after each removal step. The results give a timeless insight into the cumulative impact of small and easily ignored design details on the total drag.

One of the aircraft investigated was the Seversky P-35 that had been designed for the US Army Air Corps in the early 1930s (see Figure 16-18). At the time, it was an innovative single-engine fighter that offered a number of firsts. It was the Air Corps first all metal fighter, the first to feature retractable landing gear, and the first with an enclosed cockpit. Its promised maximum airspeed was 280KTAS [18], but its actual speed was some 28KTAS

lower. While its engine could not develop the advertised power, which contributed to the problem, it did not fully explain the difference between practice and prediction. This simply implied its drag was higher than predicted—something common to the other 10 aircraft also studied in the report. This highlights a scenario to which anyone estimating the drag of a new airplane may be subject—to analyze Airplane 1 in Ref. [17], when in reality it will be closer to Airplane 18.

Such underpredictions are not limited to aircraft of the yesteryear. They still happen. A recently developed small twin-engine business jet was unable to meet the predicted performance advertised on the company website. This led to a costly redevelopment effort [19, 20]. A small single-engine propeller aircraft developed by a prominent car manufacturer also didn't meet the predicted performance due to higher than predicted drag [21]. Both aircraft were designed by very capable people. It shows that drag prediction must be treated with utmost respect.

Going back to Ref. [17], the source presents a detailed listing of the changes made to the airplane presented in a graphic and tabulates their effect on the total drag. The graphic is reproduced as Ref. [17] and the table is recreated as Table 16-1. It is of great value to review the table to see how contributions of seemingly insignificant modifications, such as a sanded walkway or an opened cowl flap affect the overall drag of the airplane. The problem is not the individual contribution, but their collective effect. To make the numbers easier to relate to, the impact of the change on maximum level airspeed (at 12,000ft) is calculated. It shows that the airspeed change between the actual (ID18) and ideal airplane (ID1) is 44KTAS.

<sup>2</sup> It was demolished between 2010 and 2014.

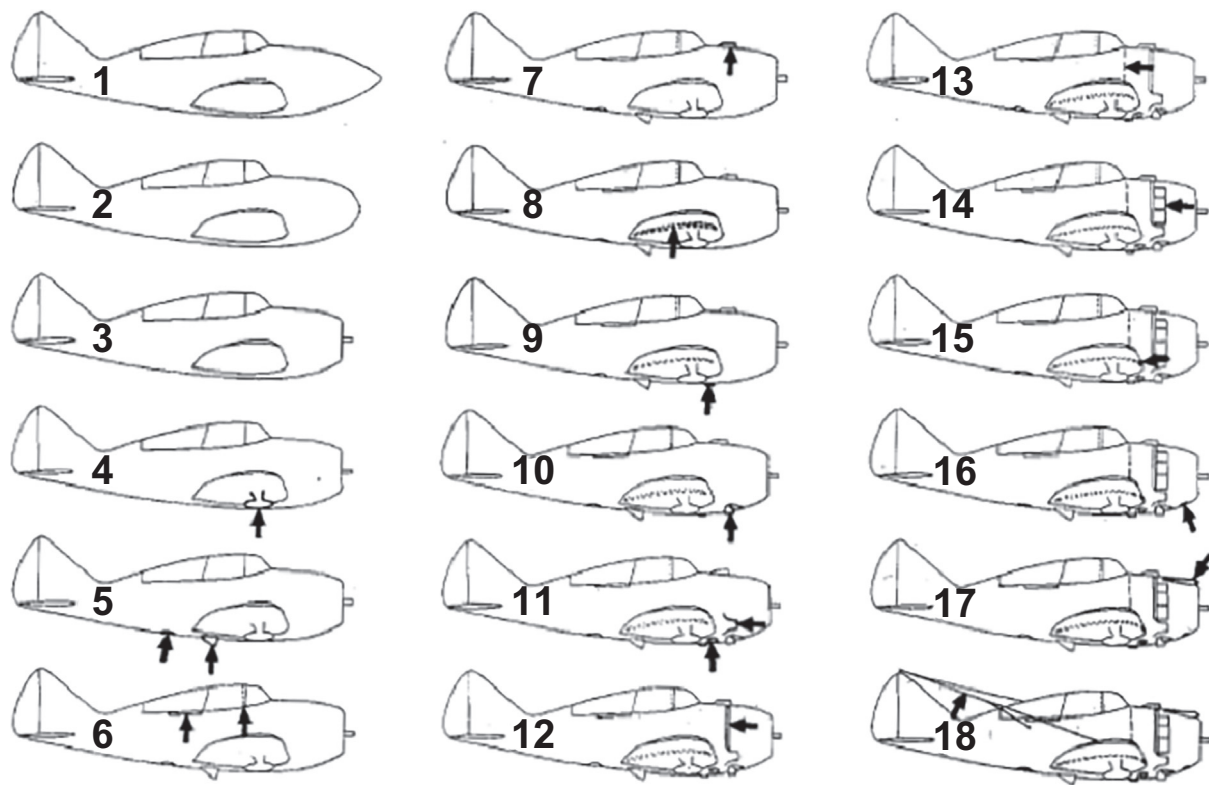


**FIGURE 16-18** Order of modifications made to the Seversky P-35 aircraft during wind tunnel testing. *Figure from C.H. Dearborn, and A. Silverstein, Drag Analysis of Single-Engine Military Airplanes Tested in the NACA Full-Scale Wind Tunnel, NACA WR-L-489, 1940.*

**TABLE 16-1** Component contribution to drag for the Seversky P-35 [17].

ID	Airplane Conditions	$C_D$	$\Delta C_D$	$\Delta C_D \%$	$V_{max}, KTAS$
1	Completely faired condition with long nose fairing	0.0166	0	0	296
2	Completely faired condition with blunt nose fairing	0.0169	0.0003	1.8%	296
3	Completely faired condition with original NACA cowling (no air flowing through cowling)	0.0186	0.0020	12.0%	288
4	Same as 3 except landing gear seals and fairing removed	0.0188	0.0002	1.2%	287
5	Same as 4 except original oil cooler installed	0.0205	0.0017	10.2%	279
6	Same as 5 except canopy fairing removed	0.0203	-0.0002	-1.2%	280
7	Same as 6 except carburetor scoop added	0.0209	0.0006	3.6%	277
8	Same as 7 except sanded walkway added	0.0216	0.0007	4.2%	274
9	Same as 8 except ejector chute added	0.0219	0.0003	1.8%	272
10	Same as 9 except exhaust stacks added	0.0225	0.0006	3.6%	270
11	Same as 10 except intercoolers added	0.0236	0.0011	6.6%	266
12	Same as 11 except cowling exit opened	0.0247	0.0011	6.6%	261
13	Same as 12 except accessory exit opened	0.0252	0.0005	3.0%	260
14	Same as 13 except cowling fairing and seals removed	0.0261	0.0009	5.4%	257
15	Same as 14 except cockpit ventilator opened	0.0262	0.0001	0.6%	256
16	Same as 15 except cowling venturis installed	0.0264	0.0002	1.2%	256
17	Same as 16 except blast tubes added	0.0267	0.0003	1.8%	255
18	Same as 17 except radio aerial installed	0.0275	0.0008	4.8%	252
TOTAL DRAG CHANGE			0.0109	65.7%	

Percentages are based on ID 1

### 16.2.7 Various Means to Reduce Drag

It has already been stated that, generally, drag is a detrimental force in aircraft design, in particular, for fuel efficiency. In addition to “obvious” means to reduce drag, such as retractable landing gear and smooth NLF surfaces, people have been creative in the pursuit of reduced drag. This section introduces a few fruits of this labor.

#### (1) Reduction of Wing Drag via Laminar Flow Control (LFC)

The history of LFC dates back to 1930s and is well documented by Chambers [22] and in particular Braslow [23]. LFC is also referred to as *artificial laminar flow* (ALF) to contrast *natural laminar flow* (NLF). LFC attempts to maintain laminar boundary layer over a large surface area by “sucking” the turbulent boundary layer through tiny perforations in the wing skin. A variation of LFC, called *hybrid LFC* (HLFC), relies on NLF for a larger portion of the wing to reduce the power required for the ALF. The primary drawback of these methods is that they are *active* rather than *passive*. Thus, additional energy is required to draw in the external boundary layer. Furthermore, the perforations are detrimental to the structural integrity of the wing and require the operator to deal with nuisances such as insect removal that can clog the perforations, reducing system performance.

Figure 16-19 shows the difference in airflow over an airfoil with and without LFC. The left photo shows the airfoil at an AOA of 20 degrees with a fully separated wake behind it. The right photo shows the same airfoil with the LFC turned on. The change in the nature of the flow is clearly evident, with the separation being eliminated as far aft as 70% of the chord. This “unstalls” the airfoil, giving it a higher  $C_{l_{max}}$  and reduced drag. It demonstrates the promising potential of LFC technology, although being severely hampered by a number of factors discussed in Ref. [22].

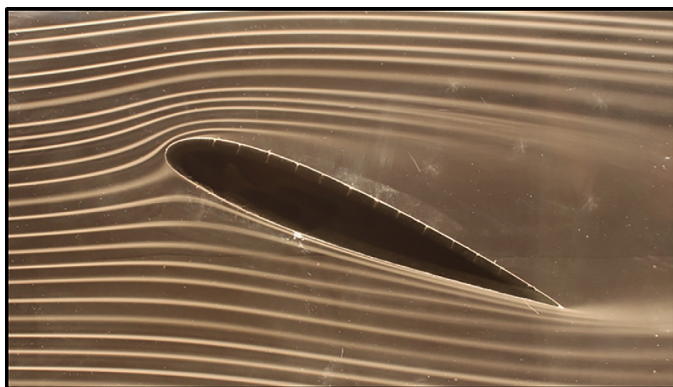


**FIGURE 16-19** The effect of Laminar Flow Control. The AOA is approximately 20 degrees. *Photos by Phil Rademacher.*

Early experiments involve the Northrop X-21A, a heavily modified Douglas WB-66D aircraft. Its two original Allison J71 engines, originally on the wing, were replaced with two GE XJ79s that were mounted to the rear fuselage. The bleed air from these engines was used to drive a compressor that, effectively, sucked the wing boundary layer through slots in the wing. While the system demonstrated the effectiveness of LFC, it turned out to be a manufacturing and maintenance nightmare and too costly to be practical.

In 1999, Marshall [24] investigated the effectiveness of a variable-porosity suction glove on the F-16XL-2 aircraft to demonstrate the feasibility of ALF for supersonic operation. It showed that at Mach 2 at 53,000 ft ( $R_e$  of the order of  $22.7 \times 10^6$ ) laminar boundary layer was sustained as far aft as 46% of the chord. In 2010, van de Wal [25] showed merely 3.2% reduction in total drag of a small GA aircraft (ENAER Namcu), citing that installing a boundary layer suction system was not beneficial to its operation.

#### (2) Reduction of Lift-Induced Drag using Winglets

Winglets and the potential for a reduction in lift-induced drag is discussed in Section 10.5.9, *The Winglet*.

#### (3) Reduction of Wing Profile Drag using NLF Airfoils

*Natural laminar flow* airfoils are an obvious choice when trying to reduce drag. Of course, they have to be selected before the airplane is built. NLF airfoils are discussed in great detail earlier in this section and Chapter 8, *The Anatomy of the Airfoil*.

#### (4) Reduction of Fuselage Drag

Wortman [26] suggests that installing relatively large fixed pitch vortex generators on the bottom, near the beginning of the upsweep of the lower fuselage of transport aircraft can reduce the total drag by 1%–2%. The idea

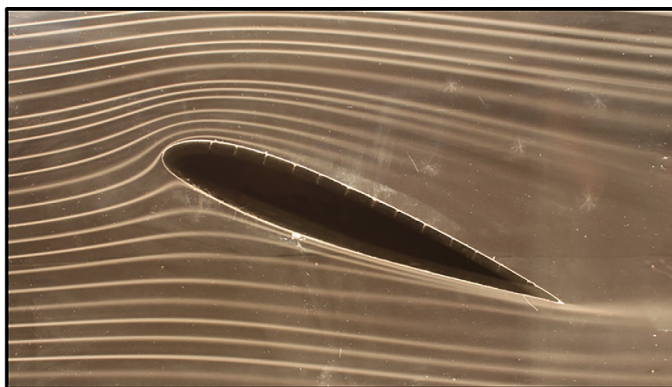




**FIGURE 16-20** Vortex generators on the aft fuselage of a B-52 Stratofortress. Photo by Phil Rademacher.

was validated in extensive wind tunnel tests using fuselage models of the Boeing 747 and Lockheed C-5 Galaxy transport aircraft. The author suggests the vortex generators can be installed on such aircraft for a fraction of the cost of their monthly operational cost. Such vortex generators are shown mounted to the aft lower fuselage of the B-52 Stratofortress in [Figure 16-20](#).

Kentfield [27] suggests that using a stepped after-body can significantly reduce the drag of an axis-symmetric fuselage style bodies. The unorthodox idea forms entrapped vortices at each step of the conical after-body, which allows the airflow to better follow its geometry, ultimately reducing its drag. The method is untraditional and results in an unusual after-body geometry that would be hard to justify from an aesthetics standpoint, not to mention there could be some structural challenges.

A clear way to reduce fuselage drag is to employ tadpole fuselages, like those used for sailplanes. Naturally, such fuselages are not always practical considering the mission of the airplane. Tadpole fuselages are discussed in [Section 12.2.3, The Tadpole Fuselage](#).

In evaluating the importance of smooth surfaces in maintaining NLF on lifting surfaces (wing, HT, and

VT), Quast and Horstmann [28] demonstrate the magnitude of fuselage drag. Using the Airbus 300 as an example, they estimate the drag of the fuselage alone amounts to about 49% of the minimum drag. Such studies remind us it is easy to spend a tremendous effort eliminating a few dragcounts from the lifting surfaces, while overlooking the largest source of drag—the fuselage.

### (5) Reduction of Fuselage/Wing Juncture Drag

The juncture of the fuselage and wing can be particularly bothersome as it is not always easy to estimate tendency for flow separation. The steep adverse pressure gradients that frequently form in the region promote flow separation, even at low AOAs. This increases drag during climb and even cruise, reducing performance.

Modern methodologies are being developed that use state-of-the-art *Navier-Stokes computational fluid dynamics* (NS CFD) tools to shape the wing fairing using genetic algorithms. Using such a tool, Peigin and Epstein [29] demonstrated a 43 dragcount drag reduction in a before-and-after investigation of a business jet.

## 16.3 ESTIMATING THE DRAG OF A COMPLETE AIRCRAFT

The focus of this section is the development of a drag model for an entire aircraft. This is a complex task that must be broken down into several subtasks. For typical aircraft, it is compounded by configuration changes. There is a *clean configuration* intended for cruise. There is a *T-O configuration*, which is the clean configuration with the addition of landing gear (if not fixed) and a high-lift system deployed for T-O. Then, there is a *landing configuration*, which comprises the clean configuration with landing gear and a high-lift system deployed for landing. Hence, the analyst must develop at least three drag models. The task is made simpler by starting with the clean aircraft configuration and then add contributions by the landing gear and high-lift devices.

[Figure 16-21](#) shows a rudimentary plan of attack that applies to all configurations. The section numbers for the required analyses are shown right of each task. The product of this work is shown at the bottom of the figure: It is the *drag model*. [Figure 16-22](#) further highlights important contributors to the drag. If you are new to this process you must first learn the ropes. You must learn how to calculate skin friction. This is required for wings, HT, VT, fuselage, and all components that resemble a wing or an axisymmetric body. You must learn how to boost the resulting coefficients to include pressure drag. Then, how to account for contributions made by small components that “dirty up” the airplane. You must also learn how to calculate lift-induced drag and, if your airplane

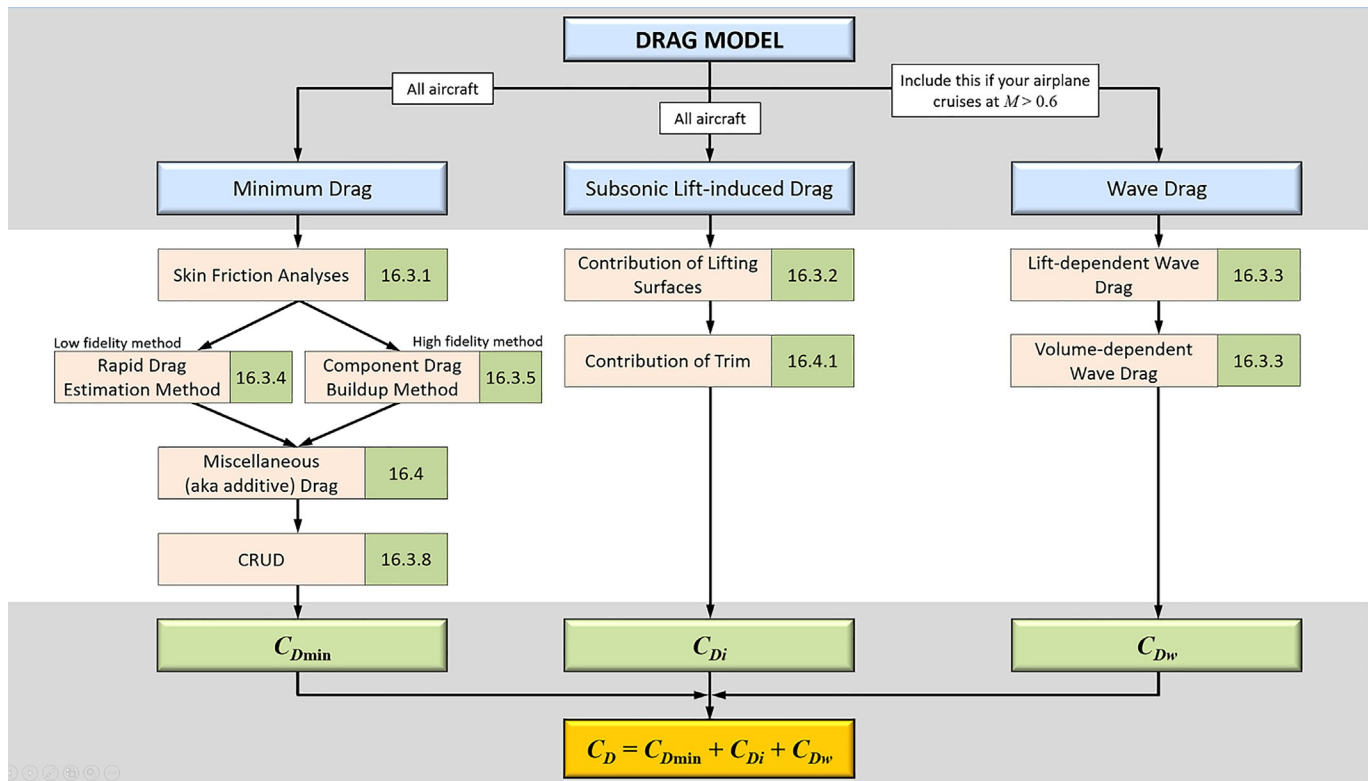


**FIGURE 16-21** A flow chart depicting the development of the *drag model*.

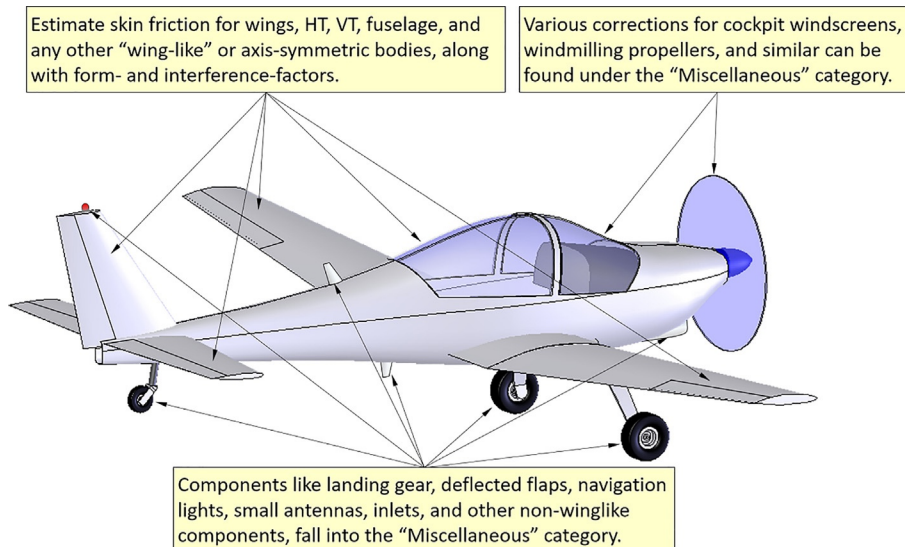


**FIGURE 16-22** Contributions to the *drag model*.

operates in the transonic range, wave drag. This section is written for this purpose.

The tasks listed in Figure 16-22 are best tackled in the following (logical) order:

- Calculate skin friction per [Section 16.3.1](#).
- Calculate aircraft profile drag per [Section 16.3.4](#) or [16.3.5](#) (preferred).

- Calculate miscellaneous drag contributions per [Section 16.4](#).
- Apply crud per [Section 16.3.8](#).
- Calculate minimum drag coefficient per [Section 16.3.9](#).
- Calculate lift-induced drag per [Section 16.3.2](#).
- Calculate trim drag per [Section 16.4.1](#).
- Calculate wave drag per [Section 16.3.3](#).

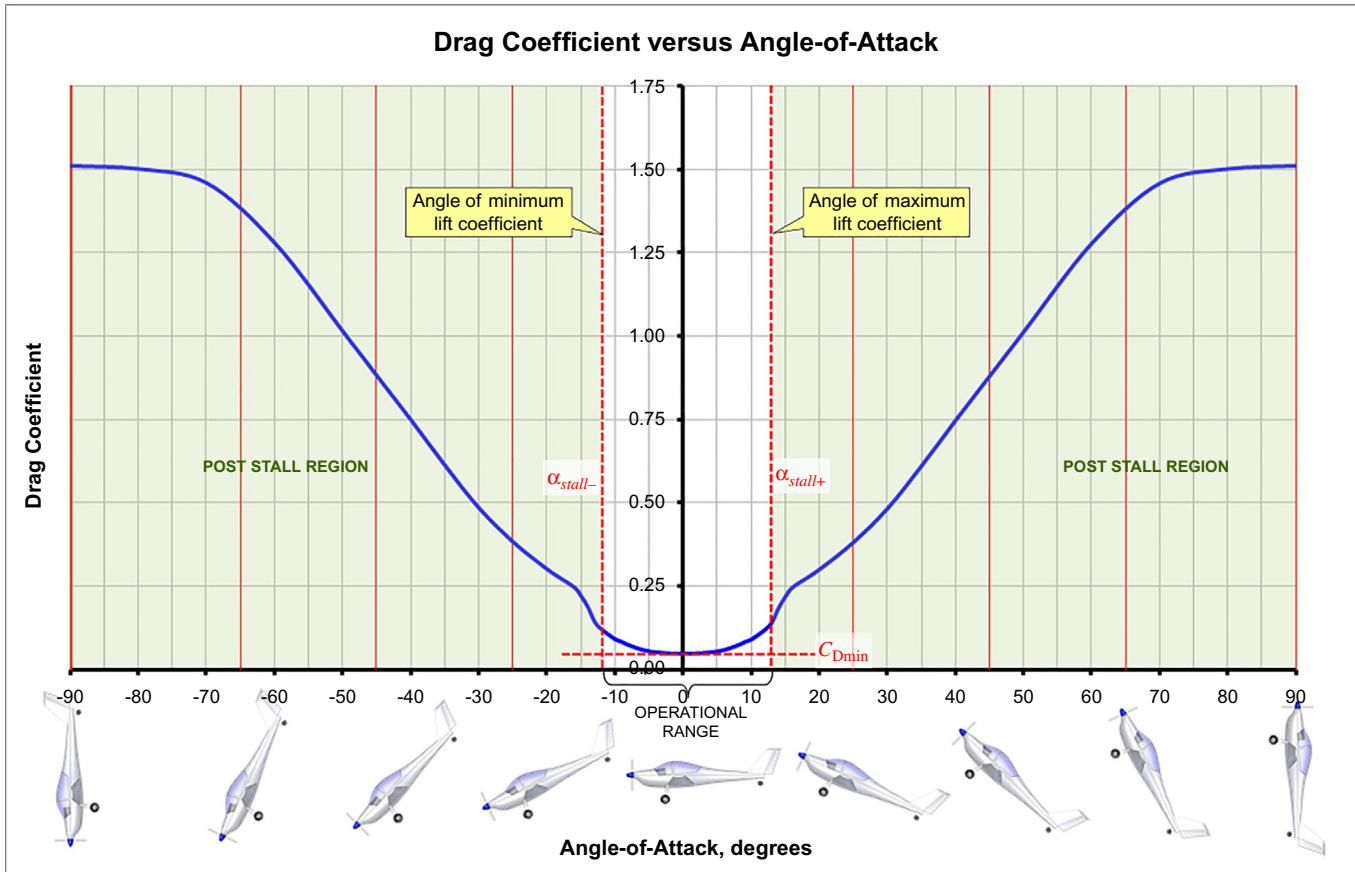


**FIGURE 16-23** Typical variation of the drag coefficient for angle-of-attack between  $-90$  degrees and  $+90$  degrees.

Figure 16-23 shows a typical variation of the 3-dimensional drag coefficient for a complete aircraft (wings, fuselage, tail, etc.) with angle-of-attack for an AOA range of  $-90$  degrees  $\leq \alpha \leq +90$  degrees. It is based on actual wind tunnel test data. The drag coefficient at the extreme AOAs typically ranges from 1.5 to 1.7. That beats the drag of the parachute in [Section 16.4.14, Drag of Parachutes](#). Standard drag modeling is usually limited to the unshaded region in the center of the graph (the operational range).

### 16.3.1 Estimating Skin Friction Drag: $C_{Df}$

Recall that the drag of a body is caused by surface friction and pressure difference. This section focuses on the former—surface friction. Familiarity with [Sections 8.1.6 \(Chordwise Pressure Distribution\)](#), [8.1.7 \(Forces and Moment per Unit Span\)](#), and [8.1.10 \(Boundary Layer Basics\)](#) is an essential preparation for this section.

The formulation presented in subsequent subsections are the product of the *boundary layer theory*. The formulae are extracted from numerous sources, including Schlichting [30], Schetz and Bowersox [31], and Young [32]. Derivations of the formulae is provided in these texts. Only results important to aircraft drag analysis are presented

here. The resulting relationships are plotted in [Figure 16-26](#).

#### (1) Introduction

Figure 16-24 shows an airfoil immersed in airflow and illustrates several regions of interest. For skin friction, we are interested in the extent of *laminar* and *turbulent boundary layer* (BL) and *flow separation region*. The thick blue line that wraps around the leading edge represents a region of laminar BL. It terminates on both surfaces at the *transition point* (denoted by  $x_{tr_u}$  and  $x_{tr_d}$ ) where it transforms into turbulent BL. Its extent depends on the geometry of the airfoil. The extent is shorter than shown for non-NLF airfoils. Eventually, this develops into separated flow. Figure 16-24 shows how angle-of-attack causes the two transition points move forward or aft. Other parameters affecting its extent are detailed in [Section 8.1.10](#).

The extent of the laminar and turbulent BL impacts the airfoil's skin friction and, thus, its drag polar. Airfoils featuring geometries such as that shown in [Figure 8-11](#), develop pressure distribution with extensive favorable pressure gradient ( $dp/dx$ ). They sustain laminar BL over a large part of their surface. Such airfoils are called *natural laminar flow* (NLF) airfoils (see [Sections 8.1.6](#) and [8.1.10](#)).

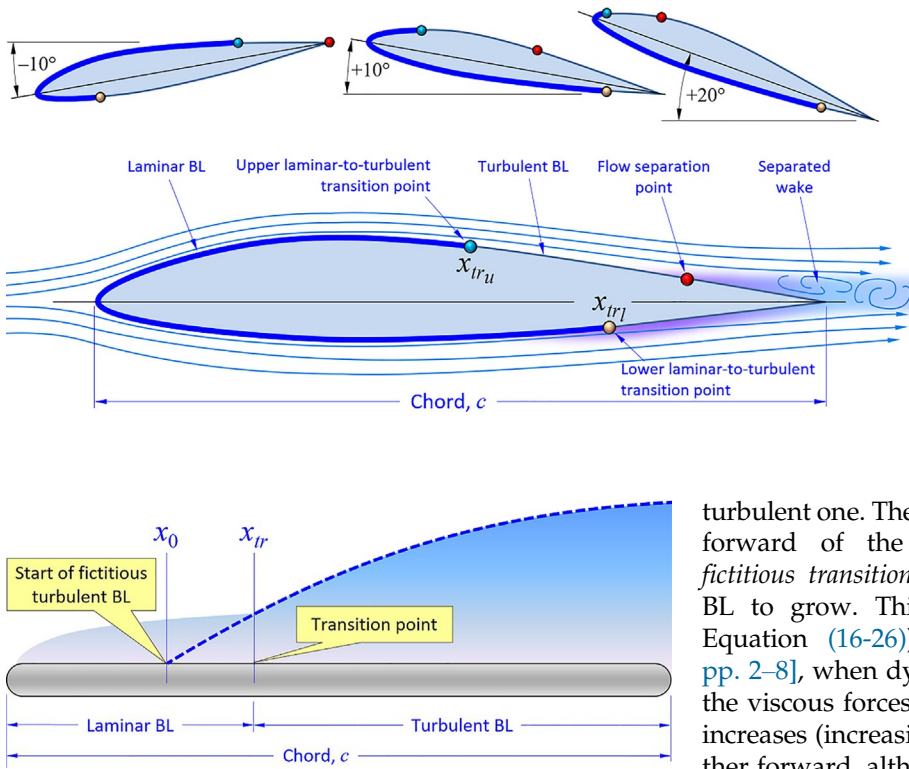


**FIGURE 16-25** Transition from laminar to turbulent flow inside a mixed boundary layer.

Their primary advantage is considerably lower drag at low angles-of-attack, during cruise. The effect of such geometry differences is depicted in Figure 8-21.

The boundary layer develops on a curved surface similar to what it does on a flat plate. It is affected by all the same shortcomings. Figure 16-25 illustrates the transformation that takes place as the laminar BL transitions into

turbulent one. The transition can be thought to take place forward of the transition point, at the so-called *fictitious transition point*. It causes the thickness of the BL to grow. This tends to occur once the  $R_{ex}$  (see Equation (16-26)) approaches and exceeds  $10^6$  [33, pp. 2-8], when dynamic flow forces become larger than the viscous forces (see Figure 16-25). As the flow speed increases (increasing  $R_{ex}$ ) the transition points move farther forward, although never quite to the LE.

The laminar BL is sensitive to surface contamination. The presence of rivet-heads, uneven plate joints, insects, and even paint chips can destabilize it and initiate an early transition (see Section 8.3.7, *The Effect of Leading-Edge Roughness and Surface Smoothness*). The laminar BL is even sensitive to uncontrollable factors like the quality of the airflow. Figure 16-26 shows how the flat plate drag coefficient for laminar and turbulent BL changes with Reynolds number. Figure 16-26 shows how susceptible to transitioning the laminar

Laminar BL  
Turbulent BL  
Mixed BL

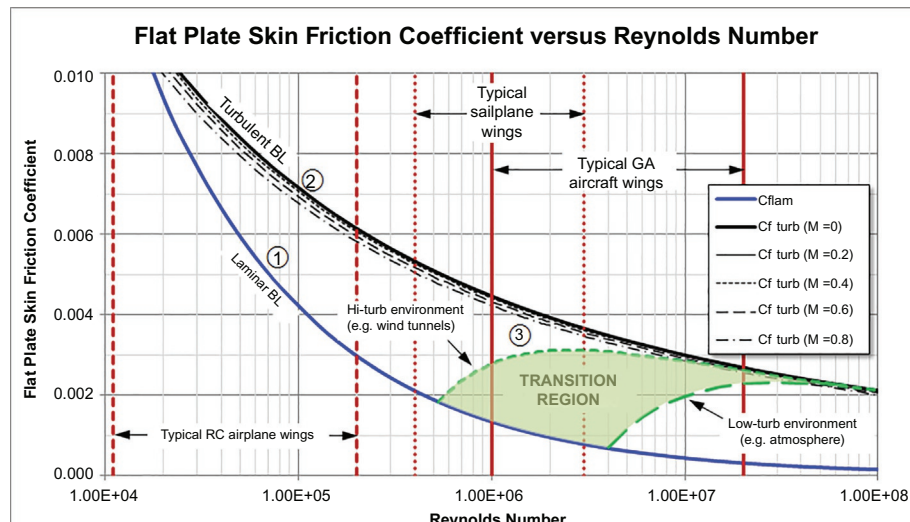


**FIGURE 16-26** Change in skin friction with Reynolds number. ① is Equation (16-40), ② is Equation (16-43), ③ is Equation (16-46).

boundary layer is as it flows over a flat plate, operating within  $4 \times 10^5 < R_e < 1 \times 10^7$ .

## (2) Basic Analysis Procedure

(A) List all components that can be classified as "winglike." This includes the wings, HT, VT, pylons, fuselage, engine nacelles, wingtip tanks, and so forth. Smaller components like small, wing-shaped antennas can be omitted, as these are treated as "miscellaneous" drag. (B) List geometric properties of each component, primarily chord-lengths and wetted areas. (C) Calculate the skin friction coefficients for each component using any of the applicable methods that follow. A similar approach is also used in the *component drag buildup method*, presented in [Section 16.3.5](#).

## (3) Skin Friction Drag Coefficient, $C_{Df}$

The skin friction drag coefficient applies to the entire aircraft. It is defined as

$$C_{Df} = \frac{2D_f}{\rho V_\infty^2 S} = C_f \left( \frac{S_{wet}}{S} \right) \quad (16-23)$$

Where  $D_f$  is skin friction drag force,  $S$  is the reference wing area,  $S_{wet}$  is wetted area,  $C_{Df}$  is *skin friction drag coefficient*, and  $C_f$  is *skin friction coefficient*. Note the difference between the two coefficients;  $C_f$  and  $C_{Df}$ .

## (4) Viscosity

See introduction in [Section 8.1.10, Boundary Layer Basics](#). The viscosity of air is given by the empirical Sutherland's formula [34]:

SI-system:

$$\mu = 1.458 \times 10^{-6} \left( \frac{T^{1.5}}{110.4 + T} \right) \quad \left[ \frac{\text{Ns}}{\text{m}^2} \right] \quad (16-24)$$

UK-system:

$$\mu = 3.170 \times 10^{-11} \left( \frac{734.7T^{1.5}}{216 + T} \right) \quad \left[ \frac{\text{lb}_f \text{s}}{\text{ft}^2} \right] \quad (16-25)$$

Equation (16-25) is presented in Ref. [35] and cited by [36]. There are two kinds of viscosities of interest to the aircraft designer. (1) *Dynamic viscosity* ( $\mu$ ) is simply known as *viscosity* or *viscosity coefficient*. Common units are  $\text{kg}/\text{m}\cdot\text{s}$ ,  $\text{Ns}/\text{m}^2$ , or  $\text{slugs}/\text{fts}$ . (2) *Kinematic viscosity* ( $\nu$ ) is the ratio of viscous to inertia forces in a fluid. Common units are  $\text{m}^2/\text{s}$  or  $\text{ft}^2/\text{s}$ . It is defined below:

$$\nu = \frac{\mu}{\rho} = \frac{\text{viscous force}}{\text{inertia force}} \quad (16-26)$$

## (5) Reynolds Number

The Reynolds number is a measure of the ratio of inertial forces to viscous forces in fluid flow. It is derived

using dimensional analysis. It is of great importance in the analysis of the boundary layer. It is defined as follows:

$$\text{Reynolds number: } R_e \equiv \frac{\rho V_\infty c}{\mu} = \frac{V_\infty c}{\nu} \quad (16-27)$$

Where:  $c$ =Reference length, in ft or m,

$V_\infty$ =Reference airspeed, in ft/s or m/s,

$\rho$ =Air density, in slugs/ $\text{ft}^3$  or  $\text{kg}/\text{m}^3$ ,

$\mu$ =Air viscosity, in  $\text{lb}_f \text{s}/\text{ft}^2$  or  $\text{Ns}/\text{m}^2$ ,

$\nu$ =Kinematic viscosity, in  $\text{ft}^2/\text{s}$  or  $\text{m}^2/\text{s}$ .

Note that *local*  $R_e$  is represented as a function of the distance from the leading edge of a body to a point of interest. It is written as follows:

$$R_{e_x} \equiv \frac{\rho V_\infty x}{\mu} = \frac{V_\infty x}{\nu} \quad (16-28)$$

The expression is used to estimate friction on a surface using integration (see later). The Reynolds number for a standard day, sea-level conditions only, is found from:

$$\text{UK-system } (V_\infty \text{ in ft/s, } c \text{ in ft}): \quad R_e \approx 6400 V_\infty c \quad (16-29)$$

$$\text{SI-system } (V_\infty \text{ in m/s, } c \text{ in m}): \quad R_e \approx 68,500 V_\infty c \quad (16-30)$$

## (6) Cutoff Reynolds Number

Ref. [37] contends that poor surface qualities result in skin friction higher than that predicted by equations such as Equation (16-40) or (16-43). To remedy this discrepancy a special  $R_e$ , called a *cutoff*  $R_e$ , is calculated. When the actual  $R_e$  exceeds the cutoff  $R_e$ , the latter is used. It is calculated using the following expressions

$$\text{Subsonic: } R_{e_{cutoff}} = 38.21 \left( \frac{c}{\kappa} \right)^{1.053} \quad (16-31)$$

$$\text{Trans \& supersonic: } R_{e_{cutoff}} = 44.62 \left( \frac{c}{\kappa} \right)^{1.053} M^{1.16} \quad (16-32)$$

Where  $M_\infty$  is the far-field Mach number and  $\kappa$  is the skin roughness value specified in [Table 16-2](#).

**TABLE 16-2** Skin roughness values.

Surface type	$\kappa$ (C in ft)
Camouflage paint on aluminum	$3.33 \times 10^{-5}$
Smooth paint	$2.08 \times 10^{-5}$
Production sheet metal	$1.33 \times 10^{-5}$
Polished sheet metal	$0.50 \times 10^{-5}$
Smooth molded composite	$0.17 \times 10^{-5}$

*Based on D.E. Hoak, USAF Stability and Control DATCOM, Flight Control Division, Air Force Flight Dynamics Laboratory, 1978, Section 4.1.5.1.*

## (7) Viscous Shear Stress

Two concepts of interest regarding viscous shear in the BL are *shear stress* (aka wall stress) and *shear force* (aka friction). The shear stress is determined as follows

$$\tau_w = \mu \left( \frac{du}{dy} \right)_{y=0} \quad (16-33)$$

Where  $u$  is the flow speed in the boundary layer and  $y$  is the axis normal to the surface. Units are  $\text{N/m}^2$  (Pa) or  $\text{lb}_f/\text{ft}^2$ . The subscript  $y=0$  indicates the shear stress should be evaluated at the surface (because the stress of interest takes place between the fluid and the surface). Note that Equation (16-33) is only valid for so-called *Newtonian fluids* (air, water, avgas). Non-Newtonian fluids are beyond the scope of this introduction.

## (8) Skin Friction Coefficient, $C_f$

We prefer to relate skin friction to the dynamic pressure ( $q_\infty$ ) in the flow. This is defined as follows

$$\tau_w \equiv q_\infty C_f \Rightarrow C_f = \frac{\tau_w}{q_\infty} \quad (16-34)$$

## (9) Average Skin Friction Coefficient

The friction coefficients come in two forms: (A) As a *local* function of  $R_{ex}$  or (B) *averaged* based on the  $R_e$  of the body's length (see Bullet (5)). Figure 16-27 plots the  $C_f$  for laminar, turbulent, and mixed boundary layers assuming  $x_{tr}/c=0.5$ . It also illustrates the resulting average values. Figure 16-27 shows how three skin friction coefficients,  $C_{f_{laminar}}$ ,  $C_{f_{turbulent}}$ , and  $C_{f_{mixed}}$ , vary along the surface of the airfoil as functions of  $x$  (implicit functions of  $R_{ex}$ ).

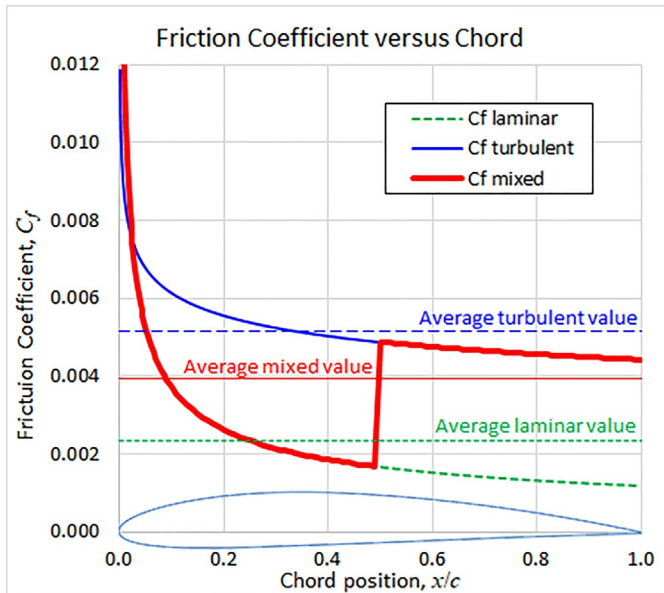


FIGURE 16-27 Distribution of  $C_f$  over an airfoil.

Their average value between the leading and trailing edges can be calculated using the following expression:

$$\underbrace{\bar{C}_f}_{\text{Averaged}} = \frac{1}{c} \int_0^c \underbrace{C_f}_{\text{Local}} dx \quad (16-35)$$

## (10) Friction Force, $f$

Knowing the viscous shear stress, we can calculate the friction ( $f$ ) (aka *skin friction* and *shear force*) acting on surface area  $A$ . There are two ways to do this; using *average shear stress* and *integration*. The former is convenient for rapid estimation and is determined as follows:

$$f = A\tau_w = A\mu \left( \frac{du}{dy} \right)_{y=0} \quad (16-36)$$

### EXAMPLE 16-4

The “average” boundary layer velocity profile of air flowing over the surface of a flat plate with total surface area  $50 \text{ m}^2$  is described by

$$u(y) = u_{\max} \sin \left( \frac{\pi y}{2\delta} \right)$$

Where  $u_{\max} = 100 \text{ m/s}$  and  $\delta = 0.0012 \text{ m}$ . Estimate the total skin friction developed by the plate if  $\mu = 1.73 \times 10^{-5} \text{ Ns/m}^2$ .

#### SOLUTION:

First, let us evaluate the derivative:

$$u = u_{\max} \sin \left( \frac{\pi y}{2\delta} \right) \Leftrightarrow \left( \frac{du}{dy} \right)_{y=0} = \frac{\pi u_{\max}}{2\delta} \cos \left( \frac{\pi 0}{2\delta} \right) = \frac{\pi u_{\max}}{2\delta} = 1$$

Thus, the shear force is determined as shown:

$$f = A\mu \left( \frac{du}{dy} \right)_{y=0} \Rightarrow f = A\mu \left( \frac{\pi u_{\max}}{2\delta} \right)$$

$$f = (50)(1.73 \times 10^{-5}) \left( \frac{\pi \cdot 100}{2 \cdot 0.0012} \right) = 113.2 \text{ N}$$

A more precise method is to integrate the *skin friction coefficient* (see Table 16-3) over the surface using Equation (16-65). Omitting the contribution of the pressure, the second equation becomes:

$$f = \int_{LE}^{TE} \tau_u \cos \theta_u ds_u + \int_{LE}^{TE} \tau_l \cos \theta_l ds_l = \int_0^c (\tau_u + \tau_l) dx$$

$$= q_\infty \int_0^c (C_{f_u} + C_{f_l}) dx \quad (16-37)$$

Where the subscripts  $u$  and  $l$  refer to the upper and lower surfaces, respectively.

**TABLE 16-3** Properties of the boundary layer.

Property	Laminar	Turbulent	Turbulent (for pipe flow)
Boundary layer thickness	$\delta_{lam} = \frac{4.91x}{\sqrt{R_{ex}}}$	$\delta_{turb} \approx \frac{0.16x}{R_{ex}^{1/7}}$	$\delta_{turb} \approx \frac{0.38x}{R_{ex}^{1/5}}$
Displacement thickness	$\delta_{lam}^* = \frac{1.72x}{\sqrt{R_{ex}}}$	$\delta_{turb}^* \approx \frac{0.020x}{R_{ex}^{1/7}}$	$\delta_{turb}^* \approx \frac{0.048x}{R_{ex}^{1/5}}$
Momentum thickness	$\theta_{lam} = \frac{0.664x}{\sqrt{R_{ex}}}$	$\theta_{turb} \approx \frac{0.016x}{R_{ex}^{1/7}}$	$\theta_{turb} \approx \frac{0.037x}{R_{ex}^{1/5}}$
Skin friction coefficient	$C_{f, lam} = \frac{0.664}{\sqrt{R_{ex}}}$	$C_{f, turb} \approx \frac{0.027}{R_{ex}^{1/7}}$	$C_{f, turb} \approx \frac{0.059}{R_{ex}^{1/5}}$
Skin friction per unit width	$\frac{F}{w} = \rho V^2 \theta$	w = width normal to page	

Based on Y.A. Cengel, J.M. Cimbala, *Fluid Mechanics—Fundamentals and Applications*, McGraw-Hill, 2006.

### (11) Laminar, Turbulent, and Mixed Boundary Layer

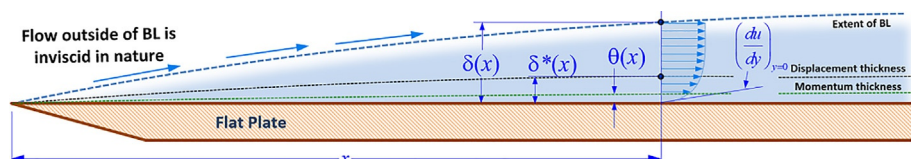
In this book,  $C_{f, lam}$  represents the skin friction coefficient associated with *laminar* BL,  $C_{f, turb}$  is associated with *turbulent* BL, and  $C_{f, mixed}$  refers to *mixed* BL. A mixed boundary layer combines laminar and turbulent BL, such that  $C_{f, lam}$  extends from the leading edge to the specified transition point,  $x_{tr}$ , after which  $C_{f, turb}$  takes over (see Figure 16-27). The mixed skin friction coefficient can be defined as follows

$$C_{f, mixed} \equiv \begin{cases} C_{f, lam} & \text{if } x < x_{tr} \\ C_{f, turb} & \text{if } x \geq x_{tr} \end{cases} \quad (16-38)$$

### (12) Estimation of Boundary Layer Properties

The derivation of the formulae in Table 16-3 is presented in Refs. [7, 38]. These assume flow over a smooth, flat plate. The *boundary layer thickness* ( $\delta$ ) is the height above the plate surface where the horizontal velocity component is 99% of the flow speed outside the BL. *Displacement thickness* ( $\delta^*$ ) refers to the distance that a streamline just outside the BL is deflected due to mass conservation. Its effect is analogous to an increase in the thickness of the plate. *Momentum thickness* ( $\theta$ ) is like the displacement thickness, except it accounts for loss

**FIGURE 16-28** The thickness of the boundary layer depends on whether it is laminar and turbulent.



of momentum flow inside the BL. These are illustrated in Figure 16-28. Finally, *skin friction coefficient* ( $C_f$ ) is used to estimate friction force developed by the plate.

### (13) Skin Friction Coefficient for Laminar Boundary Layer

The classical Blasius<sup>3</sup> solution for a laminar boundary layer yields the following *local skin friction coefficient*

$$C_{f, lam} = \frac{0.664}{\sqrt{R_{ex}}} = \frac{0.664}{\sqrt{\rho V_\infty x / \mu}} = \frac{0.664}{\sqrt{x}} \sqrt{\frac{\mu}{\rho V_\infty}} \quad (16-39)$$

Where  $x$  is the distance from the leading edge. Consider the theoretical possibility that laminar flow is fully sustained over a flat plate surface. This permits the *averaged skin friction coefficient* to be determined. It is presented below.

$$\bar{C}_{f, lam} = \frac{1.328}{\sqrt{R_e}} \quad (16-40)$$

Where  $R_e$  is the Reynolds number based on the airfoil chord,  $c$ .

### DERIVATION OF EQUATION (16-40)

Substitute Equation (16-39) into Equation (16-35) and solve.

$$\begin{aligned} \bar{C}_{f, lam} &= \frac{1}{c} \int_0^c C_{f, lam} dx = \frac{1}{c} \int_0^c \left( \frac{0.664}{\sqrt{R_{ex}}} \right) dx \\ &= \frac{0.664}{c} \sqrt{\frac{\mu}{\rho V_\infty}} \int_0^c x^{-1/2} dx = \frac{0.664}{c} \sqrt{\frac{\mu}{\rho V_\infty}} [2\sqrt{c}] = \frac{1.328}{\sqrt{R_e}} \end{aligned}$$

### (14) Skin Friction Coefficient for Turbulent Boundary Layer

The following local skin friction coefficient for turbulent boundary layer is commonly referred to as *Prandtl's one-seventh power law coefficient* [8]:

$$C_{f, turb} \approx \frac{0.027}{R_{ex}^{1/7}} = \frac{0.027}{(\rho V_\infty x / \mu)^{1/7}} = \frac{0.027}{x^{1/7}} \left( \frac{\mu}{\rho V_\infty} \right)^{1/7} \quad (16-41)$$

If it is assumed that turbulent flow is fully sustained over a flat plate surface, Equation (16-41) yields the following averaged skin friction coefficient

<sup>3</sup> Named after the German scientist Paul Blasius (1883–1970), one of Ludwig Prandtl's first doctoral students.

$$\bar{C}_{f_{turb}} = \frac{0.0315}{R_e^{1/7}} \quad (16-42)$$

## DERIVATION OF EQUATION (16-42)

Substitute Equation (16-41) into Equation (16-35) and solve.

$$\begin{aligned} \bar{C}_{f_{turb}} &= \frac{1}{c} \int_0^c C_{f_{turb}} dx = \frac{1}{c} \int_0^c \left( \frac{0.027}{R_{e_x}^{1/7}} \right) dx \\ &= \frac{0.027}{c} \left( \frac{\mu}{\rho V_\infty} \right)^{1/7} \int_0^c x^{-1/7} dx \\ &= \frac{0.027}{c} \left( \frac{\mu}{\rho V_\infty} \right)^{1/7} \left[ \frac{7}{6} c^{6/7} \right] = \frac{0.0315}{R_e^{1/7}} \end{aligned}$$

There are other averaged turbulent skin friction coefficients used. In fact, comparing those to experiment reveals Equation (16-42) underpredicts the drag. Thus, it should be avoided unless its use is supported by experiment. The so-called *Prandtl-Schlichting relation* [30, p. 438] is a commonly used model that agrees well with experiment.

$$\bar{C}_{f_{turb}} = \frac{0.455}{(\log_{10} R_e)^{2.58}} \quad (16-43)$$

The equation has roots in the so-called Schoenherr's friction equation [39];  $1/\sqrt{\bar{C}_{f_{turb}}} = 4.13 \log_{10}(R_e \bar{C}_{f_{turb}})$ . Schlichting attributes that formula to the work of Theodore von Kármán [30, p. 439] from 1930. It shows up in Figure 4 of Ref. [40] as a translation of von Kármán's work from 1930, 2 years prior that of Schoenherr. Regardless, its transcendental nature makes it unwieldy for use. Prandtl evaluated its solution for Reynolds numbers between  $10^5 < R_e < 1.5 \times 10^9$  [41]. Equation (16-43) is Schlichting's curve fit to Prandtl's data [30, 32].

Lazauskas [42] presents a collection of turbulent local and averaged skin friction coefficients, largely compiled using the work of Gadd [43] and Granville [44]. Some of these are listed in Table 16-4.

## (15) Compressibility Corrections for Drag

As the far-field Mach number,  $M_\infty$ , increases, the aerodynamic heating increases viscosity and decreases density. This increases BL thickness and reduces  $du/dy$  at the wall. This effect calls for a special compressibility correction, employed when  $M_\infty > 0.3$  [45].

$$C_{f_c} = C_{f_{inc}} (1 + 0.144 M_\infty^2)^{-0.65} \quad (16-44)$$

Where  $C_{f_c}$  is the compressible value of the incompressible skin friction  $C_{f_{inc}}$ . Another correction method is that of Frankl-Voishel [46, 47]:

$$\begin{aligned} C_{f_c} &= C_{f_{inc}} (0.000162 M_\infty^5 - 0.00383 M_\infty^4 + 0.0332 M_\infty^3 \\ &\quad - 0.118 M_\infty^2 + 0.0204 M_\infty + 0.996) \end{aligned} \quad (16-45)$$

## (16) Laminar-to-Turbulent Transition Model

The transition of laminar to turbulent boundary layer can be estimated using the so-called *Prandtl-Schlichting skin friction formula for a smooth flat plate at zero incidence* [30, p. 439], presented below.

$$C_{f_{turb}} = \frac{0.455}{(\log_{10} R_e)^{2.58}} - \frac{A}{R_e} \quad (16-46)$$

**TABLE 16-4** Local and averaged turbulent skin friction coefficients.

Author	Formula	
<b>Local Coefficients</b>		
Prandtl-Schlichting (1932)	$C_{f_{turb}} = (2 \log_{10} R_{e_x} - 0.65)^{-2.3}$	(16.47)
Th. Von Kármán (1935)	$\frac{1}{\sqrt{C_{f_{turb}}}} = 4.15 \log_{10}(R_{e_x} C_{f_{turb}}) + 1.7$	(16.48)
Schultz-Grunow (1940)	$C_{f_{turb}} = 0.37 (\log_{10} R_{e_x})^{-2.584}$	(16.49)
Dhawan (1953)	$\frac{1}{\sqrt{C_{f_{turb}}}} = 5.06 \log_{10}(R_{e_x} C_{f_{turb}}) - 0.91$	(16.50)
ITTC (1957)	$C_{f_{turb}} = 0.075 \left( 1 - \frac{0.869}{\log_{10} R_{e_x} - 2} \right) (\log_{10} R_{e_x} - 2)^{-2}$	(16.51)
<b>Averaged Coefficients</b>		
Prandtl (1927)	$\bar{C}_{f_{turb}} = 0.074 R_e^{-1/5}$	(16.52)
Telfer (1927)	$\bar{C}_{f_{turb}} = 0.34 R_e^{-1/3} + 0.0012$	(16.53)
Schoenherr (1932)	$\bar{C}_{f_{turb}} = 0.0586 (\log_{10}(R_e \bar{C}_{f_{turb}}))^{-2}$	(16.54)
Schultz-Grunow (1940)	$\bar{C}_{f_{turb}} = 0.427 (\log_{10} R_e - 0.407)^{-2.64}$	(16.55)
Kempf-Karman (1951)	$\bar{C}_{f_{turb}} = 0.055 R_e^{-0.182}$	(16.56)
Lap-Troost (1952)	$\bar{C}_{f_{turb}} = 0.0648 \left( \log_{10}(R_e \sqrt{\bar{C}_{f_{turb}}}) - 0.9526 \right)^{-2}$	(16.57)
Landweber (1953)	$\bar{C}_{f_{turb}} = 0.0816 (\log_{10} R_e - 1.703)^{-2}$	(16.58)
Hughes (1954)	$\bar{C}_{f_{turb}} = 0.067 (\log_{10} R_e - 2)^{-2}$	(16.59)
Wieghardt (1955)	$\bar{C}_{f_{turb}} = 0.52 (\log_{10} R_e)^{-2.685}$	(16.60)
ITTC (1957)	$\bar{C}_{f_{turb}} = 0.075 (\log_{10} R_e - 2)^{-2}$	(16.61)
Gadd (1967)	$\bar{C}_{f_{turb}} = 0.0113 (\log_{10} R_e - 3.7)^{-1.15}$	(16.62)
Granville (1977)	$\bar{C}_{f_{turb}} = 0.0776 (\log_{10} R_e - 1.88)^{-2} + 60/R_e$	(16.63)
Date-Turnock (1999)	$\bar{C}_{f_{turb}} = (4.06 \log_{10}(R_e \bar{C}_{f_{turb}}) - 0.729)^{-2}$	(16.64)

Based on L.V. Lazauskas, *Hydrodynamics of Advanced High-Speed Sealift Vessels*, (Master's thesis), University of Adelaide, 2005; G.E. Gadd, *A new turbulent friction formulation based on a re-appraisal of Hughes' results*, Trans. RINA 109 (1967) 511–539; P.S. Granville, *The viscous resistance of surfaces vessels and the skin friction of flat plates*, Trans. SNAME 64 (1956) 209–240.

**TABLE 16-5** Transition parameters.

Condition	High turbulence (e.g., wind tunnels)	Low-turbulence (e.g., atmosphere)	
Critical $R_e$	$0.3 \times 10^6$	$0.6 \times 10^6$	$1.0 \times 10^6$
Constant A	1050	1700	3300

Where  $A$  is read from Table 16-5 and is selected based on the  $R_e$  at which transition is expected (critical  $R_e$ ).

### (17) Method 1: Mixed Laminar-Turbulent Flow Skin Friction by Surface Integration

If the distribution of pressure and shear stress over the surface of a body (e.g., an airfoil), is known, we can estimate the *normal and chordwise force per unit length* ( $f_n$  and  $f_c$ ) using the first two equations of Equation (8-20) (shown below for convenience)

$$\begin{aligned} f_n &= - \int_{LE}^{TE} (p_u \cos \theta_u + \tau_u \sin \theta_u) ds_u + \int_{LE}^{TE} (p_l \cos \theta_l - \tau_l \sin \theta_l) ds_l \\ f_c &= - \int_{LE}^{TE} (p_u \sin \theta_u - \tau_u \cos \theta_u) ds_u + \int_{LE}^{TE} (p_l \sin \theta_l + \tau_l \cos \theta_l) ds_l \end{aligned} \quad (16-65)$$

Where  $p_u, \tau_u$  and  $p_l, \tau_l$  are the pressure and viscous shear stress along the upper and lower surfaces, respectively.  $\theta_u$  and  $\theta_l$  are the angles between the tangent and the coordinate system on the upper and lower surfaces, respectively (see Figure 8-13). To obtain the lift and drag per unit length,  $f_n$  and  $f_c$  must be transformed using Equation (8-19).

In order to only extract the skin friction, we set all pressure terms to zero. For airfoil geometry, this largely sets the upper equation of Equation (16-65) to zero. Using Equation (16-34), the lower equation becomes

$$f_c = q_\infty \int_0^c (C_{f_u} + C_{f_l}) dx \quad (16-66)$$

Where  $C_{f_u}$  and  $C_{f_l}$  are the skin friction coefficients along the upper and lower surfaces. The estimate of  $f_c$  is per unit span (so area is  $c(1)=c$ ), the averaged skin friction coefficient becomes

$$\bar{C}_f = \frac{f_c}{qc} = \frac{1}{c} \int_0^c (C_{f_u} + C_{f_l}) dx \quad (16-67)$$

When applying Equation (16-66) to NLF airfoils, where the transition point is known to occur at  $x_{tr_u}$  on the upper surface and at  $x_{tr_l}$  on the lower one, the integrals are split up as follows

$$f_c = q_\infty \left[ \int_0^{x_{tr_u}} C_{f_{lam}} dx + \int_{x_{tr_u}}^c C_{f_{turb}} dx + \int_0^{x_{tr_l}} C_{f_{lam}} dx + \int_{x_{tr_l}}^c C_{f_{turb}} dx \right] \quad (16-68)$$

Then substitute this value into Equation (16-67).

### EXAMPLE 16-5

The flat plate airfoil of chord 1 m is operated at S-L at airspeed of 100 m/s. It develops laminar boundary layer over the first 25% of the chord and turbulent boundary layer over the remaining 75% of the chord, on both upper and lower surface. Estimate the airfoil's skin friction coefficient  $C_f$ . Assume the slope of both surfaces to be small enough to be considered parallel to the chord-line.  $\mu = 1.8 \times 10^{-5}$  Ns/m<sup>2</sup> and  $\rho = 1.225$  kg/m<sup>3</sup>.

#### SOLUTION:

Taking advantage of the symmetry of the problem, we get

$$\begin{aligned} \bar{C}_f &= \frac{1}{c} \left[ \int_0^{c_{xtr_u}} C_{f_{lam}} dx + \int_{c_{xtr_u}}^c C_{f_{turb}} dx + \int_0^{c_{xtr_l}} C_{f_{lam}} dx + \int_{c_{xtr_l}}^c C_{f_{turb}} dx \right] \\ &= \frac{2}{c} \left[ \int_0^{c_{xtr_u}} C_{f_{lam}} dx + \int_{c_{xtr_u}}^c C_{f_{turb}} dx \right] \\ &= \frac{2}{(1)} \left[ \int_0^{0.25} C_{f_{lam}} dx + \int_{0.25}^c C_{f_{turb}} dx \right] \\ &= 2 \left[ 0.664 \sqrt{\frac{\mu}{\rho V_\infty}} \int_0^{0.25} x^{-1/2} dx + 0.027 \left( \frac{\mu}{\rho V_\infty} \right)^{1/7} \int_{0.25}^c x^{-1/7} dx \right] \\ &\approx 0.0005091 \left[ 2x^{1/2} \right]_0^{0.25} + 0.005705 \left[ \frac{7}{6} x^{6/7} \right]_{0.25}^c = 0.005137 \end{aligned}$$

### (18) Method 2: Mixed Laminar-Turbulent Flow Skin Friction—Young's Method

Young [32, pp. 162–164] presents a two-step method to calculate the skin friction coefficient when the extent of the laminar flow is known. The first step requires the location of the *fictitious transition point*,  $x_0$  (see Figure 16-25) to be calculated:

$$\left( \frac{x_0}{c} \right) = 36.9 \times \left( \frac{x_{tr}}{c} \right)^{0.625} \left( \frac{1}{R_e} \right)^{0.375} \quad (16-69)$$

Then, the skin friction coefficient is determined as follows:

$$\bar{C}_{f_{mixed}} = \frac{0.074}{R_e^{0.2}} \left( 1 - \left( \frac{x_{tr} - x_0}{c} \right) \right)^{0.8} \quad (16-70)$$

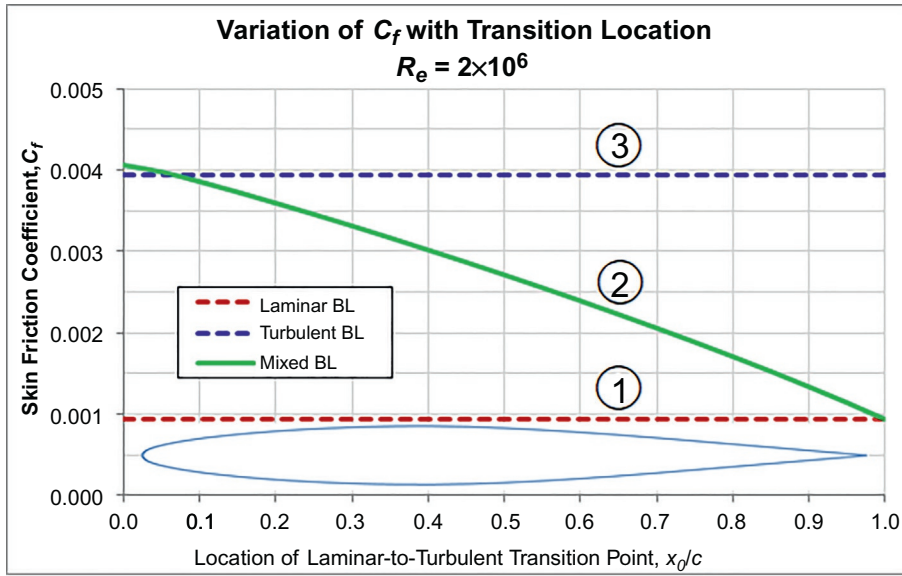


**FIGURE 16-29** Skin friction coefficient as a function of transition point calculated using fully laminar, turbulent, and mixed theory. ① is Equation (16-40), ② is Equation (16-70), and ③ is Equation (16-43).

It is evident its origin lies in Prandtl's expression of Equation (16-52). It is of interest to compare Equations (16-40), (16-43), and (16-70) as done in Figure 16-29. The first two are independent of transition location, whereas the mixed boundary layer methodology depends on  $x_{tr}$ . It is seen to deviate from Equation (16-43) when  $x_{tr}/c < 0.06$ . This is to be expected since the model is based on Prandtl's expression.

#### (19) Skin Friction Coefficient for Multisurface Components

The skin friction of any component consisting of several subcomponents can be estimated as follows:

Skin friction coefficient:

$$C_f = \frac{1}{S_{wet}} \sum_{i=1}^N C_{f_i} \times S_{wet_i} \quad (16-71)$$

Skin friction drag coefficient:

$$C_{Df} = \left( \frac{S_{wet}}{S} \right) C_f = \left( \frac{1}{S} \right) \sum_{i=1}^N C_{f_i} \times S_{wet_i} \quad (16-72)$$

Where  $C_{f_i}$  is the skin friction coefficient of subcomponent  $i$ ,  $S_{wet_i}$  is wetted area of subcomponent  $i$ ,  $S_{wet}$  is the total wetted area, and  $N$  is the number of subcomponents.

#### (20) Compute the Skin Friction Drag Force

The skin friction drag force acting on each subcomponent can be calculated by two means: (A) Based on their wetted area or (B) on the reference area,  $S$ :

Using the skin friction coefficient:

$$D_f = \frac{1}{2} \rho V^2 C_f S_{wet} \quad (16-73)$$

Using the skin friction drag coefficient:

$$D_f = \frac{1}{2} \rho V^2 C_{Df} S \quad (16-74)$$

#### (21) Step-by-Step: Procedure to Calculate Skin Friction for a Specific Component

This Step-by-Step presents how to calculate skin friction drag force for a specific component (e.g., a wing, HT, VT, etc.). It does not require form factors because these are used to account for the component's pressure drag.

##### *Step 1: Determine the Viscosity of Air*

Calculate  $\mu$  using Equations (16-24) or (16-25).

##### *Step 2: Determine Reynolds Number*

Calculate  $R_e$  using Equation (16-27).

##### *Step 3: Determine Cutoff Reynolds Number*

Calculate the  $R_{e_{cutoff}}$  for the surface. If smaller than  $R_e$  from Step 2, use it to determine the appropriate  $C_f$ .

##### *Step 4: Determine the Skin Friction Coefficient*

Select one of the previously discussed methodologies for calculating  $C_f$ . The most realistic options are (A) mixed boundary layer (bullets (17) and (18)) or (B) fully developed turbulent boundary layer (Bullet (14)). A fully developed laminar boundary layer is the aerodynamicist's folly. Calculate  $C_f$  per Equation (16-71).

##### *Step 5: Compute Skin Friction Drag Coefficient*

Calculate the skin friction drag coefficient,  $C_{Df}$ , per Equation (16-72).

##### *Step 6: Compute the Total Skin Friction Drag Force*

Calculate the total skin friction drag force for the component using Equation (16-73) or (16-74).

### EXAMPLE 16-6 SKIN FRICTION DRAG OF A WING

In this example, the skin friction drag of the SR22 wing will be estimated. The wing's pertinent dimensions are shown in [Figure 16-30](#), but these were obtained by scaling by the reported wing span of 38.3 ft. Assume a single NACA 65<sub>2</sub>-415 class airfoil, capable of sustaining a laminar boundary layer on the upper and lower surfaces as indicated in the figure. Assume the wing's wetted area is 7% greater than that of the shaded planform area shown.

Determine  $C_{Df}$  and  $D_f$  acting on the wing due to the mixed laminar and turbulent BL regions when the airplane is cruising at 185 KTAS at S-L ISA. Compare to a wing with fully laminar or fully turbulent BL.

**SOLUTION:**

Note that the solution below was calculated using the spreadsheet software Microsoft Excel. A reader repeating the calculations should expect slight difference from the numbers shown.

**Step 1: Determine the viscosity of air.**

Use Sutherland's formula to compute the viscosity assuming an OAT of 518.67 °R:

$$\begin{aligned}\mu &= 3.170 \times 10^{-11} T^{1.5} \left( \frac{734.7}{T + 216} \right) \\ &= 3.170 \times 10^{-11} (518.67)^{1.5} \left( \frac{734.7}{518.67 + 216} \right) \\ &= 3.745 \times 10^{-7} \text{ lb}_f \text{s}/\text{ft}^2\end{aligned}$$

**Step 2: Determine the Reynold's Number for Root Airfoil.**

Compute  $R_e$  for the root airfoil, using ISA density of 0.002378 slugs/ft<sup>3</sup> and an airspeed of 185 KTAS.

$$R_{e_1} = \frac{\rho V_\infty C_r}{\mu} = \frac{(0.002378)(185 \times 1.688)(4.88)}{3.745 \times 10^{-7}} = 9,667,562$$

**Step 3: Determine the Reynold's Number for Tip Airfoil.**  
Compute  $R_e$  for the tip airfoil:

$$R_{e_2} = \frac{\rho V_\infty C_t}{\mu} = \frac{(0.002378)(185 \times 1.688)(2.59)}{3.745 \times 10^{-7}} = 5,126,287$$

**Step 4: Fictitious Turbulent BL on Root Airfoil—Upper surface**

For the upper surface of the root airfoil (45% coverage), we get:

$$\begin{aligned}\left( \frac{x_0}{c_r} \right) &= 36.9 \times \left( \frac{x_{tr}}{c_r} \right)^{0.625} \left( \frac{1}{R_{e_1}} \right)^{0.375} \\ &= 36.9 \times (0.45)^{0.625} \left( \frac{1}{9,667,562} \right)^{0.375} = 0.05380\end{aligned}$$

**Step 5: Fictitious Turbulent BL on Root Airfoil—Lower surface**

For the lower surface of the root airfoil (45% coverage), we get the same value as on the upper surface:

$$(x_0/c_r) = 0.05380$$

**Step 6: Fictitious Turbulent BL on Tip Airfoil—Upper surface**

For the upper surface of the tip airfoil (60% coverage), we get the same value as on the lower surface:

$$\left( \frac{x_0}{c_t} \right) = 36.9 \times (0.60)^{0.625} \left( \frac{1}{5,126,287} \right)^{0.375} = 0.08169$$

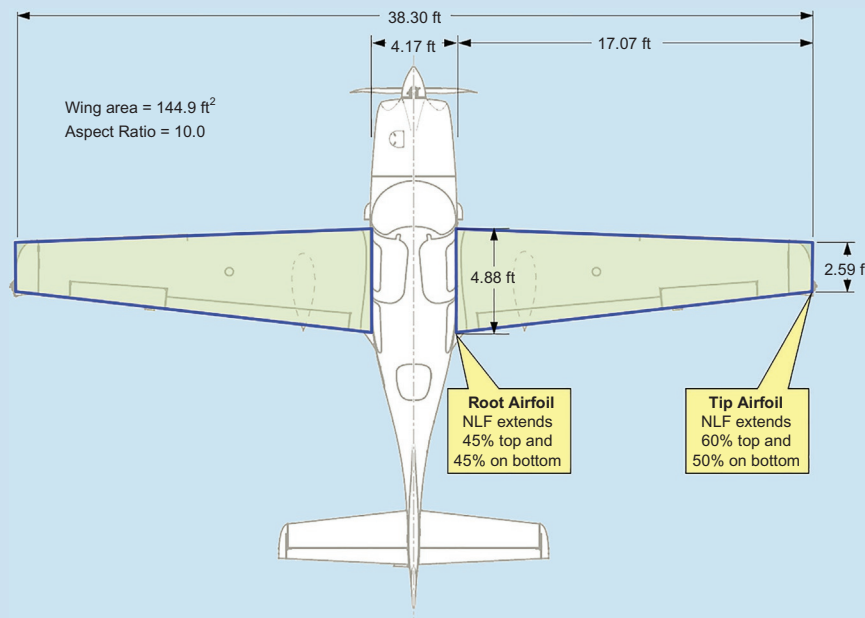


**FIGURE 16-30** Dimension resulting from scaling the top-view based on the wing span. Courtesy of Cirrus Aircraft. Copyright 2021 Cirrus Aircraft or its Affiliates. All Rights Reserved. Image reproduced with the permission of Cirrus.

**EXAMPLE 16-6**  
**SKIN FRICTION DRAG OF A WING (cont'd)**

**Step 7: Fictitious Turbulent BL on Tip Airfoil—Lower surface**

For the lower surface of the tip airfoil (50% coverage), we get:

$$\left(\frac{x_0}{c_t}\right) = 36.9 \times (0.50)^{0.625} \left(\frac{1}{5,126,287}\right)^{0.375} = 0.07290$$

**Step 8: Skin Friction for Root Airfoil—Upper surface**

For the upper surface of the root airfoil (45% coverage), we get:

$$\begin{aligned} \bar{C}_{f_{upper\ 1}} &= \frac{0.074}{R_{e1}^{0.2}} \left(1 - \left(\frac{x_{tr} - x_0}{c_r}\right)\right)^{0.8} \\ &= \frac{0.074}{9,667,562^{0.2}} (1 - (0.45 - 0.05380))^{0.8} = 0.001981 \end{aligned}$$

**Step 9: Skin Friction for Root Airfoil—Lower surface**

For the lower surface of the root airfoil (45% coverage), we get:

$$\bar{C}_{f_{lower\ 1}} = 0.001981$$

**Step 10: Average Skin Friction for Root Airfoil**

The average of the upper and lower surfaces of the root airfoil yields:

$$\bar{C}_{f_1} = \frac{1}{2}(0.001981 + 0.001981) = 0.001981$$

**Step 11: Skin Friction for Tip Airfoil—Upper surface**

For the upper surface of the tip airfoil (60% coverage), we get:

$$\begin{aligned} \bar{C}_{f_{upper\ 2}} &= \frac{0.074}{R_{e2}^{0.2}} \left(1 - \left(\frac{x_{tr} - x_0}{c_t}\right)\right)^{0.8} \\ &= \frac{0.074}{5,126,287^{0.2}} (1 - (0.60 - 0.08169))^{0.8} = 0.001877 \end{aligned}$$

**Step 12: Skin Friction for Tip Airfoil—Lower surface**

For the lower surface of the tip airfoil (50% coverage), we get:

$$\begin{aligned} \bar{C}_{f_{lower\ 2}} &= \frac{0.074}{R_{e2}^{0.2}} \left(1 - \left(\frac{x_{tr} - x_0}{c_t}\right)\right)^{0.8} \\ &= \frac{0.074}{5,126,287^{0.2}} (1 - (0.50 - 0.07290))^{0.8} = 0.002156 \end{aligned}$$

**Step 13: Average Skin Friction for Tip Airfoil**

The average of the upper and lower surfaces of the tip airfoil yields:

$$\bar{C}_{f_2} = \frac{1}{2}(0.001877 + 0.002156) = 0.002017$$

**Step 14: Average Skin Friction for Complete Wing**

The skin friction coefficient for the total wetted surface is simply the average of the average coefficients for both airfoils, i.e.:

$$\bar{C}_f = \frac{1}{2}(0.001981 + 0.002017) = 0.001999$$

**Step 15: Wing's Wetted Area**

The wing's total wetted area is:

$$S_{wet} = 2 \times 1.07 \times \left[\frac{1}{2}(4.88 + 2.59) \times (38.3 - 4.17)\right] = 272.8 \text{ ft}^2$$

**Step 16: Skin Friction Drag Coefficient for Complete Wing**

The wing's skin friction drag coefficient is:

$$C_{Df} = \left(\frac{S_{wet}}{S_{ref}}\right) \bar{C}_f = \left(\frac{272.8}{144.9}\right) (0.001999) = 0.003758$$

**Step 17: Skin Friction Drag Force for Complete Wing**

Estimate skin friction drag due to the mixed boundary layer.

$$\begin{aligned} D_f &= \frac{1}{2} \rho V^2 \times S_{wet} \times \bar{C}_f \\ &= \frac{1}{2} (0.002378) (185 \times 1.688)^2 (272.4) (0.001999) = 63.1 \text{ lb}_f \end{aligned}$$

This means that the total flat plate skin friction drag for the wing only of the SR22 at cruising speed amounts to 63 lb<sub>f</sub>. The contributions of interference with the fuselage and airfoil shape are not accounted for. It also omits drag due to the presence of control surfaces.

**Step 18: Skin friction coefficient for 100% Laminar Flow.**  
Laminar flow coefficient for the root:

$$\bar{C}_{flam} = \frac{1.328}{\sqrt{R_{e1}}} = \frac{1.328}{\sqrt{9,667,562}} = 0.0004271$$

Laminar flow coefficient for the tip:

$$\bar{C}_{flam} = \frac{1.328}{\sqrt{R_{e2}}} = \frac{1.328}{\sqrt{5,126,287}} = 0.0005865$$

Average for the wing:

$$\bar{C}_f = \frac{0.0004271 + 0.0005865}{2} = 0.0005068$$

**Step 19: Skin friction coefficient for 100% Turbulent Flow.**  
Turbulent flow coefficient for the root:

$$\bar{C}_{flurb} = \frac{0.455}{(\log_{10}(R_{e1}))^{2.58}} = \frac{0.455}{(\log_{10}(9,667,562))^{2.58}} = 0.003020$$

Turbulent flow coefficient for the tip:

$$\bar{C}_{flurb} = \frac{0.455}{(\log_{10}(R_{e2}))^{2.58}} = \frac{0.455}{(\log_{10}(5,126,287))^{2.58}} = 0.003350$$

Average for the wing:

$$\bar{C}_f = \frac{1}{2}(0.003020 + 0.003350) = 0.003185$$

**Step 20: Comparison.**

See [Table 16-6](#) for a comparison of the analysis techniques.

**EXAMPLE 16-6  
SKIN FRICTION DRAG OF A WING (cont'd)**

The comparison shows that were it possible to maintain laminar flow over the entire wing, its drag would be 25% of that predicted by the mixed boundary layer theory. Alternatively, if the wing sustained turbulent BL only, it would be almost 60% draggier than the NLF airfoils. It demonstrates the value of employing such airfoils.

**TABLE 16-6** Comparing skin friction analysis methods.

Method	$C_f$	Comparison
Fully Laminar BL	0.0005068	25%
Fully Turbulent BL	0.003185	159%
Mixed BL	0.001999	100%

**EXAMPLE 16-7  
TOTAL SKIN FRICTION OF A MULTIPANEL WING**

Figure 16-31 shows a half-span of a three section Schuemann wing. The skin friction coefficient for each section has been determined and is tabulated with the corresponding planform areas. If operating at 100 KCAS, estimate the following: (a) Total skin friction coefficient, (b) total skin friction drag coefficient, (c) skin friction drag force for individual surfaces, and (d) skin friction drag. Use the wing area as the reference area ( $S$ ) and assume its wetted area amounts to 2S times a wetted area booster factor,  $K_b$ , of 1.1.

**SOLUTION:**

(a) Assemble Table 16-7 as shown (where  $S_{wet_i} = 2K_b S_i$ ). Thus, the wetted area for panel ① is given by  $S_{wet_1} = 2K_b S_1 = 2(1.1)(35.0) = 77.0 \text{ ft}^2$ . Multiplying this by  $C_{f1} = 0.0050$  and  $q = \frac{1}{2}\rho V_\infty^2 = \frac{1}{2}(0.002378)(100 \times 1.688)^2 = 33.88 \text{ lb}_f/\text{ft}^2$  yields the other two columns. Complete similar calculations for the other two rows. Next, the three rightmost columns summed. Note that these apply to only one of the two wing halves.

The total skin friction coefficient can be found by the weighted contribution from each panel:

$$\begin{aligned} \bar{C}_f &= \frac{\sum_{i=1}^N C_{fi} \times S_{wet_i}}{S_{wet}} \\ &= \frac{77.0 \times 0.0050 + 69.3 \times 0.0055 + 46.2 \times 0.0065}{77.0 + 69.3 + 46.2} \\ &= \frac{1.100}{192.5} = 0.00554 \end{aligned}$$

**TABLE 16-7** Comparing skin friction analysis methods.

	$S_i$	$C_{fi}$	$S_{wet_i}$	$S_{wet_i} \cdot C_{fi}$	$q \cdot S_{wet_i} \cdot C_{fi}$
Part ①	35.0	0.0050	77.0	0.3850	13.04
Part ②	31.5	0.0055	69.3	0.3812	12.91
Part ③	21.0	0.0065	46.2	0.3003	10.17
<b>TOTALS:</b>			<b>192.5</b>	<b>1.1</b>	<b>36.1</b>

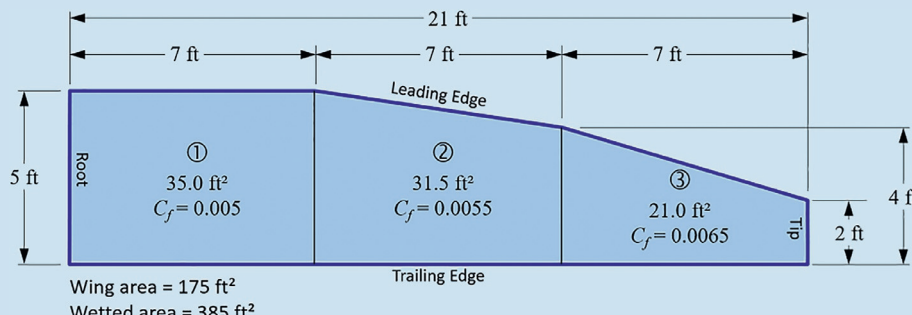


**FIGURE 16-31** The multipanel wing used in this example.

**EXAMPLE 16-7**  
**TOTAL SKIN FRICTION OF A MULTIPANEL WING (cont'd)**

This is the averaged skin friction coefficient for the wing.

(b) The total skin friction drag coefficient is always based on the reference area, which here is  $S = 175 \text{ ft}^2$ :

$$C_{Df} = \frac{S_{wet}}{S} C_f = \frac{385}{175} \times 0.00554 = 0.01219$$

This amounts to 121.9 dragcounts.

(c) And (d) since the skin friction coefficient differs from one panel to the next, the drag force on each surface must be determined using the wetted area of the individual surface per Equation (16-73):

$$D_f = \frac{1}{2} \rho V^2 C_{fi} S_{wet,i} = q C_{fi} S_{wet,i}$$

The total skin friction drag generated by both wing halves is the sum of the individual contributions:

$$\begin{aligned} D_f &= 2 \times q \sum_{i=1}^3 C_{fi} S_{wet,i} = 2 \times (33.88)[(0.0050)(77.0) \\ &\quad + (0.0055)(69.3) + (0.0065)(46.2)] \\ &= 2 \times (33.88)[0.3850 + 0.3812 + 0.3003] = 72.3 \text{ lb}_f \end{aligned}$$

or:  $D_f = \frac{1}{2} \rho V^2 C_f S_{wet} = (33.88)(0.00554)(385) = 72.3 \text{ lb}_f$

or:  $D_f = \frac{1}{2} \rho V^2 C_{Df} S_{ref} = (33.88)(0.01219)(175) = 72.3 \text{ lb}_f$

We can also calculate the skin friction drag coefficient,  $C_{Df,i}$ , for each panel for each wing half (assuming only half of the reference wing area) as shown below. Note the results are presented in Table 16-8:

$$\begin{aligned} C_{Df_1} &= \frac{C_{f1} \cdot S_{wet,1}}{S_{ref}} = \frac{0.0050 \cdot 77.0}{(175/2)} = 0.004400 \\ C_{Df_2} &= \frac{C_{f2} \cdot S_{wet,2}}{S_{ref}} = \frac{0.0055 \cdot 69.3}{(175/2)} = 0.004356 \\ C_{Df_3} &= \frac{C_{f3} \cdot S_{wet,3}}{S_{ref}} = \frac{0.0065 \cdot 46.2}{(175/2)} = 0.003432 \end{aligned}$$

**TABLE 16-8** Total skin friction of the multipanel wing.

	$S_i$	$C_{fi}$	$S_{wet,i}$	$q \cdot S_{wet,i} \cdot C_{fi}$	$C_{Df,i}$
Part ①	35.0	0.0050	77.0	0.3850	0.004400
Part ②	31.5	0.0055	69.3	0.3812	0.004356
Part ③	21.0	0.0065	46.2	0.3003	0.003432
TOTALS:	192.5	1.1	36.1	0.01219	

### 16.3.2 Estimating Lift-Induced Drag: $C_{D_i}$

Consider a finite wing featuring a single airfoil at some specific AOA and airspeed. Contrast that with a straight wing segment featuring exactly the same airfoil, extending from wall-to-wall in a wind tunnel, at the same AOA and airspeed. The finite wing generates less lift per unit span than the one in the wind tunnel. It does so because the air must flow around its wingtips, which it does through the formation of *wingtip vortices*. Their presence absorbs a fraction of the energy present in the airflow, leaving less available for lift generation. Thus, the finite wing must be placed at a higher AOA to generate the same amount of lift as the wing in the wind tunnel. This process increases the drag of the finite wing beyond that attributed to the airfoil only. This additional drag is called a *lift-induced*, or *induced*, or *vortex* drag and is denoted by  $D_i$ . As usual the standard formulation of this drag involves the determination of a *lift-induced drag coefficient*. A number of methods to determine this drag coefficient are presented below. The lift induced drag is a pressure drag force.

#### (1) Method 1: Lift-Induced Drag from the Momentum Theorem

Familiarity with Section 8.1.9, *The Generation of Lift* is an essential preparation for this section. Consider Equation (8-27), repeated below for convenience. It expresses the average downwash ( $w$ ) behind the wing in terms of lift coefficient ( $C_L$ ), aspect ratio ( $AR$ ), and airspeed ( $V_\infty$ ):

$$w = \frac{2C_L}{\pi AR} V_\infty \quad (16-75)$$

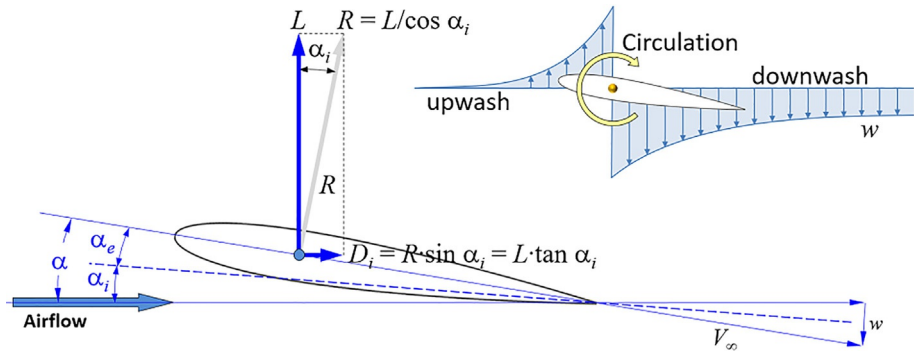
This is shown in Figure 16-32. The circulation introduces an upwash and downwash into the flow around the airfoil. The downwash is compounded by the contribution from the wingtip vortices. This reduces the *geometric AOA* ( $\alpha$ ) by an amount called the *induced AOA* ( $\alpha_i$ ). It amounts to half the theoretical downwash angle, given by  $w/V$ . The difference between the two is the *effective AOA* ( $\alpha_e$ ). Mathematically, the relation between  $w/V$  and  $\alpha_i$  is given by

$$\frac{w}{V_\infty} = \frac{2C_L}{\pi AR} = 2\alpha_i \quad (16-76)$$

Using small angle relations, the induced AOA is found from

$$\alpha_i \approx \tan \alpha_i = \frac{1}{2} \frac{w}{V_\infty} = \frac{C_L}{\pi AR} \quad (16-77)$$

**FIGURE 16-32** A schematic showing how the induced drag is a component of the lift force.



Referring to Figure 16-32, we see that the presence of the induced AOA effectively tilts the lift force back by the amount  $\alpha_i$ . In the process, an additional force component,  $D_i$ , is developed. This is the *lift-induced drag*. It is calculated as shown in the figure.

$$D_i = R \sin \alpha_i = \frac{L}{\cos \alpha_i} \sin \alpha_i = L \tan \alpha_i \quad (16-78)$$

In coefficient form, this becomes:

$$C_{D_i} = C_L \tan \alpha_i = C_L \left( \frac{C_L}{\pi AR} \right) = \frac{C_L^2}{\pi AR} \quad (16-79)$$

The above derivation assumes an elliptical lift distribution or, alternatively, the distribution of constant spanwise section lift coefficients<sup>4</sup> ( $C_l$ ). As shown in Chapter 9, *The Anatomy of the Wing*, this requires an elliptical planform. However, most wing planforms are not elliptical and, consequently, the distribution of section lift coefficients is not constant. This is corrected through *span efficiency*, discussed in Section 9.5.12, *Determination of Span Efficiency*.

The following representation of the lift-induced drag is of importance from an aircraft design standpoint. Using Equation (16-79) to determine induced drag leads to

$$D_i = qS \left( \frac{C_L^2}{\pi AR} \right) = qS \left( \frac{(W/qS)^2}{\pi(b^2/S)} \right) = qS \left( \frac{W^2 S}{\pi b^2 q^2 S^2} \right) = \frac{W^2}{\pi b^2 q} \quad (16-80)$$

Where  $b$  is wing span,  $S$  is wing area,  $q$  is dynamic pressure, and  $W$  is weight. The result shows that the lift-induced drag force depends on the wing span rather than wing area. Thus, only a span increase reduces the drag. Reducing chord to increase  $AR$  will not help.

## (2) Method 2: Generic Formulation of the Lift-Induced Drag Coefficient

A generic formulation of wing characteristics is presented in Ref. [48], based on the work of Glauert [49]

and Hueber [50]. It allows several wing characteristics associated with tapered wings to be evaluated, with and without rounded wingtips (popular when it was written). It presents the following formulation for  $C_{D_i}$

$$C_{D_i} = \frac{2}{S} \int_0^{b/2} \alpha_i \cdot C_l \cdot c \cdot dy = \frac{2}{S} \int_0^{b/2} \left( \alpha - \frac{C_l}{C_{l_a}} \right) \cdot C_l \cdot c \cdot dy \quad (16-81)$$

Where  $c$  is wing chord and  $y$  is spanwise location along the half-span. A more general version of this expression, which treats asymmetric wing loading, is presented below:

$$C_{D_i} = \frac{1}{S} \int_{-b/2}^{b/2} \alpha_i \cdot C_l \cdot c \cdot dy \quad (16-82)$$

## DERIVATION OF EQUATION (16-81)

The effective lift coefficient can be calculated as  $C_l = C_{l_a} C_{l_a} \alpha_e = C_{l_a} (\alpha - \alpha_i)$ . Thus,  $\alpha_i$  at any section along the wing can be computed based on section lift coefficients,  $C_l$ , and section lift curve slopes,  $C_{l_a}$ :

$$\alpha_i = \alpha - C_l / C_{l_a} \quad (16-83)$$

Using small angle relations, the induced drag of the airfoil section can be computed from:

$$C_{d_i} = \alpha_i C_l = (\alpha - C_l / C_{l_a}) C_l = (\alpha C_l - C_l^2 / C_{l_a}) \quad (16-84)$$

The total lift-induced drag for the wing is the sum of the weighted contribution of all the sections, extending from tip-to-tip, or:

$$C_{D_i} = \frac{2}{S} \int_0^{b/2} C_{d_i} \cdot c \cdot dy \quad (16-85)$$

The weighted form is necessary as the planform shape is may be changing or affected by washout. Thus, multiplying it with the chord,  $c$ , inserting the result from Equation (16-84) and manipulate will yield Equation (16-81).

<sup>4</sup> Also refer to the derivation of Equation (9-162) using the lifting-line theory.

### EXAMPLE 16-8

Estimate the induced drag coefficient for a Hershey bar wing for which wing area, span, and chord are given by,  $S=145 \text{ ft}^2$ ,  $b=38 \text{ ft}$ , and  $c=4 \text{ ft}$ , respectively. The wing is operating at  $\alpha=5^\circ=0.08727 \text{ rad}$ . The spanwise distribution of section lift coefficients is approximated by  $C_l=0.5\cdot\cos(\pi y/b)$  (yes, it is just an approximation), as shown in Figure 16-33. The wing features an airfoil whose  $C_{l_a}=5.730$  per radian and is untwisted.

#### SOLUTION:

Solution is obtained by evaluating the integral of the distribution of the section lift coefficients along the half-span of the aircraft per Equation (16-81):

$$\begin{aligned} C_{D_i} &= \frac{2}{S} \int_0^{b/2} \left( \alpha - \frac{C_l}{C_{l_a}} \right) \cdot C_l \cdot c \cdot dy \\ &\approx \frac{2}{145} \int_0^{38/2} \left( 0.08727 - \frac{0.5\cos\left(\frac{\pi y}{38}\right)}{5.730} \right) \left( 0.5\cos\left(\frac{\pi y}{38}\right) \right) (4) dy \\ &\approx \frac{4}{145} \int_0^{38/2} \left( 0.08727 - 0.08726\cos\left(\frac{\pi y}{38}\right) \right) \cos\left(\frac{\pi y}{38}\right) dy \\ &\approx 0.006251 \end{aligned}$$

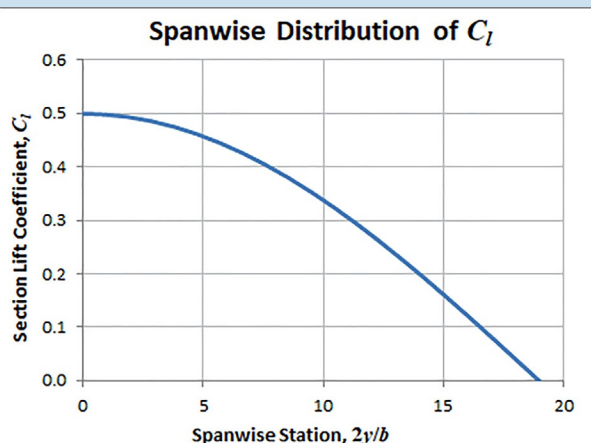


FIGURE 16-33 Spanwise distribution of section lift coefficients.

### (3) Method 3: Simplified $k \cdot C_L^2$ Method

This is the simplest representation of lift-induced drag. As has already been demonstrated, is derived directly from the momentum theorem, or by using the lifting-line theory presented in Section 9.7, *Prandtl's Lifting-Line Theory*.

$$C_{D_i} = \frac{C_L^2}{\pi \cdot AR \cdot e} = k \cdot C_L^2 \quad (16-86)$$

Where  $e$  is Oswald's efficiency and  $k$  is the lift-induced drag constant. Methods to estimate  $e$  are presented in Section 9.5.12, *Determination of Span Efficiency*. Also see Method 5 below. Note an important dependency of the induced drag coefficient on wing area,  $S$ , and wing span,  $b$ :

$$C_{D_i} = \frac{C_L^2}{\pi \cdot AR \cdot e} = \left( \frac{S}{b^2} \right) \frac{C_L^2}{\pi \cdot e} \quad (16-87)$$

Like Equation (16-80), this reinforces the importance of wing span on induced drag.

### (4) Method 4: Adjusted $k \cdot (C_L - C_{L_{minD}})^2$ Method

As already discussed, the adjusted drag model provides far superior estimate of lift-induced drag than the simplified model. This model is presented below:

$$C_{D_i} = \frac{(C_L - C_{L_{minD}})^2}{\pi \cdot AR \cdot e} = k \cdot (C_L - C_{L_{minD}})^2 \quad (16-88)$$

Where  $C_{L_{minD}}$  is the lift coefficient of minimum drag.

### (5) Method 5: Lift-Induced Drag Using the Lifting-Line Theory

To determine the lift-induced drag constant,  $k$ , numerical methods such as the lifting-line or vortex-lattice methods may be used. Of the two, the former, presented in Section 9.7, *Prandtl's Lifting-Line Theory*, is relatively easy to apply, although it requires a matrix solver to calculate the constants of simultaneous linear equations. These are used to evaluate a special constant, called the *lift-induced drag factor*, denoted by the Greek letter  $\delta$ . Once known, the lift-induced drag coefficient is calculated from:

$$\text{Simplified drag model: } C_{D_i} = \frac{C_L^2}{\pi \cdot AR} (1 + \delta) \quad (16-89)$$

$$\text{Adjusted drag model: } C_{D_i} = \frac{(C_L - C_{L_{minD}})^2}{\pi \cdot AR} (1 + \delta) \quad (16-90)$$

Note that these underestimate  $C_{D_i}$  and must be corrected per Section 9.5.12, *Determination of Span Efficiency*. Figure 9-75 shows the variation of the lift-induced drag factor,  $\delta$ , for a range of taper ratios,  $\lambda$ , and aspect ratios,  $AR$ , as calculated by the lifting-line method. A code snippet, using Visual Basic for Applications, is also presented in Section 9.7.4, *Computer Code: Prandtl's Lifting-Line Method*, allowing the reader to determine the factor using Microsoft Excel. Note that the Oswald's span efficiency,  $e$ , is related to the lift-induced drag factor per Equations (9-127) and (9-128), repeated below for convenience.

$$e = e_{theo} \cdot k_{corr_1} \cdot k_{corr_2} \cdot \dots = \left( \frac{1}{1 + \delta} \right) \cdot k_{corr_1} \cdot k_{corr_2} \cdot \dots \quad (9-127)$$

### EXAMPLE 16-9

An aircraft featuring an  $AR=10$  and a  $\lambda=0.5$  is flying at a condition that generates a  $C_L=0.5$ . Determine the lift-induced drag coefficient using Figure 9-75. For this example, assume  $C_{L_{\min D}}=0$ .

#### SOLUTION:

Figure 9-75 shows that  $\delta \approx 0.022$ . This means that the lift-induced drag coefficient can be determined as follows:

$$C_{D_i} = \frac{C_L^2}{\pi \cdot AR} (1 + \delta) = \frac{0.5^2}{\pi \cdot (10)} (1 + 0.022) = 0.008133$$

This value is 2.2% higher than that for an elliptical wing of the same  $AR$ .

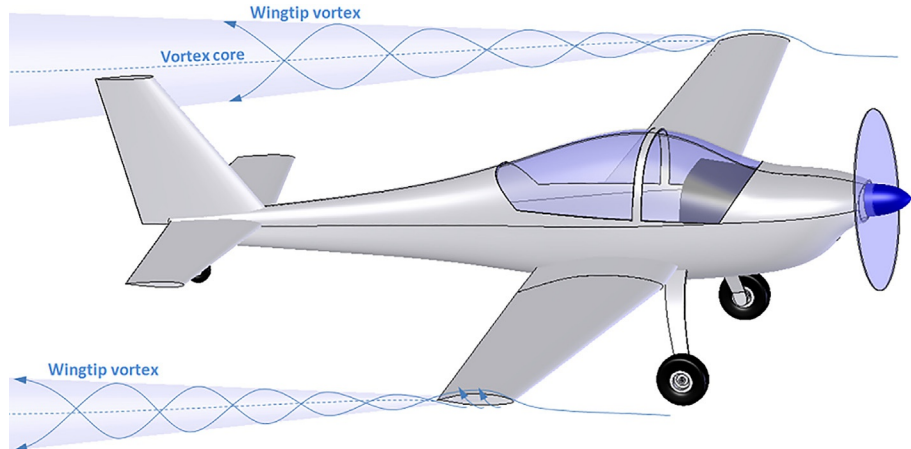
### (6) Method 6: Prandtl-Betz integration in the Trefftz<sup>5</sup> plane

This method was developed by Ludwig Prandtl (1875–1953) and Albert Betz (1885–1968) around the year 1918. The method computes the induced drag of a wing based on disturbance it inflicts on the fluid flow in the far-field. By evaluating the disturbances in a plane, placed infinitely behind the wing (the *Trefftz plane*), the velocity component in the  $x$ -direction (denoted by  $u$ ) can be eliminated from the integration. This way, a volumetric integration can be reduced to a surface integration.

$$D_i = \frac{\rho}{2} \iint_{\text{Trefftz Plane}} (v^2 + w^2) dS \quad (16-91)$$

The method is in computational fluid dynamics (CFD) methods, such as the vortex-lattice method and is

**FIGURE 16-34** Pressure difference between the upper and lower surfaces forms the wingtip vortex.



<sup>5</sup> Named after the German mathematician Erich Trefftz (1888–1937).

primarily presented here for completeness. It requires  $v$  and  $w$  to be obtained using the concept of *velocity potential*.

### (7) Correcting the Lift-Induced Drag

There may be reasons to consider several of the following corrections to the lift-induced drag estimate.

#### Wingtip Correction

In addition to the effect of  $AR$  and  $\lambda$ , the lift-induced drag is also affected by the wingtip geometry (see Section 10.5, *Wingtip Design*). It is usually assumed that the distance between the core of the two wingtip vortices equals that of the wingspan. However, the wingtip affects the roll-up of the vortices (see Figure 16-34). The wingtip geometry modifies the 3-dimensional flow field, shifting the wingtip vortices inboard or outboard. The separation changes the effective  $AR$  of the wing (see Equation 10-4).

Hoerner [33, pp. 7–5] presents this effect due to several wingtips (see Figure 16-35). The terms  $\Delta AR$  are values that should be added to correct the geometric  $AR$ . The resulting value, denoted by  $AR_{corr}$ , is then used when calculating lift-induced drag,  $C_{D_i}$ . For instance, consider a wing whose  $AR=7$ . The selection of a round frontal view and round top view shows a  $\Delta AR=-0.20$ . Therefore, the  $AR$  to use with Equations (16-86) and (16-88) would be 6.8 and not 7. Generally, the figure shows that rounded tips reduce the effectiveness of the wing—it is simply better to feature a square rectangular tip. It is cheaper too. Other wingtips are presented in Section 10.5, *Wingtip Design*.

The effect of how the wingtip shape influences the lift-induced drag is based on how air flows around the wingtip. Three examples are shown in Figure 16-36. The top wingtip shape is round. It allows air to flow to the upper surfaces such the vortex core resides inside and on top of

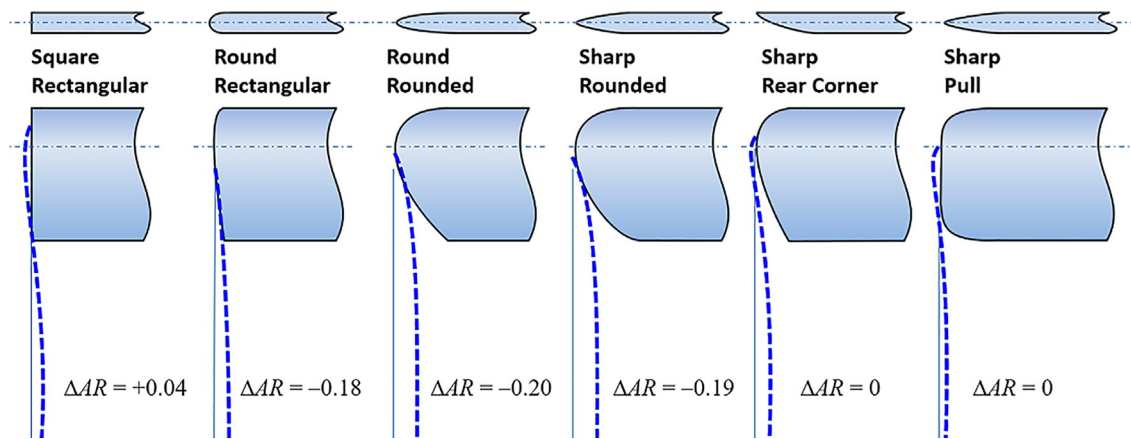


**FIGURE 16-35** Effect of several types of wingtips on the separation of the cores of the wingtip vortices. Tested at  $R_e = 10^6$  and  $AR = 3$ . Reproduced from S.F. Hoerner, *Fluid-Dynamic Drag*, L. Hoerner, 1965.

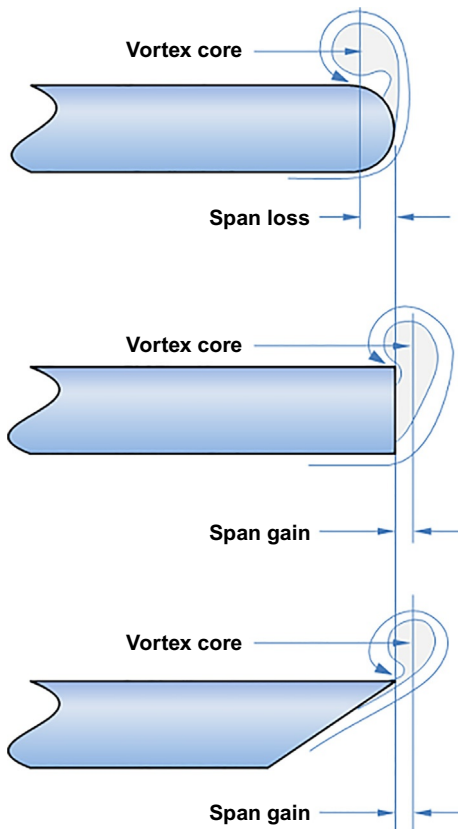


**FIGURE 16-36** Location of vortex core for three different wingtip shapes.

the wingtip. This results in a wingtip vortex that is closer to the plane of symmetry than the physical wingtip, effectively reducing the wingspan. The center wingtip is square. It forces the spanwise flow component of the lower surface to make the turn around a very sharp corner. This forces the vortex core to reside farther away from the plane-of-symmetry than the actual wing span—it increases the effective wingspan, albeit by a fraction. The bottom wingtip is representative of the so-called Hoerner wingtip. It promotes spanwise flow outboard

and upward that is forced to make a turn around a sharp corner.

This forces the vortex core to reside even farther outboard than the square wingtip in the middle. This idea is extended to the so-called upturned or downturned booster wingtip that helps placing the vortex such that a small effective wingspan increase is achieved, although this is not always realized in practice.

#### Correction of Lift-Induced Drag in Ground Effect

As shown in [Section 9.5.11, Ground Effect](#), the lift-induced drag is reduced when the aircraft is operated close to the ground. This fact should be taken into account during T-O and landing analysis. The effect is favorable during the T-O ground run as the total drag of the airplane is reduced. It is unfavorable during the landing ground roll, for the same reason. Use any of the methods in the section to correct the lift-induced drag based on the height if the MGC above the ground.

#### Correcting Lift-Induced Drag due to Wing Washout

Horner suggest the following correction for lift-induced drag of a wing due to wing washout. It was shown in [Chapter 9, The Anatomy of the Wing](#) how the lift distribution is altered as wing twist is introduced. This can lead to an appreciable lift-induced drag, even when the wing is at an AOA for which no lift is generated.

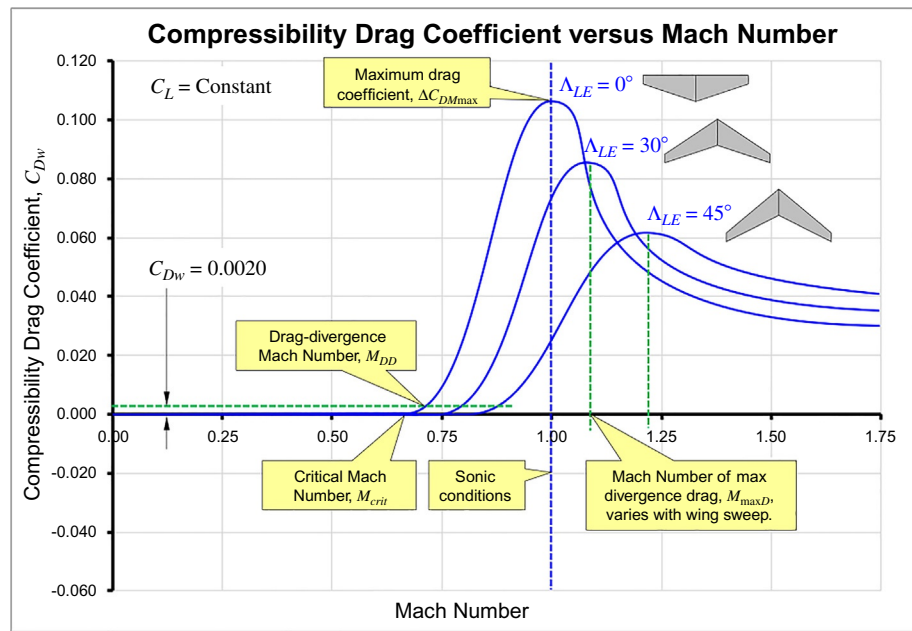
$$\Delta C_{D_{i\phi}} = 0.00004 (\phi_{tip} - \phi_{MGC}) = 0.00004 \cdot \Delta\phi \quad (16-92)$$

Where  $\phi_{tip}$  is the angle of the tip and  $\phi_{MGC}$  is the angle of the MGC, both with respect to the root of the wing and both in degrees.

#### 16.3.3 Estimating Wave Drag: $C_{D_w}$

Familiarity with [Section 8.3.8, The Effect of Compressibility](#) is an essential preparation for this section. The lift, drag, and moment of a body operating at a fixed  $\alpha$  changes rapidly as it approaches the speed of sound. This

**FIGURE 16-37** The effect of compressibility on drag. Based on R. Whitford, *Design for Air Combat*, Jane's Publishing Company Limited, 1987; E. Torenbeek, *Synthesis of Subsonic Aircraft Design*, Delft University Press, 1986.



change is called *compressibility effect*. Its onset begins at a specific airspeed called the *critical Mach number*,  $M_{crit}$ , defined in Bullet (3) of Section 8.3.8. It is driven by the formation of a normal shock that separates the flow on the aft part of an airfoil (e.g., see Figure 8-47). It can form in more than one place on an aircraft. The drag increase, called *wave drag*, is denoted by  $C_{dw}$  for 2D bodies and  $C_{Dw}$  for 3D bodies. An airplane with thick airfoils will experience it perhaps as early as  $M=0.6$ , whereas a sleek high-performance jetliner begins to experience it at  $M\approx 0.80$ . The Mach number at which this happens is the *drag-divergence Mach number*. Figure 16-37 shows a hypothetical scenario in which an airplane flying at a constant  $C_L$  experiences a sharp rise in the compressible drag coefficient near  $M=0.7$ . It further illustrates how  $M_{crit}$ ,  $M_{DD}$ , and  $M_{maxD}$  are affected by wing sweep.

### (1) Wing Drag Divergence Mach Number, $M_{DD}$

An introduction to *drag divergence* and *drag divergence Mach number* of airfoils is provided in Section 8.3.8. Thus, this section focuses only on wings. For wings,  $M_{DD}$  ranges from 1.02 to  $1.04M_{crit}$ , depending on wing sweep [51]. Drag divergence refers to the sudden rise of drag soon after  $M_{crit}$  is reached (see Figure 16-37). There are two common definitions used to establish when this happens: one is attributed to Boeing, the other to Douglas (see Figure 8-67 for graphical representation) [52]:

Boeing definition:  $M_{DD} = M_\infty$  when  $C_{Dw} = +0.002$  (16-93)

Douglas definition:  $M_{DD} = M_\infty$  when  $dC_{Dw}/dM = 0.10$  (16-94)

### (2) Simple Sweep Theory

Consider the swept wing in Figure 16-38. The *simple sweep theory* contends that, at transonic speeds, the component of the airspeed normal to the line-of-sweep ( $V_N$ ) dictates when shock begins to form. The far-field airspeed ( $V_\infty$ ) is broken into two components:  $V_P$  and  $V_N$  (see Figure 16-38); the acute angle is denoted by  $\Lambda_{eff}$ . The literature is surprisingly lax in what constitutes sweep angle. Authors tend to use one of the following: (1) Leading-edge sweep [53, 54] (2) quarter-chord sweep (e.g., Refs. [53, 55–58]), (3) mid-chord sweep (e.g., Refs. [53, 59, 60]), and (4) the angle of the normal-shock front along the span—which may be close to the mid-chord sweep (e.g., Refs. [61, 62]). In this text,  $\Lambda_{eff}$  is the sweep of the mid-chord, unless the weighted average of the shock-front is known (see Figure 16-38). If so, it is used based on [62]. The basic results of simple sweep theory follow:

$$V_N = V_\infty \cos \Lambda_{eff} \quad (16-95)$$

$$C_{L_N} = C_{L_\infty} / \cos^2 \Lambda_{eff} \quad (16-96)$$

$$V_P = V_\infty \sin \Lambda_{eff} \quad (16-97)$$

$$C_{D_N} = C_{D_\infty} / \cos^3 \Lambda_{eff} \quad (16-98)$$

$$M_N = M_\infty \cos \Lambda_{eff} \quad (16-99)$$

$$(t/c)_N = (t/c)_\infty / \cos \Lambda_{eff} \quad (16-100)$$

$$(M_N)_{crit} = (M_\infty)_{crit} \cos \Lambda_{eff} \quad (16-101)$$

$$C_{p_N} = C_{p_\infty} / \cos^2 \Lambda_{eff} \quad (16-102)$$

$$q_N = q_\infty \cos^2 \Lambda_{eff} \quad (16-103)$$

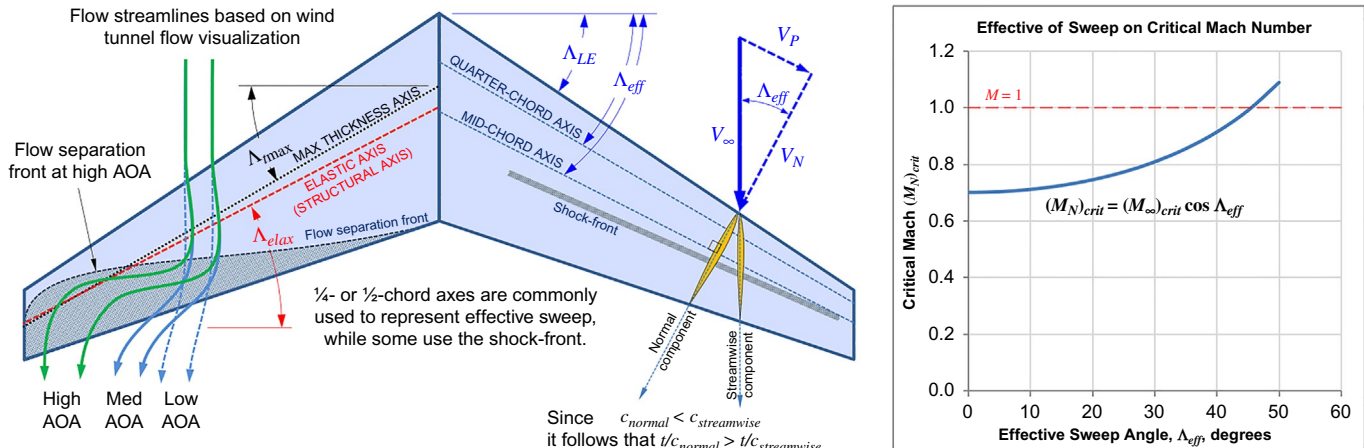


**FIGURE 16-38** The deconstruction of the far-field airspeed into a normal (N) and parallel (P) components (left). Note the flow-separation front (left). The effect of sweeping the effective critical Mach number (right).

### (3) The Korn Relation for Swept Wings

The *Korn relation*<sup>6</sup> was introduced in Section 8.3.8 as  $M_{dd} = \kappa - t/c - 0.1C_{ld}$ , where  $M_{dd}$  is the drag-divergence Mach number for an airfoil with thickness ratio  $t/c$  at a specific lift coefficient ( $C_{ld}$ ). This simple empirical expression permits Mach-versus-lift trades to be conducted for airfoils [62]. Using the simple sweep theory, it can be adapted to swept wings as follows [59, 62, 63]:

$$M_{DD} \cos \Lambda_{eff} = \kappa - \frac{t/c}{\cos \Lambda_{eff}} - \frac{C_{Lc}}{10 \cos^2 \Lambda_{eff}} \quad (16-104)$$

Where  $C_{Lc}$  = design lift coefficient and  $\kappa$  = airfoil class constant, obtained using airfoil specific CFD analyses. Refer to the above references for details. In the absence of such work, use  $\kappa = 0.87$  for conventional airfoils and 0.95 for NASA-style supercritical airfoils. The  $C_{Lc}$  for typical commercial jetliners ranges between  $0.4 < C_{Lc} < 0.7$ , depending on weight and altitude.  $M_{DD}$  is obtained from Equation (16-104) as follows:

$$M_{DD} = \frac{\kappa}{\cos \Lambda_{eff}} - \frac{t/c}{\cos^2 \Lambda_{eff}} - \frac{C_{Lc}}{10 \cos^3 \Lambda_{eff}} \quad (16-105)$$

In short, too little wing sweep and  $M_{DD}$  will be low. Too much and structural weight increases and exceeds the benefits of the higher  $M_{DD}$  [60]. Thus, a compromise in the sweep angle selection is necessary. It is also possible to apply the *Korn relation* to identify limits on  $M_{crit}$  for selected airfoils as follows:

$$M_{crit} = \frac{\kappa}{\cos \Lambda_{eff}} - \frac{t/c}{\cos^2 \Lambda_{eff}} - \frac{C_{Lc}}{10 \cos^3 \Lambda_{eff}} - 0.1077 \quad (16-106)$$

The coefficient  $-0.1077$  is derived in Ref. [60]. These expressions allow wave drag to be estimated.

### (4) Mason's Optimum Sweep Angle

By solving for  $C_{Lc}$  in Equation (16-105), Mason [59] showed that, in terms of  $M_{DD}$ , the optimum (mid-chord) sweep angle for a long-range transonic transport is given by:

$$\Lambda_{opt} = \cos^{-1} \left\{ \frac{\kappa}{3M_{DD}} + \sqrt{\left( \frac{\kappa}{3M_{DD}} \right)^2 - \left( \frac{t/c}{3M_{DD}} \right)} \right\} \quad (16-107)$$

This expression yields  $\Lambda_{opt} \approx 44$  degrees, for an Airbus 320/Boeing 737 class aircraft, for which  $t/c = 0.12$ ,  $\kappa = 0.95$ , and assuming  $M_{DD} = 0.80$ . Both aircraft have a quarter-chord sweep of 25 degrees [64]. Wing design for commercial jets considers other factors too.

### DERIVATION OF EQUATION (16-107)

Differentiate the  $C_{Lc}$  obtained from Equation (16-105) with respect to sweep angle and set to zero

$$\begin{aligned} \frac{dC_{Lc}}{d\Lambda} &= \frac{d}{d\Lambda} [10\kappa \cos^2(\Lambda) - 10(t/c) \cos \Lambda - 10M_{DD} \cos^3 \Lambda] \\ &= 10 \sin \Lambda [(t/c) - 2\kappa \cos \Lambda + 3M_{DD} \cos^2 \Lambda] = 0 \end{aligned}$$

The nontrivial solution is inside the brackets. It is a second-order polynomial in terms of  $\cos \Lambda$ . It is solved in the standard form. Then, solving for  $\Lambda$  yields Equation (16-107).

### (5) Method to Approximate Drag Divergence at Subsonic Airspeed

The following method uses a spline to approximate the typical shape of the drag divergence at high subsonic Mach numbers. It requires three following parameters to be known: (1) the critical Mach number,  $M_{crit}$ , (2) the

<sup>6</sup> Attributed to Dr. David Korn formerly of New York University's Courant Institute.

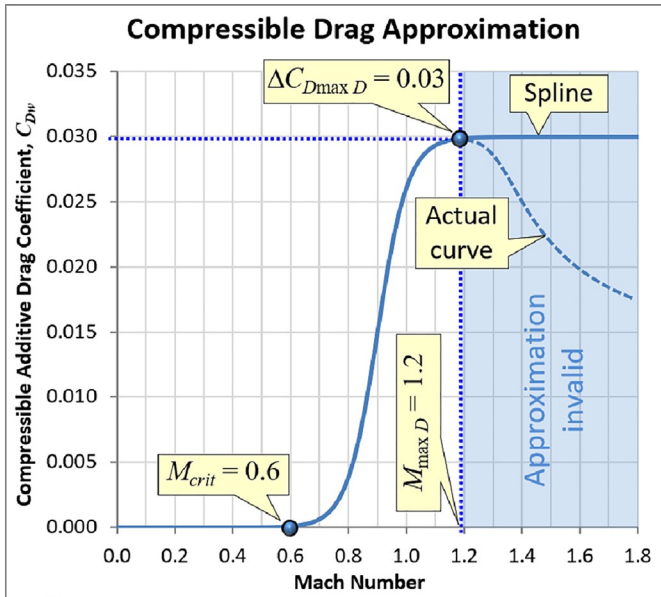


**FIGURE 16-39** Method shown in action using  $M_{crit}=0.6$ ,  $M_{maxD}=1.2$ , and  $\Delta C_{D_{maxD}}=0.03$ .

maximum Mach divergence drag,  $\Delta C_{D_{maxD}}$ , and (3) the Mach number at which it occurs,  $M_{maxD}$  (see Figure 16-39). If these

**TABLE 16-9** Token values of  $M_{maxD}$  and  $\Delta C_{D_{maxD}}$ .

Description	$M_{crit}$	$M_{maxD}$	$\Delta C_{D_{maxD}}$	Reference
Straight wing "clean"	Eq. (16-105) or (8-62)	≈1.10	0.055	[33]
Swept wing $\Lambda_{c/4}=34^\circ$ "clean"		≈1.25	0.030	
Swept wing $\Lambda_{c/4}=45^\circ$ "clean"		≈1.65	0.020	
Swept wing $\Lambda_{c/4}=60^\circ$ "clean"		≈1.90	0.013	
Axisymmetric body ( $l/d=10$ )		≈1.03	0.004-0.012	[65]
Axisymmetric body ( $l/d=10$ ) + wing ( $\Lambda_{c/4}=45^\circ$ )		≈1.03	0.0145	
Axisymmetric body ( $l/d=10$ ) ( $C$ in ref) ( $\Lambda_{LE}=23^\circ$ )		≈1.05	0.019	
Axisymmetric body ( $l/d=10$ ) with waist ( $B$ in ref)		≈1.05	0.0165	[66]

## DERIVATION OF EQUATIONS (16-108)-(16-110)

Assume a spline function of the type:

$$C_{D_w} = \frac{\Delta C_{D_{maxD}}}{2} (1 + \tanh(AM_\infty + B))$$

Since the hyperbolic tangent has asymptotes at  $y = -1$  and  $y = 1$ , it is necessary to divide  $\Delta C_{maxD}$  by 2 (because the asymptotes are separated by a value of 2). The value "1" is added to shift tanh upward, so the lower asymptote will be at  $y = 0$ , rather than  $y = -1$ . The resulting function is a spline that can be used to approximate the drag divergence. This requires the constants  $A$  and  $B$  to be determined to fit the function through specific points on the drag versus Mach curve (see Figure 16-37). These points are: (1)  $M_{crit}$ , where the drag begins to rise and (2)  $M_{maxD}$ , where it reaches its maximum value,  $\Delta C_{maxD}$ . To work around the lower asymptote, we assume a very small increase in  $C_{D_w}$  at  $M_{crit}$ ; Here assume 1 dragcount or 0.0001. To work

are known, the additional drag for Mach numbers ranging from 0 to  $M_{maxD}$  can be estimated using the following expression:

$$C_{D_w} = \frac{\Delta C_{D_{maxD}}}{2} (1 + \tanh(AM_\infty + B)) \quad (16-108)$$

Where  $M_\infty$  is the Mach number and the constants  $A$  and  $B$  are determined using the following expressions:

$$A = \frac{\tanh^{-1}\left(\frac{2\Delta C_{D_{maxD}} - 0.0002}{\Delta C_{D_{maxD}}} - 1\right) - \tanh^{-1}\left(\frac{0.0002}{\Delta C_{D_{maxD}}} - 1\right)}{M_{maxD} - M_{crit}} \quad (16-109)$$

$$B = \tanh^{-1}\left(\frac{0.0002}{\Delta C_{D_{maxD}}} - 1\right) - AM_{crit} \quad (16-110)$$

It is unlikely that  $\Delta C_{D_{maxD}}$  and  $M_{maxD}$  are known early during conceptual design. In this case, Table 16-9 can provide some guidance. Note that performance analysis for subsonic aircraft does not wander into the supersonic regime. Therefore, we only need to approximate trends on the subsonic side of the drag rise in Figure 16-39.

around the upper asymptote, where  $C_{D_w}$  reaches its maximum value ( $\Delta C_{maxD}$ ) we assume its value is  $C_{D_w} = \Delta C_{maxD} - 0.0001$ . Thus, we write:

At  $M_\infty = M_{crit}$ :

$$\Delta C_{DM} = \frac{\Delta C_{D_{maxD}}}{2} (1 + \tanh(AM_{crit} + B)) \\ = 0.0001$$

At  $M_\infty = M_{maxD}$ :

$$\Delta C_{DM} = \frac{\Delta C_{D_{maxD}}}{2} (1 + \tanh(AM_{maxD} + B)) \\ = \Delta C_{D_{maxD}} - 0.0001$$

We readily see that we can solve for the argument of the hyperbolic tangent as follows:

$$AM + B = \tanh^{-1}\left(\frac{2\Delta C_{DM}}{\Delta C_{D_{maxD}}} - 1\right)$$

This allows us to write:

At  $M_\infty = M_{crit}$ :

$$\begin{aligned} AM_{crit} + B &= \tanh^{-1}\left(\frac{2\Delta C_{D_M}}{\Delta C_{D_{maxD}}} - 1\right) \\ &= \tanh^{-1}\left(\frac{0.0002}{\Delta C_{D_{maxD}}} - 1\right) \end{aligned}$$

At  $M_\infty = M_{maxD}$ :

$$\begin{aligned} AM_{maxD} + B &= \tanh^{-1}\left(\frac{2\Delta C_{D_M}}{\Delta C_{D_{maxD}}} - 1\right) \\ &= \tanh^{-1}\left(\frac{2\Delta C_{D_{maxD}} - 0.0002}{\Delta C_{D_{maxD}}} - 1\right) \end{aligned}$$

Solving for  $A$  and  $B$  yields Equations (16-109) and (16-110).

### EXAMPLE 16-10

Determine drag divergence spline for the Learjet 45 (see Section 17.5.2, *Learjet 45*) assuming the following parameters:  $M_{crit} = 0.80$ ,  $\Delta C_{D_{maxD}} = 0.03$ , and  $M_{maxD} = 1.05$ . Plot the drag coefficient as a function of calibrated airspeed between 0 and 500 KCAS for the aircraft at S-L, 25,000 ft, 35,000 ft, and 45,000 ft, if  $C_{D_{min}} = 0.0200$ ,  $k = 0.05236$ ,  $C_{L_{minD}} = 0.20$ , and physical data provided in Table 17.8.

#### SOLUTION:

This is largely a “plug-and-chug” problem. Use Equation (16-109) to get constant  $A$ :

$$A = \frac{\tanh^{-1}\left(\frac{2(0.03) - 0.0002}{0.03} - 1\right) - \tanh^{-1}\left(\frac{0.0002}{0.03} - 1\right)}{1.05 - 0.80} = 22.80$$

Use Equation (16-110) to get constant  $B$ :

$$B = \tanh^{-1}\left(\frac{0.0002}{0.03} - 1\right) - (22.80)(0.80) = -21.09$$

The wave drag spline is given by:

$$\begin{aligned} C_{D_w} &= \frac{0.03}{2}(1 + \tanh(22.80M_\infty - 21.09)) \\ &= 0.015(1 + \tanh(22.80M_\infty - 21.09)) \end{aligned}$$

In interest of space, only the requested graph is shown in Figure 16-40. It plots  $C_D = C_{D_{min}} + k(C_L - C_{L_{minD}})^2 + C_{D_w}$ . It shows clearly how the drag divergence moves to a lower calibrated airspeed with altitude, a consequence of the reduced sonic speed and effect of density on the calibrated airspeed. Note that this model is also corrected using the high AOA correction of Equation (16-20). Also see Figure (20-4), which breaks down the total drag into minimum, lift-induced, and wave drag contributions.

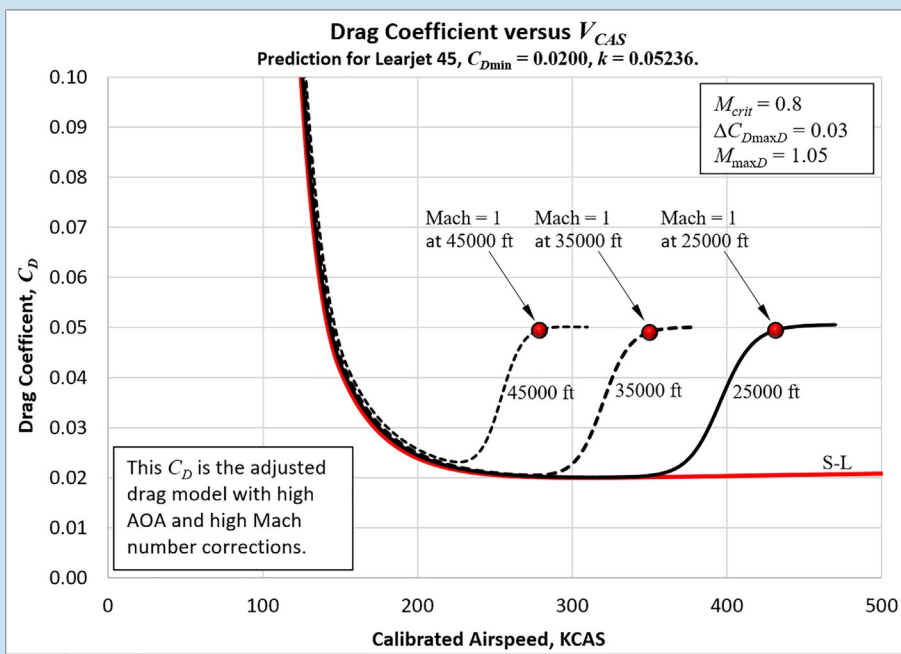


FIGURE 16-40 The incorporation of the wave drag spline to the drag coefficient.

## (6) Transonic Area Rule

Refers to a method of estimating transonic and supersonic wave drag for aircraft. It was first conceived and formulated by the German scientist Otto Frenzl (1909–96) [67]. Frenzl theorized that the steepness of the drag rise of a body approaching the speed of sound was related to its distribution of cross-sectional area. As an employee of Junkers Aircraft, it should not surprise anyone that his invention shows up in a Junkers-owned patent number 932410 from 1944. The idea was further developed by Wallace D. Hayes (1918–2001) in his 1947 Ph.D. dissertation, where it was called the “supersonic area rule.” [68] It is also called the “Hayes drag formula” in Ref. [69]. Its application to aircraft design was shown by the American aerodynamicist Richard T. Whitcomb (1921–2009). In 1951, Whitcomb attended a symposium on transonic flow presented by the renowned German aerodynamicist Dr. Adolf Busemann (1901–86) [70]. Afterward, Whitcomb hypothesized that narrowing the fuselage at the wing-juncture (called “waisting”) should reduce the supersonic drag. He published an experimental confirmation of this approach in 1952 in Ref. [71], later superseded by Ref. [65].

A theoretical treatment of the method is provided by Jones [72] and Ashley and Landahl [69]. The theory presumes flow disturbances are independent of the body's arrangement. This is justified on the basis that no information about its shape is carried upstream because of its high speed. Thus, the cross section of a body at any fuselage station ( $x$ ) can be regarded circular in shape. To calculate the wave drag requires a complicated numerical analysis of the geometry. The procedure passes multiple cutting planes along the length (along the  $x$ -axis) of the body. Each is rotated in steps through 180 degrees about the  $x$ -axis and the wave drag for each step is determined. The complete wave drag is then calculated per the procedure in Refs. [73, 74]. If  $M_\infty = 1$ , then the cross sections are *normal* to the  $x$ -axis. If  $M_\infty > 1$ , then the cross-sections are parallel to the Mach angle,  $\mu$ , given by

$$\mu = \sin^{-1}(1/M_\infty) \quad (16-111)$$

This is illustrated in Figure 16-41. Moreover, the area distribution,  $S(x)$ , is done for several roll angles ( $\phi$ ) (each resulting in a different  $S(x)$ ), which are then averaged. The wave drag is then calculated using the expression

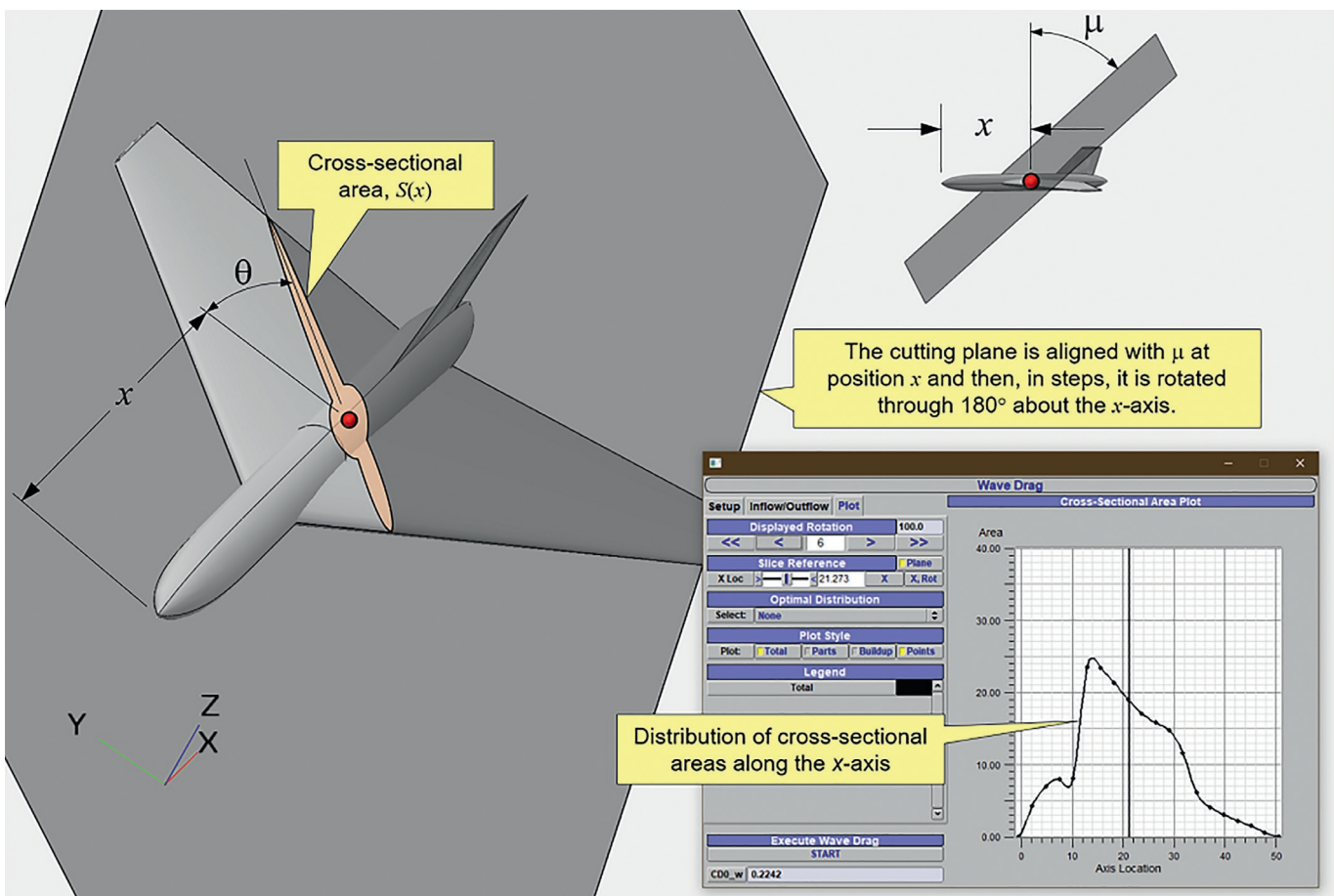
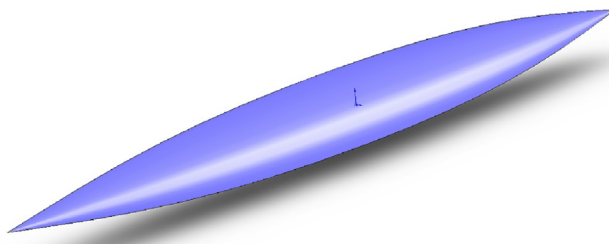


FIGURE 16-41 Implementation of the transonic area rule in the software OpenVSP [75].



**FIGURE 16-42** A Sears-Haack body.

$$C_{D_w} = \frac{-1}{2\pi S} \int_0^l \int_0^l S''(x)S''(\xi) \ln(x-\xi) dx d\xi \quad (16-112)$$

Where  $l$  is the length of the body,  $S$  is the cross-sectional area,  $x$  refers to the longitudinal axis,  $\xi$  is an integration variable. The expression is derived in Ref. [69]. The configuration will develop its minimum wave drag coefficient at its operational Mach number when its distribution of  $S(x)$  resembles the area distribution of a Sears-Haack body (see Figure 16-42). The Sears-Haack distribution develops the least wave drag. Therefore, the designer of supersonic vehicles tries to reshape the aircraft to match the Sears-Haack distribution.

Radius ( $R_{\max}$  is maximum body radius):

$$r(x) = R_{\max} [4x(1-x)]^{3/4}$$

Cross-sectional area:

$$S(x) = \pi R_{\max}^2 [4x(1-x)]^{3/2}$$

First derivative of  $S(x)$ :

$$S'(x) = 12\pi R_{\max}^2 (1-2x) \sqrt{(x-x^2)}$$

Second derivative of  $S(x)$ :

$$S''(x) = 12\pi R_{\max}^2 \left[ \frac{(1-2x)^2}{2\sqrt{x-x^2}} - 2\sqrt{x-x^2} \right]$$

$$\text{Volume (body only): } V = \frac{3\pi^2}{16} R_{\max}^2 l$$

$$\text{Wave drag (body only): } D_w = \frac{9\pi^3 R_{\max}^4}{4l^2} \rho V_\infty^2 = q_\infty \frac{9\pi^3 R_{\max}^4}{2l^2}$$

$$\text{Wave drag coefficient (body only): } C_{D_w} = \frac{D_w}{q_\infty S} = \frac{9\pi^3 R_{\max}^4}{2l^2 S}$$

The minimum supersonic drag of an aircraft is given by R.T. Jones' approximation [76, 77]:

$$D_{\min} = q_\infty S C_{D_{\min}} + \underbrace{\frac{W^2}{q_\infty \pi b^2}}_{\text{Wing's lift-induced drag}} + \underbrace{\frac{(M_\infty^2 - 1) W^2}{q_\infty \pi l^2}}_{\text{Fuselage's lift-induced drag}} + \underbrace{\frac{q_\infty \frac{128}{\pi} V^2}{l^4}}_{\text{Fuselage's volume dependent drag (for Sears-Haack)}} \quad (16-113)$$

Where  $q_\infty$  is dynamic pressure,  $W$  is weight (which equals lift),  $b$  is wingspan,  $l$  is the overall (fuselage) length, and  $V$  is volume. It shows how wave drag depends on lift, length, and volume. The approximation applies only at low supersonic speeds for wings whose leading-edge sweep is greater than the sweep of the Mach shock-lines.

### 16.3.4 Calculate $C_{D_{\min}}$ Using the Rapid Drag Estimation Method

The *rapid drag estimation method* (RDEM) is the fastest way to estimate the drag of an airplane. However, it is a low-fidelity method. It presumes a relationship between the airplane's averaged skin friction coefficient ( $\bar{C}_f$ ), total wetted area ( $S_{\text{wet}}$ ), and  $C_{D_{\min}}$ . Due to its low-fidelity nature, the method should only be used to check drag estimates by the *component drag buildup method* (CDBM). It allows for contributions by flaps and landing gear. The method calculates  $C_{D_{\min}}$  using the concept of EFPA (see Section 16.2.1, *Fundamental Definitions*) and Equation (16-9):

$$C_{D_{\min}} = (f/S + \Delta C_{D_{\min}}) k_{\text{crud}} \quad (16-114)$$

Where  $f$  is the equivalent flat plate (parasite) area,  $\Delta C_{D_{\min}}$  is the additive (miscellaneous) drag, and  $k_{\text{crud}}$  is the crud factor (see Section 16.3.9). The method involves using  $\bar{C}_f$  and  $S_{\text{wet}}$  to extract the value of  $f$  for a "clean" aircraft from Figure 16-43, using the approach outlined in the figure. An accurate estimate of the aircraft's wetted area is essential. An example of the application of the method is shown in Figure 16-43.

The drag increments due to flaps, landing gear, speed brakes, etc., are accounted for using the following relation and then added to  $C_{D_{\min}}$ :

$$\Delta C_{D_{\min}} = \frac{1}{S} \sum C_{D_\pi} A_\pi \quad (16-115)$$

Where  $\Delta C_{D_{\min}}$  is the drag increment,  $C_{D_\pi}$  is the component's equivalent drag coefficient, and  $A_\pi$  is the equivalent parasite area. The equivalent parasite areas and coefficients are obtained from the Table 16-10, where  $A_C$  stands for maximum cross-sectional area,  $S$  is the wing reference area and  $S_{HT}$  is the HT planform area.

### 16.3.5 Calculate $C_{D_{\min}}$ Using the Component Drag Buildup Method

The *component drag buildup method* (CDBM) estimates total drag by summing the skin friction of all external components comprising the airplane. Since pressure drag depends on viscous effects (e.g., through flow separation), the skin friction coefficient is corrected using a special factor called the *form factor* ( $FF$ ). It accounts for the difference in drag generated by dissimilar geometries

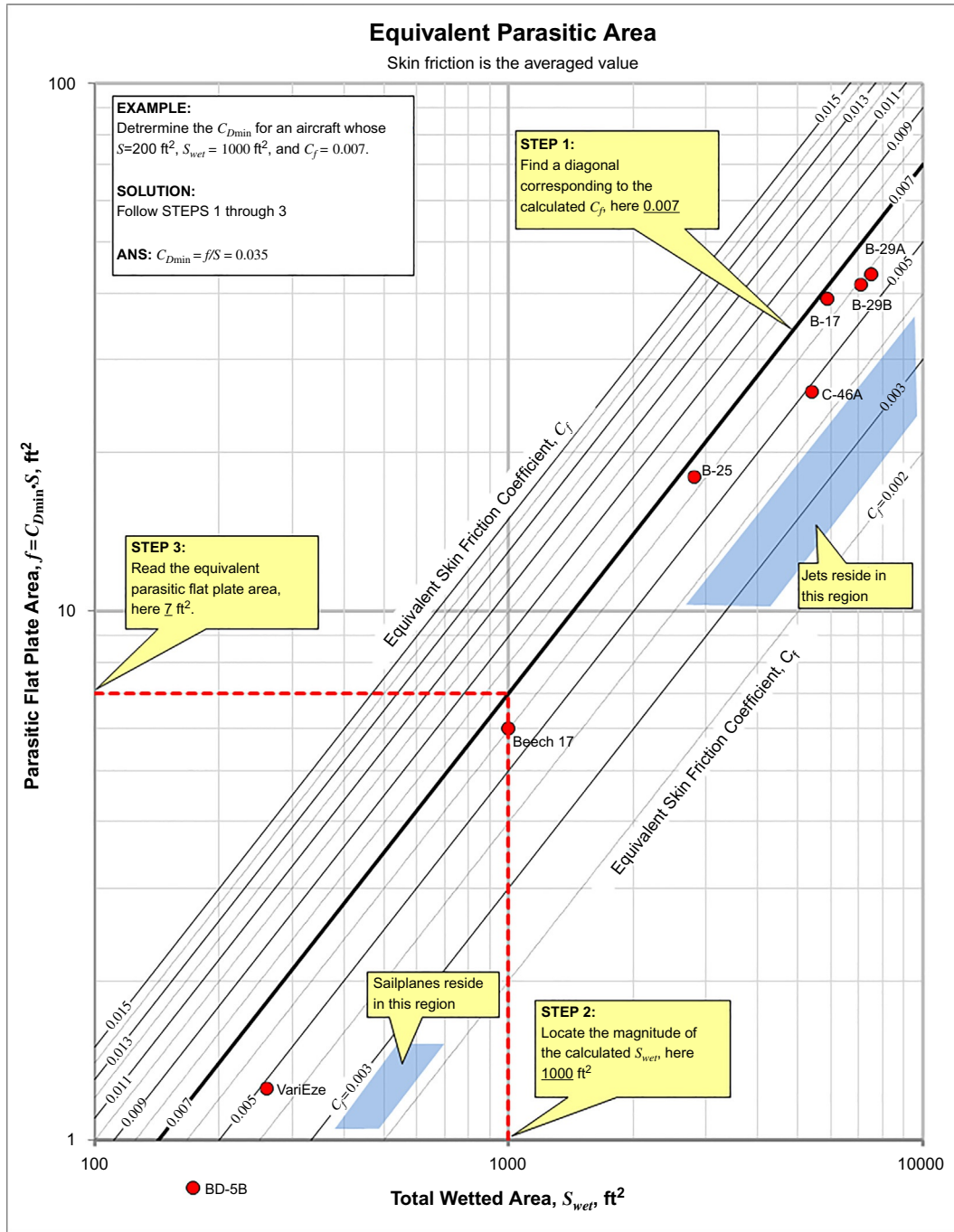


**FIGURE 16-43** Determination of equivalent parasite area. Based on C.D. Perkins, R.E. Hage, *Airplane Performance, Stability, and Control*, John Wiley & Sons, 1949; J. Roskam, *Methods for Estimating Drag Polars of Subsonic Airplanes*, 4<sup>th</sup> printing, 1984.

that happen to have equal wetted area or skin friction coefficients. The CDBM also incorporates effects caused by the proximity of components to each other (interferences), using a so-called *interference factor (IF)*. The procedure is illustrated in Figure 16-44 and implemented in Example 16-10. In the flow chart, the “+” sign means that contributions are added, whereas the “×” sign means multiplication. The following Step-by-Step describes how to implement the procedure.

#### Step 1: Identify and List Components

Tabulate all “winglike” components that constitute the external (wetted) geometry of the airplane. Identify each component using an index  $j=1,2,\dots,N$  (= number of components) and specify their wetted areas,  $S_{wet,j}$ . This typically includes the wing, winglets, HT, VT, fuselage, pylons, nacelles, external fuel tanks, dorsal and ventral fins, and so forth. While it is easily argued that some of

**TABLE 16-10** Equivalent parasite areas and coefficients.

Item	Comment	$C_{D_a}$	Area on which $C_{D_a}$ is based
Wing	Standard operational roughness, airfoil $t/c=10\%-20\%$ .	0.005–0.009 $S$	
HT and VT	Standard operational roughness, airfoil $t/c=8\%-12\%$ .	0.006–0.008 $S_{HT}$	
Wing flaps	Plain, 60% span at 30-degree deflection	0.02–0.03 $S$	
Fuselage	Streamlined and very smooth body	0.05 $A_C$	
Fuselage	Small aircraft with engine in nose	0.09–0.13 $A_C$	
Fuselage	Large transport aircraft (DC-4, DC-5)	0.07–0.10 $A_C$	
Fuselage	Bomber (B-17)	0.08–0.12 $A_C$	
Landing gear	Typical light twin, wheel wells closed	0.014 $S$	
Landing gear	Typical light twin, wheel wells open	0.017 $S$	
Nacelle, propeller	Above wing on a small aircraft (e.g., Cessna 310 type)	0.25 $A_C$	
Nacelle, propeller	Relatively small leading-edge nacelle on a large aircraft	0.05–0.09 $A_C$	
Nacelle, turbojet	Mounted on wing (e.g., Me-262)	0.05–0.07 $A_C$	
Wingtip tank	Suspended below wingtip	0.10 $A_C$	
Wingtip tank	Centrally mounted at wingtip	0.06 $A_C$	
Wing tank	Suspended below wing, incl. support	0.19–0.21 $A_C$	
Bomb	Suspended below wing, incl. support	0.22–0.25 $A_C$	
Cooling flaps	Depends strongly on size, no realistic representative data		
Speed brakes	can be given		

Based on C.D. Perkins, R.E. Hage, *Airplane Performance, Stability, and Control*, John Wiley & Sons, 1949; J. Roskam, *Methods for Estimating Drag Polars of Subsonic Airplanes*, 4<sup>th</sup> printing, 1984.

these are not quite winglike, these are included and the method is applied identically to all. However, components like a fuselage are analyzed using length in lieu of a chord. Exclude smaller wing-like components such as antennas. These are treated using the methods of **Section 16.4, Miscellaneous or Additive Drag**. The total wetted area,  $S_{wet}$ , of the aircraft is given by

$$S_{wet} = \sum_{j=1}^N S_{wet_j} \quad (16-116)$$

### Step 2: Estimate Skin Friction of All Listed Components

Calculate the averaged skin friction,  $\bar{C}_f$ , of all listed components using the methods of **Section 16.3.1, Estimating Skin Friction Drag**. This is shown in **Figure 16-44** as ①.

### Step 3: Estimate the FF and IF of All Listed Components

Calculate the form- and interference-factors for all listed components. For **FF** use the methods of **Section 16.3.6, Form Factors**. For **IF** use the methods of **Section 16.3.7, Interference Factors**. This is shown in **Figure 16-44** as ② and ③.

### Step 4: Estimate the $C_{D_{misc}}$ of Remaining Components

This includes drag contributions of components like landing gear, inlets, outlets, antennas, fuel caps, flaps, canopies, control system components (bellcranks, hinges, etc.) and other nonwing-like parts. This is accomplished using the methods of **Section 16.4, Miscellaneous or Additive Drag**. This is shown in **Figure 16-44** as ④.

### Step 5: Estimate the $C_{D_{min}}$

The minimum drag is estimated using the following expression

$$C_{D_{min}} = (C_{D_1} + C_{D_2} + C_{D_p} + C_{D_{misc}}) k_{crud} \quad (16-117)$$

Where the coefficients  $C_{D_1}$ ,  $C_{D_2}$ , and  $C_{D_p}$  are given by the expressions below.  $C_{D_{misc}}$  is the miscellaneous drag per **Section 16.4**, and  $k_{crud}$  is the crud factor ⑤ (see **Section 16.3.8**). The coefficient  $C_{D_1}$  is estimated per the above Step-by-Step, where the tabulated component contributions are added as follows

$$C_{D_1} = \frac{1}{S} \left( \sum_{j=1}^N \bar{C}_{f_j} \times FF_j \times S_{wet_j} \times IF_j \right) \quad (16-118)$$

Where  $FF_j$ ,  $S_{wet_j}$ , and  $IF_j$  are the form factor, wetted area, and interference factor of component  $j$ , respectively.

The coefficient  $C_{D_2}$  is optional. It accounts for drag of a wing-like component (e.g., wing, HT, VT) when a 2D drag polar of its airfoil is available. In this case,  $C_{d_j}$  represents the average airfoil profile drag obtained from the drag polar and  $S_j$  is the planform area. Of course, if using this scheme, the component must be excluded from the  $C_{D_1}$ .  $C_{D_2}$  is calculated using the expression

$$C_{D_2} = \frac{1}{S} \left( \sum_{j=1}^M C_{d_j} \times S_j \times IF_j \right) \quad (16-119)$$

Where  $M$  is the number of components. Note that the airfoil's  $C_{d_j}$  already includes the wetted area and contributions from pressure drag. Its use can be easily extended to account for drag rise with section lift coefficients. Additionally, it is scaled based on the component's planform area  $S_j$ . Therefore,  $C_{d_j}$  can be related to  $\bar{C}_f$  as follows

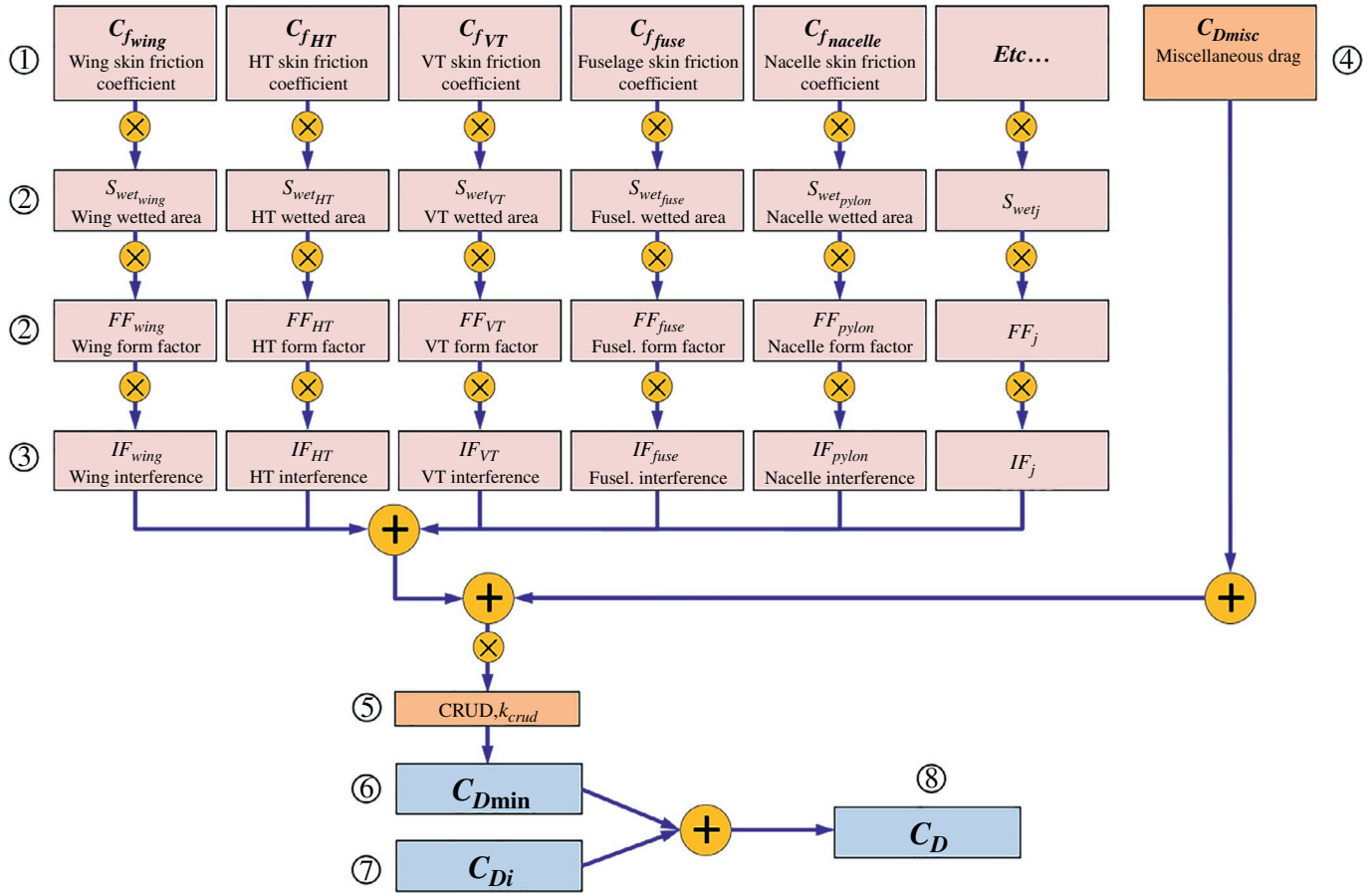


FIGURE 16-44 Flow chart describing the component drag buildup method.

$$C_{d_j} = \left( \frac{S_{wet_j}}{S_j} \right) \bar{C}_{f_j} \times FF_j \quad (16-120)$$

It can be seen that if substituted into Equation (16-119) it acquires the form of Equation (16-118). Thus,  $\bar{C}_{f_j}$  can be written in terms of  $C_{d_j}$  as shown below

$$\bar{C}_{f_j} = \frac{1}{FF_j} \left( \frac{S_j}{S_{wet_j}} \right) C_{d_j} \quad (16-121)$$

The coefficient  $C_{D_p}$  is also optional. It provides an alternative to  $C_{D_2}$  to account for the profile drag of the wing and incorporate AOA dependency in the drag estimate. This is accomplished through Equation (16-16), repeated below for convenience.

$$C_{D_p} = C_{d_{min}} + \frac{2m}{b} \int_0^{b/2} (f(y) - C_{l_{minD}})^2 dy \quad (16-16)$$

If  $C_{D_2}$  and  $C_{D_p}$  are disregarded, the component drag buildup is expressed in the following simpler form:

$$C_{D_{min}} = \left( C_{D_{misc}} + \frac{1}{S} \sum_{j=1}^N \bar{C}_{f_j} \times FF_j \times S_{wet_j} \times IF_j \right) k_{crud} \quad (16-122)$$

### 16.3.6 Form Factors

As stated earlier, the form factor ( $FF$ ) accounts for a component's pressure drag by boosting its skin friction drag. There are numerous methods available for this purpose. Some are only intended for wing-like components, while others are intended for axisymmetric components like fuselages. These form factors are typically derived by semiempirical methods that emphasize the component's thickness-to-chord ratio. The following form factors are found in the literature.

#### (1) Form Factors for Wing-like Components

The following  $FF$  are used with lifting surfaces like wings, HT, VT, streamlined wing-struts, engine pylons, wing-shaped antennas, and landing gear pant fairings, to name a few. This forces the designer to ask "which one do I pick?" Unless specific applications are cited the answer is often: "Use engineering judgment." The unsure designer can also take the average of two or more methods.

Hoerner [33, pp. 6-6] suggests the following  $FF$  for lifting surfaces featuring airfoils whose  $(x/c)_{max} = 0.30$ :

$$FF = 1 + 2(t/c) + 60(t/c)^4 \quad (16-123)$$

Hoerner [33] suggests the following *FF* for lifting surfaces featuring airfoils whose  $(x/c)_{\max} = 0.40\text{--}0.50$ , such as NACA 64 and 65 series airfoils:

$$FF = 1 + 1.2(t/c) + 70(t/c)^4 \quad (16-124)$$

Torenbeek [54, p. 499] suggests the following *FF* for lifting surfaces featuring airfoils whose  $t/c \leq 0.21$ :

$$FF = 1 + 2.7(t/c) + 100(t/c)^4 \quad (16-125)$$

None of the above models account for wing sweep nor compressibility effects. Shevell [51] suggests the following *FF* for lifting surfaces and introduces compressibility and sweep effects:

$$FF = 1 + \frac{(2 - M_{\infty}^2) \cos \Lambda_{c/4}}{\sqrt{1 - M_{\infty}^2 \cos^2 \Lambda_{c/4}}} (t/c) + 100(t/c)^4 \quad (16-126)$$

Nicolai [78] and Raymer [79] suggest the following *FF* for lifting surfaces that also corrects for compressibility and the sweep of the maximum thickness line. The equation is only valid for  $M_{\infty} \geq 0.2$  because the compressibility correction (the bracket on the right-hand side) is less than 1 for  $M_{\infty} < 0.2$ . Thus, omit the compressibility correction when  $M_{\infty} < 0.2$ .

$$FF = \left[ 1 + \frac{0.6}{(x/c)_{\max}} (t/c) + 100(t/c)^4 \right] \cdot \left[ 1.34M_{\infty}^{0.18} (\cos \Lambda_{t\max})^{0.28} \right] \quad (16-127)$$

Jenkinson [80] suggests two kinds of *FF*; one for the wing, the other for tail surfaces. The *FF* for a wing is given by:

$$FF = \left[ 3.3(t/c) - 0.008(t/c)^2 + 27.0(t/c)^3 \right] \cos^2 \Lambda_{c/2} + 1 \quad (16-128)$$

Furthermore, the reference recommends *IF* to use with the expression:  $IF = 1.0$  for well-filleted low or mid wings, and  $1.1\text{--}1.4$  for small or no fillet. It recommends an  $IF = 1.2$  for tail surfaces. The *FF* for tail surfaces is given by:

$$FF = [3.52(t/c)] \cos^2 \Lambda_{c/2} + 1 \quad (16-129)$$

In the previously mentioned equations:

$M_{\infty}$ =Mach number,

$\Lambda_{c/4}$ =Sweep angle of the quarter-chord line,

$\Lambda_{c/2}$ =Sweep angle of the mid-chord line,

$\Lambda_t$  max=Sweep angle of maximum thickness line,

$(x/c)_{\max}$ =Location of maximum airfoil thickness,

$(t/c)$ =Airfoil thickness ratio.

Note that Equations (16-126) and (16-127) approach Torenbeek's form of Equation (16-125) for wings whose quarter-chord (Shevell) or maximum thickness (Nicolai, Raymer) sweep angle is 0 degrees, when  $M_{\infty} = 0$  (Shevell) or  $M_{\infty} = 0.2$  (Nicolai, Raymer).

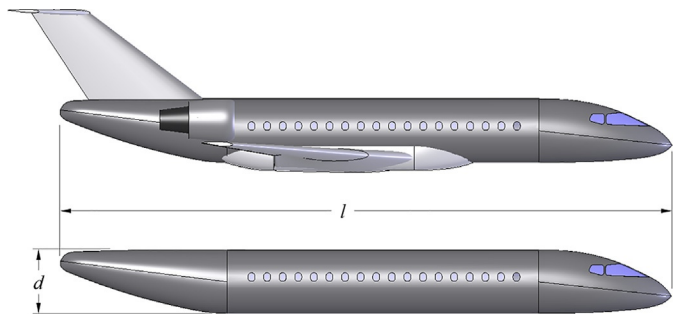


**FIGURE 16-45** Definition of terms for use with the estimation of form factors for a fuselage.

## (2) Form Factors for a Fuselage and a Smooth Canopy

The following *FF* are used with *streamlined bodies* (which typically represent fuselages) and *smooth canopies*. These can also be used for engine nacelles and external, streamlined fuel tanks. These typically use *fineness ratio*, defined as length (*l*) divided by the average diameter (*d*), as shown in Figs. 16-45 and 16-46. The former illustrates how to strip the fuselage of the wing, tail, and engines to extract the dimensions needed. Sometimes the distinction is not so clear, leaving no option besides engineering judgment.

A streamlined body usually refers to a body-of-revolution, whose cross section is similar to what is shown in Figure 16-46. A streamlined body is used to represent many types of fuselages, including airship hulls and engine nacelles. A canopy is sized geometrically as shown in Figure 16-46. For more realistic canopies, refer to Section 16.4.10, *Drag of Canopies*.

### Fuselage as a Body of Revolution

In the following expressions, the *fineness ratio* (*f*) is a measure of the slenderness of a body-of-revolution. It is defined as follows:

$$f = l/d \quad (16-130)$$

Although devised for bodies-of-revolution, the expressions for the *FF* below are also applicable to bodies that feature noncircular cross sections (see Figure 16-46). For instance, a cross section might be shaped like an egg, or be box-shaped. Such shapes are treated based on their maximum cross-sectional area,  $A_{\max}$ , which is related to that of a circular cross section using a "representative" fineness ratio as shown below:

$$f = l/d = \frac{l}{2} \sqrt{\frac{\pi}{A_{\max}}} \quad (16-131)$$

### Form Factors at Subcritical Reynolds Numbers

Hoerner [33, pp. 6–16] derives and suggests the following *FF* for streamlined bodies at subcritical Reynolds numbers ( $R_e < 10^5$ ). This  $R_e$  applies to small vehicles, such as RC aircraft, or small Unmanned Aerial Vehicles. Note that

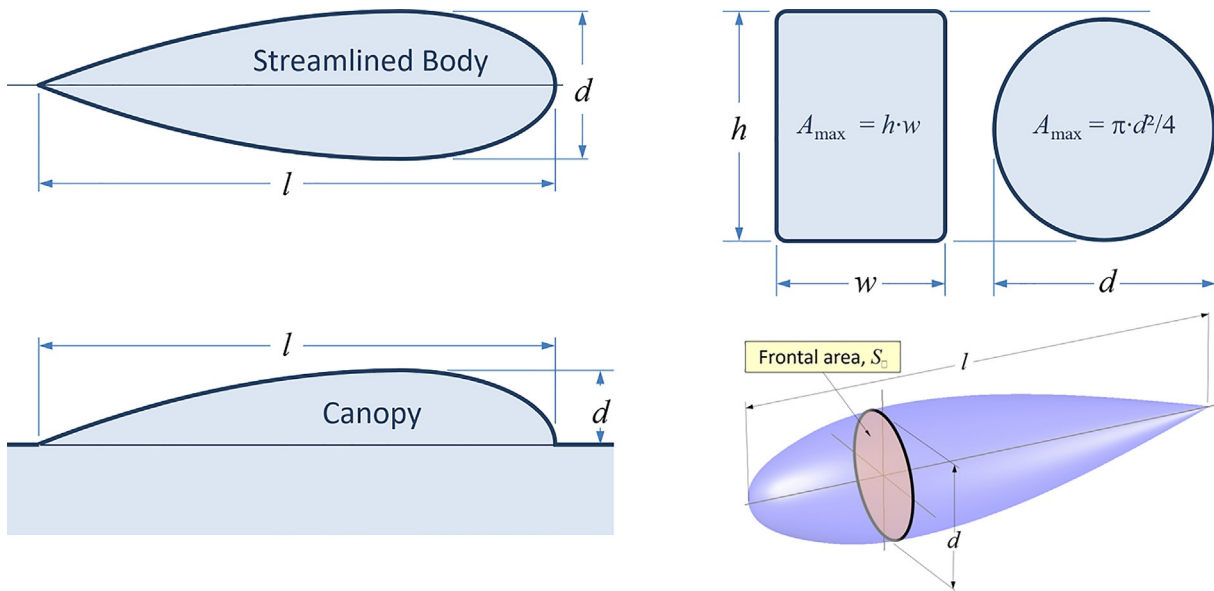


**FIGURE 16-46** Definition of terms for use with streamlined bodies and canopies.

since the expression includes the pressure drag component, it is not represented as a standalone form factor, but rather what the product of the  $\bar{C}_f \times FF_i$  in Equation (16-122). It also requires the skin friction coefficient for laminar boundary layer of Equation (16-40) to be used:

$$\begin{aligned} \bar{C}_f \cdot FF &= C_{f,lan} [1 + f^{-1.5}] + 0.11f^{-2} \\ &= \frac{1.328}{\sqrt{R_e}} [1 + f^{-1.5}] + 0.11f^{-2} \end{aligned} \quad (16-132)$$

#### Form Factors at Supercritical Reynolds Numbers

Hoerner [33, pp. 6–17] suggests the following form factor for streamlined bodies in airflow whose  $R_e > 10^5$ :

$$FF = 1 + 1.5f^{-1.5} + 7f^{-3} \quad (16-133)$$

Torenbeek [54] suggests the following form factor for a generic fuselage:

$$FF = 1 + 2.2f^{-1.5} + 3.8f^{-3} \quad (16-134)$$

Likewise, Nicolai [78], Raymer [79], and Roskam [81] present the following form factor for a fuselage:

$$FF = 1 + 60f^{-3} + \frac{f}{400} \quad (16-135)$$

Shevell [82] also provides a model for a fuselage given by:

$$\begin{aligned} FF &= 2.939 - 0.7666f + 0.1328f^2 - 0.01074f^3 + 3.275 \\ &\times 10^{-4}f^4 \end{aligned} \quad (16-136)$$

Finally, Jenkinson's [80] model is given by:

$$FF = 1 + 2.2f^{-1.5} - 0.9f^{-3} \quad (16-137)$$

Fuselage fineness ratios and wetted areas for selected GA aircraft are shown in Table 16-11.

**TABLE 16-11** Fuselage fineness ratios and wetted areas for selected GA aircraft.

Aircraft	Fineness ratio, $l/d$	Wing area, $S$ , $\text{ft}^2$	Fuselage $S_{wet,ff}$ , $\text{ft}^2$	$S_{wet}/S$
Beech Baron	5.69	199.2	362	1.82
Beech Bonanza (1958)	4.98	181	323	1.78
Beech Duke	5.59	212.9	586	2.75
Beech King Air	6.06	294	652	2.22
Beech Sierra	5.22	146	332	2.27
Cessna 185	5.15	176	292	1.66
Cessna 207	5.69	174	425	2.44
Cessna 210	5.02	175	319	1.82
Cessna 310	5.4	179	306	1.71
Cessna 414	5.52	195.7	488	2.49
Cirrus SR22	5.38	144.9	258	1.78
Gates Learjet 24	8.8	232	502	2.16
Piper Navajo	5.97	229	502	2.19
Piper Seneca	5.68	206.5	356	1.72

Mostly based on J. Roskam, Some comments about fuselage drag, in: Proceedings of the NASA-Industry-University GA Drag Reduction Workshop, Lawrence, KS, July 14–16, 1975.

#### Optimum Fineness Ratio, $f_{opt}$

The determination of the optimum fineness ratio involves the contribution of both the length ( $l$ ) and diameter ( $d$ ) of the body. Using the body's frontal ( $A_{max}$ ) and wetted area ( $S_{wet}$ ), this is accomplished through  $FF \times S_{wet}/A_{max}$ . The wetted area of a streamlined axisymmetric body ranges between 0.7 and 0.8

times its perimeter<sup>7</sup> ( $\pi d$ ) times its length,  $l$ . For this discussion, assume this is  $S_{wet} = 0.75\pi ld$  or  $\frac{3}{4}\pi ld$ . The frontal area is given by  $A_{max} = \pi d^2/4$ . Thus, the drag coefficient based on frontal area is given by

$$C_{D_A} = \bar{C}_f \times FF \times \frac{S_{wet}}{A_{max}} \quad (16-138)$$

$$\text{Where the area ratio is given by: } \frac{S_{wet}}{A_{max}} = \frac{\frac{3}{4}\pi ld}{\frac{1}{4}\pi d^2} = 3 \frac{l}{d} = 3f$$

Substituting an  $FF$  of choice, e.g., per Equation (16-133), leads to

$$\begin{aligned} C_{D_A} &= \bar{C}_f \times FF \times \frac{S_{wet}}{A_{max}} \\ &= \bar{C}_f (1 + 1.5f^{-1.5} + 7f^{-3}) (3f) \\ &= \bar{C}_f (3f + 4.5f^{-1/2} + 21f^{-2}) \end{aligned} \quad (16-139)$$

Differentiating  $C_{D_A}$  with respect to  $f$  and setting equal to zero, yields the optimum fineness ratio

$$\begin{aligned} \frac{dC_{D_A}}{df} &= 3\bar{C}_f (1 - 0.75f^{-3/2} - 14f^{-3}) = 0 \\ \Leftrightarrow \quad 0.75f^{-3/2} + 14f^{-3} &= 1 \end{aligned}$$

From which we determine that  $f_{opt} \approx 2.58$ . A minimum fineness ratio of 2.6–3.5 for such bodies is well supported by experimental data and explains why fuselages of transport aircraft typically feature this fineness ratio for the aft end. A number of the previously mentioned form factors are plotted in Figure 16-47.

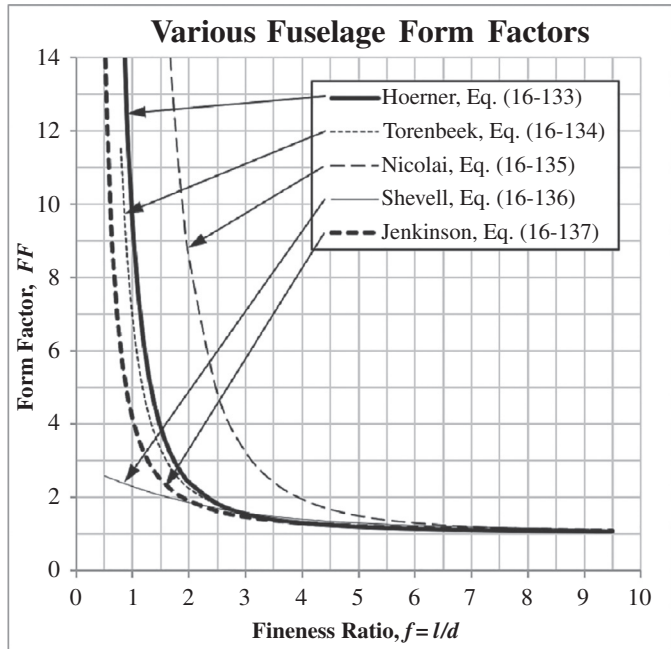


FIGURE 16-47 Comparison of various FFs.

#### Form Factor for Nacelle and Smooth External Store

Raymer [79] suggest the following form factors for nacelles:

$$FF = 1 + 0.35f^{-1} \quad (16-140)$$

Jenkinson [80] recommends simply using the constant  $FF \cdot IF = 1.2$  for wing mounted nacelles and  $FF \cdot IF = 1.44$

#### EXAMPLE 16-11

Use the *component drag buildup method* (CDBM) to determine the  $C_{D_{min}}$  for the SR22 (see Figure 16-48). Note that this task begins here and is supported by multiple smaller examples to follow. The completed  $C_{D_{min}}$  is presented in Example 16-22.

- Assume:
- (1) Flight condition at S-L and 185 KTAS.
  - (2) Wing sustains laminar flow as detailed in Example 16-6.
  - (3) HT sustains 50% laminar flow on lower and upper surfaces.
  - (4) VT sustains 50% laminar flow on left and right surfaces.
  - (5) Fuselage sustains 5% laminar flow, cut short due to engine cowling assembly.
  - (6) Wetted area booster coefficient of 1.07 for wing and 1.05 for HT and VT.
  - (7) Max thickness for wing, HT, and VT is at 50% of the chord for all.

- (8)  $t/c = 0.15$  for wing, 0.1 for HT and VT, and  $4.17/22.42 = 0.186$  for the fuselage.
- (9) Skin roughness value from Table 16-2.
- (10) Assume the max thickness lines for the wing, HT, and VT is  $0^\circ$ ,  $5^\circ$ , and  $18^\circ$ , respectively.
- (11)  $C_{D_{misc}}$  is 74.4 dragcounts (see Example 16-22).
- (12)  $k_{crud}$  is 25% of the sum of the above ( $\times 1.25$ ).

#### SOLUTION:

The solution to this problem is extensive due to the number of components involved. Luckily, many of the calculations are similar and, thus, conveniently implemented in a spreadsheet (see Figures 16-49 through 16-51). Each row is numbered for convenience and sample calculations provided below for selected rows. The spreadsheet allows geometry for other aircraft to be

<sup>7</sup> Depending on its “pudginess.”

## EXAMPLE 16-11 (cont'd)

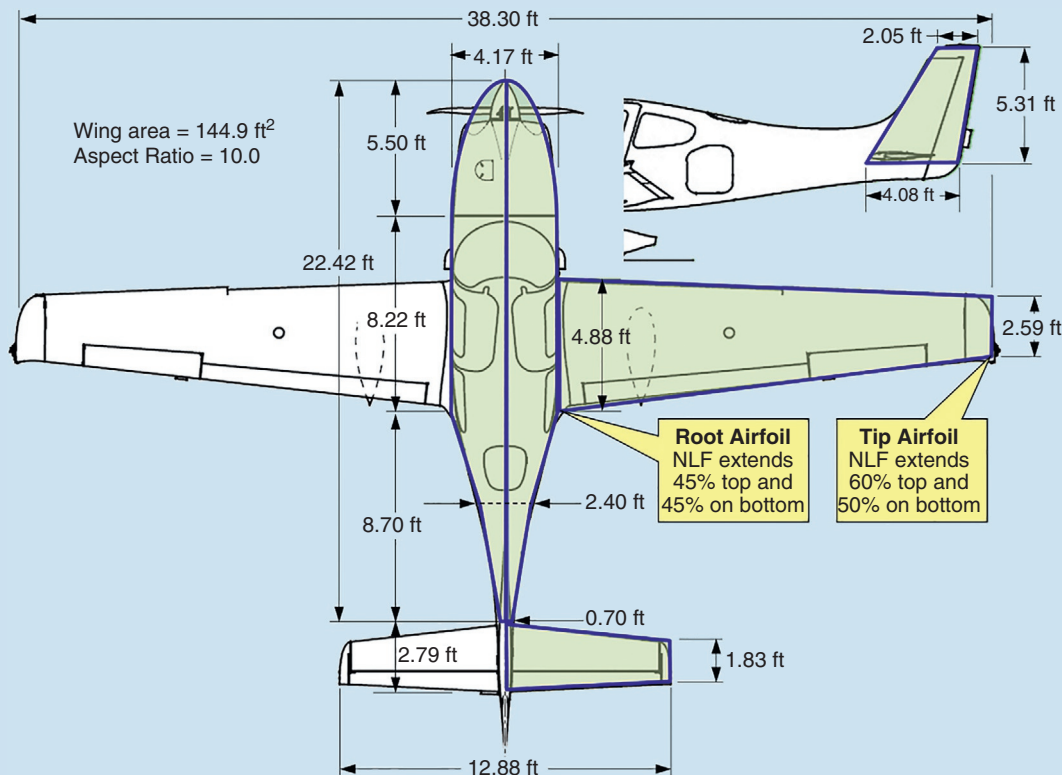


**FIGURE 16-48** Geometry of the example aircraft showing the approximation of its wetted area. Note that for clarity some dimensions have been rounded off to two decimals. Copyright 2021 Cirrus Aircraft or its Affiliates. All Rights Reserved. Image reproduced with the permission of Cirrus.

## FLIGHT CONDITION

1	Airspeed	$V_\infty =$	312.3	ft/s	User entry
2	Viscosity of air	$\mu =$	3.745E-07	lb <sub>f</sub> s/ft <sup>2</sup>	Formula
3	Altitude	$H =$	0		
4	Density of air	$\rho =$	0.002378	slugs/ft <sup>3</sup>	
5	Dynamic pressure	$q =$	115.95	lb/ft <sup>2</sup>	

		WING	HT	VT	FUSELAGE
6	Chord, root	$c_r =$	4.875	2.792	4.083
7	Chord, tip	$c_t =$	2.585	1.834	2.050
8	Exposed halfspan	$b/2 =$	17.07	6.442	5.313
9	Exposed planform area	$S_i =$	127.30	29.79	16.29
10	Reference area	$S =$	144.9		
11	Reference wing span	$b =$	38.30		
12	Aspect Ratio	$AR = b^2/S =$	10.12		
13	Wetted area booster	$k_b =$	1.07	1.05	1.05
14	Wetted area	$S_{wetj} = 2 \cdot S_i \cdot k_b =$	272.4	62.6	34.2
15	Location of max t	$(x/c)_{max} =$	0.50	0.50	0.50
16	Thickness-to-chord ratio	$t/c =$	0.150	0.100	0.100
17	Skin roughness value	$k =$	1.7E-06	1.7E-06	1.7E-06

**FIGURE 16-49** Geometric information of the example aircraft.

## EXAMPLE 16-11 (cont'd)

ROOT CHORD					
18 Upper surface transition	$x_{tr\ upper} =$	0.45	0.50	0.30	0.05
19 Lower surface transition	$x_{tr\ lower} =$	0.45	0.50	0.30	0.05
20 Reynolds Number based on $c_r$	$Re_{Cr} =$	9.668E+06	5.536E+06	8.098E+06	4.446E+07
21 Cutoff Reynolds Number	$Re_{cutoff\ root} =$	2.410E+08	1.340E+08	1.999E+08	1.202E+09
22 Analysis Reynolds Number	$Re_{root} =$	9.668E+06	5.536E+06	8.098E+06	4.446E+07
23 Upper surface fictitious trans	$x_{0\ upper} =$	0.05380	0.07082	0.04463	0.00769
24 Upper surface skin friction	$C_{fupper} =$	0.001981	0.002117	0.002427	0.002112
25 Lower surface fictitious trans	$x_{0\ lower} =$	0.05380	0.07082	0.04463	0.00769
26 Lower surface skin friction	$C_{flower} =$	0.001981	0.002117	0.002427	0.002112
27 Average root skin friction	$C_{favg} =$	0.001981	0.002117	0.002427	0.002112

TIP CHORD					
28 Upper surface transition	$x_{tr\ upper} =$	0.60	0.50	0.30	0.05
29 Lower surface transition	$x_{tr\ lower} =$	0.50	0.50	0.30	0.05
30 Reynolds Number based on $c_t$	$Re_{Ct} =$	5.126E+06	3.636E+06	4.065E+06	4.446E+07
31 Cutoff Reynolds Number	$Re_{cutoff\ tip} =$	2.410E+08	1.340E+08	1.999E+08	1.202E+09
32 Analysis Reynolds Number	$Re_{tip} =$	5.126E+06	3.636E+06	4.065E+06	4.446E+07
33 Upper surface fictitious trans	$x_{0\ upper} =$	0.08169	0.08292	0.05779	0.00769
34 Upper surface skin friction	$C_{fupper} =$	0.001877	0.002342	0.002825	0.002112
35 Lower surface fictitious trans	$x_{0\ lower} =$	0.07290	0.08292	0.05779	0.00769
36 Lower surface skin friction	$C_{flower} =$	0.002156	0.002342	0.002825	0.002112
37 Average tip skin friction	$C_{favg} =$	0.002017	0.002342	0.002825	0.002112
38 Average skin friction for panel	$C_{favg\ panel} =$	0.001999	0.002230	0.002626	0.002112

FIGURE 16-50 Calculated skin friction coefficients.

DRAG ANALYSIS					
		Wing	HT	VT	Fuselage
39 Sweep angle	$\Lambda_{t\ max} =$	0.00	5.00	18.00	*
40 Form Factor	$FF_j =$	1.311	1.203	1.187	1.399
41 Interference Factor, IF	$IF_j =$	1	1.05	1.05	1
42 Weighted drag factor	$C_{ff} \cdot FF_j \cdot IF_j \cdot S_{wet,j} =$	0.7140	0.1762	0.1120	0.7607
43 Skin friction drag	$(1/S) \sum C_{ff} \cdot FF_j \cdot IF_j \cdot S_{wet,j} =$	0.01217			

FIGURE 16-51 Minimum drag analysis. See discussion about Line 43 in the text.

entered for analysis. Note that green colored cells are intended for user entry and blue cells contain formulas.

Begin by considering Figure 16-49, which shows cells with the given information (green cells) and five rows which show some calculation results (blue cells). Note the setup of the columns dedicated to the inboard and outboard wing elements, as well as the HT and VT.

**Line 1:** Airspeed is  $185 \text{ KTAS} \times 1.688 \text{ ft/s} = 312.3 \text{ ft/s}$ .

**Line 2:** Viscosity of air:

$$\begin{aligned}\mu &= 3.170 \times 10^{-11} T^{1.5} \left( \frac{734.7}{T + 216} \right) \\ &= 3.170 \times 10^{-11} (518.67)^{1.5} \left( \frac{734.7}{518.67 + 216} \right) \\ &= 3.745 \times 10^{-7} \text{ lb}_f \text{s/ft}^2\end{aligned}$$

**Line 4:** Density of air:  $\rho = 0.002378 (1 - 0.0000068756h)^{4.2561} = 0.002378 \text{ slugs/ft}^3$

**Line 5:** Dynamic pressure:

$$q = \frac{1}{2} \rho V^2 = \frac{1}{2} (0.002378) (312.3)^2 = 115.95 \text{ lb}_f/\text{ft}^3$$

## EXAMPLE 16-11 (cont'd)

**Lines 6–8, 10–13, and 16–17:** Geometric data are obtained from [Figure 16-48](#) and other data are entered based on the problem statement. Note that the exposed half-span (and planform area) excludes the area of the surface that is inside the fuselage. Here it will be assumed that, of the components shown, only a part of the wing is inside the fuselage and this is reflected as the exposed half-span and planform area.

**Line 9:** Exposed planform area.

Wing:	$S_W = (38.30 - 4.17)((4.875 + 2.585)/2)$ $= 127.3 \text{ ft}^2$
HT:	$S_{HT} = \frac{1}{2}(2.792 + 1.834) \times 12.88 = 29.79 \text{ ft}^2$
VT:	$S_{VT} = \frac{1}{2}(4.083 + 2.050) \times 5.313 = 16.29 \text{ ft}^2$
Fuselage:	A different method is used to determine its wetted area.

**Line 14:** Total wetted area of all components (exposed wing, HT, VT, and fuselage):

Wing wetted area:	$S_{wet\_W} = 1.07 \times 2 \times S_W = 272.4 \text{ ft}^2$
HT wetted area:	$S_{HT\_wet} = 1.05 \times 2 \times S_{HT} = 62.6 \text{ ft}^2$
VT wetted area:	$S_{VT\_wet} = 1.05 \times 2 \times S_{VT} = 34.2 \text{ ft}^2$

The total wetted area of the fuselage is estimated using the method of [Section 12.4.3, Surface Areas and Volumes of a Typical Tubular Fuselage](#), and the fuselage geometry of [Figure 16-48](#), using [Equation \(12-13\)](#), repeated here for convenience:

$$S_{fuse} = \pi D \left[ \frac{(D^2 + 16L_1^2)^{3/2} - D^3}{96L_1^2} + L_2 + \frac{\sqrt{D^2 + 4L_3^2}}{4} \right]$$

Where:  $D$  = Maximum fuselage diameter = 4.17 ft

$L_1$  = Length of nose section = 5.50 ft

$L_2$  = Length of center section = 8.22 ft

$L_3$  = Length of tail section = 8.70 ft

Plugging and chugging those numbers into this equation yields 217 ft<sup>2</sup>. However, the author's own approximation, which accounts for more details in the fuselage and spinner geometry, returned the following value:

Fuselage wetted area :  $S_{FUSE} = 257.6 \text{ ft}^2$

Note that it would be prudent to subtract the cross-sectional area of the wing on the left and right sides, where it enters the fuselage, but in the interest of simplicity it is left out of these calculations. To calculate this cross-sectional area, the reader can use the approximation of [Section 9.2.6, Wing Volume Approximation](#). Now, let's consider [Figure 16-50](#), which shows the skin friction analysis for the root and tip chords.

**Lines 18–19 and 28–29:** Data entered are based on the problem statement.

**Line 20:** Reynolds number for the root chord (using the wing column as an example).

$$Re_{root} = \frac{\rho VL}{\mu} = \frac{(0.002378)(312.3)(4.875)}{3.745 \times 10^{-7}} = 9,667,562$$

**Lines 21–22 and 30–31:** Here, the calculations for Lines 21–22 are used (see [Figure 16-50](#)). The cutoff Reynolds number for the root chord (again using the wing column as an example) using Equation (16-31).

$$Re_{cutoff} = 38.21 \left( \frac{c_r}{\kappa} \right)^{1.053} = 38.21 \left( \frac{4.875}{1.7 \times 10^{-6}} \right)^{1.053} = 240,963,686$$

Since the  $R_e$  based on  $c_r$  is less than this value, it will be used throughout the remainder of these calculations. If the opposite had been the case, then the cutoff  $R_e$  would have been used.

**Line 23–27 and 33–38:** Steps 4 through 14 of Example 16-6 detail how the values for the wing column were obtained. All the values in the other three columns are calculated in an identical fashion, yielding the table shown in Line 42. Finally, consider [Figure 16-51](#) which shows how the minimum drag coefficient is calculated.

**Line 39:** Thickness sweep angles for the wing, HT, and VT are given in the problem statement as 0°, 5°, and 18°, respectively.

**Line 40:** The Form factor for the wing, HT, and VT is calculated using Equation (16-127) and Equation (16-135) for the fuselage. Note that 185 KTAS at sea level corresponds to  $M_\infty \approx 0.28$ .

Wing FF:

$$FF = \left[ 1 + \frac{0.6}{(x/c)_{max}} \left( \frac{t}{c} \right) + 100 \left( \frac{t}{c} \right)^4 \right] \left[ 1.34 M^{0.18} (\cos \Lambda_{tmax})^{0.28} \right] \\ = \left[ 1 + \frac{0.6}{0.50} (0.15) + 100 (0.15)^4 \right] \left[ 1.34 (0.28)^{0.18} (\cos 0^\circ)^{0.28} \right] \\ = 1.311$$

HT FF:

$$FF = \left[ 1 + \frac{0.6}{0.50} (0.10) + 100 (0.10)^4 \right] \left[ 1.34 (0.28)^{0.18} (\cos 5^\circ)^{0.28} \right] \\ = 1.203$$

VT FF:

$$FF = \left[ 1 + \frac{0.6}{0.50} (0.10) + 100 (0.10)^4 \right] \left[ 1.34 (0.1513)^{0.18} (\cos 18^\circ)^{0.28} \right] \\ = 1.187$$

Fuselage:  $FF = \left[ 1 + \frac{60}{f^3} + \frac{f}{400} \right] = \left[ 1 + \frac{60}{5.376^3} + \frac{5.376}{400} \right] = 1.399$

**EXAMPLE 16-11 (cont'd)**

Where  $f$  is the fineness ratio, calculated from  $f=l/d=22.42/4.17=5.376$ .

**Line 41:** Interference factors are selected from Table 16-12.

**Line 42:** Weighted drag factor calculated as shown in table. For instance, for the wing, we get

$$C_{f_j} \cdot FF_j \cdot IF_j \cdot S_{wet_j} = 0.001999 \times 1.311 \times 1 \times 272.4 = 0.7140$$

**Line 43:** Skin friction drag is calculated by summing up the cells in Line 42 and dividing by the reference area of  $144.9 \text{ ft}^2$ . The resulting total skin friction coefficient, which includes interference and form drag is:

$$\frac{1}{S} \sum_{j=1}^N C_{f_j} \times FF_j \times IF_j \times S_{wet_j}$$

$$= \frac{1}{144.9} (0.7140 + 0.1762 + 0.1120 + 0.7607) = 0.01217$$

This only partially completes the drag analysis—drag due to miscellaneous sources remains to be determined and added to the above value, in addition to other corrections that must be made. This will be done in the next section.

**TABLE 16-12** Typical interference factors.

Component	IF
Nacelle or external store, directly under a fuselage.	1.5
Nacelle or external store, under a fuselage, less than about 1 diameter away.	1.3
Nacelle or external store, under a fuselage, more than about 1 diameter away.	1.0
Object, such as a fuel tank, mounted to a wingtip.	1.25
High wing or mid wing with carefully designed fairing	1.0
Unfilled low wing	1.1–1.4
Whitcomb winglet	1.04
"Airbus" style winglet	1.04
Modern blended winglet	1.00–1.01
Aerodynamic or square leaf-spring main landing gear strut entering wing or fuselage	1.10
Aerodynamic wing strut entering wing on one end and fuselage on the other	1.10
Boundary layer diverter	~1.0
Conventional tail	1.04–1.05
Cruciform tail	1.06
V-tail	1.03
H-tail (B-25 Mitchell or A-10 Warthog style)	1.08
H-tail (Lockheed Model 10 Electra style)	1.13
H-tail (Beech D-18 style)	1.06
Triple-tail (Lockheed Constellation style)	1.10
T-tail	1.04

In part based on S.F. Hoerner, *Fluid-Dynamic Drag*, L. Hoerner, 1965; D. Raymer, *Aircraft Design: A Conceptual Approach*, fourth ed., AIAA Education Series, 2006.

for nacelles mounted on the rear of the airplane (a Sud-Est Caravelle configuration).

### 16.3.7 Interference Factors

As previously stated, *interference factors (IF)* account for the proximity of one component to another. For instance, consider the juncture between the wing and fuselage, which constrains the airflow compared to that of the individual components. This increases the local airspeeds, increasing the drag. However, the *IFs* do not account for additional drag that arises due to early separation in poorly designed wing/fuselage junctures.

**Table 16-12** lists typical *IFs*, partially derived from Refs. [33, 79] and partially using factors that have worked well in drag analyses performed by the author. No claim is made about their accuracy beyond that. Note that when using the factors for multiple objects, e.g., the triple-tail of the L-1049 Constellation, the presented *IF* must be applied to all surfaces. Thus, when using the CDBM, each of the four surfaces constituting the tail (one HT and three VTs) must be multiplied by  $IF=1.10$ . The following formulation illustrates how its contribution would be accounted for in the CDBM:

$$\begin{aligned} \sum_{i=1}^N \bar{C}_{f_i} \times FF_i \times S_{wet_i} \times IF_i &= \dots + \overbrace{\bar{C}_{f_{HT}} \times FF_{HT} \times S_{wet_{HT}} \times IF_{HT}}^{HT} \\ &+ \overbrace{\bar{C}_{f_{VT_1}} \times FF_{VT_1} \times S_{wet_{VT_1}} \times IF_{VT_1}}^{VT 1 \text{ of } 3} + \overbrace{\bar{C}_{f_{VT_2}} \times FF_{VT_2} \times S_{wet_{VT_2}} \times IF_{VT_2}}^{VT 2 \text{ of } 3} \\ &+ \overbrace{\bar{C}_{f_{VT_3}} \times FF_{VT_3} \times S_{wet_{VT_3}} \times IF_{VT_3}}^{VT 3 \text{ of } 3} + \dots \end{aligned}$$

For this application, we would use

$$IF_{HT} = IF_{VT1} = IF_{VT2} = IF_{VT3} = 1.10.$$

### 16.3.8 Cumulative Result of Undesirable Drag (CRUD)

The above title is a play on words. The word crud means dirt, filth, or refuse. In aircraft design, it stands for the undesirable drag caused by exhaust stacks, misaligned sheet-metal panels, antennas, small inlets and outlets, sanded walkways, and so on. These contributions are easily overlooked when performing drag analysis, primarily because they appear small. But they add up. The aspiring designer should be aware of this additional drag and account for it appropriately. This section introduces how this is typically done. The crud factor is typically 25%, which means that Equations (16-117) and (16-122) are multiplied by  $k_{crud} = 1.25$ .

It is strongly recommended that the designer estimates the  $C_{D_{min}}$  of similar aircraft and compares to  $C_{D_{min}}$  extracted from published (or otherwise reliable) sources. This information should be used to evaluate an aircraft specific  $k_{crud}$ . This can be accomplished using some of the methods presented in [Section 16.5, Special Topics Involving Drag](#).

### 16.3.9 Total Drag Coefficient: $C_D$

Once the drag contributions developed in this section have been estimated, the total drag coefficient at any flight condition is determined as follows:

$$C_D = C_{D_{min}} + C_{D_i} + C_{D_w} \quad (16-141)$$

## 16.4 MISCELLANEOUS OR ADDITIVE DRAG

This section presents methods for evaluating drag caused by components that are not conveniently analyzed using the *component drag buildup method* (CDBM), discussed in [Section 16.3.5](#). This includes methods to estimate the drag of landing gear, antennas, sharp corners, joints, fasteners, inlets, outlets, fairings, and various other protuberances generally found on aircraft. This drag, justifiably called *miscellaneous or additive drag*, can cause substantial increase in total drag. As shown in Equation (16-117) or (16-122), it is denoted by  $C_{D_{misc}}$  and is given by

$$C_{D_{misc}} = \Delta C_{D_1} + \Delta C_{D_2} + \dots + \Delta C_{D_N} \quad (16-142)$$

Where the terms  $\Delta C_{D_1}, \Delta C_{D_2}, \dots$  represent contributions by all known components (sources) that were not accounted for using the CDBM. These contributions comprise many disparate sources, many of which use reference areas other than the reference wing area,  $S$ . Thus, each  $\Delta C_{D_i}$  has undergone adjustments to prepare its use with the reference wing area,  $S$ . How this is accomplished is shown in the derivation of Equation (16-144).

The geometric shape of protrusions common to aircraft is inherently irregular. For instance, consider the dissimilar geometry of antennas, blisters, or the main landing gear typical of ordinary aircraft. All lack consistent dimensions like those shared by lifting surfaces (e.g., span, root and tip chord). And most are geometrically complex enough to require drag estimation rooted in empirical formulation. Their drag is based on parameters like the thickness-to-length ratio (or fineness ratio), the location of the maximum thickness, frontal area, lengthwise distribution of thickness, leading-edge radius, trailing-edge angle, and camber, to name a few.

The first step in miscellaneous drag analysis is to evaluate each contribution independently. Each contribution is called a *source*. Descriptive subscripts add clarity when treating each source. It provides clarity to call the drag coefficient of an antenna  $\Delta C_{D_{antenna}}$  than, say,  $\Delta C_{D_s}$ . This naming convention is adopted here.

The next step is to establish a general method to handle reference areas for drag coefficients. Consider a source of interest whose drag force of magnitude  $D_S$  (where the subscript stands for *source*) was measured in a wind tunnel at dynamic pressure  $q$ . Furthermore, assume that  $D_S$  references some area,  $S_S$ , specific to the component (e.g., frontal area). This measurement can be converted into a drag coefficient,  $\Delta C_{D_S}$ , based on  $S_S$ , as follows

$$D_S = qS_S \Delta C_{D_S} \Rightarrow \Delta C_{D_S} = \frac{D_S}{qS_S} \quad (16-143)$$

As stated above, we prefer to use this coefficient in terms of the reference wing area,  $S$ . This calls for a scaling procedure. To guarantee we get the same drag regardless of using  $\Delta C_{D_S}$  or  $\Delta C_D$ , the product  $S \cdot \Delta C_{D_S}$  must equal  $S \cdot \Delta C_D$ . Assuming, the source is the above antenna, the drag coefficient based on  $S$  is

$$S \Delta C_{D_{antenna}} = S_S \Delta C_{D_S} \Rightarrow \Delta C_{D_{antenna}} = \Delta C_{D_S} \left( \frac{S_S}{S} \right) \quad (16-144)$$

Thus,  $\Delta C_{D_S}$  refers to  $S_S$ , while  $\Delta C_{D_{antenna}}$  (which is used with  $C_{D_{misc}}$ ) refers to the reference wing area,  $S$ .

### 16.4.1 Trim Drag

*Trim drag* is the penalty paid for providing static stability. It is caused by (A) The difference in lift-induced drag of the airplane with and without balancing forces and (B) the increase in drag due to the deflection of the elevator (see Section 16.2.6, Additional Topics on Drag). Note that this drag is NOT added to  $C_{D_{\text{misc}}}$ . Rather, like  $C_{D_{\text{min}}}$ , it is added directly to the sum constituting total drag (see Figure 16-21).

#### (1) Drag Contribution of Elevator Deflection

It is denoted by  $\Delta C_{D_{\delta_e}}$ . Its value typically ranges from 0.0003 to 0.0007 per degree of elevator deflection (see Table 24-3). The total contribution depends on the elevator deflection to trim,  $\delta_e$ . Note that this derivative *only* constitutes the change in drag of the surface and not the contribution of its lift to the trim drag. This is treated next.

#### (2) Drag Contribution of a Simple Wing-HT-Thrust Combination

If it were possible to sustain steady-level flight without a balancing force, there would be no trim drag. However, this is not an option. Instead, the balancing force of a conventional, statically stable tail-aft aircraft is added to the weight. This means the total lift generated exceeds the weight alone. Therefore, the aircraft must operate at a higher AOA and, thus, higher lift-induced drag than otherwise. Ordinarily, in cruise, trim drag constitutes a small fraction of the total drag of the airplane; it should range from 1% to 2%. It increases at higher AOAs. During conceptual design, it is practical to estimate the trim drag using the simple formulation presented below. This methodology can be revised for more complex situations.

Consider the simple wing-HT system operating at a low AOA, as shown in Figure 16-52. For this system, the trim drag is given by<sup>8</sup>:

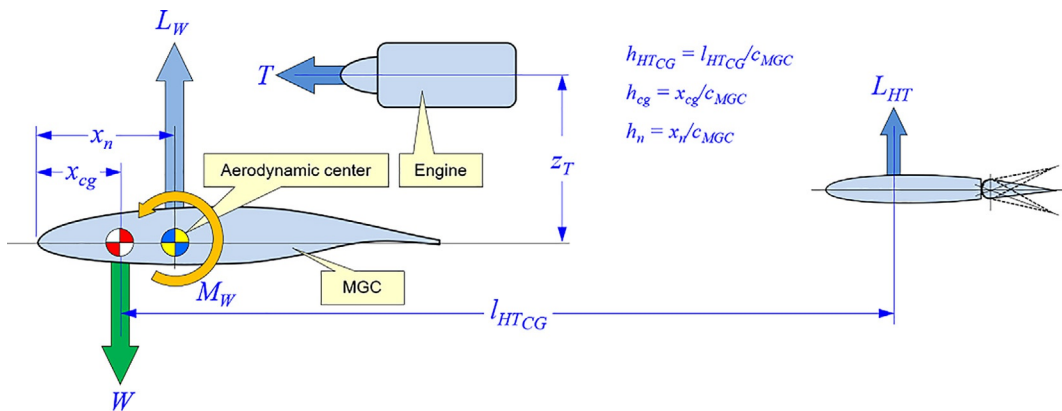


FIGURE 16-52 A simple free-body diagram used to derive the simplest formulation of trim drag.

$$\Delta C_{D_{\text{trim}}} = B \left( h_{HTCG} A - C_{M_W} + C_{M_{\theta_T}} \right)^2 - k A^2 + \Delta C_{D_{\delta_e}} \cdot \delta_e \quad (16-145)$$

Where:  $A = \frac{W}{qS}$        $B = \frac{k}{(h_{HTCG} + h_{cg} - h_n)^2}$       (16-146)

and

$W$  = Weight at condition,

$l_{HTCG}$  = Tail arm (see Figure 16-52),

$C_{LW}$  = Wing lift coefficient,

$C_{M_W}$  = Wing pitching moment coefficient,

$h_{cg}$  = Fractional distance between LE of  $c_{MGC}$  and the CG,

$h_n$  = Fractional distance between LE of  $c_{MGC}$  and the AC,

$h_{HTCG}$  = Fractional tail arm (see Figure 16-52),

$C_{M_{\theta_T}}$  = Pitching moment due to thrust.

Other variables have already been defined in multiple places. Also see relations in the derivation of the equations.

### DERIVATION OF EQUATIONS (16-145) AND (16-146)

Referring to Figure 16-52, statics requires the following to hold in steady level flight (nose-up rotation is positive):

$$\sum F_z = 0; \quad L_W + L_{HT} - W = 0$$

$$\sum M_{CG} = 0; \quad (x_{cg} - x_n)L_W - l_{HTCG}L_{HT} + M_W - z_T T = 0$$

<sup>8</sup> Note that this expression has been improved over that of the first edition of this book.

Note that  $M_W$  is a negative (nose-down) value. Next, divide through by  $qSc_{MGC}$  to convert the moment equation to coefficient form and noting the fractional distances of Chapter 24,  $h_{cg} = x_{cg}/c_{MGC}$ ,  $h_n = x_n/c_{MGC}$ , and  $h_{HT_{CG}} = l_{HT_{CG}}/c_{MGC}$ , we get

$$(h_{cg} - h_n)C_{LW} - h_{HT_{CG}}C_{L_{HT}} + C_{M_W} - z_T \frac{T}{qSc_{MGC}} = 0$$

Then, replace the thrust contribution by  $C_{M_{\theta_T}}$  per Equation (24-109) and solve for the balancing force the HT must generate (in a coefficient form). Note that  $z_T$  is positive if the thrustline is above the CG and otherwise negative.

$$C_{L_{HT}} = \frac{(h_{cg} - h_n)C_{LW} + C_{M_W} - C_{M_{\theta_T}}}{h_{HT_{CG}}} \quad (\text{i})$$

Convert the force equation into coefficient form by dividing through by  $qS$  and substitute Equation (i) into the force equation to get:

$$C_{LW} + C_{L_{HT}} - \frac{W}{qS} = 0 \Rightarrow C_{LW} = \frac{h_{HT_{CG}}W/(qS) - C_{M_W} + C_{M_{\theta_T}}}{h_{HT_{CG}} + h_{cg} - h_n} \quad (\text{ii})$$

The trim drag is the difference between the lift coefficient with and without stabilizing moments. Thus, we write

$$\begin{aligned} \Delta C_{D_{trim}} &= (C_{D_i})_{stab} - (C_{D_i})_{no\ stab} + \Delta C_{D_{\delta_e}} \cdot \delta_e \\ &= k \left( C_{LW}^2 - \left( \frac{W}{qS} \right)^2 \right) + \Delta C_{D_{\delta_e}} \cdot \delta_e \end{aligned} \quad (\text{iii})$$

Substituting Equation (ii) into Equation (iii), followed by some algebraic manipulations, leads to

$$\begin{aligned} \Delta C_{D_{trim}} &= k \left( \frac{1}{(h_{HT_{CG}} + h_{cg} - h_n)^2} \left( h_{HT_{CG}} \frac{W}{qS} - C_{M_W} + C_{M_{\theta_T}} \right)^2 \right. \\ &\quad \left. - \left( \frac{W}{qS} \right)^2 \right) + \Delta C_{D_{\delta_e}} \cdot \delta_e \end{aligned} \quad (\text{iv})$$

$$\text{Next let } A = \frac{W}{qS} \quad B = \frac{k}{(h_{HT_{CG}} + h_{cg} - h_n)^2}$$

These constitute Equation (16-146). Substitute Equation (ii) into Equation (iii), using  $A$  as defined above.

$$\Delta C_{D_{trim}} = B \left( h_{HT_{CG}}A - C_{M_W} + C_{M_{\theta_T}} \right)^2 - kA^2 + \Delta C_{D_{\delta_e}} \cdot \delta_e$$

This is Equation (16-145).

### EXAMPLE 16-12

Estimate the trim drag coefficient and drag force for an SR22 cruising at 185KTAS at S-L, assuming the following parameters:

### EXAMPLE 16-12 (cont'd)

$W = 3400 \text{ lb}_f$	$S = 144.9 \text{ ft}^2$	$T = 450 \text{ lb}_f$
$k = 0.04207$	$C_{M_W} = -0.060$	$\Delta C_{D_{\delta_e}} \cdot \delta_e = 0$
$l_{HT_{CG}} = 14.06 \text{ ft}$	$z_T = 0.6 \text{ ft}$	$c_{MGC} = 3.783 \text{ ft}$
$h_{cg} = 0.25$	$h_n = 0.40$	$h_{HT_{CG}} = 3.717$

#### SOLUTION:

Dynamic pressure:

$$q = \frac{1}{2} \rho V^2 = \frac{1}{2} (0.002378) (185 \times 1.688)^2 = 115.9 \text{ lb}_f/\text{ft}^2$$

Pitching moment due to thrust:

$$C_{M_{\theta_T}} = z_T \frac{T}{qSc_{MGC}} = (0.6) \frac{450}{(115.9)(144.9)(3.783)} = 0.004248$$

$$\text{Constant } A: \quad A = \frac{W}{qS} = \frac{3400}{(115.9)(144.9)} = 0.2024$$

Constant  $B$ :

$$B = \frac{k}{(h_{HT_{CG}} + h_{cg} - h_n)^2} = \frac{0.04207}{(3.717 + 0.25 - 0.40)^2} = 0.003307$$

Therefore, the trim drag amounts to

$$\begin{aligned} \Delta C_{D_{trim}} &= B \left( h_{HT_{CG}}A - C_{M_W} + C_{M_{\theta_T}} \right)^2 - kA^2 + \Delta C_{D_{\delta_e}} \cdot \delta_e \\ &= (0.003307)((3.717)(0.2024) - 0.06 + 0.004248)^2 \\ &\quad - (0.04207)(0.2024)^2 + (0) \\ &= 0.0004812 \end{aligned}$$

Thus, the trim drag force amounts to

$$D_{trim} = qS \Delta C_{D_{trim}} = (115.9)(144.9)(0.0004812) = 8.1 \text{ lb}_f$$

### 16.4.2 Cooling Drag

The term *cooling drag* refers to drag associated with cooling the engine of a propeller driven aircraft. Its determination is not needed for jet engines; it is accounted for in their net thrust (which equals gross thrust minus engine drag). The aircraft designer must still account for nacelle/pylon drag (using the CDBM). See more about jet engine drag in Refs. [83, 84].

The overarching concern of cooling drag involves the design of the nacelle. It is a major contributor to wing drag (especially in climb) and cooling drag. The former is evaluated using the CDBM, the latter is treated here. The magnitude of cooling drag depends on external and internal contributions. The designer is urged to review the design guidelines of Section 7.2.7, *Piston Engine Inlet and Exit Sizing*, in particular of Refs. [85–90]. These provide excellent guidance for the inlet and exit design to help reduce cooling drag.

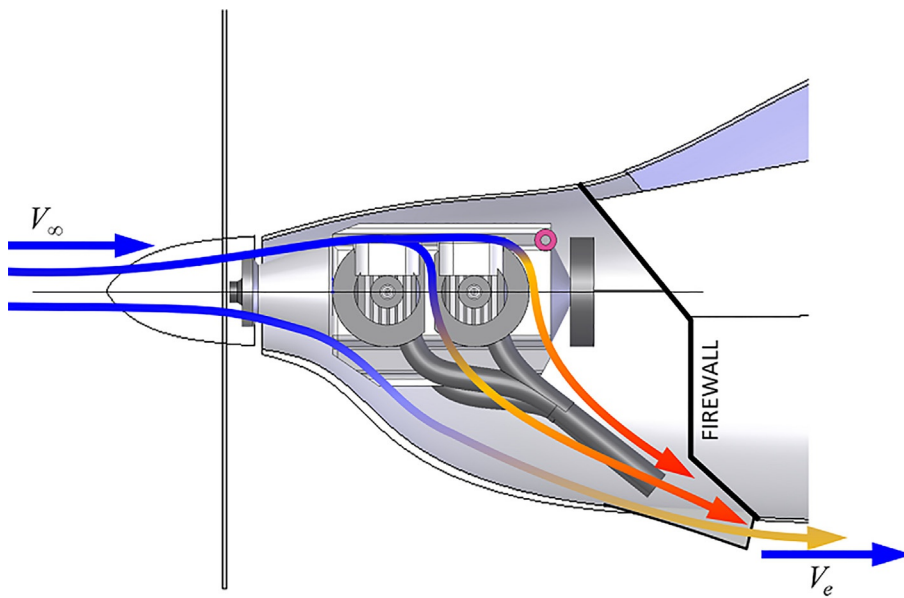


**FIGURE 16-53** Idealization of a conventional engine installation.

The operation of powered aircraft affects drag through heat transfer. This exposes heat exchangers to the free stream airflow. The cylinder head fins of a piston engine and radiators for oil-cooling (and water-cooling if present) constitute a heat exchanger. The flow entering the heat exchanger has a total head of which some is lost as the air flows through it. This causes a drop in the total pressure of the flow and reduces its energy. Some of this energy loss is made up by adding heat to the flow. However, if the heat energy added is less than the energy lost due to the pressure drop, the flow's momentum flux is reduced. This reduction is manifested as a drag force and constitutes the *cooling drag*.

Cooling drag is hard to estimate due to the complexity of the flow field inside the engine compartment (see idealization in Figure 16-53). Typically, it is estimated using empirical methods based on testing performed by the engine manufacturer. The following method for estimating cooling drag is an example of such a methodology; here largely based on McCormick [91]. It yields the following expression for the cooling drag coefficient.

$$\Delta C_{D_{cool}} = \frac{\dot{m}(V_\infty - V_e)}{qS} \quad (16-147)$$

Where  $\dot{m}$  is the mass flow rate through the engine compartment,  $V_\infty$  is the far-field airspeed (represents the inlet airspeed), and  $V_e$  is the average airspeed at the exit of the engine cowling.

### DERIVATION OF EQUATION (16-147)

This derivation is based, in part, on Ref. [91]. The flow through the engine changes its kinetic energy from  $E_\infty$  in the far-field to  $E_e$  at the exit. This change in energy can be expressed as the rate of change of work

$$\Delta W = \frac{1}{2} \dot{m} (V_\infty^2 - V_e^2) \quad (i)$$

Algebraically, this can be rewritten as follows:

$$\Delta W = \frac{1}{2} \dot{m} (V_\infty^2 - V_e^2) = \dot{m} (V_\infty - V_e) \frac{(V_\infty + V_e)}{2} \quad (ii)$$

Where the term  $\dot{m}(V_\infty - V_e)$  is the momentum flux (force) associated with the change in energy. Calling this force  $D_{cool}$ , we write

$$\Delta W = \overbrace{\dot{m}(V_\infty - V_e)}^{\equiv D_{cool}} \frac{(V_\infty + V_e)}{2} = D_{cool} \frac{(V_\infty + V_e)}{2} \quad (iii)$$

In order to convert  $D_{cool}$  to an additive drag coefficient, we write:

$$D_{cool} = qS \Delta C_{D_{cool}} = \dot{m}(V_\infty - V_e) \Rightarrow \Delta C_{D_{cool}} = \frac{\dot{m}(V_\infty - V_e)}{qS} \quad (iv)$$

### EXAMPLE 16-13

Estimate the cooling drag and cooling drag coefficient of the airplane of Example 7-5, if its wing area is  $S = 144.9 \text{ ft}^2$ , far-field airspeed is  $V_\infty = 185 \text{ KTAS}$  at 10,000 ft, engine compartment exit airspeed is  $V_e = 199.3 \text{ ft/s}$ , and flow of cooling air is  $2.7 \text{ lb}_f/\text{s}$  (i.e.,  $\dot{m} = 0.08392 \text{ slugs/s}$ ).

#### SOLUTION:

The cooling drag is calculated per the momentum conservation. The momentum of air exiting the engine is less than that entering. Thus, per Equation (14-35), where the input values are taken from Example 7-5, we get

$$D_{cool} = -\dot{m}(V_e - V_\infty) = 0.08392((185)(1.688) - 199.3) = 9.481 \text{ lb}_f$$

The cooling drag coefficient is estimated from Equation (16-147), where the dynamic pressure was given (in Example 7-5) as  $q = 80.60 \text{ lb}_f/\text{ft}^2$ :

**EXAMPLE 16-13 (cont'd)**

$$\Delta C_{D_{cool}} = \frac{\dot{m}(V_\infty - V_e)}{qS} = \frac{9.481}{(80.60)(144.9)} = 0.0008118$$

This amounts to about 8.12 dragcounts.

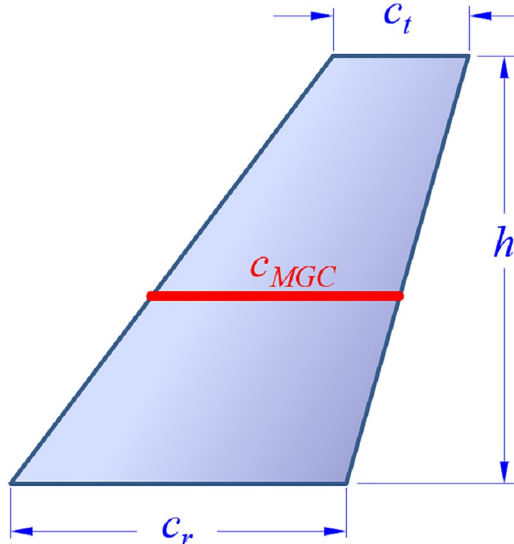
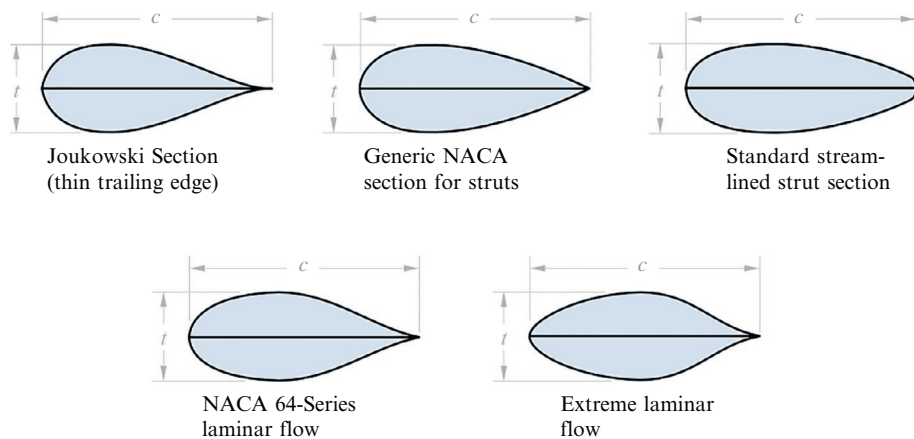


**FIGURE 16-54** Geometric definition of a small wing-like surface.

#### 16.4.3 Drag of Simple Wing-like Surfaces

Consider the wing-like surface in [Figure 16-54](#). It represents an aerodynamically shaped antenna, or some other fin, and features a single airfoil. Its drag can be determined by estimating the averaged skin friction coefficient of the  $c_{MGC}$  or the average chord of the surface. The additive drag coefficient of this surface, here denoted by  $\Delta C_{D_{fin}}$ , can be estimated from:

**FIGURE 16-55** Selected standard cross sections for wing- and landing gear struts. Reproduced from S.F. Hoerner, *Fluid-Dynamic Drag*, L. Hoerner, 1965.



$$\Delta C_{D_{fin}} = \bar{C}_f \left[ 1 + 2.7(t/c) + 100(t/c)^4 \right] \frac{h(c_r + c_t)}{2S} \quad (16-148)$$

This additive drag coefficient is based on the reference area, as can be seen in the equation. Here the form factor is based on Equation [\(16-125\)](#).

**EXAMPLE 16-14**

Determine the additive drag coefficient for a COM antenna for the SR22 airplane, if its root chord is 4.5 in., tip is 2 in., and height is 13.5 in. Assume an averaged skin friction coefficient of 0.0035 and a  $t/c = 0.25$ .

**SOLUTION:**

$$\begin{aligned} \Delta C_{D_{fin}} &= \bar{C}_f \left[ 1 + 2.7(t/c) + 100(t/c)^4 \right] \frac{h(c_r + c_t)}{2S} \\ &= (0.0035) \left[ 1 + 2.7(0.25) + 100(0.25)^4 \right] \\ &\quad \cdot \frac{(13.5/12)((4.5+2)/12)}{2(144.9)} = 0.00001520 \end{aligned}$$

This amounts to about 0.152 dragcounts.

#### 16.4.4 Drag of Streamlined Struts and Landing Gear Pant Fairings

The cross sections in [Figure 16-55](#) are typical of those used for wing struts or to reduce the drag of leaf-spring landing gear legs. Such shapes typically operate in a low  $R_e$  region (based on chord,  $c$ ). The drag of such sections is typically related to their thickness-to-chord ratios ( $t/c$ ). The additive source drag coefficient for the strut,  $\Delta C_{D_s}$ , is given by Ref. [33, pp. 6–5] and is based on empirical results:

$$\Delta C_{D_s} = \frac{D_s}{qS} = 2\bar{C}_f [1 + (t/c)] + (t/c)^2 \quad (16-149)$$

Where  $S_S$  is the planform area of the strut (i.e., its length  $\times$  chord) and the coefficient "2" accounts for the two sides of the planform. The additive drag coefficient for a strut,  $\Delta C_{D_{strut}}$ , of length  $l$  and chord  $c$  in terms of  $S$  is thus estimated from:

$$\Delta C_{D_{strut}} = \left[ 2\bar{C}_f(1+t/c) + (t/c)^2 \right] \left( \frac{l \times c}{S} \right) \quad (16-150)$$

### EXAMPLE 16-15

Determine the additive drag of a (Cessna-like) wing strut of 5-ft length, 4-in. chord, and  $t/c=0.2$  at 110KTAS airspeed at S-L. The reference area is  $160 \text{ ft}^2$ . Assume no interference and  $\bar{C}_f = 0.008$ .

**SOLUTION:**

Using Equation (16-150), we get:

$$\begin{aligned} \Delta C_{D_{strut}} &= \left[ 2\bar{C}_f(1+t/c) + (t/c)^2 \right] \left( \frac{l \times c}{S} \right) \\ &= \left[ 2(0.008)(1+0.2) + (0.2)^2 \right] \left( \frac{5 \times (4/12)}{160} \right) \\ &= 0.0006167 \end{aligned}$$

This amounts to about 6.2 dragcounts. Therefore, the resulting drag amounts to:

$$\begin{aligned} D_{strut} &= \frac{1}{2} \rho V^2 S \Delta C_{D_{strut}} \\ &= \frac{1}{2} (0.002378) (100 \times 1.688)^2 (160) (0.0006167) \\ &= 3.34 \text{ lb}_f \end{aligned}$$

This means that each strut (assuming there are two) adds 3.34  $\text{lb}_f$  of drag to the total drag.

### EXAMPLE 16-16

Determine the additive drag coefficient of a step onto the wing to help occupants enter the cabin of an SR22 aircraft. There are two such entry steps, whose cross section is the *standard streamlined strut section* that are approximately 12 in. long, 3-in. chord and 1-in. thickness. Assume no interference, ignore the break in the step where it changes from a step to a strut and  $\bar{C}_f=0.008$ .

**SOLUTION:**

The  $t/c$  is  $1/3$  or about 0.333. Therefore, using Equation (16-150), we get for each step:

$$\Delta C_{D_{strut}} = \left[ 2(0.008)(1+0.333) + (0.333)^2 \right] \left( \frac{(12/12) \times (3/12)}{144.9} \right) = 0.0002281$$

This amounts to about 2.28 dragcounts and 4.56 dragcounts for two steps.

### Thick Fairings

A fairing is a streamlined structure whose purpose is to reduce the drag that would be caused by the geometry it conceals. Hoerner [33, pp. 6–9] presents the following expression to determine the (2-dimensional) drag of a fairing whose chord is  $c$ , height is  $t$ , and length is  $l$ :

$$\Delta C_{D_{fairing}} = \bar{C}_f \left( 4 + \frac{2}{(t/c)} + 120(t/c)^3 \right) \quad (16-151)$$

The term inside the parenthesis is the form factor. It accounts for pressure and friction (see Figure 16-56). This means that  $\Delta C_{D_{strut}}$  for a strut of length  $l$  and thickness  $t$  (it is based on frontal area) in terms of  $S$  can be estimated from:

$$\Delta C_{D_{fairing}} = \bar{C}_f \left( 4 + \frac{2}{(t/c)} + 120(t/c)^3 \right) \left( \frac{l \times t}{S} \right) \quad (16-152)$$

This allows the optimum thickness-to-chord ratio to be determined by determining the derivative, setting it equal to zero, and solve for the optimum  $t/c$ , as shown below:

$$\begin{aligned} FF &= \left( 4 + \frac{2}{(t/c)} + 120(t/c)^3 \right) \\ \Rightarrow \frac{dFF}{d(t/c)} &= 360(t/c)^2 - \frac{2}{(t/c)^2} = 0 \\ \Rightarrow (t/c)_{opt} &= \sqrt[4]{\frac{1}{180}} = 0.273 \end{aligned}$$

Therefore, the optimum thickness-to-chord ratio is 0.273. This corresponds to a fineness ratio of  $\approx 3.7$ .

### 16.4.5 Drag of Landing Gear

**(1) Drag of Tires Only**

Figure 16-57 shows several types of aircraft tires, identified as A, B, C, and D. The drag generated by these styles is the focus of Ref. [92]. The drag coefficient of tires is usually based on their frontal area, defined as their diameter,  $d$ , times width,  $w$ . This is done in Figure 16-57 and Table 16-13. The additive drag coefficient of the tire can be estimated from:

$$\Delta C_{D_{tire}} = \frac{(d \times w)}{S} \Delta C_{D_s} \quad (16-153)$$

**FIGURE 16-56** Form Factor plotted against the fineness ratio for wing- and landing gear struts.

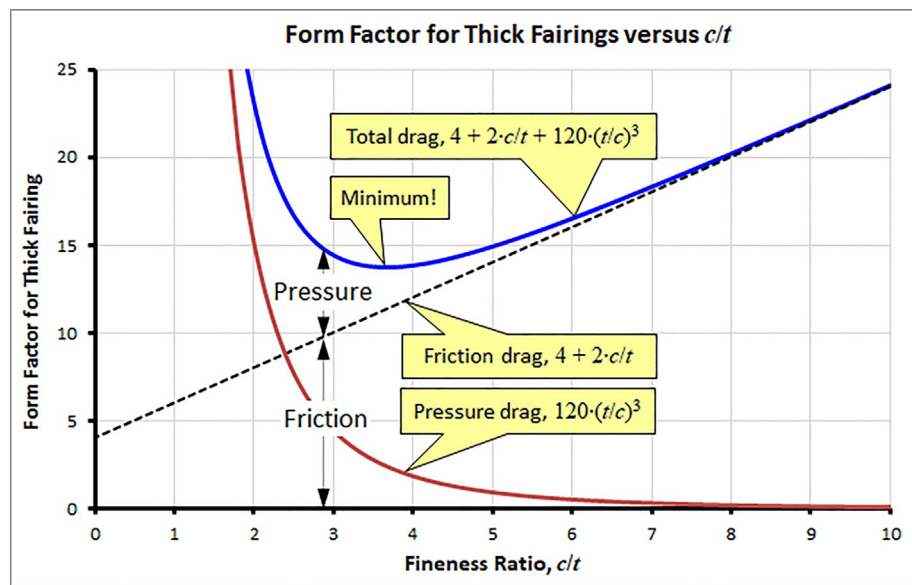


**FIGURE 16-57** Most common types of modern tires for aircraft landing gear. Based on W.H. Herrnstein, D. Biermann, *The Drag of Airplane Wheels, Wheel Fairings, and Landing Gears—I*, NACA R-485, 1935.

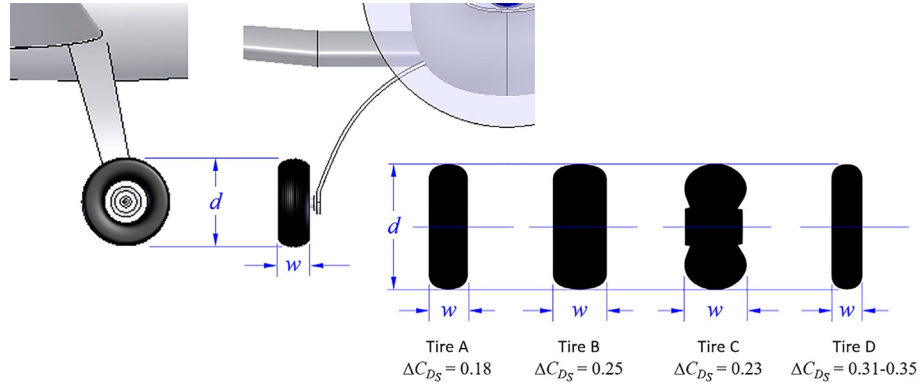


**TABLE 16-13** Drag of tires ( $d$ =diameter of tire,  $w$ =width of tire).

Tire Type	Corresponds to	Reference Area	$\Delta C_{D_S}$	Reference
A	Three Part Type (GA)	$d \times w$	0.18	
B	Type III	$d \times w$	0.25	NACA R-485
C	Type III High Floatation (tundra)	$d \times w$	0.23	
D	Old fashioned disc wheel types	$d \times w$	0.31-0.35	

## (2) Drag of Tires with Wheel Fairings

A wheel fairing reduces the aerodynamic drag of the tire. Figure 16-58 shows several fairing styles and Table 16-14 lists the applicable drag coefficients based on (1) the frontal area of the fairing and (2) the frontal area

of the tire. It is left to the reader to select which one to use. While the data are based on a Type III tires, for preliminary design purposes it may be assumed the drag coefficients are independent of the type of tire. The additive drag coefficient of the tire with the fairing can be estimated from:

$$\Delta C_{D_{\text{fairing}}} = \frac{(H \times W)}{S} \Delta C_{D_S} \quad (16-154)$$

Note that this coefficient is for a single tire with a fairing. This is emphasized because some texts present the drag coefficient for two wheels (e.g., assuming both main landing gear). However, some aircraft feature fairings on the main wheel only, while others have all three wheels (main and nose landing gear) with fairings.

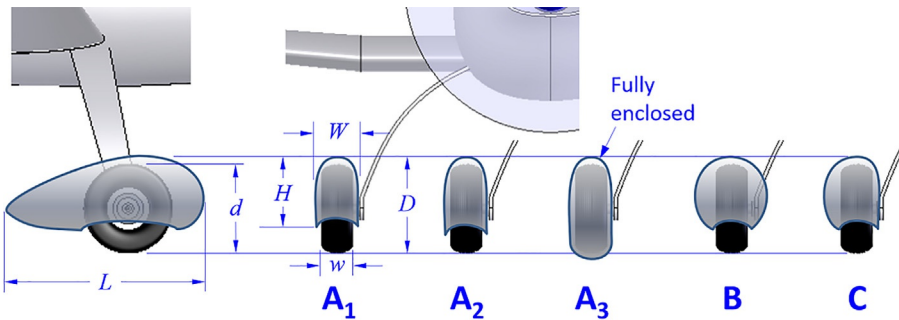


**FIGURE 16-58** Selected types of landing gear wheel fairings. The drag of the landing gear wheel fairing styles denoted by “A” through “C” is presented in **Table 16-13**. Based on W.H. Herrnstein, D. Biermann, *The Drag of Airplane Wheels, Wheel Fairings, and Landing Gears—I*, NACA R-485, 1935.

**TABLE 16-14** Drag of tires with fairings ( $H$ =fairing height,  $W$ =fairing width,  $d$ =tire diameter,  $w$ =tire width).

Fairing Type	Tire Type	$\Delta C_{D_S}$ Reference Area = $H \times W$	$\Delta C_{D_S}$ Reference Area = $d \times w$	Reference
A1	Type III (B)	0.130	0.143	NACA R-485
A2	Type III (B)	0.090	0.119	
A3 (tire fully covered)	Type III (B)	0.044	0.070	
B	Type III (B)	0.117	0.217	
C	Type III (B)	0.129	0.188	

### (3) Drag of Fixed Landing Gear Struts with Tires

Drag coefficients for a number of typical fixed main landing gear with tires are presented in **Table 16-15**. All the drag coefficients are based on the dimensions of a single tire per side but apply to the entire installation (both wheels and support structure). The coefficients include interference drag, but exclude the nose landing gear, however. The additive drag coefficient of the fixed landing gear with the fairing can be estimated from:

$$\Delta C_{D_{fixed}} = \frac{(d \times w)}{S_{ref}} \Delta C_{D_S} \quad (16-155)$$

Refer to **Figure 16-59** for the shape of the landing gear configuration. Each configuration is identified with a letter ranging from A to Q. Ref. [92] presents results for these configurations, some of which feature more than one type of tire and even fairings. These differences are presented in **Table 16-15** using numbers following the letter (note that only configurations A through N are featured in the table). For instance, configurations A and B both feature a Type III tire, whereas configuration C is presented with five different tires, of which one configuration is supported by a streamlined tension wire and the other with a tubular tension support. The remainder of the configurations utilizes that same tubular support.

**TABLE 16-15** Drag of landing gear struts with and without fairings ( $h$ =height of tire,  $w$ =width of tire).

Strut Type	Tire Type	Reference Area	$\Delta C_{D_S}$	Reference
A	8.5-10	B	1.112	NACA R-485
B	8.5-10	B	1.204	
C1	8.5-10 + streamline wire	B	1.151	
C2	8.5-10 + tubular support	B	1.178	
C3	27-inch streamline + tube	A	1.082	
C4	25x11-4 X-low press + tube	C	0.940	
C5	30x5 disk wheel hi-press + tube	D1	1.779	
C6	32x6 disk wheel hi-press + tube	D2	1.373	
D1	8.5-10	B	1.230	
D2	8.5-10	B	1.191	
E	8.5-10	B	1.125	
F1	8.5-10	B	1.138	
F2	8.5-10 + Fairing C	B	0.877	
F3	27-inch streamline + tube	A	1.014	
F4	25x11-4 X-low press + tube	C	0.858	
F5	30x5 disk wheel hi-press + tube	D1	1.628	
G1	8.5-10	B	1.151	
G2	8.5-10+Fairing A2	B	0.733	
H	8.5-10	B	0.994	
I1	8.5-10 + Fairing B	B	0.536	
I2	8.5-10 + Fairing C	B	0.484	
I4	27-inch streamline + tube	A	0.564	
I5	27-inch streamline + tube	A	0.496	
J1	8.5-10	B	0.615	
J2	8.5-10 + Fairing A1	B	0.458	
J3	27-inch streamline	A	0.485	
K1	8.5-10	B	0.981	
K2	8.5-10 + Fairing C	B	0.641	
L	8.5-10	B	0.992	
M1	8.5-10 + Fairing A1	B	0.484	
M2	8.5-10+Fairing A1+Expanding fillet	B	0.315	
N	8.5-10	B	0.315	

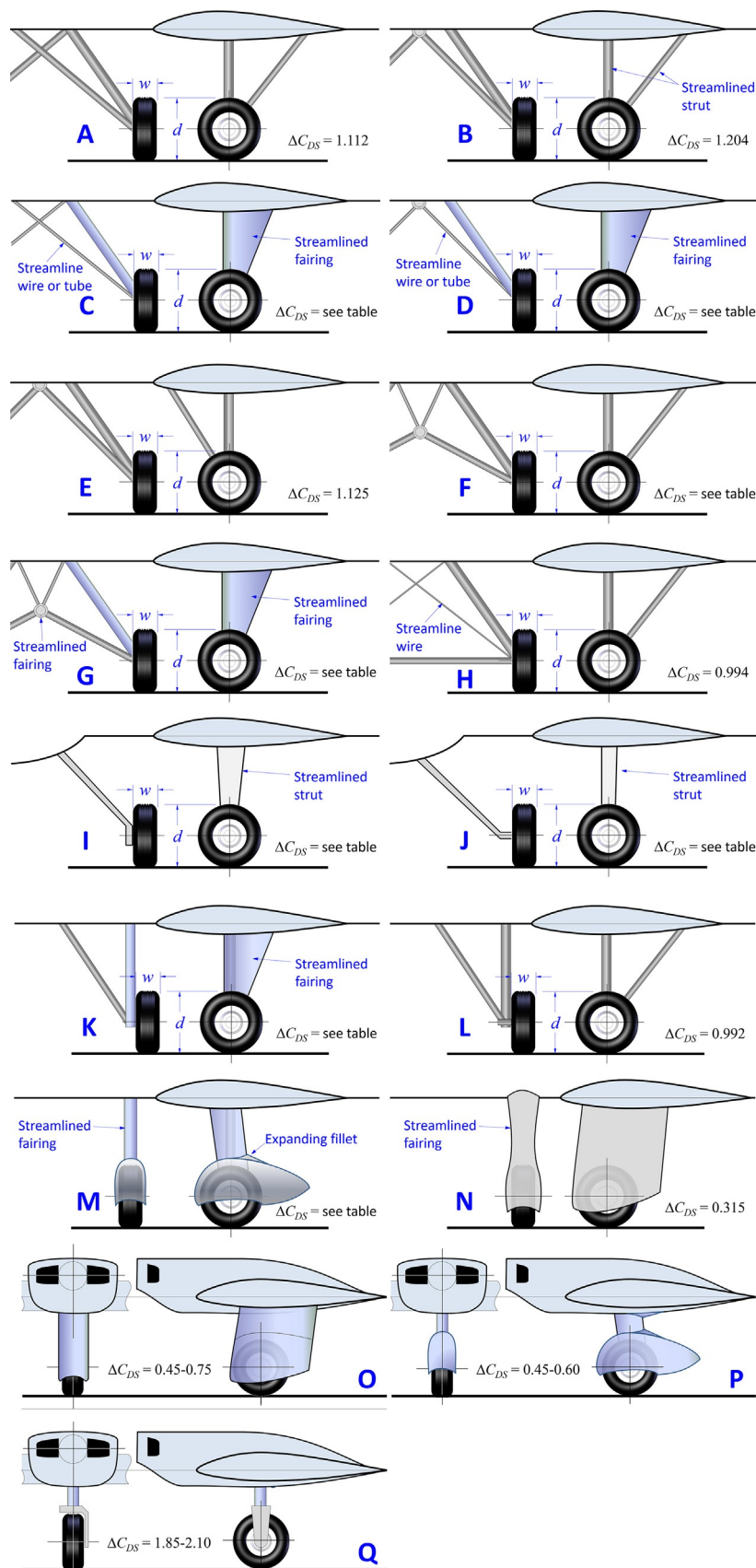


**FIGURE 16-59** Drag of selected types of fixed landing gear installations. All struts are streamlined. All drag coefficients are based on the tire geometry and pertain to the entire installation (two main gear). See Table 16-15 for additional detail. Based on W.H. Herrnstein, D. Biermann, *The Drag of Airplane Wheels, Wheel Fairings, and Landing Gears—I*, NACA R-485, 1935; J. Roskam, *Methods for Estimating Drag Polars of Subsonic Airplanes*, 4<sup>th</sup> printing, 1984.

**EXAMPLE 16-17**

Determine the additive drag coefficient for the fixed landing gear of the SR22 airplane. Its wing area is  $144.9 \text{ ft}^2$  and assumes the main landing gear tire dimensions are 15-in. diameter and 6-in. width and the nose gear tire is 14 by 5 in.

**SOLUTION:**

Approximate the main landing gear using Configuration I2 since the landing gear fairing (Style C) is similar in some ways to that of the SR22. The additive drag coefficient for I2 is  $\Delta C_{D_s} = 0.484$ . The nose landing gear can be represented using Configuration M1, for which  $\Delta C_{D_s} = 0.484$  as well. Note that the drag refers to the entire installation, which consists of two wheels. Since the nose gear is a single wheel, we reduce this number by a factor of two, i.e.,  $\Delta C_{D_s} = 0.242$  for the nose gear. Thus, the drag contribution of the main and nose landing gear can be represented by (note that a factor of 144 is used to convert in.<sup>2</sup> to ft<sup>2</sup>):

$$\text{Main: } \Delta C_{D_{\text{main}}} = \frac{(d \times w)}{S} \Delta C_{D_s} = \frac{(15 \times 6)/144}{144.9} (0.484) \\ = 0.00209$$

$$\text{Nose: } \Delta C_{D_{\text{nose}}} = \frac{(d \times w)}{S} \Delta C_{D_s} = \frac{(14 \times 5)/144}{144.9} (0.242) \\ = 0.00081$$

This amounts to about 20.9 dragcounts due to the main gear and 8.1 counts due to the nose landing gear.

**(4) Drag of Retractable Landing Gear**

Mair and Birdsall [93] give the following empirical expressions for the additive drag of landing gear in the absence and presence of flaps. In other words, one expression applies to deployed landing gear and retracted flaps. The other applies to the both the landing gear and flaps extended. The equations are based on historical data and are presented in terms of weight,  $W$  (in lb<sub>f</sub>) in the UK-system, or mass,  $m$  (in kg) in the SI-system. They are representative of commercial jetliners and business jet, and should not be used with lighter GA aircraft. The drag of landing gear with the flaps stowed is given as follows in the SI- and UK-systems, respectively, where subscripts indicate units required for terms:

Flaps retracted :

$$\Delta C_{D_{RG}} = \begin{cases} w_{\text{N/m}^2} (5.81 \times 10^{-5}) m_{\text{kg}}^{-0.215} & \frac{5.698 \times 10^{-4} m_{\text{kg}}^{0.785}}{S_{\text{m}^2}} \\ & \frac{0.003297 W_{\text{lb}_f}^{0.785}}{S_{\text{ft}^2}} \end{cases} \quad \begin{matrix} \text{SI} \\ \text{UK} \end{matrix} \quad (16-156)$$

If the flaps are fully deflected the expression becomes:

Flaps deployed :

$$\Delta C_{D_{RG}} = \begin{cases} w_{\text{N/m}^2} (3.16 \times 10^{-5}) m_{\text{kg}}^{-0.215} & \frac{3.099 \times 10^{-4} m_{\text{kg}}^{0.785}}{S_{\text{m}^2}} \\ & \frac{0.001793 W^{0.785}}{S_{\text{ft}^2}} \end{cases} \quad \begin{matrix} \text{SI} \\ \text{UK} \end{matrix} \quad (16-157)$$

**EXAMPLE 16-18**

Determine the additive drag coefficient of the retractable landing gear for an airplane that weighs 22,000 lb<sub>f</sub> and whose wing area is 300 ft<sup>2</sup>, with and without flaps.

**SOLUTION:**

Using Equations (16-156) and (16-157), we get:

Without flaps:

$$\Delta C_{D_{\text{wheel}}} = \frac{0.003297 W^{0.785}}{S} = \frac{0.003297 (22,000)^{0.785}}{300} \\ = 0.02817$$

With flaps:

$$\Delta C_{D_{\text{wheel}}} = \frac{0.001793 W^{0.785}}{S} = \frac{0.001793 (22,000)^{0.785}}{300} \\ = 0.01532$$

This amounts to 282 and 153 dragcounts respectively.

Jenkinson [80] gives the following expression for the drag of the landing gear of commercial jetliners. Formulation for two classes of jetliners is given; for medium-to-large jetliners like the Boeing 747, 757, 767, DC-10, L-1011, etc. and for smaller jetliners, such as the F-100, DC-9, and B-737. The expressions are presented in terms of the flat plate area,  $\Delta D/q$ . However, these have been modified using the following relation, to adhere to the presentation in this book.

$$\Delta D/q \rightarrow \Delta C_D = \Delta D/(qS)$$

Medium to large jetliners:

$$\Delta C_{D_{RG}} = \begin{cases} \frac{0.00157(m_{NLG} + m_{MLG})^{0.73}}{S} & \text{SI} \\ \frac{0.0025(W_{NLG} + W_{MLG})^{0.73}}{S} & \text{UK} \end{cases} \quad (16-158)$$

Small jetliners:

$$\Delta C_{D_{RG}} = \begin{cases} \frac{0.00093(m_{NLG} + m_{MLG})^{0.73}}{S} & \text{SI} \\ \frac{0.006(W_{NLG} + W_{MLG})^{0.73}}{S} & \text{UK} \end{cases} \quad (16-159)$$

Where  $W_{NLG}$  and  $W_{MLG}$  is the weight (in lb<sub>f</sub>) of the nose and main landing gear, respectively and  $m_{NLG}$  and  $m_{MLG}$  is the mass (in kg) of the nose and main landing gear, respectively. The result applies to the entire landing gear. It underpredicts smaller aircraft and should only be used for large aircraft.

Roskam [94] presents a simple method for determining the additive drag of retractable landing gear. To calculate the additive drag coefficient, it uses the ratio of the actual frontal area of the landing gear to the area of a rectangle enclosing the gear (see Figure 16-60). The method assumes an open wheel well, but suggests a 7% reduction to correct for closed wells. The formulation is presented below for open and closed wheel wells:

$$\text{Open wheel wells: } \Delta C_{D_{RG}} = 0.05328 \left( \frac{d \times w}{S} \right) e^{5.615m} \quad (16-160)$$

$$\text{Closed wheel wells: } \Delta C_{D_{RG}} = 0.04955 \left( \frac{d \times w}{S} \right) e^{5.615m} \quad (16-161)$$

Where  $m = S_A / (d \times w)$ . Note that even though the drag coefficient is based on the ratio  $m$ , the value of  $\Delta C_{D_{RG}}$  applies to both legs of the main landing gear (the nose landing gear is not included). Also note a common error is to forget to convert  $d$  and  $w$  (which often are in inches)

to ft, to ensure unit consistency with  $S$  in ft<sup>2</sup>. If  $m = 0.75$  and  $S / (d \times w) = 130$ , then the open wheel well  $\Delta C_{D_{RG}} \approx 0.0272$ .

### (5) Drag of Nose Landing Gear

This method applies to both fixed and retractable nose landing gear (NLG). Essentials of the method are presented in Figure 16-61. It requires the distance of the NLG from the nose,  $a$ , its total length,  $e$ , and tire diameter,  $d$ , to be known. First, determine the ratio  $a/d$ . Use it to select the appropriate curve. Interpolate for values falling between curves. Next, calculate the wheel height ratio,  $e/d$ . Use it with the selected curve to read the source drag coefficient,  $\Delta C_{D_s}$ , on the vertical axis. Finally, calculate the additive drag coefficient,  $\Delta C_{D_{NLG}}$  (which is based on the reference wing area), as follows:

$$\Delta C_{D_{NLG}} = \frac{(d \times w)}{S} \Delta C_{D_s} \quad (16-160)$$

#### 16.4.6 Drag of Floats

Floats are a popular option for many GA aircraft. Their primary drawbacks include a healthy dose of additive drag, inherent destabilizing moment, and weight. This section presents a method to estimate the drag. Ref.

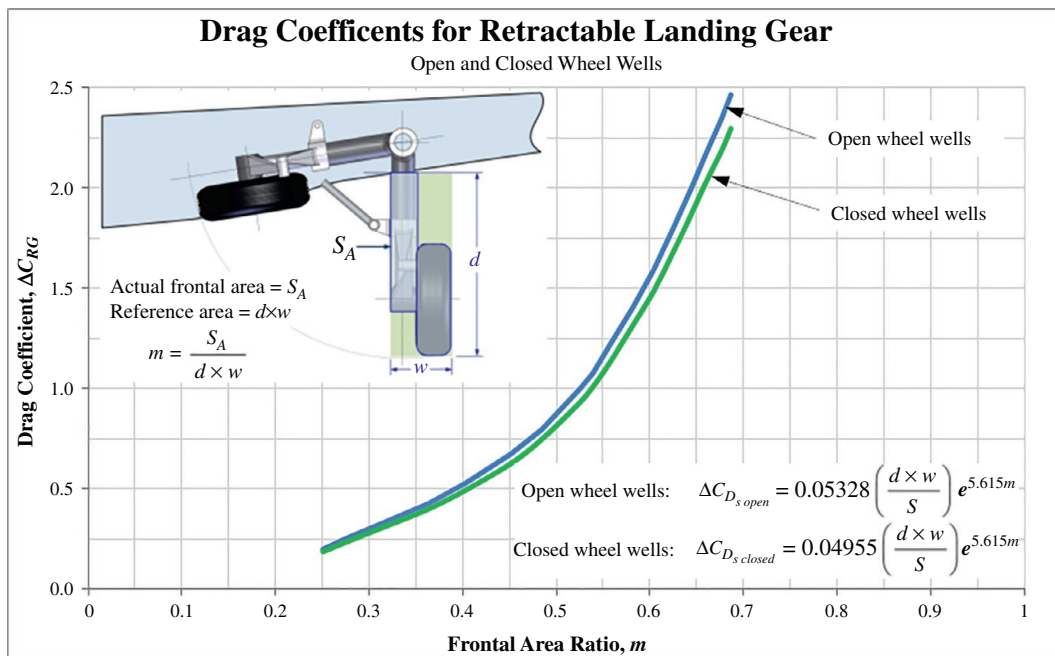


**FIGURE 16-60** Estimating the drag contribution of a retractable landing gear. Based on J. Roskam, *Methods for Estimating Drag Polars of Subsonic Airplanes*, 4<sup>th</sup> printing, 1984.

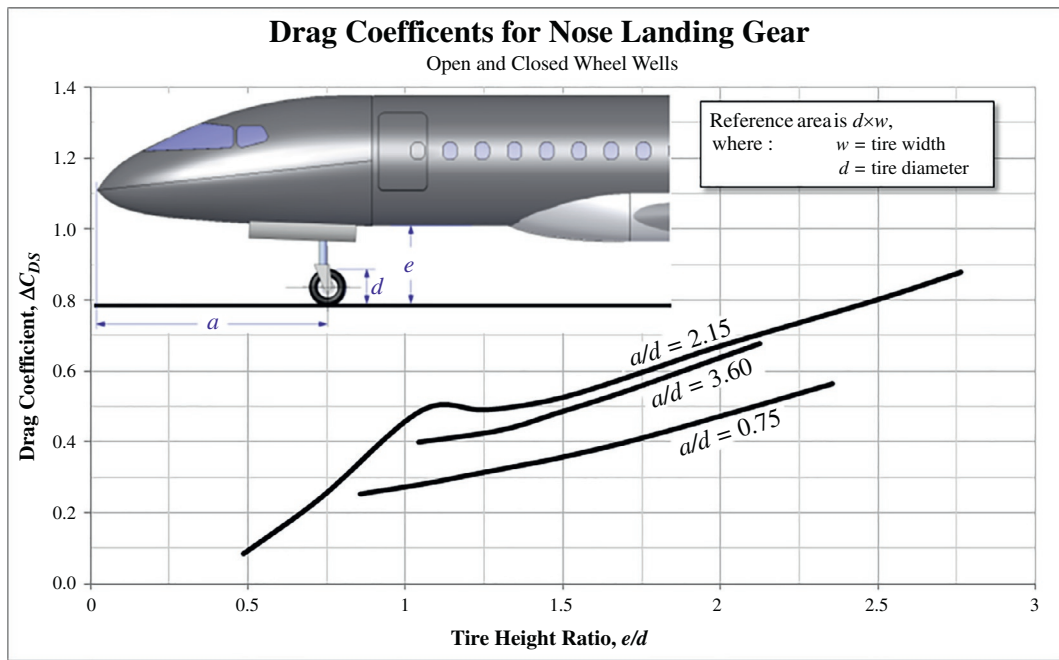


**FIGURE 16-61** Estimating the drag contribution of a nose landing gear. Based on J. Roskam, *Methods for Estimating Drag Polars of Subsonic Airplanes*, 4<sup>th</sup> printing, 1984.

[95] investigated the drag of four full-scale floats used as a single float for large single-engine military aircraft, such as the Vought OS2U Kingfisher. The floats varied in length, ranging from about 24.8 to 26.6 ft (7.56 to 8.11 m), with maximum cross-sectional area ranging from 6.63 to 9.25 ft<sup>2</sup> (0.616 to 0.859 m<sup>2</sup>). While larger than what is typically used for single-engine GA aircraft, the results permit the drag of smaller floats to be estimated. The reference concluded that the step constituted about 10% of the drag and adding a tail fairing reduced it by 8%. It found no benefit by counter-sunk rivets over normal universal head rivets aft of the step.

The following expressions refer to the configurations A, B, and C in Figure 16-62. The term  $A_{\max}$  is the maximum cross-sectional area of the float and  $\alpha$  is the AOA with respect to the horizontal upper surface. No provision was made to reduce the drag specifically, e.g., by removing hardware. The drag measurements included support fairings, except wire-bracings were not present. The  $R_e = 25$  million, based on the length of the float. The drag was measured using an  $\alpha$ -sweep from -6 degrees to +6 degrees at an airspeed of 87 KTAS. The drag applies to a single float only, so if using two floats, the additive drag coefficient must be doubled.

Ref. [96] investigated special NACA designed floats, referred to as the NACA 57 series. It was found that

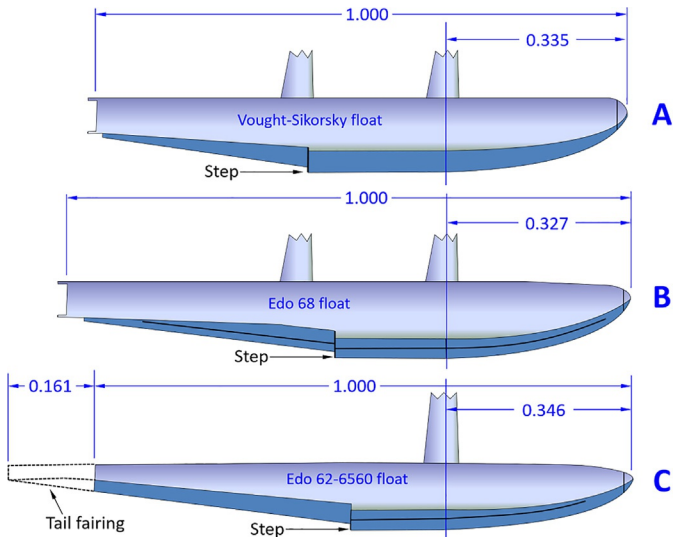


**FIGURE 16-62** Float geometries. The drag of the float styles denoted by "A," "B," and "C" is presented in Equations (16-163), (16-164), and (16-165), respectively. Based on R.N. Conway, J.D. Maynard, Wind-Tunnel Tests of Four Full-Scale Seaplane Floats, NACA WR-L-238, 1943.

the dead-rise angle (the angle between the horizontal and the "v" of the float) had a small effect on the total drag: The greater the dead-rise angle the higher the drag. The drag coefficients increase with the AOA similar to that reflected by Equation (16-163); however, the minimum drag ( $\Delta C_{D_s}$ ) is less or about 0.13–0.155.

$$\text{Float A: } \Delta C_{D_{\text{float}}} = \left( \frac{A_{\max}}{S} \right) (0.00165\alpha^2 + 0.00413\alpha + 0.2142) \quad (16-163)$$

$$\text{Float B: } \Delta C_{D_{\text{float}}} = \left( \frac{A_{\max}}{S} \right) (0.00109\alpha^2 + 0.00052\alpha + 0.1771) \quad (16-164)$$

$$\text{Float C: } \Delta C_{D_{\text{float}}} = \left( \frac{A_{\max}}{S} \right) (0.00176\alpha^2 - 0.00105\alpha + 0.1981) \quad (16-165)$$

### 16.4.7 Drag of Deployed Flaps

Deflecting flaps modifies the drag model in two ways: (1) minimum drag and (2) lift-induced drag both increase (see Figure 16-16). This section introduces methods to account for this change.

#### Increase of $C_{D_{\min}}$ due to Flaps

Young [97] presents an empirical method to estimate the drag of a number of types of flaps. The estimation depends on the flap type, flap chord ( $c_f$ ), deflection angle ( $\delta_f$ ), and its span ( $b_f$ ). The following expression is used for this estimation and it requires the two functions  $\Delta_1$  and  $\Delta_2$  to be determined. The former accounts for the contribution of the flap chord to the flap drag and the latter for the contribution of the flap deflection. These are detailed in the two graphs of Figure 16-63, and are discussed further below.

$$\Delta C_{D_{\text{flap}}} = \Delta_1 \Delta_2 \left( \frac{S_{\text{flap}}}{S} \right) \quad (16-166)$$

#### Flap Chord Contribution—The Function $\Delta_1$

As stated earlier, the function  $\Delta_1$  represents the contribution of the flap chord to the flap drag. This contribution is shown in the left image of Figure 16-63, for plain, split, and slotted flaps, for airfoils of three thickness-to-chord ratios; 0.12, 0.21, and 0.30. The author has digitized these graphs and they be reconstructed using the polynomial curvefits shown in Table 16-16. Note that the parameter  $R_f$  is the flap chord ratio, i.e.,  $R_f = \text{flap chord/wing chord} = c_f/c$ . This ratio typically ranges from 0.20 to 0.35.

#### Flap Deflection Contribution—The Function $\Delta_2$

The  $\Delta_2$  function represents the contribution of the flap deflection angle to the flap drag, shown in the right image of Figure 16-63, for plain, split, and slotted flaps, for airfoils of three thickness-to-chord ratios; 0.12, 0.21, and 0.30. These are given by the polynomial curvefits shown in Table 16-17.

Corke [98] presents additive drag for several types of flaps at the 30- and 50-degree deflection. These are reproduced in Table 16-18. It is a limitation that these apply to the specific flap span and chord of 60% and 25%, respectively. Regardless, these can come in handy for initial estimation of flap drag.

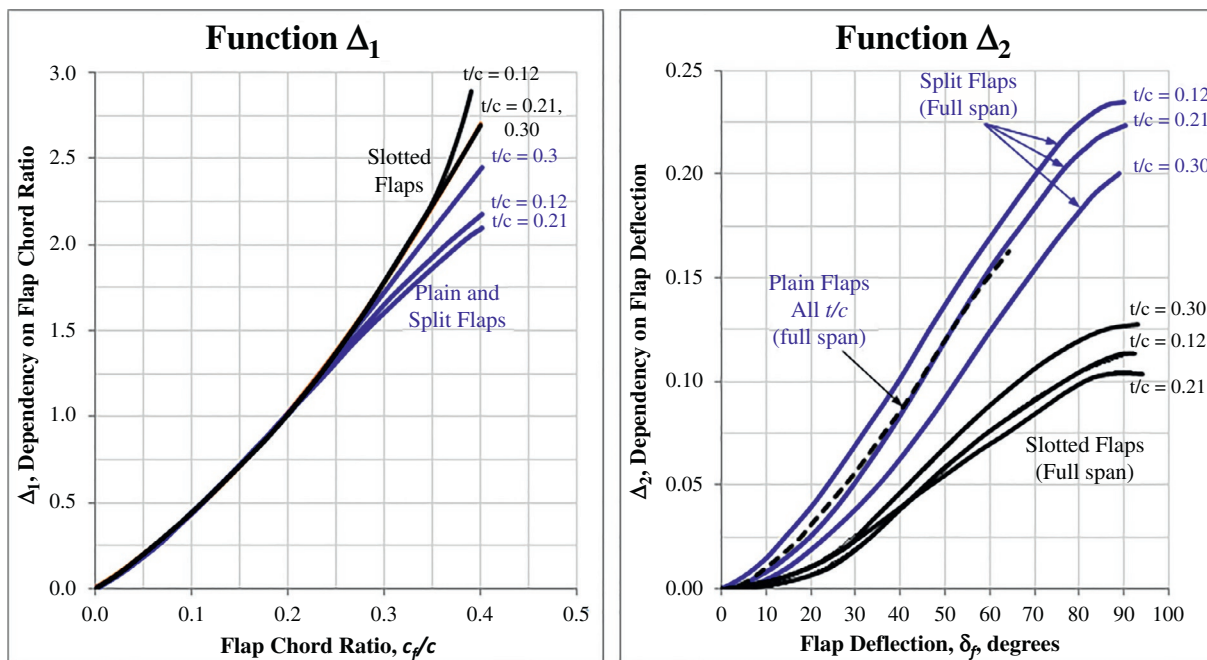


**FIGURE 16-63** Estimation of the drag contribution of the flaps calls for the  $\Delta_1$  and  $\Delta_2$  functions to be determined. Based on A.D. Young, *The Aerodynamic Characteristics of Flaps*, R.&M. No. 2622, British A. R. C., 1947.

**TABLE 16-16** Polynomial representations of the function  $\Delta_1$  for plain, split, and slotted flaps.

Plain and Split Flaps:	
t/c	Function ( $R_f = c_f/c$ )
0.12	$\Delta_1 = -21.090R_f^3 + 14.091R_f^2 + 3.165R_f - 0.00103$
0.21	$\Delta_1 = -19.988R_f^3 + 12.682R_f^2 + 3.363R_f - 0.0050$
0.30	$\Delta_1 = 4.6945R_f^2 + 4.3721R_f - 0.031$
Slotted Flaps:	
0.12	$\Delta_1 = 179.32R_f^4 - 111.6R_f^3 + 28.929R_f^2 + 2.3705R_f - 0.0089$
0.21, 0.30	$\Delta_1 = 8.2658R_f^2 + 3.4564R_f + 0.0054$

### 16.4.8 Drag of Deployed Spoilers

Deflecting wing spoilers modifies the flow field in complex ways, depending on chord- and spanwise position and spanwise extent of the device (see [Figure 16-64](#)). The geometry of the device itself (height, deflection angle, and perforations) also play an important role. It is recommended the reader investigates the literature for experimental data, with which it is rich. For instance, refer to Refs. [33, 99–101], to name a few. Also, study some of their supporting references. In the absence of such data, the spoiler can be approximated as a 3-dimensional flat plate. In this capacity refer to [Figure 16-76](#), which gives a  $C_{D_s} = 1.17$  for a circular plate. The planform shape of plates has surprisingly small effect on the drag once the flow on the leeward side is fully separated. Thus, we can devise the following approximation:

$$\Delta C_{D_{sp}} \approx 1.17 \frac{b_{sp} h_{sp}}{S} \left( \frac{\delta_{sp}}{90} \right) \quad (16-167)$$

**TABLE 16-17** Polynomial representations of the function  $\Delta_2$  for plain, split, and slotted flaps.

t/c	Function
Plain Flaps:	
0.12	$\Delta_2 = -3.795 \times 10^{-7} \delta_f^3 + 5.387 \times 10^{-5} \delta_f^2 + 6.843 \times 10^{-4} \delta_f - 1.4729 \times 10^{-3}$
Split Flaps:	
0.12	$\Delta_2 = -4.161 \times 10^{-7} \delta_f^3 + 5.5496 \times 10^{-5} \delta_f^2 + 1.0110 \times 10^{-3} \delta_f - 2.219 \times 10^{-5}$
0.21	$\Delta_2 = -5.1007 \times 10^{-7} \delta_f^3 + 7.4060 \times 10^{-5} \delta_f^2 - 4.8877 \times 10^{-5} \delta_f + 8.1775 \times 10^{-4}$
0.30	$\Delta_2 = -3.2740 \times 10^{-7} \delta_f^3 + 5.598 \times 10^{-5} \delta_f^2 - 1.2443 \times 10^{-4} \delta_f + 5.1647 \times 10^{-4}$
Slotted Flaps:	
0.12	$\Delta_2 = -2.4416 \times 10^{-12} \delta_f^6 + 6.3942 \times 10^{-10} \delta_f^5 - 6.2028 \times 10^{-8} \delta_f^4 + 2.4984 \times 10^{-6} \delta_f^3 - 1.8922 \times 10^{-5} \delta_f^2 + 3.1582 \times 10^{-4} \delta_f + 6.9698 \times 10^{-5}$
0.21	$\Delta_2 = 6.2317 \times 10^{-11} \delta_f^5 - 1.3354 \times 10^{-8} \delta_f^4 + 6.4833 \times 10^{-7} \delta_f^3 + 2.1134 \times 10^{-5} \delta_f^2 - 2.6425 \times 10^{-4} \delta_f + 5.2279 \times 10^{-4}$
0.30	$\Delta_2 = -3.7252 \times 10^{-7} \delta_f^3 + 5.4024 \times 10^{-5} \delta_f^2 - 4.4994 \times 10^{-4} \delta_f + 1.1175 \times 10^{-3}$

**TABLE 16-18** Additive flap drag coefficients.

Flap type	Reference deflection, $\delta_f$ (degrees)	$\Delta C_{flaps}$
Split or plain flap	30	0.05
	50	0.10
Slotted flap	30	0.02
	50	0.05
Fowler flap	30	0.032
	50	0.083

Assumes 60% flap span and 25% chord.

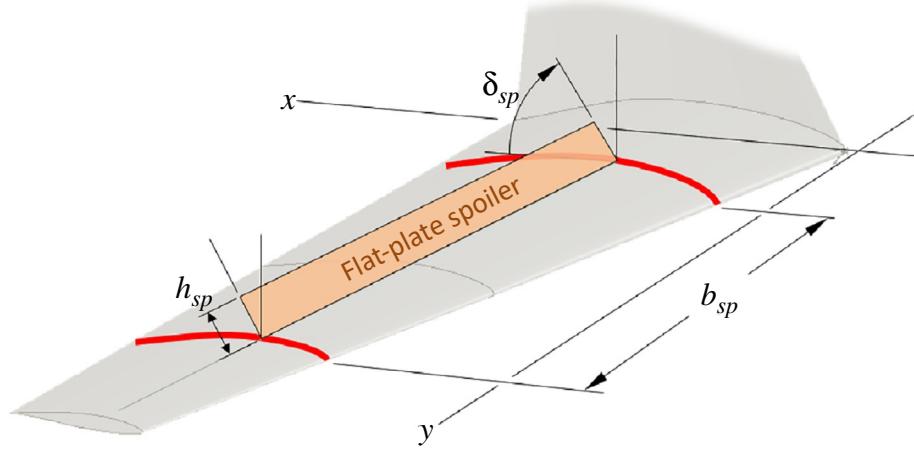
Based on T.C. Corke, *Design of Aircraft*, Prentice-Hall, 2003.

Where  $b_{sp}$ ,  $h_{sp}$ , and  $\delta_{sp}$  are the span, height, and deflection angle (in degrees, where 0 degrees  $\leq \delta_{sp} \leq 90$  degrees) shown in [Figure 16-64](#), respectively. The expression applies to one spoiler only. Thus, the additive drag coefficient of two (4 ft)  $\times$  (0.5 ft) spoilers, deflected 45 degrees, on a wing of area 150 ft<sup>2</sup>, is 156 dragcounts.

### 16.4.9 Drag Correction for Cockpit Windows

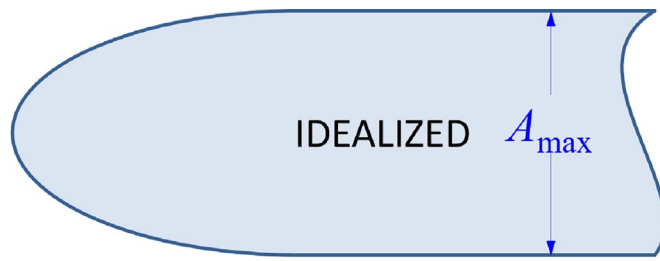
The form-factor estimation methods presented earlier assume a fuselage with a smooth round forward geometry that provides a smooth contour for air to flow across. Such smoothness is normally not present in airplanes; they often feature a sharp discontinuity around the cockpit windows. Cockpit windows are often flat, in particular in pressurized aircraft, with heated windscreens to improve bird-strike resistance and minimize optical distortion.

**FIGURE 16-64** Idealized, unperforated, flat-plate spoiler.



### (1) Drag of Conventional Cockpit Windows

A consequence of this discontinuity is a high-pressure region, caused by the reduction in airspeed over the geometry. This increases the drag of the airplane and must be accounted for using an additive drag contribution. Ref. [94], presents such a method, assuming the general geometry shown in Figure 16-65. The drag coefficients refer to the maximum frontal area of the fuselage ( $A_{\max}$ ) that can be estimated using a method such as the one shown in Figure 16-46. The source drag coefficients are given in Table 16-19:



High pressure region

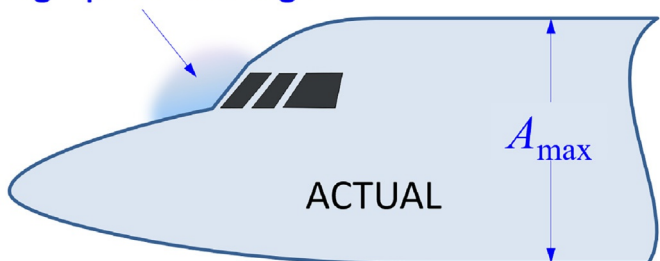


**FIGURE 16-65** Idealized and actual forward geometry of typical aircraft.

**TABLE 16-19** Additive drag coefficients for cockpit windows.

Description (drag references the fuselage frontal area)	$\Delta C_{D_s}$
Flat windscreens with a protruding frame	0.016
Flat windscreens with a flush frame	0.011
Curved windscreens with a sharp upper edge	0.005
Curved windscreens with a round upper edge	0.002

$$\Delta C_{D_{window}} = \Delta C_{D_s} \frac{A_{\max}}{S} \quad (16-168)$$

### EXAMPLE 16-19

Estimate the additive drag of the SR22 due to the cockpit window, assuming a curved windscreens with a round upper edge. The fuselage cross-sectional area is approximately  $14 \text{ ft}^2$ .

#### SOLUTION:

$$\Delta C_{D_{window}} = \Delta C_{D_s} \frac{A_{\max}}{S} = (0.002) \frac{14}{144.9} = 0.0001932$$

This amounts to about 1.93 dragcounts.

### (2) Drag of Blunt Ordinary and Blunt Undercut Cockpit Windows

A cockpit windows installation is classified as *blunt* if the windscreens faces the oncoming airflow at angles ranging from normal to around 22 degrees in the horizontal plane and  $\pm 20$  degrees from the vertical, respectively (see Figure 16-66). The vertical angle defines the *ordinary* and *undercut* configurations. The blunt installation leads to higher drag than curved geometry. The undercut installation

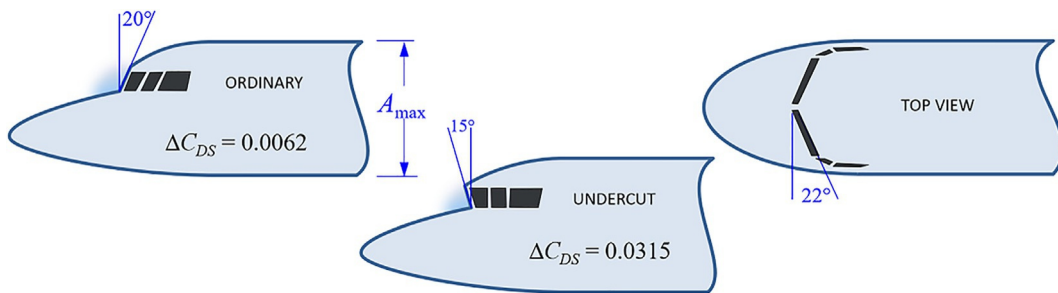


**FIGURE 16-66** Drag of blunt and undercut cockpit windows. Based on S.F. Hoerner, *Fluid-Dynamic Drag*, L. Hoerner, 1965; E.P. Hartman, *The Aerodynamic Drag of Flying-Boat Hull Model as Measured in the NACA 20-foot Wind Tunnel I*, NACA TN-525, 1935.

was a popular approach in the 1930s to reduce the reflection of instrument lights at night (e.g., on the Boeing 247 [102] and the Vultee V-1). It is a very draggy configuration and should be avoided by all means. The source drag coefficients shown in the figure are used with Equation (16-168).

#### 16.4.10 Drag of Canopies

Many single- to four-seat aircraft feature canopies rather than roofed cabins to improve the field-of-view. This section presents a simple method to estimate the drag caused by canopies. It is based on experimental data presented in Ref. [103], in which a number of dissimilar canopies were investigated at Mach numbers ranging

from 0.19 to 0.71 and AOAs up to 6 degrees. The canopies are illustrated in Figure 16-67. The reference states the contribution of a well-designed canopy to the total drag of the airplane is approximately 2% of the total drag. However, a poorly designed canopy easily exceeds that 10-fold—it is 20% of the total drag. The drag is presented in terms of the maximum cross-sectional area of the window,  $A_{\max}$ , using the following expression:

$$\Delta C_{D_{\text{canopy}}} = \Delta C_{D_s} \frac{A_{\max}}{S} \quad (16-169)$$

The values of the  $\Delta C_{D_s}$  for the various canopy geometries are shown in Figure 16-68, plotted for the cited range of Mach numbers. These data are only provided for a low AOA, although information for higher AOAs (up to

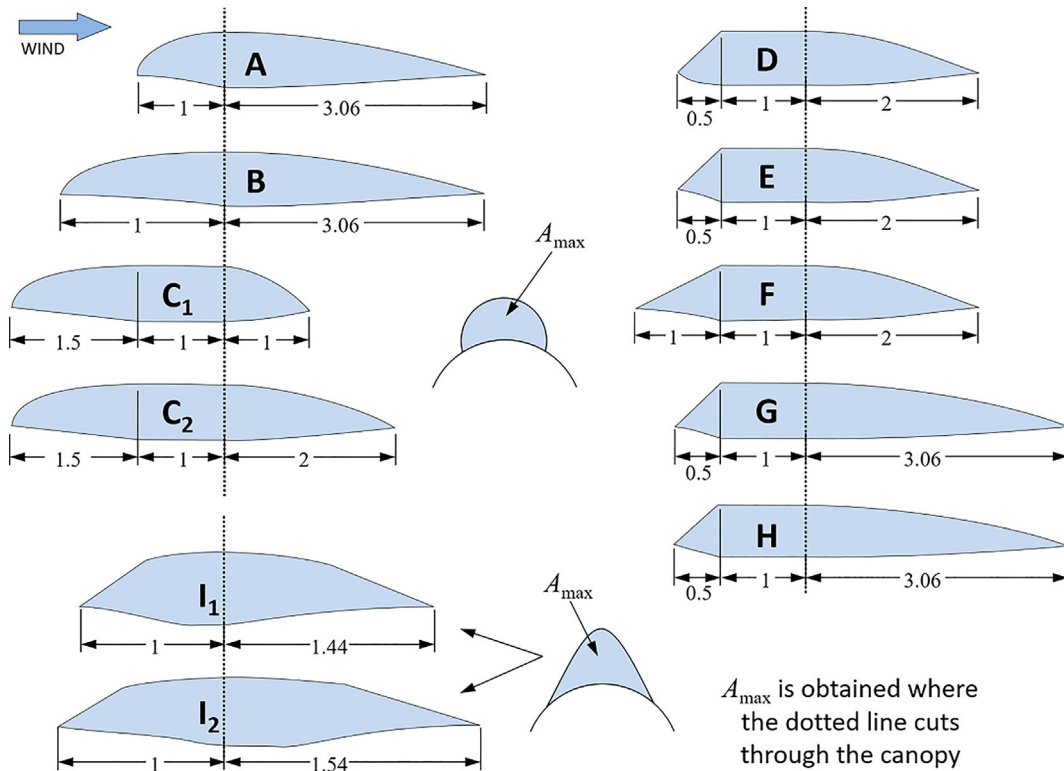
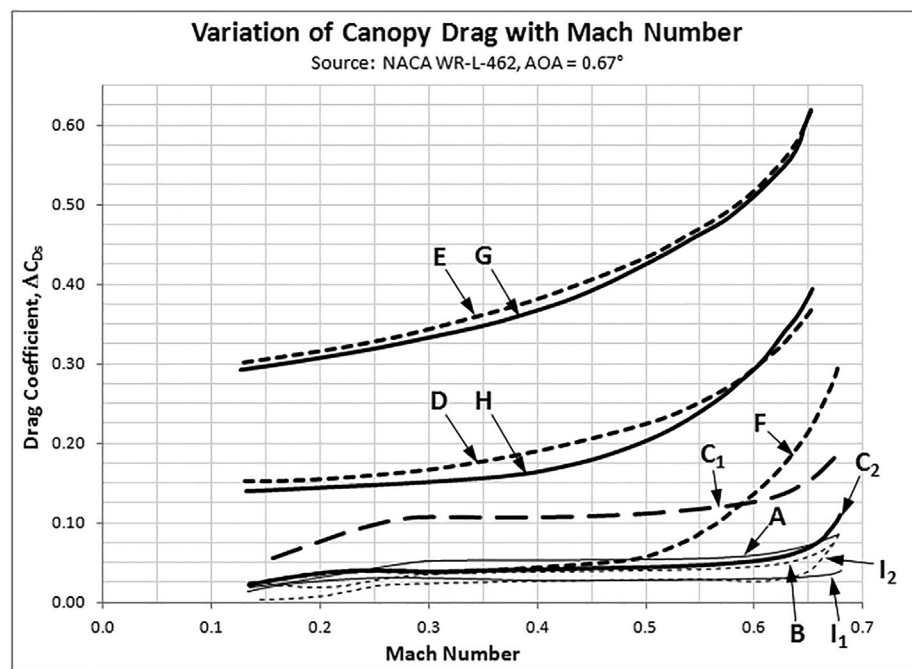


**FIGURE 16-67** Canopy styles evaluated by Ref. 103. The drag of the canopy styles denoted by "A" through "I" is presented in the graph of Figure 16-68.

**FIGURE 16-68** Drag coefficients for the canopy styles of Figure 16-67. Reproduced from R.M. Wright, *Investigation of Drag and Pressure Distribution of Windshields at High Speeds*, NACA WR-L-462, 1942.



6 degrees) is provided in Ref. [103]. The lower AOAs are important for efficient aircraft featuring canopies. The higher AOAs are important for design missions involving prolonged cruise near  $LD_{max}$  or high-speed maneuvers (where compressibility effect prevail). The reference presents the distribution of pressure coefficients, helpful when estimating critical Mach number (see Section 8.3.8, *The Effect of Compressibility*).

#### 16.4.11 Drag of Blisters

Blisters are fairings that cover components that extend beyond the intended *outside mold line* (OML).

GPS antennas are frequently shaped like blisters, as are covers for various mechanisms, such as flap actuation (e.g., Aero L-159 Alca) and landing gear (e.g., Supermarine Spitfire Mk XXI). Hoerner [33, pp. 8-5] provides source drag coefficients for several blister shapes. Thus, the additive drag coefficient for blisters can be calculated from

$$\Delta C_{D_{blister}} = \Delta C_{D_s} \left( \frac{A_{max}}{S_{ref}} \right) \quad (16-170)$$

Where:  $A_{max}$  = Cross-sectional area of shape as shown in Figure 16-69.

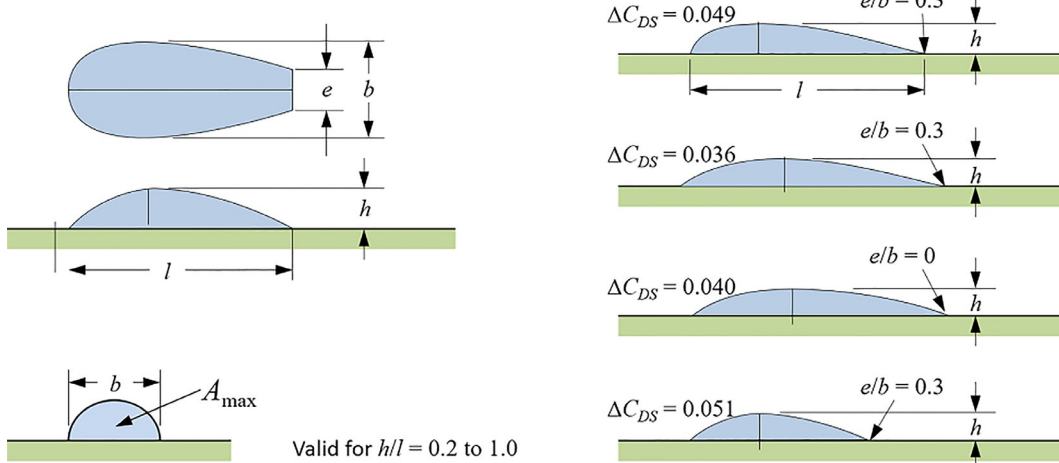


**FIGURE 16-69** Drag contribution of typical blisters (bumps). Based on S.F. Hoerner, *Fluid-Dynamic Drag*, L. Hoerner, 1965.

### EXAMPLE 16-20

Estimate the additive drag of a GPS blister antenna for the SR22, assuming a length  $\times$  width  $\times$  height of  $4.7 \times 3.0 \times 0.78$  in. Assume the base ( $e$ ) is 30% of the width ( $b$ ) and that its side view resembles that of the top blister in Figure 16-69. Furthermore, assume a maximum cross-sectional area of  $14.1 \text{ in.}^2$ .

#### SOLUTION:

The height ratio is about  $0.78/4.7 = 0.17$ , a tad outside of the limits cited in Figure 16-69, but close enough to warrant using Equation (16-170).

$$\Delta C_{D_{\text{blister}}} = \Delta C_{D_S} \left( \frac{A_{\max}}{S} \right) = 0.049 \left( \left( \frac{14.1}{12 \times 12} \right) / 144.9 \right) = 0.00003311$$

This amounts to approximately 0.33 dragcounts. Note that this antenna is about two times "draggier" than the wing-shaped antenna of Example 16-14.

### 16.4.12 Drag of Antennas

There are typically three kinds of antenna geometries planted on aircraft: (1) blister type, (2) wire type, and (3) wing type. Their drag can be estimated using the methods already presented in here. Typical placement and shapes of such antennas are shown in Figure 16-70. Their number can easily turn your nice, smooth airplane into something resembling a porcupine! If possible, try to mount as many antennas internally as practical, although this is often impossible due to reduced effectiveness of the antenna. Also, ask the manufacturer for an additive drag

coefficient or drag force<sup>9</sup> associated with their antenna. Many have this readily available—it may save you analysis work. Others do not and for those you will have to estimate the drag based on the geometry using the approximations below.

- For wire antennas perpendicular to the airstream, use Equation (16-178).
- For wire antennas at an angle  $\theta$  to the airstream, use Equation (16-181).
- For blister antennas, use Equation (16-170).
- For wing antennas, use Equation (16-148).

### 16.4.13 Drag of Windmilling and Stopped Propellers

Engine failure in propeller-driven aircraft leads to two possible scenarios: (1) Windmilling or (2) stopped propellers. In addition to loss of thrust, both increase the drag, but for different reasons. For single-engine aircraft, this dangerously cuts glide capability. For multiengine aircraft, it reduces range and climb performance, because of increased drag driven by the asymmetric thrust.

#### (1) Drag due to Windmilling Propellers

The rotating propeller acts as a wind turbine that drives the engine and must develop enough torque to overcome the internal friction of the engine. A thorough analysis of the phenomenon is beyond the scope of this book, but some experimental data are provided in Ref. [104]. The following methods are provided for initial estimation only.

Hoerner [33] proposes a method in which the power required to turn the engine is 10% of its rated power and the propeller efficiency expected through the

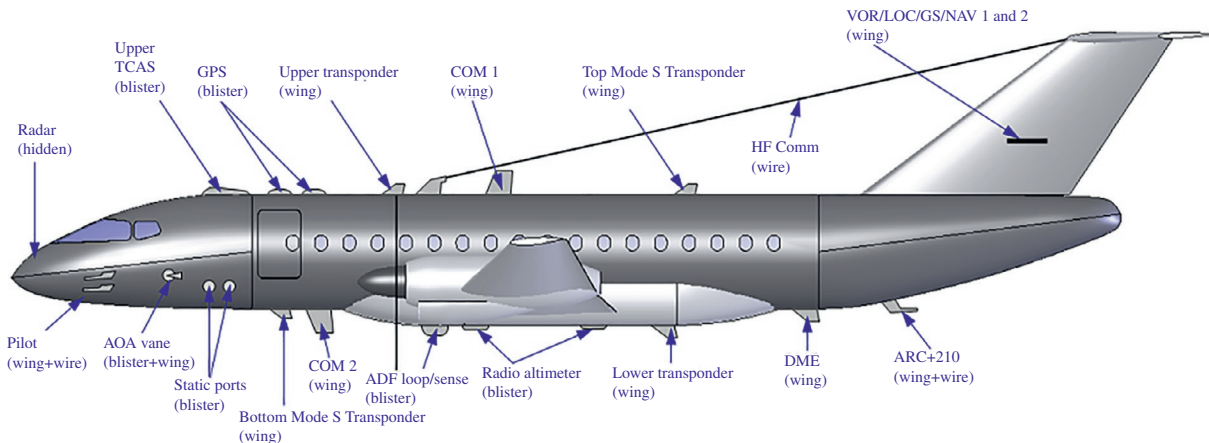


FIGURE 16-70 Typical placement and shape of various antennas and flight control components. Actual size is exaggerated for clarity.

<sup>9</sup> Convert to a drag coefficient per Equation (16-144).

windmilling is approximately 50%. In other words, 50% of the drag power is converted into the rotational power. This allows us to write:

$$0.1 \times 550 \times P_{HP,\max} = 0.5 \times D_{windmill} \times V_\infty \quad (16-171)$$

Assuming the windmilling drag to depend on dynamic pressure and propeller disk area,  $A_p$ , we can write:

$$D_{windmill} = \frac{1}{2} \rho V^2 A_p C_{D_s} = \frac{1}{2} \rho V^2 S \Delta C_{D_{windmill}}$$

Substitute this into Equation (16-169). Solving for the drag coefficient and referencing the reference area yields:

$$\Delta C_{D_{windmill}} = \frac{220 P_{HP,\max}}{\rho V_\infty^3 S} \quad (16-172)$$

Where  $V_\infty$  is the glide speed and  $\rho$  the density at condition. Comparison to existing aircraft reveals that Equation (16-172) over predicts the additive drag by a factor of 2–4. For this reason, for small engines with low internal friction, multiply the value by 0.25 and for larger engines with a high internal friction multiply by 0.33. The author's unpublished study of single-engine aircraft reveals that, on the average, windmilling propeller increased drag by approximately:

$$\Delta C_{D_{windmill}} \approx 0.0150 \quad (16-173)$$

With several excursions nearing and even exceeding 300 dragcounts! The above value will easily reduce the  $LD_{\max}$  of a sleek airplane by a whopping one-third.

## (2) Drag due to Stopped Propellers

When an engine malfunction causes the propeller to stop completely, the drag penalty is less than if it windmills. The resulting drag can be estimated using the blade planform area, assuming inclined flat-plate drag based on the blade angle at the 0.7R blade station ( $\beta$ ). This angle is close to the airfoil's pitch angle (e.g., see Figure 15-9). When  $\beta=0$ , the blade drag is high and when  $\beta=90$  degrees, the drag is at minimum. Hoerner [33], citing experiments from Ref. [104], provides the following expression to estimate the source drag coefficient of such a blade:

$$C_{D_s} = 0.1 + \cos^2 \beta \quad (16-174)$$

Where  $\beta$  may or may not be equal to the pitch angle referenced in Chapter 15, *Thrust Modeling for Propellers*. The blade drag coefficient varies between  $0.1 < \Delta C_{D_s} < 1.1$ . Thus, the drag of the stopped propeller ( $D_{sp}$ ) can be written as follows:

$$D_{sp} = \frac{1}{2} \rho V^2 N_B S_B C_{D_s} = \frac{1}{2} \rho V^2 S \Delta C_{D_{sp}}$$

Where  $N_B$  is the number of blades and  $S_B$  is the planform area of the blade. Solving for  $\Delta C_{D_{sp}}$  (which is based on  $S$ ) yields the following expression:

$$\Delta C_{D_{sp}} = \left( \frac{S_B}{S} \right) N_B C_{D_s} = \left( \frac{S_B}{S} \right) N_B (0.1 + \cos^2 \beta) \quad (16-175)$$

## 16.4.14 Drag of Parachutes

While the drag of parachutes may appear simple, it is surprisingly complicated. Accurate estimation of parachute drag and the time history of its development during deployment is a serious scientific discipline, applicable to a range of applications, including the deployment of re-entry parachutes or ejection seats.

Hoerner [33] provides a practical insight into the drag of parachutes. In general, the drag coefficient of inflated parachutes is based on simple geometric features, such as the height, diameter, and the projected frontal area of the inflated canopy. For initial sizing, the drag coefficient,  $C_{D_{parachute}}$ , can be estimated based on the aspect ratio ( $AR$ ) of the parachute; defined as its inflated height,  $h$ , by the inflated diameter,  $d$ . This is shown in the graph of Figure 16-71, which shows the inflated drag coefficient as a function of  $h/d$ . An empirical expression based on the graph is given below. It is valid only for  $h/d < 1.1$  and  $10^5 < R_e < 10^6$ , where  $R_e$  is based on the inflated diameter. The maximum drag coefficient is obtained for an  $AR=0.5$ , which represents a hemispherical geometry. Further increase of the  $AR$  will make the parachute partially "fill in" the flow separation region, which will reduce the drag coefficient until it reaches a theoretical minimum of 1.0.

$$C_{D_{parachute}} = 2.239 \left( \frac{h}{d} \right)^4 - 4.202 \left( \frac{h}{d} \right)^3 + 1.227 \left( \frac{h}{d} \right)^2 + 0.6167 \left( \frac{h}{d} \right) + 1.174 \quad (16-176)$$

The coefficient is then used to evaluate the total drag force of the parachute using the following expression, where  $S$  is the projected area of the chute and  $S=\pi d^2/4$ :

$$D = q S C_{D_{parachute}} = \frac{1}{2} \rho V^2 S C_{D_{parachute}} \quad (16-177)$$

### EXAMPLE 16-21

The Cirrus SR22 is equipped with the so-called Cirrus Airframe Parachute System (CAPS), to be deployed in case of an emergency. The POH for the SR22 states that the "the airplane will descend at less than 1700 feet-per-minute (or 28.3 ft/s) with a lateral speed equal to the velocity of the surface wind" (at a gross weight of 3400 lb<sub>f</sub>) the airplane will not exceed 1700 fpm. The company website states the diameter of the canopy is 55 ft. Using this information, estimate the drag coefficient of the parachute.

#### SOLUTION:

Solve for  $C_{D_{parachute}}$  using Equation (16-177):

$$C_{D_{parachute}} = \frac{2D_{parachute}}{\rho V^2 S} = \frac{2W}{\rho V^2 S} = \frac{2(3400)}{(0.002378) \left( \frac{1700}{60} \right)^2 \left( \frac{\pi}{4} 55^2 \right)} = 1.499$$

Note that the  $R_e$  is close to  $10^7$ .

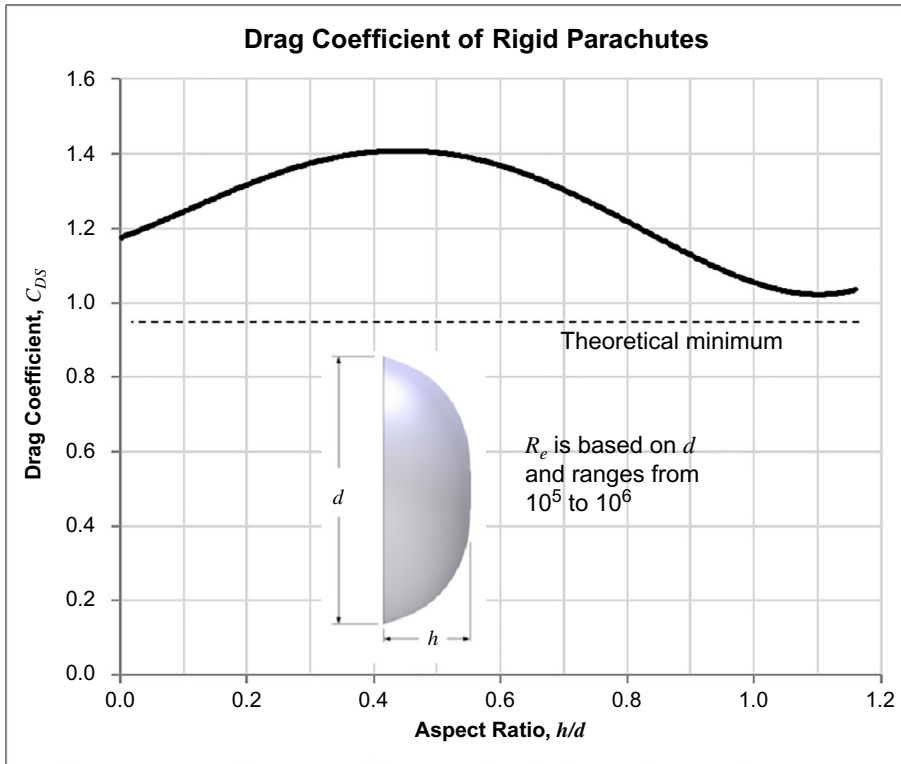


**FIGURE 16-71** Drag coefficients of rigid objects shaped like parachutes. Valid only for  $10^5 < R_e < 10^6$  and  $h/d < 1.1$ . Reproduced from S.F. Hoerner, *Fluid-Dynamic Drag*, L. Hoerner, 1965.

### 16.4.15 Drag of Various Sources

Figure 16-72 shows the 3-dimensional drag coefficient for a sphere and a circular cylinder, based on Schlichting [30]. The drag coefficient is defined using Equation (16-143), where  $S_S$  is the cross-sectional area ( $\pi d^2/4$  for the sphere and  $d \cdot l$ , where  $l$  is the length of the cylinder). Schematics showing the nature of the separation have been superimposed to demonstrate how the drag coefficient depends on the nature of the flow separation that occurs. The dashed line indicates a specific region where the said flow takes place. Of importance is the sharp dip near a  $R_e$  of 300,000 (sphere) and 500,000 (cylinder), first discovered by Alexander Gustave Eiffel (1832–1923) [105]. This dip is indicative of the formation of a turbulent boundary layer that better follows the geometric shape of the solid, reducing the wake size and, thus, the pressure drag. The figure also shows the relatively constant drag coefficient of geometry over the range  $10^3 < R_e < 10^5$ . This is indicative of the formation of a laminar boundary layer (presuming smooth surface).

The range of  $R_e$  starting at  $10^3$  and higher includes most aircraft, even small RC aircraft, and is of great interest to the aircraft designer. This region is usually broken into four separate subregions called *subcritical*, *critical*, *supercritical*, and *transcritical* (see Figure 16-73).

In the subcritical region, laminar boundary layer is formed that separates once it flows to latitude of approximately 80 degrees (see the schematic to the

right in Figure 16-73). In this range  $10^3 < R_e < 10^5$  the  $C_D$  is largely independent of the  $R_e$ . In the critical region, the  $C_D$  drops sharply over a relatively narrow range of  $R_e$ , reaching a minimum value called the *critical Reynolds number*. This is caused by a sudden movement of the laminar boundary layer separation point to latitude of almost 95 degrees. At the critical  $R_e$ , a separation bubble is formed at this location that forces the laminar boundary layer to transition into a turbulent one. This, in turn, more easily follows the shape of the object, moving the separation point farther downstream to approximately 120 degrees. This reshapes the separation region, reducing its diameter and consequently the pressure drag. In the supercritical region, laminar-to-turbulent transition occurs in the attached boundary layer, causing the separation to begin to crawl upstream, gradually increasing the drag coefficient. In the transcritical region, the transition point has moved upstream closer to the stagnation point, eventually causing the drag to become independent of the  $R_e$ .

Figures. 16-74 and 16-76 show drag coefficients for selected geometry reproduced from Hoerner [33].

#### (1) 3D Drag of 2D Cross Sections of Given Length

Research shows that the drag coefficients for the 2-dimensional shapes shown in Figure 16-74 depends on their fineness ratio, here denoted by  $h/d$  (shown on

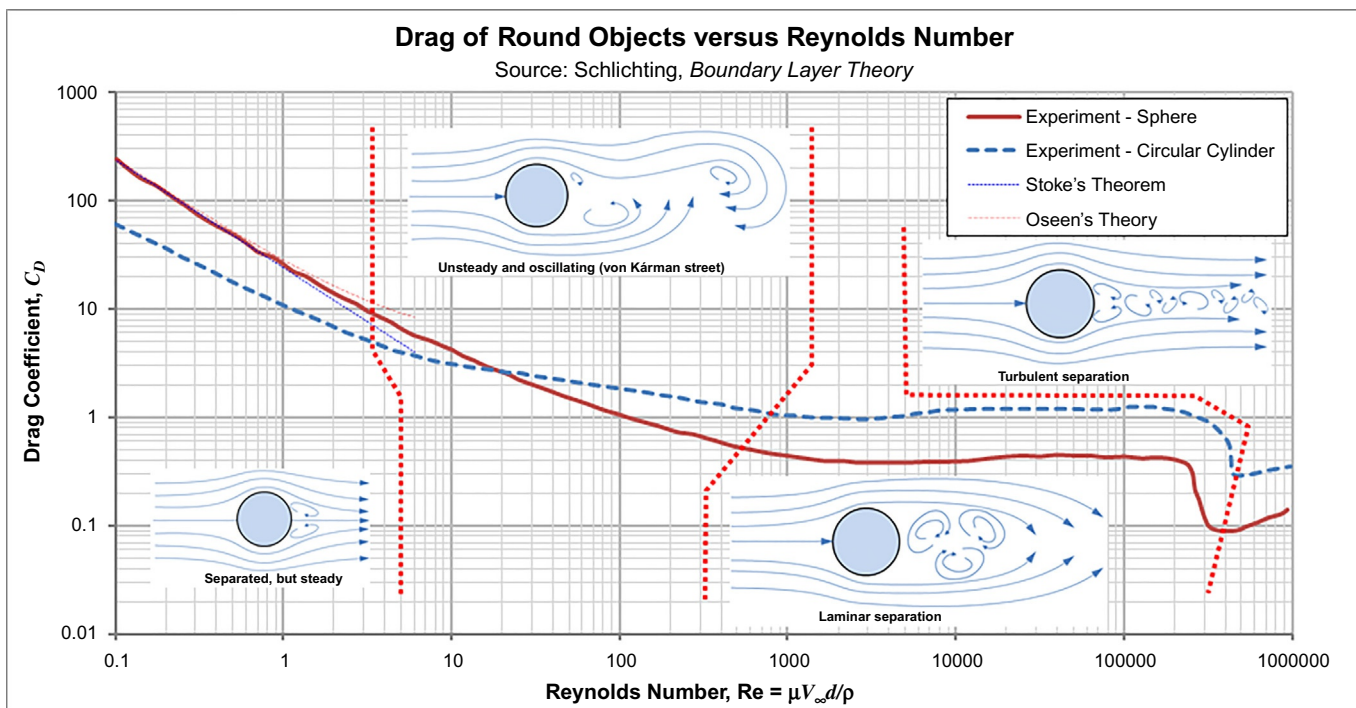


**FIGURE 16-72** The drag coefficient of a sphere and a circular cylinder as a function of  $R_e$ . Insets are schematics showing the nature of the separation, whose consequence is the  $C_D$  shown in the graph.

**FIGURE 16-73** The classification of flow regions on a sphere.

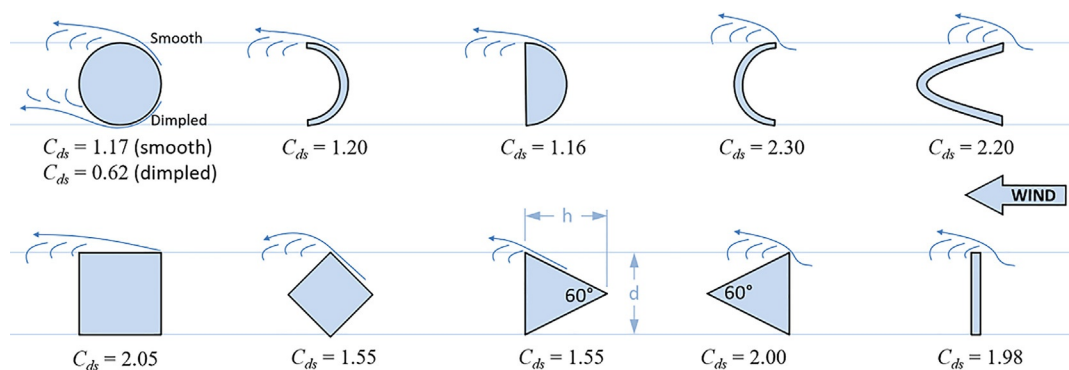
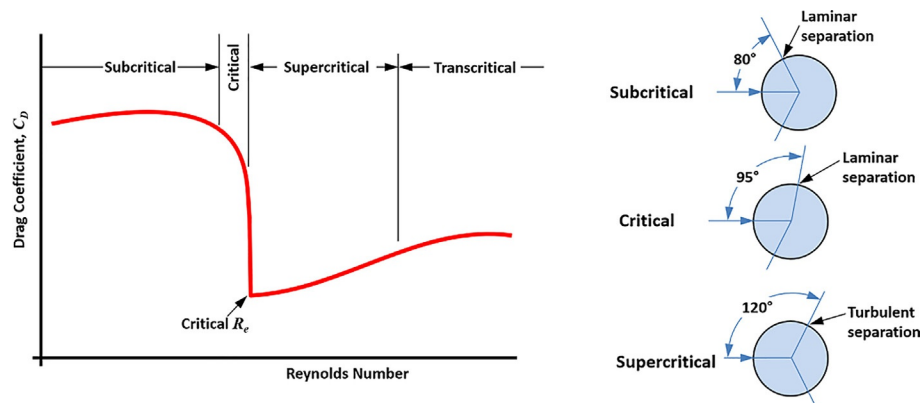


**FIGURE 16-74** 2-dimensional drag coefficients of several cross sections. Valid only for  $10^4 < R_e < 10^5$ .

the triangular shape in the center, lower row). However, their drag is determined using their frontal areas. Thus, the 3D drag of the shapes is calculated from:

$$\Delta C_{D_{2D-shape}} = \Delta C_{d_s} \left( \frac{d \times l}{S} \right) \quad (16-178)$$

Where  $d$  is the shape thickness, as shown in Figure 16-74, and  $l$  is the length of shape in the out-of-plane direction.

### The Cross-Flow Principle

Hoerner [33] presents a practical method to calculate the drag of wires that are inclined with respect to the airflow (see Figure 16-75). This is referred to as the *cross-flow principle*. It can be used to estimate the drag and lift of a tube or cylinder of a given length,  $l$ , and a particular cross section whose 2-dimensional drag coefficient is known. The formulation below is used to calculate the coefficients in terms of the reference wing area so it (primarily the drag) can be added directly to the miscellaneous drag coefficient.

Note that the absolute sign in Equation (16-181) guarantees the drag is always greater than zero. Also note that the inclination angle of  $\theta = 90$  degrees means the cylinder is perpendicular to airstream.

The cross-flow principle is very helpful in determining the drag of external aircraft components, such as HF radio wire antennas.

Resultant coefficient:  $\Delta C_{R_{cyl}} = \Delta C_{d_s} \left( \frac{d \times l}{S} \right) \sin^2 \theta \quad (16-179)$

Lift coefficient:  $\Delta C_{L_{cyl}} = \Delta C_{d_s} \left( \frac{d \times l}{S} \right) \sin^2 \theta \cos \theta \quad (16-180)$

Drag coefficient:  $\Delta C_{D_{cyl}} = \Delta C_{d_s} \left( \frac{d \times l}{S} \right) \cdot |\sin^3 \theta| \quad (16-181)$

Where  $\theta$  is the angle of inclination (see Figure 16-75).

### (2) Drag of 3-dimensional Objects

Figure 16-76 shows a number of 3-dimensional objects and the corresponding drag coefficients. The drag of these objects is also based on the cross-sectional area normal to the flow direction. Therefore, the cross-sectional area normal to the flow direction for the sphere is given

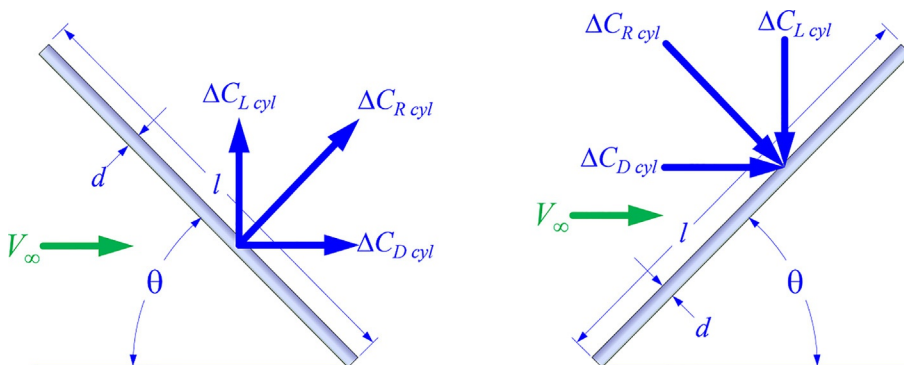


**FIGURE 16-75** Dimensions for the applications of the cross-flow principle.

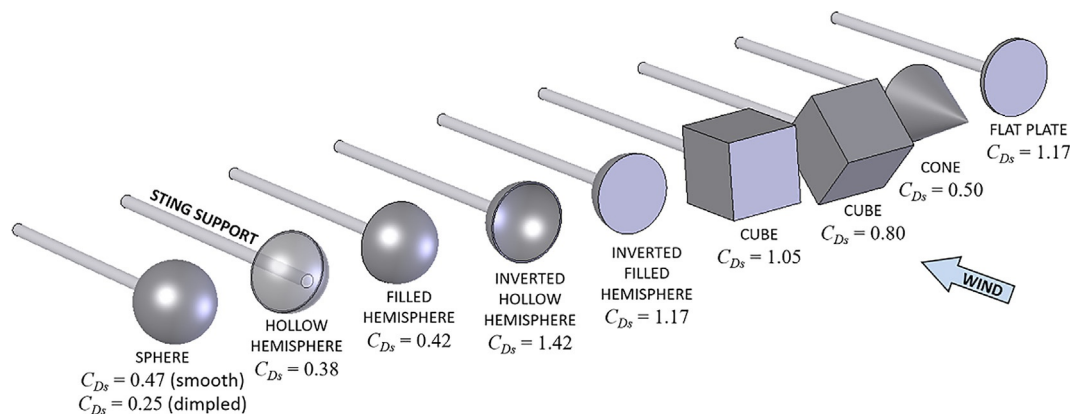


**FIGURE 16-76** 3-dimensional drag coefficients of various geometric shapes. Valid only for  $10^4 < R_e < 10^5$ .

by  $\pi d^2/4$ , where  $d$  is its diameter. In general, if  $S_N$  denotes this area (i.e.,  $S_N = \pi d^2/4$ ), the 3-dimensional drag coefficient is calculated from:

$$\Delta C_{D_{3D-shape}} = \Delta C_{D_S} (S_N/S) \quad (16-182)$$

### (3) Drag of Sanded Walkway on Wing

As shown in Table 16-1, Ref. [17] indicates adding a sanded walkway (both sides of the fuselage) adds 7 drag counts to the total drag. Thus, assume the following drag increase per side:

$$\Delta C_{D_{walkway}} = 0.00035 \quad (16-183)$$

### (4) Drag of Gun Ports in the Nose of an Airplane

NACA WR-L-502 [106] presents the results from drag analysis of the introduction of openings for eight machine gun barrels in a P-38 Lightning style fuselage. It found the drag increase amounted to 5 dragcounts or 0.0005 total, based on the wing reference area. Based on this result, it is possible to estimate drag increase per opening as follows:

$$\Delta C_{D_{gunport}} = 0.0000625 \quad (16-184)$$

### (5) Drag due to Ice Accretion

Drag due to ice accretion on the aircraft poses a serious challenge to safe flight. All aircraft can be classified as

those that have been certified for *flight into known icing* (FIKI) and those that have not. Regardless of classification, all aircraft can accrete ice during operation. Ice formation was studied as early as 1938 by Gulick [107]. He concluded that airfoil  $C_d$  almost doubles and  $C_{l_{max}}$  reduced from 1.32 to 0.80, without changing the angle of stall. Further research took place in the early 1950s (e.g., see a paper by Gray and Glahn [108]). Since then, considerable research effort has been dedicated to the subject. The sheer volume of work cannot be adequately presented here. The interested reader is directed toward work published by NASA, SAE, and AIAA, to name a few.

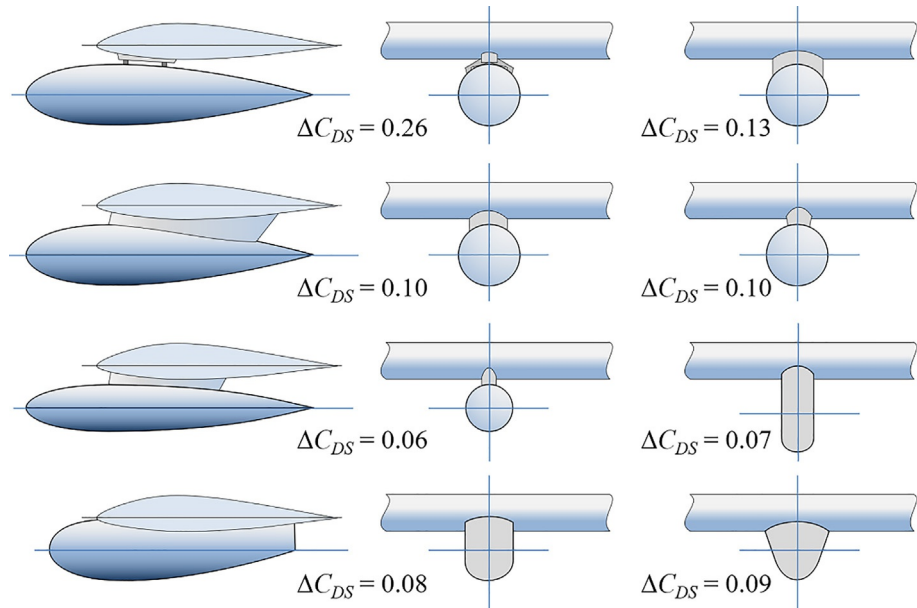
### (6) Drag of Streamlined External Fuel Tanks

External fuel tanks store additional fuel for military aircraft. However, they are also a plausible solution to a long-range operation of some GA aircraft. A similar shape is often used to house weather radars for GA aircraft. It is for this reason that their drag is presented here.

The drag of streamlined tanks depends on the interference between the tank and the wing. Careless installation can easily increase drag by a factor of four, as shown in Figure 16-77. The installation should always be improved using streamlined fairings. The drag coefficients shown in the figure are based on the frontal area of the tank,  $S_{tank}$ , and are related to the reference area as follows:

$$\Delta C_{D_{tank}} = \Delta C_{D_S} \left( \frac{S_{tank}}{S} \right) \quad (16-185)$$

**FIGURE 16-77** Drag of external fuel tanks. Based on S.F. Hoerner, *Fluid-Dynamic Drag*, L. Hoerner, 1965.



## EXAMPLE 16-22

(a) Evaluate the complete minimum drag coefficient of the SR22 assuming the results from the component drag buildup method of Example 16-11, and the various additive drag contributions evaluated in this section. How does it compare to the  $C_{D_{\min}} = 0.02541$  calculated from published performance information?

(b) Perform this evaluation at other altitudes as well (only change will be in the skin friction). How will this affect the  $C_{D_{\min}}$ ?

**SOLUTION:**

(a) See Table 16-16 for the result and the discussion that follows:

The table shows the estimated drag is in reasonable agreement with the one reverse-engineered from published performance data, or  $100 \times 0.02495 / 0.02541 = 98.2\%$ . There are many areas that can be refined; for instance, the airplane's tie-down rings and control surface gaps are not included. These would add to the total. On the other hand, it is debatable whether a 20 drag-counts penalty due to the presence of the engine cowling is justifiable (see row 44 in Table 16-20). This penalty is attributed to the fact the front

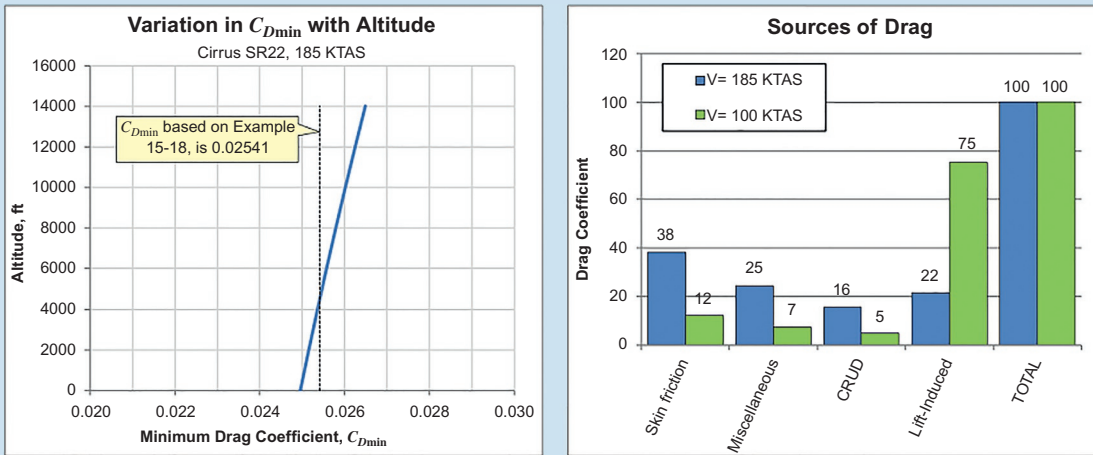
part of the airplane features a cowling with an inlet and exit, which generates substantially higher drag than the smooth nose shape assumed by the fuselage skin friction estimation of Example 16-11. The 20 dragcounts in row 44 are based on an airplane (the P-35) that has a radial engine. It may be draggier than the horizontally opposed piston engine of the SR22. The important point is that while a careful prediction ought to put one in the neighborhood of the drag obtained by experiment, any contribution should be carefully reviewed and justified.

(b) Since the drag analysis was prepared in a spreadsheet, it is easy to change the altitude and get a new estimate. This has been done for altitudes ranging from S-L to 14,000 ft and this is shown in left graph of Figure 16-78. The flight test value of  $C_{D_{\min}} = 0.02541$  is shown as the vertical dashed line. Interestingly, this value was obtained using cruise data at 8000 ft (see Example 16-24). The right graph of Figure 16-78 shows the contribution of various sources of drag at two airspeeds. Note the large contribution of the lift-induced drag at the lower airspeed.

TABLE 16-20 Drag analysis.

DRAG ANALYSIS				
		Wing	HT	VT
39	<b>Sweep angle</b>	$\Delta C_{D_{\text{wing}}} = 0.00$	$5.00$	$18.00$
40	<b>Form Factor</b>	$FF_j = 1.311$	$1.203$	$1.187$
41	<b>Intereference Factor, IF</b>	$IF_j = 1$	$1.05$	$1.05$
42	<b>Weighted drag factor</b>	$C_f \cdot FF_j \cdot IF_j \cdot S_{\text{wet},j} = 0.7140$	$0.1762$	$0.1120$
43	<b>Skin friction drag</b>	$(1/S) \sum C_f \cdot FF_j \cdot IF_j \cdot S_{\text{wet},j} = 0.01217$		
44	Presence of engine cowling	$\Delta C_{D_{\text{cowl}}} = 0.002000$		Same penalty as that of the Severski P-35
45	Cooling drag	$\Delta C_{D_{\text{cool}}} = 0.000812$		See Example 16-12
46	Two COM antennas	$2 \times \Delta C_{D_{\text{fin}}} = 0.000030$		See Example 16-13
47	Four half-sized "COM" antennas	$4 \times 0.5 \times \Delta C_{D_{\text{fin}}} = 0.000030$		See Example 16-13
48	Two GPS antennas	$2 \times \Delta C_{D_{\text{blister}}} = 0.000066$		See Example 16-19
49	Two wing entry steps	$\Delta C_{D_{\text{entry}}} = 0.000456$		See Example 16-15
50	6 Flap fairings (double "COM" drag)	$6 \times 2 \times \Delta C_{D_{\text{fin}}} = 0.000182$		Each fairing assumed 2x the COM geometry
51	External wing tip nav lights	$2 \times \Delta C_{D_{\text{blister}}} = 0.000066$		Assumed to cause same drag as GPS antenna
52	Main landing gear	$\Delta C_{D_{\text{main}}} = 0.002090$		See Example 16-16
53	Nose landing gear	$\Delta C_{D_{\text{nose}}} = 0.000810$		See Example 16-16
54	Cockpit window drag correction	$\Delta C_{D_{\text{window}}} = 0.000193$		See Example 16-18
55	Sanded walkway, both sides	$\Delta C_{D_{\text{walkway}}} = 0.000700$		0.00035 per side
56	Miscellaneous drag coeff.	$C_{D_{\text{misc}}} = 0.00744$		
57	CRUD	$k_{\text{crud}} = 1.25$		
58	Minimum drag coefficient	$C_{D_{\min}} = 0.02450$		$= (0.01217 + 0.00780) \cdot 1.25$
59				

## EXAMPLE 16-22 (cont'd)

FIGURE 16-78 Variation in the  $C_{D\min}$  of the SR22 with altitude.

## 16.5 SPECIAL TOPICS INVOLVING DRAG

Estimating drag for existing aircraft is common in aircraft design. This is helpful for validation or to evaluate the strength of a competitor. This section presents several methods for this purpose. Naturally, there are shortcomings to these methods and some extract less data than others. All assume the simplified or adjusted drag models of [Section 16.2, The Basics of Drag Modeling](#).

First, a note of caution: The extraction of drag data for existing aircraft relies on published data. However, care must be exercised, for the source matters. The ideal source is manufacturer's *pilot's operating handbook* (POH) for said aircraft. This is followed by *Jane's All the World's Aircraft* (JAWA) [109]. A common shortcoming in other sources is ambiguity. Lack of clarity in airspeed units is frequent. It is frequently presented using unidentifiable knots. To laypeople a knot is "just a knot." However, to engineers (and pilots) this is far from the truth. An indicated knot (KIAS) is not equal to a calibrated knot (KCAS) and neither is equal to an equivalent knot, let alone a true knot (KTAS). When the only data available are vague, one must rely on sound judgment. A knot next to a stalling or climb speed is most likely KCAS. Yes, it could be KIAS, but this is less likely. A knot next to a cruising speed is most likely KTAS.

### 16.5.1 Step-by-Step: Extracting Drag from $LD_{\max}$

The simplest method uses  $LD_{\max}$  and the airspeed at which it is achieved. This information is commonly available from aircraft Pilot's Operating Handbooks (POH)

and is almost always based on actual flight testing. The information this particular method extracts is the  $C_{D\min}$ , and assumes the UK-system of units. It is a limitation of the method that it uses the simplified drag model. However, since the  $C_{L_{\max}D}$  will primarily shift the drag polar sideways (see [Section 16.2.2, Quadratic Drag Modeling](#)) there really is no error introduced in the extraction of the  $C_{D\min}$ . Another issue is the extraction of drag for propeller powered aircraft. The  $LD_{\max}$  reported in the POH will include drag from the wind milling propeller (since the purpose is to present the pilot with potentially life-saving information). This can easily double the minimum drag coefficient when compared to the other methods in this section and renders it much higher than required for accurate performance analyses. Therefore, care must be exercised when using these numbers.

#### Step 1: Gather Information from the Vehicle's POH

Assuming the reader has access to the aircraft's POH, gather the following information: Gross weight ( $W_0$ ) in lb<sub>f</sub>, best glide airspeed ( $V_{LD_{\max}}$ ), wing area ( $S$ ) in ft<sup>2</sup>, and wing Aspect Ratio ( $AR$ ). If  $AR$  is not known, use wing span ( $b$ ) in ft and compute it from  $b^2/S$ .

#### Step 2: Convert $V_{LD_{\max}}$ into Units of ft/s

Consistent units must be used. Therefore, if  $V$  is read in KTAS it must be converted to ft/s. Similarly, if  $V_V$  is given in fpm (ft/min) it must be converted to ft/s. Use the following conversion factors:

Convert KTAS or mph to ft/s:

$$V_{\text{ft/s}} = 1.688 \times V_{\text{KTAS}} = 1.688 \times 1.15 \times V_{\text{mph}}$$

Convert fpm to ft/s:  $V_{\text{ft/s}} = V_{\text{fpm}}/60$

Often the POH will report the best glide airspeed in units of KIAS or KCAS. This must be converted to KTAS for this method is to be applied at altitude (see [Section 17.3.2, Airspeeds: Instrument, Calibrated, Equivalent, True, and Ground Airspeeds](#) for methods).

### Step 3: Calculate the Optimum Glide Lift Coefficient

Calculate the lift coefficient at the best glide speed from:

$$C_{L_{opt}} = 2W_0 / (\rho V_{LD_{max}}^2 S) \quad (16-186)$$

### Step 4: Calculate Span Efficiency

Estimate the span efficiency,  $e$ , from any of the methods of [Section 9.5.12, Determination of Span Efficiency](#).

### Step 5: Compute Minimum Drag

Compute the minimum drag from the following expression:

$$C_{D_{min}} = \frac{C_L}{LD_{max}} - \frac{C_L^2}{\pi \cdot AR \cdot e} \quad (16-187)$$

## DERIVATION OF EQUATION (16-187)

The simplified drag model is given by:

$$C_D = C_{D_{min}} + \frac{C_L^2}{\pi \cdot AR \cdot e}$$

Knowledge of the lift-to-drag ratio at a specific condition (here conveniently selected to be the  $LD_{max}$ , since many aircraft manufacturers graciously reports this for us), and the lift coefficient associated with it can then be used to extract the minimum drag coefficient.

$$\begin{aligned} LD_{max} &= \frac{C_L}{C_D} = \frac{C_L}{C_{D_{min}} + \frac{C_L^2}{\pi \cdot AR \cdot e}} \\ \Leftrightarrow C_{D_{min}} &= \frac{C_L}{LD_{max}} - \frac{C_L^2}{\pi \cdot AR \cdot e} \end{aligned}$$

## 16.5.2 Step-by-Step: Extracting Drag From a Flight Polar Using the Quadratic Spline Method

This method can be used if the Flight Polar (or Rate-of-Sink versus Airspeed or  $V_V$  versus  $V$  plot) is available, as it often is for sailplanes, gliders, and motor gliders. Usually, this polar is not available for powered airplanes. It can be used to extract  $C_{D_{min}}$ ,  $C_{L_{min,D}}$ , and  $e$ . This method will not retrieve a drag model that features a drag bucket, but a quadratic one.

Consider the sample Flight Polar in [Figure 16-79](#). Follow the following the stepwise procedure to extract  $C_{D_{min}}$ ,  $C_{L_{min,D}}$ , and  $e$ .

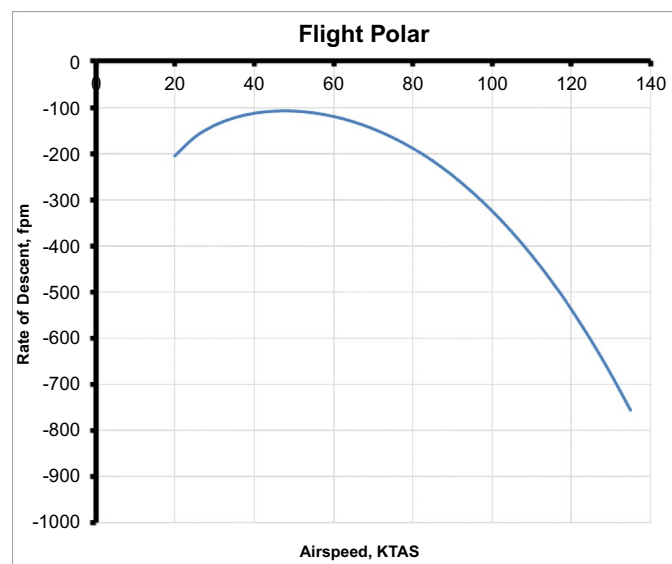


**FIGURE 16-79** A typical Flight Polar.

### Step 1: Select Data Points from the Flight Polar

Select three arbitrary points on the Flight Polar and record the corresponding  $V_V$  and  $V$ . For instance, select two points that enclose the minimum (near 50KTAS in [Figure 16-79](#)) and one at a higher speed, for instance near 100 or 120KTAS.

### Step 2: Tabulate

Fill in the table below by entering the  $V_V$  and  $V$  selected in Step 1 in Columns 1 and 2 below. Calculate the values in Columns 3 through 5.

ID	1 $V$	2 $V_V$	3 $x = V^2$	4 $x^2 = V^4$	5 $y = V \cdot V_V$
1	$V_1$	$V_{V1}$	$V_1^2$	$V_1^4$	$V_1 \cdot V_{V1}$
2	$V_2$	$V_{V2}$	$V_2^2$	$V_2^4$	$V_2 \cdot V_{V2}$
3	$V_3$	$V_{V3}$	$V_3^2$	$V_3^4$	$V_3 \cdot V_{V3}$

**Note 1:** It is important that consistent units be used. Therefore, if  $V$  is read in KTAS is must be converted to ft/s. Similarly, if  $V_V$  is given in fpm (ft/min), it must be converted to ft/s. Use the conversion factors shown under the Note 1 of Step 2 of [Section 16.6.1, Step-by-Step: Extracting Drag from LDmax](#):

**Note 2:** This formulation assumes the absolute value of the rate-of-sink. Thus, if the  $V_V$  is reported with a negative sign it must be converted to a positive number.

### Step 3: Fill in the Conversion Matrix and Invert

Fill in the matrix below using the values in Column 4 for the first row in the matrix and Column 3 for the second row. This order is imperative. Then, invert the

matrix. This can be done by some software, for instance, any spreadsheet software offers means to invert matrices:

$$\begin{bmatrix} V_1^4 & V_1^2 & 1 \\ V_2^4 & V_2^2 & 1 \\ V_3^4 & V_3^2 & 1 \end{bmatrix} \rightarrow \begin{bmatrix} V_1^4 & V_1^2 & 1 \\ V_2^4 & V_2^2 & 1 \\ V_3^4 & V_3^2 & 1 \end{bmatrix}^{-1}$$

#### Step 4: Determine the Coefficients to the Quadratic Spline

Calculate the constants  $A$ ,  $B$ ,  $C$  by multiplying the inverted matrix in STEP 3 with the vector formed by Column 5 in the table above:

$$\begin{Bmatrix} A \\ B \\ C \end{Bmatrix} = \begin{bmatrix} V_1^4 & V_1^2 & 1 \\ V_2^4 & V_2^2 & 1 \\ V_3^4 & V_3^2 & 1 \end{bmatrix}^{-1} \begin{Bmatrix} V_1 \cdot V_{V1} \\ V_2 \cdot V_{V2} \\ V_3 \cdot V_{V3} \end{Bmatrix}$$

#### Step 5: Extract Aerodynamic Properties

Using the constants,  $A$ ,  $B$ ,  $C$  calculated in the previous step, extract the aerodynamic properties:

$$\text{Induced drag constant: } k = \left( \frac{\rho S}{2W} \right) C \quad (16-188)$$

$$\text{Location of minimum drag: } C_{L_{\min D}} = -\frac{B}{2k} \quad (16-189)$$

$$\text{Minimum drag coefficient: } C_{D_{\min}} = A \left( \frac{2W}{\rho S} \right) - k C_{L_{\min D}}^2 \quad (16-190)$$

$$\text{Oswald efficiency: } e = \frac{1}{\pi \cdot AR \cdot k} \quad (16-191)$$

### DERIVATION OF EQUATIONS (16-188) THROUGH (16-191)

The adjusted drag model is given by:

$$C_D = C_{D_{\min}} + k(C_L - C_{L_{\min D}})^2 \quad (\text{i})$$

This can be expanded as follows:

$$C_D = (C_{D_{\min}} + kC_{L_{\min D}}^2) - 2kC_{L_{\min D}}C_L + kC_L^2$$

Recall that the lift coefficient and the *rate-of-descent* (ROD) are given by:

$$C_L = \frac{2W}{\rho V^2 S} \quad (\text{ii})$$

and

$$V_V = \frac{DV}{W} = \frac{\rho V^3 S C_D}{2W} \quad (\text{iii})$$

Substitute Equation (i) into Equation (iii) and expand:

$$\begin{aligned} V_V &= \frac{\rho V^3 S C_D}{2W} \\ &= \frac{\rho V^3 S ((C_{D_{\min}} + kC_{L_{\min D}}^2) + (-2kC_{L_{\min D}})C_L + (k)C_L^2)}{2W} \end{aligned}$$

$$= \frac{\rho V^3 S (kC_L^2 + (-2kC_{L_{\min D}})C_L + (C_{D_{\min}} + kC_{L_{\min D}}^2))}{2W}$$

Substitute Equation (ii) into this and expand:

$$\begin{aligned} V_V &= \frac{\rho V^3 S \left( k \left( \frac{2W}{\rho V^2 S} \right)^2 + (-2kC_{L_{\min D}}) \left( \frac{2W}{\rho V^2 S} \right) + (C_{D_{\min}} + kC_{L_{\min D}}^2) \right)}{2W} \\ &= \frac{\rho V^3 S \left( k \frac{4W^2}{\rho^2 V^4 S^2} + (-2kC_{L_{\min D}}) \frac{2W}{\rho V^2 S} + (C_{D_{\min}} + kC_{L_{\min D}}^2) \right)}{2W} \end{aligned}$$

Simplify:

$$\begin{aligned} V_V &= \frac{k \frac{4W^2}{\rho V^2 S} + (-2kC_{L_{\min D}}) 2WV + (C_{D_{\min}} + kC_{L_{\min D}}^2) \rho V^3 S}{2W} \\ &= k \frac{2W}{\rho V S} + (-2kC_{L_{\min D}}) V + (C_{D_{\min}} + kC_{L_{\min D}}^2) \frac{\rho V^3 S}{2W} \\ &= k \left( \frac{2W}{\rho S} \right) \frac{1}{V} + (-2kC_{L_{\min D}}) V + (C_{D_{\min}} + kC_{L_{\min D}}^2) \left( \frac{\rho S}{2W} \right) V^3 \end{aligned}$$

Multiply through by  $V$  to get:

$$\begin{aligned} V \cdot V_V &= k \overbrace{\left( \frac{2W}{\rho S} \right)}^{=C} + \overbrace{(-2kC_{L_{\min D}})}^{=B} V^2 + \overbrace{(C_{D_{\min}} + kC_{L_{\min D}}^2) \left( \frac{\rho S}{2W} \right)}^{=A} V^4 \\ &= C + BV^2 + AV^4 \end{aligned}$$

Where:

$$A = (C_{D_{\min}} + kC_{L_{\min D}}^2) \left( \frac{\rho S}{2W} \right) \quad B = -2kC_{L_{\min D}} \quad C = k \left( \frac{2W}{\rho S} \right)$$

Therefore, we can rewrite:

$$V \cdot V_V = C + BV^2 + AV^4 = C + Bx + Ax^2$$

Where  $x = V^2$ . Also, let  $y = V \cdot V_V$ . We need 3 points (i.e.,  $V_V$  corresponding to a  $V$ ) to determine the constants  $A$ ,  $B$ ,  $C$ . Obtain by inverting the matrix.

$$\begin{aligned} \begin{cases} y_1 = Ax_1^2 + Bx_1 + C \\ y_2 = Ax_2^2 + Bx_2 + C \\ y_3 = Ax_3^2 + Bx_3 + C \end{cases} &\Rightarrow \begin{bmatrix} x_1^2 & x_1 & 1 \\ x_2^2 & x_2 & 1 \\ x_3^2 & x_3 & 1 \end{bmatrix} \begin{Bmatrix} A \\ B \\ C \end{Bmatrix} = \begin{Bmatrix} y_1 \\ y_2 \\ y_3 \end{Bmatrix} \\ &\Rightarrow \begin{Bmatrix} A \\ B \\ C \end{Bmatrix} = \begin{bmatrix} x_1^2 & x_1 & 1 \\ x_2^2 & x_2 & 1 \\ x_3^2 & x_3 & 1 \end{bmatrix}^{-1} \begin{Bmatrix} y_1 \\ y_2 \\ y_3 \end{Bmatrix} \end{aligned}$$

Then, the coefficients can be found as follows:

$$C = k \left( \frac{2W}{\rho S} \right) \quad \Leftrightarrow \quad k = \left( \frac{\rho S}{2W} \right) C$$

$$B = -2kC_{L_{\min D}} \quad \Leftrightarrow \quad C_{L_{\min D}} = -\frac{B}{2k}$$

$$A = (C_{D_{\min}} + kC_{L_{\min D}}^2) \left( \frac{\rho S}{2W} \right)$$

$$\Leftrightarrow C_{D_{\min}} = A \left( \frac{2W}{\rho S} \right) - kC_{L_{\min D}}^2$$

$$\text{Also note that: } k = \frac{1}{\pi \cdot AR \cdot e} \quad \Leftrightarrow \quad e = \frac{1}{\pi \cdot AR \cdot k}$$

**EXAMPLE 16-23**

Consider the Flight Polar for a powered sailplane shown in [Figure 16-80](#). Extract its drag characteristics, ignoring the existence of a drag bucket and assuming it can be described using the adjusted drag model. Its gross weight is  $W_0 = 1876 \text{ lb}_f$ , wing area and aspect ratio are  $S = 202 \text{ ft}^2$  and  $AR = 29.29$ , respectively.

**SOLUTION:**

**Step 1 through 3:** The three selected point are shown in [Figure 16-80](#) and are tabulated below:

$$\begin{cases} A \\ B \\ C \end{cases} = \begin{bmatrix} x_1^2 & x_1 & 1 \\ x_2^2 & x_2 & 1 \\ x_3^2 & x_3 & 1 \end{bmatrix}^{-1} \begin{cases} y_1 \\ y_2 \\ y_3 \end{cases}$$

$$= \begin{bmatrix} 28,267,394 & 5317 & 1 \\ 368,383,509 & 19,193 & 1 \\ 1,104,195,089 & 33,229 & 1 \end{bmatrix}^{-1} \begin{cases} 133.7 \\ 461.8 \\ 1215.3 \end{cases}$$

**Step 4:** Calculate the constants  $A$ ,  $B$ ,  $C$ :

$$\begin{cases} A \\ B \\ C \end{cases} = \begin{cases} 1.07602 \times 10^{-6} \\ -0.00272772 \\ 117.7650518 \end{cases}$$

Selected Data							
ID	V km/h	V <sub>V</sub> fpm	V KCAS	V ft/s	x = V <sup>2</sup>	x <sup>2</sup> = V <sup>4</sup>	Y = V · V <sub>V</sub>
1	80	110	43	73	5317	28267394	133.7
2	152	200	82	139	19193	368383509	461.8
3	200	400	108	182	33229	1104195089	1215.3

**Step 5:** Extract the aerodynamic properties using the constants  $A$ ,  $B$ ,  $C$ :

Induced drag constant:

$$k = \left( \frac{\rho S}{2W} \right) C = \left( \frac{(0.002378)(201.3)}{2(1876)} \right) (117.8)$$

$$= 0.015074$$

Location of minimum drag:

$$C_{L_{\min D}} = -\frac{B}{2k} = -\frac{-0.00272772}{2 \times 0.015074} = 0.090478$$

Minimum drag coefficient:

$$C_{D_{\min}} = A \left( \frac{2W}{\rho S} \right) - k C_{L_{\min D}}^2 = 0.008283$$

Oswald efficiency:

$$e = \frac{1}{\pi \cdot AR \cdot k} = \frac{1}{\pi \cdot (29.29) \cdot (0.015074)}$$

$$= 0.72094$$

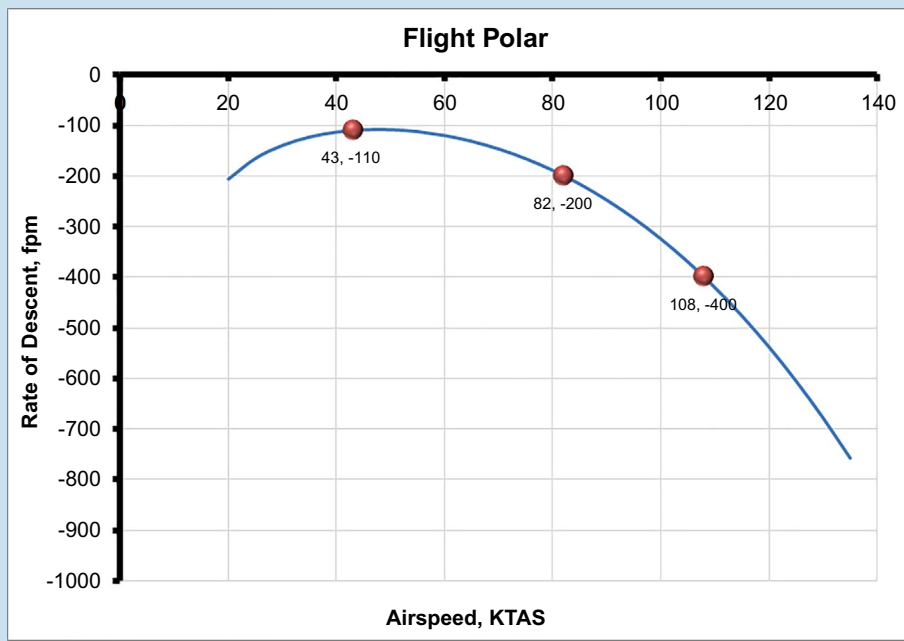


**FIGURE 16-80** A Flight Polar for a powered sailplane.

### 16.5.3 Step-by-Step: Extracting Drag Coefficient for a Piston Powered Propeller Aircraft

The drag coefficient of piston-powered airplanes can be extracted from typical data provided in the POH. The accuracy is contingent on the quality of the data provided by the manufacturer. For propeller aircraft, the hardest parameter to obtain is the propeller efficiency. An “educated guess” is usually required. The methods of [Chapter 15, Thrust Modeling for Propellers](#) should help.

#### (1) Method 1: Extracting $C_{D_{\min}}$ using Cruise Performance

The following procedure illustrates extraction of  $C_{D_{\min}}$  using cruise performance. The procedure may have to be modified for aircraft for which POH performance data of the kind shown here is not available. Here, we will illustrate the method using a data sheet for a Cirrus SR22.

[Figure 16-81](#) shows a page from the POH for a Cirrus SR22. Similar information can also be obtained from the *Type Certificate Data Sheet* (TCDS) that can be downloaded from the FAA official website ([www.faa.gov](http://www.faa.gov)). The excerpt displays a format typically used for GA aircraft.

##### Step 1:

Determine the following parameters for the type: Reference area ( $S$ ) in  $\text{ft}^2$ , aspect ratio ( $AR$ ), rated engine power ( $P_A$ ) in BHP, and gross weight ( $W_0$ ) in  $\text{lb}_f$ .

##### Step 2:

Using the POH, extract the cruising speed and the associated altitude. Usually, these numbers are normalized to the gross weight. Manufacturers present the cruising speed in KTAS. The true airspeed in KTAS is required.

##### Step 3:

Determine the density of air,  $\rho$ , at the cruise altitude using [Equation \(17-7\)](#). Then, convert the airspeed in KTAS to ft/s by multiplying it by 1.688. This airspeed is  $V$ .

8000 Feet Pressure Altitude										
		ISA -30°C (-31°C)			ISA (-1°C)			ISA + 30°C (29°C)		
RPM	MAP	PWR	KTAS	GPH	PWR	KTAS	GPH	PWR	KTAS	GPH
2700	21.7	83%	183	19.7	78%	183	18.6	75%	178	17.7
2600	21.7	79%	180	18.8	75%	180	17.8	71%	175	17.0
2500	21.7	75%	176	17.7	71%	176	16.8	67%	171	16.0
2500	20.7	70%	172	16.7	66%	172	15.8	63%	167	15.0
2500	19.7	66%	168	15.6	62%	168	14.8	59%	163	14.0
2500	18.7	61%	163	14.5	58%	163	13.8	55%	158	13.1
2500	17.7	57%	159	13.5	54%	159	12.8	51%	153	12.1

**FIGURE 16-81** Excerpt from a POH for Cirrus SR22. Courtesy of Cirrus Aircraft. Copyright 2021 Cirrus Aircraft or its Affiliates. All Rights Reserved. Image reproduced with the permission of Cirrus.

#### Step 4:

Determine the Oswald’s efficiency and the lift-induced drag constant at the condition. For a medium AR aircraft, [Equation \(9-129\)](#) can be used, repeated below for convenience:

$$\text{Oswald's efficiency: } e = 1.78(1 - 0.045AR^{0.68}) - 0.64$$

$$\text{Lift-induced drag constant: } k = 1/(\pi \cdot AR \cdot e)$$

#### Step 5:

Calculate the minimum drag coefficient from:

$$C_{D_{\min}} = \frac{\eta_p \times 1100 \times P_{BHP}}{\rho V^3 S} - k \left( \frac{2W}{\rho V^2 S} \right)^2 \quad (16-192)$$

Note that the selection of  $\eta_p$  can be consequential. Be careful. If the propeller is a fixed pitch “climb” propeller use a value ranging from 0.68 to 0.72. If the propeller is a fixed pitch “cruise” propeller, use a value ranging from 0.75 to 0.80. If the airplane is equipped with a constant-speed propeller, use a value close to 0.85.

### DERIVATION OF EQUATION (16-192)

The minimum drag can be estimated from:

$$C_D = C_{D_{\min}} + C_{D_i} \Leftrightarrow C_{D_{\min}} = C_D - C_{D_i}$$

Since thrust equals drag at this condition, we can determine the drag coefficient as follows:

$$T = D = \frac{1}{2} \rho V^2 S C_D \Leftrightarrow$$

$$C_D = \frac{2T}{\rho V^2 S} = \frac{2(\eta_p \times 550 \times P_{BHP} / V)}{\rho V^2 S} = \frac{\eta_p \times 1100 \times P_{BHP}}{\rho V^3 S}$$

Furthermore, using the simplified drag model and the lift coefficient, the lift-induced drag is given by:

$$C_{D_i} = k C_L^2 = k \left( \frac{2W}{\rho V^2 S} \right)^2$$

Inserting this into the expression for  $C_{D_{\min}}$  yields:

$$C_{D_{\min}} = C_D - C_{D_i} = \frac{\eta_p \times 1100 \times P_{BHP}}{\rho V^3 S} - k \left( \frac{2W}{\rho V^2 S} \right)^2$$

### EXAMPLE 16-24

Estimate the total, induced, and minimum drag coefficient for the Cirrus SR22, using the data in [Figure 16-81](#) using the published cruising speed of 183 KTAS (308.9 ft/s) at 8000 ft and 78% power at ISA condition.

**EXAMPLE 16-24 (cont'd)****SOLUTION:****Steps 1–3:**

Reference area:  $S = 144.9 \text{ ft}^2$

Aspect ratio:  $AR = 10.1$  (using  $b = 38.3 \text{ ft}$ ).

Engine power at condition:

$$P_A = 0.78 \times 310 \text{ BHP} = 241.8 \text{ BHP.}$$

Gross weight:  $W_0 = 3400 \text{ lb}_f$ .

Density of air at 8000 ft:

$$\rho = 0.002378(1 - 0.0000068756 \times 8000)^{4.2561} \\ = 0.001869 \text{ slugs}/\text{ft}^3.$$

**Step 4:**

Both the Oswald's efficiency factor and lift-induced drag constant have been calculated multiple times throughout this book. We need the latter one for this problem. It is  $k = 0.04207$ .

**Step 5:**

Since we don't know the propeller efficiency, we must guess. The airplane features a constant-speed propeller, specifically designed for the aircraft. Thus, its propeller efficiency is as high as 0.85 at this condition. This is a guess, so regard the resulting drag coefficient with caution. The minimum drag coefficient is estimated as follows:

$$C_{D_{\min}} = \frac{\eta_p \times 1100 \times P_{BHP}}{\rho V^3 S} - k \left( \frac{2W}{\rho V^2 S} \right)^2 \\ = \frac{0.85 \times 1100 \times 241.8}{(0.001869)(308.9)^3(144.9)} \\ - (0.04207) \left( \frac{2(3400)}{(0.001869)(308.9)^2(144.9)} \right)^2 = 0.02541$$

The total drag can be estimated using the thrust relation shown in the above derivation:

Total drag coefficient:

$$C_D = \frac{\eta_p \times 1100 \times P_A}{\rho V^3 S} = \frac{0.85 \times 1100 \times 241.8}{(0.001869)(308.9)^3(144.9)} = 0.02832$$

The lift-induced drag is the difference between the total and minimum drag:

$$C_{D_i} = C_D - C_{D_{\min}} = 0.02832 - 0.02541 = 0.00291$$

**(2) Method 2: Extracting  $C_{D_{\min}}$  using Climb Performance**

The following procedure illustrates extraction of  $C_{D_{\min}}$  using climb performance. This requires the *rate-of-climb* (ROC) and the associated airspeed and altitude to be

established. Ideally, this should be the best ROC, obtained at  $V_y$  (the best ROC airspeed). Since  $V_y$  occurs at a relatively low AOA, with less flow separation than, say,  $V_x$  (the best *angle-of-climb* airspeed) and, thus, closer adherence to the quadratic drag model. It is also better to use data at S-L as this will require fewer corrections.

**Step 1:** Same as Step 1 of Method 1.

**Step 2:**

Using the POH, extract the ROC, the associated climb airspeed, and altitude (ideally  $V_y$  at S-L). Usually, these numbers are normalized using the gross weight. Correct climb speed presented in KIAS to KCAS before it is converted to KTAS, which is required for this procedure. This conversion should be implemented using the methods of [Chapter 17, Performance—Introduction](#).

**Step 3:**

Determine the density of air ( $\rho$ ) at the climb altitude using [Equation \(17-7\)](#). Ideally, this should be at S-L ( $\rho = 0.002378 \text{ slugs}/\text{ft}^3$ ). Convert the ROC ( $V_V$ ) in fpm to ft/s per  $V_V = \text{ROC}/60$ . Convert the airspeed in KTAS to ft/s by multiplying it by 1.688. This airspeed is denoted by  $V$  in the following formulas.

**Step 4:** Same as Step 4 of Method 1.

**Step 5:**

Calculate the minimum drag coefficient from:

$$C_{D_{\min}} = \frac{\eta_p 1100 P_{BHP} - 2WV_V}{\rho V^3 S} - k \left( \frac{2W}{\rho V^2 S} \right)^2 \quad (16-191)$$

Again, note that if the propeller efficiency,  $\eta_p$ , is not known, one must rely on engineering judgment to assess its value, and this can be tricky. Assuming the flight condition to be at  $V_V$ , use a value ranging from 0.68 to 0.72 if the propeller is a fixed pitch "climb" propeller. If the propeller is a fixed pitch "cruise" propeller, use a value ranging from 0.6 to 0.7, and if equipped with a constant speed propeller, use a value ranging from 0.68–0.75. Also note that, just like for Method 1, correcting the power of normally aspirated engines to the altitude at which the aircraft is operating is crucial. For this, use the Gagg and Ferrar model of [Equation \(7-8\)](#).

**DERIVATION**

The vertical speed,  $V_V$ , is determined from:

$$V_V = \frac{\text{ROC}}{60} = \frac{TV - DV}{W}$$

Replacing the thrust ( $T$ ) and drag ( $D$ ) with the standard expressions yields:

$$V_V = \frac{\left( \frac{\eta_p 550 P_{BHP}}{V} \right) V - \left( \frac{1}{2} \rho V^2 S C_D \right) V}{W} \\ = \frac{\eta_p 550 P_{BHP} - \frac{1}{2} \rho V^3 S C_D}{W}$$

Multiplying through by  $W$  and substituting the simplified drag model and, then, the lift coefficient leads to:

$$\begin{aligned} WV_V &= \eta_p 550 P_{BHP} - \frac{1}{2} \rho V^3 S \left( C_{D_{\min}} + k C_L^2 \right) \\ &= \eta_p 550 P_{BHP} - \frac{1}{2} \rho V^3 S \left( C_{D_{\min}} + k \left( \frac{2W}{\rho V^2 S} \right)^2 \right) \end{aligned}$$

Solving for the  $C_{D_{\min}}$  returns:

$$C_{D_{\min}} = \frac{\eta_p 1100 P_{BHP} - 2WV_V}{\rho V^3 S} - k \left( \frac{2W}{\rho V^2 S} \right)^2$$

### EXAMPLE 16-25

Estimate the minimum drag coefficient for the Cirrus SR22, using the climb performance extraction method at  $V_y$  and the following data in addition to  $S$ ,  $k$ , and  $W$  from the previous example.

**SOLUTION:**

*Step 1-5:*

Engine power at condition,  $P_A = 310 \text{ BHP}$

Best rate-of-climb

$$ROC = 1398 \text{ fpm} \Rightarrow V_V = 1398/60 = 23.3 \text{ ft/s}$$

Best rate-of-climb airspeed

$$\begin{aligned} V_y &= 101 \text{ KIAS} = 101 \text{ KCAS} \\ &= 101 \text{ KTAS} = 170.5 \text{ ft/s (at S-L)} \end{aligned}$$

Propeller efficiency at  $V_y$   $\eta_p = 0.7$  (guess)

### EXAMPLE 16-25 (cont'd)

$$\begin{aligned} C_{D_{\min}} &= \frac{\eta_p 1100 P_{BHP} - 2WV_V}{\rho V^3 S} - k \left( \frac{2W}{\rho V^2 S} \right)^2 \\ &= \frac{(0.7)1100(310) - 2(3400)(23.3)}{(0.002378)(170.5)^3(144.9)} \\ &\quad - (0.04207) \left( \frac{2(3400)}{(0.002378)(170.5)^2(144.9)} \right)^2 \\ &= 0.02761 \end{aligned}$$

Note that if the propeller efficiency is 0.689, rather than 0.7, then  $C_{D_{\min}}$  will be 0.02541, which matches that of Method 1. This shows the importance of properly selecting the propeller efficiency. However, it is also possible the result reflects the presence of flow separation.

### 16.5.4 Extracting Drag Coefficient From Published Data for Piston Aircraft

The following Visual Basic for Applications routine can be used with Microsoft Excel to extract various drag-related parameters using the previously mentioned method. As shown, it estimates Oswald's efficiency assuming a straight wing. However, this is easy to modify. Also, note that the input power ( $P_{BHP}$ ) is "at-condition." For instance, the rated power for the SR22 is 310 BHP, but the at-condition power used in Example 16-24, has dropped to 241.8 BHP.

```

Function Extract_CD(Sref As Single, AR As Single, W0 As Single, P_BHP As Single, eta As Single, Vktas As Single, H As Single, Mode As Byte) As Single
    'This function uses the method of Section 16.6.3 to extract CD, CDi, CDmin and others
    'for a piston powered prop aircraft. Only valid for propeller aircraft with straight
    'wings.
    '
    'Variables: Sref = Reference wing area (ex. 145 ft2)
    '           AR = Aspect Ratio (ex. 10)
    '           W0 = Weight at condition (e.g. altitude and airspeed) (ex. 3100 lbf)
    '           P_BHP = Horsepower at condition (e.g. 205 BHP)
    '           eta = Estimated propeller efficiency at condition (ex. 0.85)
    '           Vktas = Airspeed in KTAS at condition
    '           H = Altitude in ft at condition
    '           Mode = What to return: =0 for CD, =1 for CDi, =2 for CDmin,
    '                   =3 for CL, =10 for Thrust
    '
    'Initialize
    Dim rho As Single, V As Single
    Dim T As Single, e As Single
    Dim CL As Single, CD As Single, CDi As Single, CDmin As Single

```

```

'Presets
V = 1.688 * Vktas
If V < 30 Then
    Extract_CD = -1
    Exit Function
End If
rho = 0.002378 * (1 - 0.0000068756 * H) ^ 4.2561 'Density
T = eta * 550 * P_BHP / V 'Thrust
CL = 2 * W0 / (rho * V ^ 2 * Sref) 'Lift coefficient

'Calculate CD
CD = eta * 1100 * P_BHP / (rho * V ^ 3 * Sref)

'Calculate CDi
e = 1.78 * (1 - 0.045 * AR ^ 0.68) - 0.64
CDi = CL ^ 2 / (3.14159265 * AR * e)

'Calculate CDmin
CDmin = CD - CDi

'Return
Select Case Mode
Case 0 'CD
    Extract_CD = CD
Case 1 'CDi
    Extract_CD = CDi
Case 2 'CDmin
    Extract_CD = CDmin
Case 3 'CL
    Extract_CD = CL
Case 10 'T
    Extract_CD = T
End Select
End Function

```

### 16.5.5 Determining Drag Characteristics From Wind Tunnel Data

Standard wind tunnel testing yields a number of static force and moment coefficients such as  $C_D$ ,  $C_L$ ,  $C_Y$ ,  $C_M$ , and  $C_N$ . This section focuses on the first two;  $C_L$  and  $C_D$ . A conventional alpha-sweep involves changing the AOA from some minimum value (e.g., -5 degrees) to some maximum value (e.g., +20 degrees). Thus, it returns a list of coefficients as a function of  $\alpha$ . This permits a drag polar of the form  $C_D = A \cdot C_L^2 + B \cdot C_L + C$  to be developed using a quadratic least-squares curvefit. The coefficients of this polynomial can be used to extract the coefficient

$C_{D_{\min}}$ ,  $C_{L_{\min D}}$ , and the Oswald's span efficiency factor,  $e$ , provided the airplane's  $AR$  has been established. If so, it can then be shown that these parameters are related to the constants of the curvefit polynomial as follows:

$$e = \frac{1}{\pi \cdot AR \cdot A} \quad (16-194)$$

$$C_{L_{\min D}} = -\frac{B}{2A} \quad (16-195)$$

$$C_{D_{\min}} = C - \frac{B^2}{4A} \quad (16-196)$$

**EXAMPLE 16-26**

The following data from a wind tunnel test of a complete aircraft configuration are given in the following table:

$C_L$	-0.4649	-0.3240	-0.1917	-0.0767	0.0240	0.1217	0.2367	0.3518	0.4668	0.5617	0.6537	0.7169	0.7888	0.8492
$C_D$	0.0591	0.0488	0.0400	0.0334	0.0292	0.0280	0.0298	0.0334	0.0405	0.0478	0.0571	0.0669	0.0778	0.0891

**SOLUTION:**

One way to obtain the curvefit is to use commercial spreadsheet software like Microsoft Excel, enter the data and plot using a scatter graph. Then, the user can select the curve and add a trendline with the associated equation and correlation coefficient displayed. This is shown in Figure 16-82. The resulting curvefit shows the polynomial constants are given by  $A = 0.1056$ ,  $B = -0.0226$ , and  $C = 0.0292$ . Then the drag parameters can be determined as follows:

$$e = \frac{1}{\pi \cdot AR \cdot A} = \frac{1}{\pi \cdot 6 \cdot 0.1056} = 0.5024$$

$$C_{L_{minD}} = -\frac{B}{2A} = -\frac{-0.0229}{2 \cdot 0.1056} = 0.1070$$

$$C_{D_{min}} = C - \frac{B^2}{4A}$$

$$= 0.0292 - \frac{(-0.0229)^2}{4 \cdot 0.1056} = 0.02799$$

Determine  $C_{D_{min}}$ ,  $C_{L_{minD}}$ , and  $e$  using a quadratic, least-squares curvefit of the form  $C_D = A \cdot C_L^2 + B \cdot C_L + C$ , if the aspect ratio,  $AR = 6$ .

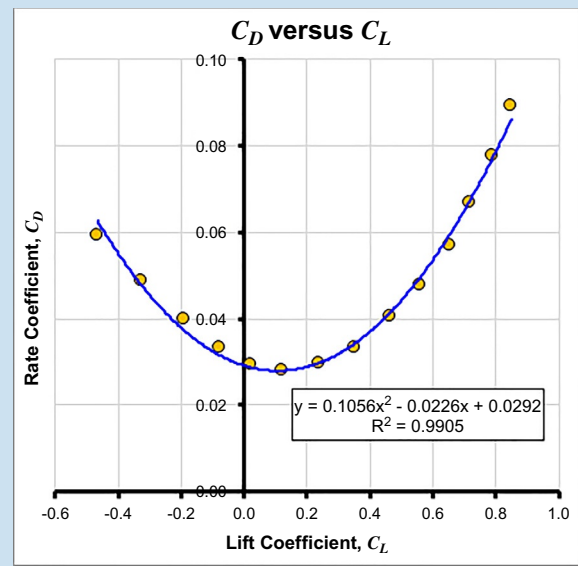


**FIGURE 16-82** Hypothetical wind tunnel test data for some complete aircraft plotted with a trendline generated in Microsoft Excel.

## DERIVATION OF EQUATIONS (16-194) THROUGH (16-196)

Begin by equating the two forms of the drag coefficients; the quadratic curvefit and the adjusted drag model of Equation (16-11):

$$C_D = AC_L^2 + BC_L + C = C_{D_{min}} + k(C_L - C_{L_{minD}})^2$$

Where  $k = 1/(\pi \cdot AR \cdot e)$ . Expand and sort coefficients based on their dependency on  $C_L^2$  and  $C_L$ :

$$AC_L^2 + BC_L + C = \underbrace{kC_L^2}_{=A} + \underbrace{(-2kC_{L_{minD}})C_L}_{=B} + \underbrace{C_{D_{min}} + kC_{L_{minD}}^2}_{=C}$$

Coefficient  $A$  yields the Oswald's efficiency:

$$k = A = \frac{1}{\pi \cdot AR \cdot e} \Rightarrow e = \frac{1}{\pi \cdot AR \cdot A}$$

Coefficient  $B$  yields the  $C_{L_{minD}}$ :

$$B = -2kC_{L_{minD}} = -2AC_{L_{minD}} \Rightarrow C_{L_{minD}} = -\frac{B}{2A}$$

Using the two previous results with Equation (iii), we get:

$$C = C_{D_{min}} + kC_{L_{minD}}^2 = C_{D_{min}} + A \left( -\frac{B}{2A} \right)^2 = C_{D_{min}} + \frac{B^2}{4A}$$

$$\Rightarrow C_{D_{min}} = C - \frac{B^2}{4A}$$

## 16.6 ADDITIONAL INFORMATION—DRAG OF SELECTED AIRCRAFT

When estimating the drag of a new aircraft design, it is strongly recommended that the designer compares own results to that of the aircraft in the below tables that most similarly resembles the new aircraft. This can help flag a possible over- or underestimation. This section presents information for selected classes and models of aircraft that is helpful when validating the drag model for a new aircraft.

### 16.6.1 General Range of Subsonic Minimum Drag Coefficients

**Table 16-21** shows the expected range of values of subsonic minimum drag coefficients for several classes of aircraft. These numbers do not bracket all possible aircraft configurations—there may be specific aircraft that are outside of the range shown. However, most aircraft reside between the lower and upper limits.

### 16.6.2 Drag of Various Aircraft by Class

**Table 16-22** lists selected drag related figures for a number of aircraft of different classes. Some of these are displayed in **Figure 16-43**. The data were gathered from a number of sources. Note that some of the data were retrieved from graphs using “careful eyeballing” and should be regarded with care.

The numbers come from a variety of sources; Perkins and Hage [110], Stinton [111], Roskam [52], Nicolai [78], NASA SP-468 [112], NASA CR-114494 [113], and the author’s own estimates. The author’s estimations utilize Method 1 of **Section 16.5.3, Step-by-Step: Extracting Drag Coefficient for a Piston Powered Propeller Aircraft**, utilizing performance data from the corresponding aircraft’s Pilots Operating Handbook (POH) or other reliable sources. The  $LD_{\max}$  estimated by the author for propeller aircraft assumes no additional drag due to windmilling or stopped propellers. Refer to **Section 16.4.13, Drag of Windmilling and Stopped Propellers**, for methods on how to account for this drag. Windmilling propellers can easily increase the minimum drag coefficient by 150 dragcounts

or more. Additionally, although expected, there is no guarantee the manufacturer has not bolstered performance values in the POH. For this reason, treat all drag data with caution.

## EXERCISES

- (1) Estimate the skin friction coefficient for an airfoil whose chord is 5.25 ft at 25,000 ft and 250 KTAS airspeed on a day at which the outside air temperature is 30°F warmer than a standard day. Do this using the following assumptions:
  - (a) fully laminar boundary layer,
  - (b) fully turbulent boundary layer assuming incompressible flow,
  - (c) fully turbulent boundary layer assuming compressible flow,
  - (d) mixed boundary layer for which the transition on the upper surface occurs at chord station 1.3 ft and at 65% chord on the lower surface.
 Ans: (a) 0.0005037, (b) 0.003186, (c) 0.003139, (d) 0.002119.
- (2) An aircraft has a drag polar given by  $C_D = 0.035 + 0.052C_L^2$ . Determine the  $C_L$  for  $LD_{\max}$  and the magnitude of the  $LD_{\max}$ . (Hint:  $\frac{d}{dx}\left(\frac{u}{v}\right) = \frac{u' \cdot v - u \cdot v'}{v^2}$ )
 Ans:  $C_L$  where  $LD_{\max}$  occurs is 0.8549,  $LD_{\max}$  is 11.71.
- (3) Consider the wing shown in **Figure 16-83** and for which the representative skin friction coefficients for

**TABLE 16-21** Range of subsonic minimum drag coefficients,  $C_{D_{\min}}$ .

Class of Aircraft	Range of $C_{D_{\min}}$	
	Lower	Upper
World War I Era Aircraft 1914-1918	0.0317	0.0771
Interwar Era Aircraft 1918-1939	0.0182	0.0585
Multi-Engine WW-II Bombers (Piston)	0.0239	0.0406
Single and Multi-Engine WW-II Fighters (Piston)	0.0157	0.0314
Multi-Engine Commercial Transport Aircraft (Piston)	0.0191	0.0258
Kitplanes (Homebuilt) and LSA	0.0119	0.0447
Single Engine GA Aircraft (Piston and Turboprop)	0.0174	0.0680
GA ag-aircraft, single engine, propeller, clean	0.0550	0.0600
GA ag-aircraft, single engine, propeller, spray-system	0.0700	0.0800
Twin Engine GA Aircraft (Piston and Turboprop)	0.0230	0.0369
Flying Boats	0.0233	0.0899
Selected Jet Fighter/Trainer Aircraft	0.0083	0.0240
Selected Jet Bomber and Attack Aircraft	0.0068	0.0160
Commercial Jetliners and Business Jets	0.0160	0.0219
Various Subsonic Military Aircraft (Props and Jets)	0.0145	0.0250
High performance sailplane	0.0060	0.0100
Tailless aircraft, propeller	0.0150	0.0200
Tailless aircraft, jet	0.0080	0.0140
Low altitude subsonic cruise missile (high W/S)	0.0300	0.0400

**TABLE 16-22** Drag characteristics of selected aircraft.

World War I Era Aircraft 1914-1918									
Make	Model	AR	S, ft <sup>2</sup>	S <sub>wet</sub> , ft <sup>2</sup>	f, ft <sup>2</sup>	C <sub>f</sub>	C <sub>Dmin</sub>	L/D <sub>max</sub>	Reference
Albatross	D-III	4.65	231	-	10.74	-	0.0465	7.5	NASA SP-468
B.E.	2c	4.47	371	-	13.66	-	0.0368	8.2	NASA SP-468
Caproni	CA.42	5.43	2223	-	98.70	-	0.0444	8.2	NASA SP-468
De Havilland	DH-2	3.88	249	-	10.71	-	0.0430	7.0	NASA SP-468
	DH-4	4.97	440	-	21.82	-	0.0422	8.1	NASA SP-468
Fokker	D-VII	4.70	221	-	8.93	-	0.0404	8.1	NASA SP-468
	D-VIII	6.58	115	-	6.34	-	0.0552	8.1	NASA SP-468
	E-III	5.70	172	-	12.61	-	0.0771	6.4	NASA SP-468
	Dr.-1 Triplane	4.04	207	-	6.69	-	0.0323	8.0	NASA SP-468
Gotha	G.V	7.61	963	-	68.45	-	0.0711	7.7	NASA SP-468
Handley Page	0/400	7.31	1655	-	70.67	-	0.0427	9.7	NASA SP-468
Junkers	D-I	5.46	159	-	9.75	-	0.0612	7.0	NASA SP-468
	J-I	6.40	522	-	17.50	-	0.0335	10.3	NASA SP-468
Nieuport	Model 17	5.51	159	-	7.81	-	0.0491	7.9	NASA SP-468
Sopwith	5F.1 Dolphin	4.85	263	-	8.35	-	0.0317	9.2	NASA SP-468
	F.1 Camel	4.11	231	-	8.73	-	0.0378	7.7	NASA SP-468
SPAD	XIII C.1	3.69	227	-	8.33	-	0.0367	7.4	NASA SP-468

Interwar Era Aircraft 1918-1939									
Make	Model	AR	S, ft <sup>2</sup>	S <sub>wet</sub> , ft <sup>2</sup>	f, ft <sup>2</sup>	C <sub>f</sub>	C <sub>Dmin</sub>	L/D <sub>max</sub>	Reference
Beechcraft	D17S	4.18	296	-	5.39	-	0.0182	11.7	NASA SP-468
Boeing	P-26A	5.24	149	-	6.68	-	0.0448	8.3	NASA SP-468
Curtiss	Hawk P-6E	4.76	252	-	9.35	-	0.0371	8.7	NASA SP-468
	JN-4H	7.76	352.6	-	17.64	-	0.0500	9.24	NASA SP-468
	R2C-1	4.18	140	-	2.88	-	0.0206	10.9	NASA SP-468
	Robin	7.54	223	-	13.10	-	0.0585	8.7	NASA SP-468
Dayton Wright RB	Hall Scott L-62	4.38	102	-	3.22	-	0.0316	9	NASA SP-468
Fokker	F-2	7.10	452	-	21.10	-	0.0466	9.4	NASA SP-468
Ford	5-AT	7.26	835	-	39.33	-	0.0471	9.5	NASA SP-468
Handley Page	W8F	4.67	1456	-	79.93	-	0.0549	7.1	NASA SP-468
Lockheed	Orion 9D	7.01	262	-	5.50	-	0.0210	14.1	NASA SP-468
	Vega 5C	6.11	275	-	7.65	-	0.0278	11.4	NASA SP-468
Northrop	Alpha	5.93	312	-	8.55	-	0.0274	11.3	NASA SP-468
Ryan	NYP	6.63	319	-	12.10	-	0.0379	10.1	NASA SP-468
Stinson	SR-8B	6.84	256	-	8.91	-	0.0348	10.8	NASA SP-468
Supermarine	S-4	6.84	136	-	3.73	-	0.0274	12.1	NASA SP-468

Multi-Engine WW-II Bombers (Piston)									
Make	Model	AR	S, ft <sup>2</sup>	S <sub>wet</sub> , ft <sup>2</sup>	f, ft <sup>2</sup>	C <sub>f</sub>	C <sub>Dmin</sub>	L/D <sub>max</sub>	Reference
Boeing	B-17	7.58	1420	5900	39.00	0.0067	0.0275	-	Perkins & Hage
	B-17G	7.58	1420	-	42.83	-	0.0302	12.7	NASA SP-468
	B-29	11.50	1736	-	41.16	-	0.0241	16.8	NASA SP-468
	B-29A	11.49	1736	7500	43.50	0.0058	0.0251	-	Roskam
	B-29B	11.49	1736	7100	41.50	0.0058	0.0239	-	Roskam
Consolidated	B-24J	11.55	1048	-	42.54	-	0.0406	12.9	NASA SP-468
North American	B-25	7.49	610	2800	18.00	0.0064	0.0295	-	Perkins & Hage

Single and Multi-Engine WW-II Fighters (Piston)									
Make	Model	AR	S, ft <sup>2</sup>	S <sub>wet</sub> , ft <sup>2</sup>	f, ft <sup>2</sup>	C <sub>f</sub>	C <sub>Dmin</sub>	L/D <sub>max</sub>	Reference
Curtiss	SB2C-1	5.88	422	-	9.52	-	0.0225	12.4	NASA SP-468
Grumman	F6F-3	5.34	334	-	7.05	-	0.0211	12.2	NASA SP-468
Lockheed	P-38	8.26	327.5	1500	8.20	0.0055	0.0250	-	Perkins & Hage
	P-38L	8.26	327.5	-	8.78	-	0.0268	13.5	NASA SP-468
Martin	B-26F	7.66	658	-	20.66	-	0.0314	12.0	NASA SP-468
North American	P-51B	5.83	235	880	3.70	0.0042	0.0157	-	Roskam
	P-51D	5.86	233	-	3.80	-	0.0163	14.6	NASA SP-468
Republic	P-47	5.54	300	1200	6.50	0.0054	0.0217	-	Perkins & Hage
Seversky	P-35	5.89	220	-	6.05	-	0.0275	11.3	NACA WR-L-489
					5.52		0.0251	11.8	NASA SP-468

**TABLE 16-22** Drag characteristics of selected aircraft—cont'd

Selected Jet Fighter/Trainer Aircraft									
Make	Model	AR	S, ft <sup>2</sup>	S <sub>wet</sub> , ft <sup>2</sup>	f, ft <sup>2</sup>	C <sub>f</sub>	C <sub>Dmin</sub>	L <sub>Dmax</sub>	Reference
Cessna	T-37	6.20	183.9	770	3.15	0.0041	0.0171	-	Roskam
Convair	F-106A	2.10	697.8	-	5.80	-	0.0083	12.1	NASA SP-468
General Dynamics	F-111D	7.56	525	-	9.36	-	0.0186	15.8	NASA SP-468
	F-16 (clean)	3.56	300	-	-	-	0.0137	13.4	AGARD Vol. 242-19
Lockheed	F-104G	2.45	196.1	-	3.37	-	0.0172	9.2	NASA SP-468
	P-80A	6.37	237.6	-	3.20	-	0.0134	17.7	NASA SP-468
McDonnell-Douglas	F-4C	2.82	530	-	12.72	-	0.0240	8.7	Nicolai
	F-4E	2.77	530	-	11.87	-	0.0224	8.6	NASA SP-468
North American	F-100D	3.76	400.2	-	5.00	-	0.0130	13.9	NASA SP-468
	F-86E	4.78	287.9	-	3.80	-	0.0132	15.1	NASA SP-468
Northrop	F-5E	3.86	186	-	3.40	-	0.0200	10.0	NASA SP-468
Republic	F-105D	3.16	385	-	6.65	-	0.0173	10.4	NASA SP-468
Vought	F-8H	3.42	375	-	5.00	-	0.0133	12.8	NASA SP-468
Selected Jet Bomber and Attack Aircraft									
Make	Model	AR	S, ft <sup>2</sup>	S <sub>wet</sub> , ft <sup>2</sup>	f, ft <sup>2</sup>	C <sub>f</sub>	C <sub>Dmin</sub>	L <sub>Dmax</sub>	Reference
Boeing	B-47E	9.42	1428	-	21.13	-	0.0148	20	NASA SP-468
	B-52H	8.56	4000	-	47.60	-	0.0119	21.5	NASA SP-468
Convair	B-58A	2.09	1542	-	10.49	-	0.0068	11.3	NASA SP-468
Grumman	A-6E	5.31	529	-	7.64	-	0.0144	15.2	NASA SP-468
Martin	B-57B	4.27	960	-	11.45	-	0.0119	15	NASA SP-468
North American	B-45C	6.74	1175	-	18.80	-	0.0160	16.3	NASA SP-468
Various Subsonic Military Aircraft (Props and Jets)									
Make	Model	AR	S, ft <sup>2</sup>	S <sub>wet</sub> , ft <sup>2</sup>	f, ft <sup>2</sup>	C <sub>f</sub>	C <sub>Dmin</sub>	L <sub>Dmax</sub>	Reference
Grumman	S2F Tracker	6.89	485	-	15.25	-	0.0315	12.0	Author
Lockheed	U-2	10.61	1000	-	10.95	-	0.0110	23.0	Author
Lockheed	C-141	7.90	3228	-	46.81	-	0.0145	18.9	Nicolai
Flying Boats									
Make	Model	AR	S, ft <sup>2</sup>	S <sub>wet</sub> , ft <sup>2</sup>	f, ft <sup>2</sup>	C <sub>f</sub>	C <sub>Dmin</sub>	L <sub>Dmax</sub>	Reference
Boeing	314	8.06	2867	-	78.56	-	0.0274	13.00	NASA SP-468
Consolidated	Commodore	9.00	1110	-	62.38	-	0.0562	9.40	NASA SP-468
	PB2Y-3	7.43	1780	-	50.02	-	0.0281	12.30	NASA SP-468
	PBY-5A	7.73	1400	-	43.26	-	0.0309	11.90	NASA SP-468
Curtiss	Curtiss F-5L	9.33	1397	-	96.95	-	0.0694	8.60	NASA SP-468
	Curtiss H16	9.40	1164	-	85.92	-	0.0768	8.40	NASA SP-468
	Curtiss HS-2L	8.24	803	-	54.24	-	0.0676	8.20	NASA SP-468
Dornier	Do X	5.12	4844	-	228.64	-	0.0472	7.70	NASA SP-468
Douglas	Dolphin	6.08	592	-	25.46	-	0.0430	8.82	NASA SP-468
Fleetwings	F-5	7.25	235	-	8.11	-	0.0345	10.60	NASA SP-468
Grumman	G-21	6.40	375	-	12.19	-	0.0325	10.50	NASA SP-468
Hall	Hall XP2H-1	5.54	2742	-	79.76	-	0.0291	10.20	NASA SP-468
Loening	Loening OA-1C	4.86	504	-	23.08	-	0.0458	7.64	NASA SP-468
Martin	130	7.88	2170	-	65.75	-	0.0303	11.90	NASA SP-468
	JRM-1	10.86	3683	-	84.34	-	0.0233	16.40	NASA SP-468
	Martin PM-1	5.19	1236	-	59.08	-	0.0478	7.70	NASA SP-468
	P5M-2	9.92	1406	-	38.67	-	0.0275	14.40	NASA SP-468
Navy-Curtiss	PBM-3D	9.89	1408	-	46.04	-	0.0327	13.20	NASA SP-468
	Navy-Curtiss NC-4	8.07	2380	-	213.96	-	0.0899	7.00	NASA SP-468
Sikorsky	S-42	9.73	1340	-	47.51	-	0.0362	12.20	NASA SP-468
	Sikorsky S-38B	7.14	720	-	39.10	-	0.0543	8.50	NASA SP-468

Continued

**TABLE 16-22** Drag characteristics of selected aircraft—cont'd

Kitplanes (Homebuilt) and LSA									
Make	Model	AR	S, ft <sup>2</sup>	S <sub>wet</sub> , ft <sup>2</sup>	f, ft <sup>2</sup>	C <sub>f</sub>	C <sub>Dmin</sub>	L <sub>D</sub> max	Reference
Bede	BD-5B	9.75	47.4	170	0.80	0.0048	0.0169	-	Stinton
Cozy	Mark IV	8.94	88.3	-	1.78	-	0.0201	16.5	Author
Falco	F.8L (160 & 180 BHP)	6.41	107.5	-	2.28	-	0.0212	14.2	Author
Flight Design	CTSW	7.29	107.4	-	3.64	-	0.0338	11.9	Author
Glassair	III (Standard Wing)	6.68	81.3	-	1.86	-	0.0229	14.0	Author
Icon	A5 (amphib)	9.03	128	-	5.72	-	0.0447	11.1	Author
Osprey	2 (amphib)	5.20	130	-	5.31	-	0.0408	9.5	Author
	GP-4	5.54	104	-	1.23	-	0.0119	18.0	Author
Progressive Aerodyne	Searey (amphib)	6.06	157	-	6.93	-	0.0441	9.7	Author
Pipistrel	Virus 912 LSA	14.10	118	-	1.50	-	0.0127	23.9	Author
Rutan	LongEz	8.31	82.0	-	1.88	-	0.0230	16.2	Author
	VariEze (wheelpants)	9.28	53.6	-	1.11	-	0.0207	16.5	Author
	VariEze (no whlpnts)	9.28	53.6	-	1.21	-	0.0226	15.8	Author
	VariEze	9.20	53.6	260	1.25	0.0047	0.0233	-	Stinton

Single Engine GA Aircraft (Piston and Turboprop)									
Make	Model	AR	S, ft <sup>2</sup>	S <sub>wet</sub> , ft <sup>2</sup>	f, ft <sup>2</sup>	C <sub>f</sub>	C <sub>Dmin</sub>	L <sub>D</sub> max	Reference
Beechcraft	Beech 17	6.91	296.5	1000	6.00	0.0059	0.0202	-	Stinton
	Bonanza V-35 (RG)	6.20	181	-	3.48	-	0.0192	13.8	NASA SP-468
Cessna	150	6.93	159.5	-	4.70	-	0.0295	12.5	Author
	152	6.93	159.5	-	5.52	-	0.0346	11.5	Author
	162 Skycatcher	7.67	120	-	3.95	-	0.0329	12.2	Author
	172 Skyhawk	7.45	174	-	5.06	-	0.0291	12.9	Author
	172 Skyhawk	7.32	175	-	5.58	-	0.0319	11.6	NASA SP-468
	177 (flaps dn)	7.40	175	-	8.23	-	0.047	8.3	Roskam
	177 (flaps up)	7.40	175	-	4.55	-	0.026	11.2	Roskam
	177 Cardinal	7.24	174	-	5.42	-	0.0312	12.3	Author
	177 Cardinal RG (RG)	7.24	174	-	3.79	-	0.0218	14.7	Author
	177 Cardinal RG II (RG)	7.66	174	-	3.88	-	0.0223	14.2	NASA SP-468
	180 Skywagon	7.45	174	700	4.30	0.0085	0.0247	-	Stinton
	180 Skywagon	7.45	174	-	5.16	-	0.0297	12.8	Author
	182 Skylane	7.45	174	-	4.69	-	0.0270	13.4	Author
	208 Caravan (FG-T)	9.71	279.4	-	9.92	-	0.0355	12.8	Author
Cirrus	SR20	9.16	135.2	-	3.45	-	0.0255	14.8	Author
	SR22	10.00	144.9	-	3.68	-	0.0254	15.3	Author
Commander	114B (RG)	7.06	152	-	4.37	-	0.0287	12.7	Author
De Havilland of Canada	DHC-2 Beaver (land)	9.22	250	-	12.19	-	0.0488	10.7	Author
	DHC-2 Beaver (floats)	9.22	250	-	17.00	-	0.0680	9.1	Author
Extra Aircraft	EA-500 (RG-T)	9.44	153.5	-	3.66	-	0.0239	15.5	Author
	M20F (RG)	7.45	174.8	-	3.46	-	0.0198	16.7	Author
	M20J (RG)	7.45	174.8	-	3.04	-	0.0174	16.7	Author
Mooney	231 (RG)	7.45	174.8	-	3.30	-	0.0189	16.0	AIAA-85-8038
	PAC-750XL (FG-T)	5.78	305	-	9.77	-	0.0320	11.1	Author
Piper	J-3 Cub	5.81	178	-	6.64	-	0.0373	9.6	NASA SP-468
	PA-28 Cherokee	6.02	170	-	6.09	-	0.0258	10.0	NASA SP-468
	PA-38 Tomahawk	9.27	124.7	-	4.85	-	0.0389	12.1	Author
	PA-46 Malibu (RG)	10.57	174.9	-	4.14	-	0.0237	16.1	Author
	PA-46 Mirage (RG)	10.57	175	-	4.07	-	0.0232	16.3	Author
	PA-46 Meridian (RG-T)	10.10	183	-	4.37	-	0.0239	15.8	Author
SOCATA	TB10 (with WF)	8.22	128.04	-	5.70	-	0.0445	10.8	Author
	TB10 (without WF)	8.22	128.04	-	7.16	-	0.0559	9.6	Author
	TBM-700 (RG-T)	8.93	193.7	-	4.78	-	0.0247	14.9	Author
	TBM-850 (RG-T)	8.93	193.7	-	4.51	-	0.0233	15.4	Author

**TABLE 16-22** Drag characteristics of selected aircraft—cont'd

Twin Engine GA Aircraft (Piston and Turboprop)									
Make	Model	AR	$S, \text{ft}^2$	$S_{\text{wet}}, \text{ft}^2$	$f, \text{ft}^2$	$C_f$	$C_{D\min}$	$LD_{\max}$	Reference
Aero	Ae-45	8.78	184	-	4.45	-	0.0242	15.0	Author
Beechcraft	D-18	6.51	349	1400	10.50	0.0080	0.0301	-	Stinton
	B55 Baron	7.19	199.2	-	4.59	-	0.0230	14.3	Author
Britten-Norman	B8 Queen Air	8.59	293.9	-	6.82	-	0.0232	15.2	Author
	BN-2	7.39	325	1350	12.00	0.0088	0.0369	-	Stinton
Cessna	310 II	7.61	179	-	4.78	-	0.0267	13.0	NASA SP-468
	310 (clean)	7.00	175.00	-	5.16	-	0.0295	12.3	Roskam
	310 (gear dn, flps 15°)	7.00	175.00	-	11.38	-	0.0650	8.6	Roskam
	310 (gear dn, flps 45°)	7.00	175.00	-	20.48	-	0.1170	6.5	Roskam
	337 Skymaster	7.18	201	-	6.08	-	0.0302	12.5	Author
Partenavia	P-68 Victor	7.74	200.2	-	5.89	-	0.0294	13.0	Author
Piper	PA-23-250 Aztec	6.67	207.6	-	6.74	-	0.0325	11.7	Author

Multi-Engine Commercial Transport Aircraft (Piston)									
Make	Model	AR	$S, \text{ft}^2$	$S_{\text{wet}}, \text{ft}^2$	$f, \text{ft}^2$	$C_f$	$C_{D\min}$	$LD_{\max}$	Reference
Boeing	247D	6.55	836	-	17.72	-	0.0212	13.5	NASA SP-468
Curtiss	C-46A	8.59	1358	5400	26.00	0.0047	0.0191	-	Roskam
Douglas	C-47B	9.24	987	3700	25.50	0.0069	0.0258	-	Roskam
	DC-3	9.14	987	-	24.58	-	0.0249	14.7	NASA SP-468
Lockheed	L-1049G	9.17	1650	-	34.82	-	0.0211	16.0	NASA SP-468

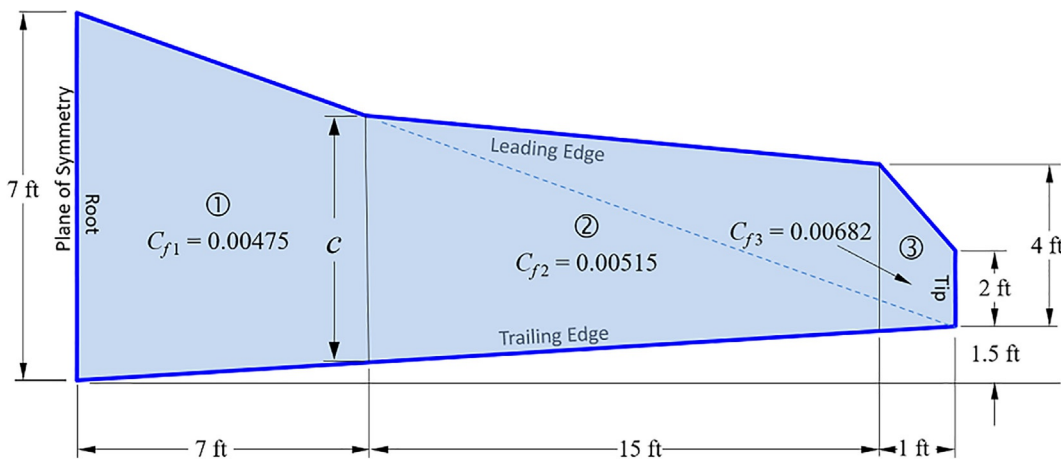
  

Commercial Jetliners and Business Jets									
Make	Model	AR	$S, \text{ft}^2$	$S_{\text{wet}}, \text{ft}^2$	$f, \text{ft}^2$	$C_f$	$C_{D\min}$	$LD_{\max}$	Reference
Boeing	B-747 (M = 0.7)	7.00	5500	-	88.00	-	0.0160	-	NASA-CR-114494
	B-747 (M = 0.8)	7.00	5500	-	96.80	-	0.0176	-	NASA-CR-114494
	B-747 (M = 0.9)	7.00	5500	-	120.45	-	0.0219	-	NASA-CR-114494
Gates	Learjet 24D	5.46	231.8	-	-	-	0.0234	-	NASA TN-D-6573

Sailplanes									
Make	Model	AR	$S, \text{ft}^2$	$S_{\text{wet}}, \text{ft}^2$	$f, \text{ft}^2$	$C_f$	$C_{D\min}$	$LD_{\max}$	Reference
DG Flugzeugbau	LS-8s	21.43	113	-	1.01	-	0.00892	43.0	Author
Stemme	S-10	29.29	202	-	1.75	-	0.00865	51.0	Author

RG = Retractable gear, FG = Fixed gear, T = Turboprop, WF = Wheel fairings,  $f$  = equivalent flat plate area =  $C_{D\min} \times S$ .



**FIGURE 16-83** Wing used in Example (3).

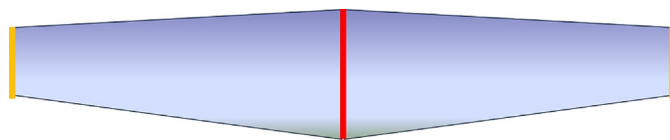


FIGURE 16-84 Wing used in Example (4).

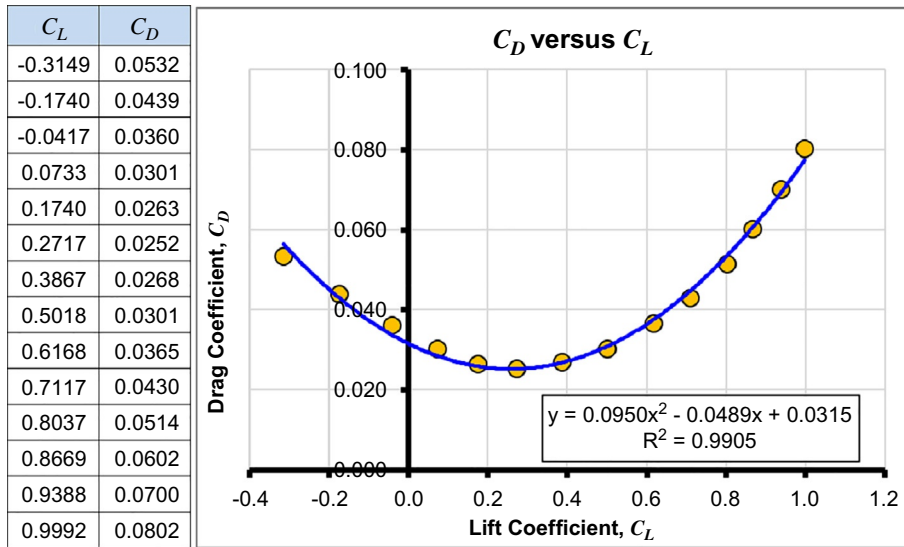


FIGURE 16-85 Information used in Example (6).

each of the three wing segments has already been calculated. Note that all data required for geometric evaluation are given in the figure. Assume wetted area booster factor of 1.07. Determine the total skin friction coefficient and total skin friction drag coefficient for the wing half. Estimate the total skin friction drag force of both wing halves at airspeed of 150 KTAS at S-L on a standard day.

Ans:  $C_f = 0.005045$ ,  $C_{Df} = 0.01080$ ,  $D_f = 183 \text{ lb}_f$ .

- (4) An airplane has two dissimilar airfoils at the root and tip of the wing (see Figure 16-84). Important dimensions to use are:

$$b = 18 \text{ ft}, c_r = 3 \text{ ft}, c_t = 2 \text{ ft}, \text{ and } S = 45 \text{ ft}^2.$$

The root airfoil is a NLF airfoil capable of sustaining 55% laminar flow on the upper surface and 35% on the lower. The tip airfoil is a turbulent flow airfoil that sustains laminar flow to 15% on the upper and lower surfaces.

If the airplane is cruising at 100 KTAS at S-L ISA, determine the skin friction drag coefficient and force acting on the wing due to the mixed laminar and turbulent BL regions. Compare to a wing with fully laminar or fully turbulent BL.

Ans:  $C_f = 0.003115$ ,  $C_{Df} = 0.006230$ ,  $D_f = 9.5 \text{ lb}_f$ .

- (5) Extract the total, induced, and minimum drag coefficient for the single-piston engine propeller

powered Cessna 172N Skyhawk II using the data below obtained from its POH. Hint: Use Equation (9-129) to estimate the Oswald's span efficiency and assume a propeller efficiency of 0.80.

Wing span is 36.08 ft, wing area is 174 ft<sup>2</sup>, cruising speed at 8000 ft and 75% power is 122 KTAS. Engine is a Lycoming O-320 rated at 160 BHP at S-L. Gross weight is 2300 lb<sub>f</sub>.

Ans:  $C_D = 0.03714$ ,  $C_{D_{min}} = 0.03141$ ,  $C_{D_i} = 0.005728$ .

- (6) Extract the  $C_{L_{min,D}}$ ,  $C_{D_{min}}$ , and  $e$  for the wind tunnel data (points) shown in the table and graph of Figure 16-85. The solid line is a least-squares curvefit whose constants and correlation coefficients are shown in the legend. The AR for the airplane being tested is 6.

Ans:  $C_{L_{min,D}} = 0.2574$ ,  $C_{D_{min}} = 0.0252$ ,  $e = 0.5584$ .

## References

- [1] D. Levy, R. Wahls, T. Zickuhr, J. Vassberg, S. Agrawal, S. Pirzadeh, M. Hemsch, AIAA CFD drag prediction workshop, data summary and comparison, in: 40th AIAA Aerospace Sciences Meeting & Exhibit, June 9-10, 2001, <https://doi.org.ezproxy.libproxy.db.erlau.edu/10.2514/6.2002-841>.
- [2] Source: 1st AIAA CFD Drag Prediction Workshop, Anaheim, CA, June 2001, <http://aiaa-dpw.larc.nasa.gov/Workshop1/workshop1.html> (Accessed 06 September 2020).
- [3] Anonymous, *A Selection of Experimental Test Cases for the Validation of CFD Codes*, AGARD-AR-303 vol. II, August 1994.

- [4] D. Gyorgyfalvy, *Performance analysis of the Horten IV flying wing*, in: 8<sup>th</sup> Congress of the Organisation Scientifique et Technique Internationale du Vol a Voile (OSTIV), June 1960.
- [5] P.W. Niewald, S.L. Parker, *Flight-test techniques employed to successfully verify F/A-18E in-flight lift and drag*, J. Aircr. 37 (2) 2000 194–200 AIAA.
- [6] I.H. Abbott, A.E. von Doenhoff, L.S. Stivers Jr., *Summary of Airfoil Data*, NACA R-824 1945.
- [7] J.D. Anderson, *Fundamentals of Aerodynamics*, sixth ed., McGraw-Hill, 2011.
- [8] Y.A. Cengel, J.M. Cimbala, *Fluid Mechanics: Fundamentals and Applications*, fourth ed., McGraw-Hill, February 27, 2017.
- [9] R.W. Fox, A.T. McDonald, *Introduction to Fluid Mechanics*, eighth ed., John Wiley and Sons, October 10, 2011.
- [10] L. Prandtl, *Applications of Modern Hydrodynamics to Aeronautics*, NACA R-116 1923.
- [11] B.M. Jones, *The streamline aeroplane*. J. R. Aeronaut. Soc. 33 (221) 1929 357–385, <https://doi.org/10.1017/S0368393100136442>.
- [12] B.M. Jones, *Flight experiments on the boundary layer*, J. Aeronaut. Sci. 5 (3) 1938 81–94.
- [13] B.H. Carmichael, *Summary of Past Experience in Natural Laminar Flow and Experimental Program for Resilient Leading Edge*, NASA CR-152276 May 1979.
- [14] B.H. Carmichael, R.C. Whites, W. Pfenninger, *Low Drag Boundary Layer Suction Experiments in Flight on the Wing Glove of an F-94A Airplane*, Rep. No. NAI-57-1163 (BLC-101) Northrop Aircraft Inc., 1957.
- [15] B.H. Carmichael, *Surface Waviness Criteria for Swept and Unswept Laminar Suction Wings*, Rep. No. NOR-59-438 (BLC-123) (Contract AF33 (616)-3168) Northrop Aircraft, Inc., 1959.
- [16] B.H. Carmichael, W. Pfenninger, *Surface Imperfection Experiments on a Swept Laminar Suction Wing*, Rep. No. NOR-59-454 (BLC-124) Northrop Aircraft Inc., 1959.
- [17] C.H. Dearborn, A. Silverstein, *Drag Analysis of Single-Engine Military Airplanes Tested in the NACA Full-Scale Wind Tunnel*, NACA WR-L-489 1940.
- [18] L. Dwyer, Seversky P-35, *The Aviation History Online Museum*, Updated April 20 <http://www.aviation-history.com/seversky/p35.htm>, 2014 (Accessed 16 December 2020).
- [19] T. Haines, *Turbine Pilot: Eclipse 500: Typed and Tried Test Driving the Eclipse 500 and Its Training Program*, AOPA Online Article <https://www.aopa.org/news-and-media/all-news/2008/august/01/turbine-pilot-eclipse-500-typed-and-tried>, August 1, 2008 (Accessed 02 November 2020).
- [20] R. Goyer, *New Eclipse*, Flying Magazine Online February 16, 2011 <https://www.flyingmag.com/aircraft/jets/new-eclipse/> (Accessed 02 November 2020).
- [21] P.J. Parmalee, *Kind of Drag*, Aviation Week and Space Technology, September 2, 2002 12–13.
- [22] J.R. Chambers, *Innovation in Flight: Research of the NASA Langley Research Center on Revolutionary Advanced Concepts for Aeronautics*, NASA SP-2005-4539 2005 pp. 123–161.
- [23] A.L. Braslow, *A History of Suction-Type Laminar-Flow Control With Emphasis on Flight Research*, Monographs in Aerospace History Number 13NASA, 1999.
- [24] L.A. Marshall, *Boundary-Layer Transition Results From the F-16XL-2 Supersonic Laminar Flow Control Experiment*, NASA TM-1999-209013 1999.
- [25] H.J.B. van de Wal, *Design of a Wing With Boundary Layer Suction*, (M.Sc. thesis) Delft University of Technology, 2010.
- [26] A. Wortman, *Reduction of fuselage form drag by vortex flows*, J. Aircr. 36 (3) 1999 501–506.
- [27] J.A.C. Kentfield, *Drag Reduction by Means of Controlled Separated Flows*, AIAA-1985-1800-493 1985.
- [28] A. Quast, K.H. Horstmann, *Profile Design for Wings and Propellers*, NASA TM-77785 Nov. 1984.
- [29] S. Peigin, B. Epstein, *Aerodynamic optimization of essentially three-dimensional shapes for wing-body fairing*, AIAA J. 46 (7) 2008 1814–1825.
- [30] H. Schlichting, *Boundary Layer Theory*, English Edition Pergamon Press, 1955, 16.
- [31] J.A. Schetz, R.D.W. Bowersox, *Boundary Layer Analysis*, American Institute of Aeronautics and Astronautics Education Series 2011.
- [32] A.D. Young, *Boundary Layers*, American Institute of Aeronautics and Astronautics Education Series 1989.
- [33] S.F. Hoerner, *Fluid-Dynamic Drag*, L. Hoerner, 1965.
- [34] W. Sutherland, *LII. The viscosity of gases and molecular force*. Philosophical Magazine Series 5 36 (223) 1893 507–531, <https://doi.org/10.1080/14786449308620508>.
- [35] V.L.E. Streeter, B. Wylie, *Fluid Mechanics*, McGraw-Hill, 1979.
- [36] J. Roskam, C.-T.E. Lan, *Aircraft Aerodynamics and Performance*, DARcorporation, 1997.
- [37] D.E. Hoak, *USAF Stability and Control DATCOM*, Flight Control Division, Air Force Flight Dynamics Laboratory, 1978 Section 4.1.5.1.
- [38] Y.A. Cengel, J.M. Cimbala, *Fluid Mechanics—Fundamentals and Applications*, McGraw-Hill, 2006.
- [39] K.E. Schoenherr, *Resistance of flat surfaces moving through a fluid*, Trans. Soc. Nav. Arch. Mar. Eng. 40 1932 279.
- [40] T. von Kármán, *Mechanical Similitude and Turbulence*, NACA TM-611 March 1931.
- [41] L. Prandtl, *Über den Reibungswiderstand Strömender Luft*, Erg. AVA, Gottingen, 1932 III series; also IV series .
- [42] L.V. Lazauskas, *Hydrodynamics of Advanced High-Speed Sealift Vessels*, (Master's thesis) University of Adelaide, 2005.
- [43] G.E. Gadd, *A new turbulent friction formulation based on a re-appraisal of Hughes' results*, Trans. RINA 109 1967 511–539.
- [44] P.S. Granville, *The viscous resistance of surfaces vessels and the skin friction of flat plates*, Trans. SNAME 64 1956 209–240.
- [45] W.D. Hayes, R.F. Probstein, *Hypersonic Flow Theory*, Academic Press, New York, 1959.
- [46] F. Frankl, V. Voishel, *Heat Transfer in the Turbulent Boundary Layer of a Compressible Gas at High Speeds*, NACA TM-1032 1942.
- [47] F. Frankl, V. Voishel, *Turbulent Friction in the Boundary Layer of a Flat Plate in a Two-Dimensional Compressible Flow at High Speeds*, NACA TM-1053 1943.
- [48] R.F. Anderson, *Determination of the Characteristics of Tapered Wings*, NACA-TR-572 1936.
- [49] H. Glauert, S.B. Gates, *The Characteristics of a Tapered and Twisted Wing With Sweep-Back*, Aeronautical Research Council, 1929 R. &M. No. 1226 .
- [50] J. Hueber, *Die Aerodynamischen Eigenschaften von Doppel-Trapezförmigen Tragflügeln*, Z.F.M., 13. Mai 1933, pp. 249–251, 29. May 1933, pp. 269–272.
- [51] R.S. Shevell, *Fundamentals of Flight*, Prentice Hall, 1983, 178.
- [52] J. Roskam, *Airplane Design*, Part VI DARcorporation, 2000.
- [53] D. Cohen, R.T. Jones, *High Speed Wing Theory*, Princeton University Press, 1960.
- [54] E. Torenbeek, *Synthesis of Subsonic Aircraft Design*, Delft University Press, 1986.
- [55] R.M. Johnson, *An Empirical Method for the Prediction of Airplane Drag Divergence Mach Number*, RAND Research Memorandum RM-1188 1953.
- [56] R.S. Shevell, F.P. Bayan, *Development of a Method for Predicting the Drag Divergence Mach Number and the Drag due to Compressibility for Conventional and Supercritical Wings*, SUDAAR 522 Department of Aeronautics and Astronautics, Stanford University, July 1980.
- [57] L.W. Hunton, *Effects of Twist and Camber on the Low-Speed Characteristics of a Large-Scale 45 Degree Swept-back Wing*, NACA RM-A50A10 1950.
- [58] W.C. Schneider, *A Comparison of the Spanwise Loading Calculated by Various Methods With Experimental Loadings Obtained on a 45 Degree Sweptback Wing of Aspect Ratio 8.02 at a Reynolds Number of 4.0x10 (6)*, NACA R-1208 1954.
- [59] W. Mason, *Analytic Models for Technology Integration in Aircraft Design*. AIAA 90-3262-CP 1990<https://doi.org/10.2514/6.1990-3262>.

- [60] B. Malone, W. Mason, *Multidisciplinary Optimization in Aircraft Design Using Analytic Technology Models*. AIAA 91-54093 1991, <https://doi.org/10.2514/6.1991-3187>.
- [61] C.W. Boppe, *Computational Aerodynamic Design: X-29, the Gulf-stream Series and a Tactical Fighter*, SAE Technical Paper Series, SAE-851789 October 1985.
- [62] C.W. Boppe, *CFD Drag Prediction for Aerodynamic Design, Technical Status Review on Drag Prediction and Analysis from Computational Fluid Dynamics: State of the Art*, AGARD AR 256 June 1989 pp. 8-1-8-27.
- [63] S.S. Chauhan, J.R.R.A. Martins, *Low-Fidelity aerostructural optimization of aircraft wings with a simplified wingbox model using Open-AeroStruct*. in: Proceedings of the 6<sup>th</sup> International Conference on Engineering Optimization, EngOpt 2008, Springer, September 2018, [https://doi.org/10.1007/978-3-319-97773-7\\_38](https://doi.org/10.1007/978-3-319-97773-7_38).
- [64] J.W.R. Taylor (Ed.), Jane's All the World's Aircraft 1987-88, Janes Yearbooks, 1988.
- [65] R.T. Whitcomb, *A Study of the Zero-Lift Drag-Rise Characteristics of Wing-Body Combinations Near the Speed of Sound*, NACA TR-1273 1956.
- [66] S. Hoffman, *Supersonic-Aera-Rule Design and Rocket-Propelled Flight Investigation of a Zero-Lift Straight-Wing-Body-Nacelle Configuration between Mach Numbers 0.8 and 1.53*, NACA RM-L56B27, April 26, 1956.
- [67] H.-U. Meier, *German Development of the Swept Wing 1935-1945*, AIAA, 2010.
- [68] Anonymous, Wallace Hayes, *Pioneer of Supersonic Flight, Dies*, Obituary from News from Princeton University, Office of Communications March 8, 2001.
- [69] H. Ashley, M. Landahl, *Aerodynamics of Wings and Bodies*, Dover Publications, 1965.
- [70] L.E. Wallace, *The whitcomb area rule: NACA aerodynamics research and innovation*, in: P.E. Mack (Ed.), From Engineering Science to Big Science: The NACA and NASA Collier Trophy Research Project Winners, NASA History Office, Washington, DC, 1998, , pp. 135-148.
- [71] R.T. Whitcomb, *A Study of the Zero-Lift Drag-Rise Characteristics of Wing-Body Combinations Near the Speed of Sound*, NACA RM-L52H08, September 3, 1952.
- [72] R.T. Jones, *Theory of Wing-Body Drag at Supersonic Speeds*, NACA TR-1284 1956.
- [73] R.J. Harris, *An Analysis and Correlation of Aircraft Wave Drag*, NASA TM-X-947 March 1964.
- [74] M.J. Waddington, *Development of an Interactive Wave Drag Capability for the OpenVSP Parametric Geometry Tool*, (Master's thesis) California Polytechnic State University, 2015.
- [75] NASA Open Source Parametric Geometry Code. <http://openvsp.org/> (Accessed 03 November 2020).
- [76] R.T. Jones, *The minimum drag of thin wings in frictionless flow*, J. Aeronaut. Sci. 18 (2) 1951 75-81.
- [77] R.T. Jones, *Theoretical determination of the minimum drag of airfoils at supersonic speeds*, J. Aeronaut. Sci. 1952 813-822.
- [78] L. Nicolai, *Fundamentals of Aircraft Design*, second ed., 1984.
- [79] D. Raymer, *Aircraft Design: A Conceptual Approach*, fourth ed., American Institute of Aeronautics and Astronautics Education Series 2006.
- [80] L.R. Jenkinson, P. Simpkin, D. Rhodes, *Civil Jet Aircraft Design*, American Institute of Aeronautics and Astronautics Education Series 1999.
- [81] J. Roskam, *Some comments about fuselage drag*, in: Proceedings of the NASA-Industry-University GA Drag Reduction Workshop, Lawrence, KS, July 14-16, 1975.
- [82] R.S. Shevell, *Fundamentals of Flight*, Prentice Hall, 1983, 179 based on the digitization of Figure 11.4.
- [83] G.C. Oates, *Aerothermodynamics of Gas Turbine and Rocket Propulsion*, American Institute of Aeronautics and Astronautics Education Series 1984.
- [84] J.D. Mattingly, W.H. Heiser, D.T. Pratt, *Aircraft Engine Design*, second ed., American Institute of Aeronautics and Astronautics Education Series 2002.
- [85] F. Monts, *The Development of Reciprocating Engine Installation Data for General Aviation Aircraft*, SAE Paper 730325, Business Aircraft Meeting, Wichita, Kansas, April 3-6 1973.
- [86] V.R. Corsiglia, J. Katz, R.A. Kroeger, *Full-scale wind-tunnel study of the effect of nacelle shape on cooling drag*. J. Aircr. 18 (2) 1981 82-88, <https://doi.org/10.2514/3.57469>.
- [87] J. Katz, V.R. Corsiglia, P.R. Barlow, *Cooling air inlet and exit geometries on aircraft engine installations*. J. Aircr. 19 (7) 1982 525-530, <https://doi.org/10.2514/3.57425>.
- [88] J. Katz, V.R. Corsiglia, P.R. Barlow, *Effect of propeller on engine cooling system drag and performance*. J. Aircr. 19 (3) 1982 193-197, <https://doi.org/10.2514/3.57375>.
- [89] S.J. Miley, E.J. Cross, J.K. Owens, *An Investigation of the Aerodynamics and Cooling of a Horizontally-Opposed Engine Installation*. SAE Technical Paper 770467 1977, <https://doi.org/10.4271/770467>.
- [90] J.V. Becker, *Wind Tunnel Tests of Air Inlet and Outlet Openings on a Streamline Body*, NACA WR-L-300 November, 1940.
- [91] B.W. McCormick, *Aerodynamics, Aeronautics, and Flight Mechanics*, John Wiley & Sons, 1979.
- [92] W.H. Herrnstein, D. Biermann, *The Drag of Airplane Wheels, Wheel Fairings, and Landing Gears—I*, NACA R-485 1935.
- [93] W. Austyn-Mair, D.L. Birdsall, *Aircraft Performance*, Cambridge University Press, Cambridge, 1992, 124 Method is based on ESDU 79015, Undercarriage Drag Prediction Methods .
- [94] J. Roskam, *Methods for Estimating Drag Polars of Subsonic Airplanes*, Roskam Aviation and Engineering Corporation, 4th Printing 1984.
- [95] R.N. Conway, J.D. Maynard, *Wind-Tunnel Tests of Four Full-Scale Seaplane Floats*, NACA WR-L-238 1943.
- [96] J.B. Parkinson, R.E. Olson, R.O. House, *Hydrodynamic and Aerodynamic Tests of a Family of Models of Seaplane Floats With Varying Angles of Dead Rise*, NACA TN-716 1939.
- [97] A.D. Young, *The Aerodynamic Characteristics of Flaps*, R.&M. No. 2622, British A. R. C. 1947
- [98] T.C. Corke, *Design of Aircraft*, Prentice-Hall, 2003.
- [99] P.E. Purser, T.R. Turner, *Wind-Tunnel Investigation of Perforated Split Flaps for Use as Dive Brakes on a Tapered NACA 23012 Airfoil*, NACA-WR-L-373 November 1, 1941.
- [100] T.R. Turner, *Aerodynamic Characteristics and Flap Loads of Perforated Double Split Flaps on a Rectangular NACA 23012 Airfoil*, NACA-WR-L-415 January 1, 1943.
- [101] J. Fischel, J.M. Wathen, *Investigation of Spoiler Ailerons for use as Speed Brakes or Glide-Path Controls on Two NACA 65-Series Wings Equipped With Full Span Slotted Flaps*, NACA-TR-1034 January 1, 1951.
- [102] F. Linden, R. Van Der, *The Boeing 247: The First Modern Airliner*, University of Washington Press, 1991.
- [103] R.M. Wright, *Investigation of Drag and Pressure Distribution of Wind-shields at High Speeds*, NACA WR-L-462 1942.
- [104] E.P. Hartman, *Negative Thrust and Torque Characteristics of an Adjustable-Pitch Metal Propeller*, NACA R-464 1934.
- [105] Eiffel is considered by many to be the father of Aerodynamics, while others place the honor on Cayley.
- [106] H.A. Fedziuk, *High-Speed Wind-Tunnel Tests of Gun Openings in the Nose of the Fuselage of a 1/4-Scale Model*, NACA WR-L-502 1942.
- [107] B.G. Gulick, *Effects of Simulated Ice Formation on the Aerodynamic Characteristics of an Airfoil*, NACA WR-L-292 1938.
- [108] V.H. Gray, U.H. Von Glahn, *Effect of Ice and Frost Formations on Drag of NACA 65(sub 1)-212 Airfoil for Various Modes of Thermal Ice Protection*, NACA TN-2962 1953.
- [109] Various editors, Jane's All the World's Aircraft, Janes Yearbooks, Various Years.
- [110] C.D. Perkins, R.E. Hage, *Airplane Performance, Stability, and Control*, John Wiley & Sons, 1949.
- [111] D. Stinton, *The Design of the Aeroplane*, Collins, 1983.
- [112] L.K. Loftin Jr., *Quest for Performance; The Evolution of Modern Aircraft*, NASA SP-468 1985.
- [113] C.R. Hanke, D.R. Nordwall, *The Simulation of a Jumbo Jet Transport Aircraft*, Modeling Datavol. 2, 1970NASA-CR-114494.